U. S. DEPARTMENT OF COMMERCE
Charles Sawyer, Secretary
NATIONAL BUREAU OF STANDARDS
E. U. Condon, Director

NOVEMBER 1948
VOLUME • 41
NUMBER 5

JOURNAL OF RESEARCH

of the

NATIONAL BUREAU OF STANDARDS

Contents

RP		Page
1930.	Calibration of accelerometers. Samuel Levy, Albert E. McPherson, and Edward V. Hobbs. (Price 10 cents)	359
1931.	Studies of the Mattson shot classifier. Raymond L. Blaine and Harold J. Valis. (Price 10 cents)	371
1932.	Compilation of thermal properties of hydrogen in its various isotopic and ortho-para modifications. Harold J. Woolley, Russell B. Scott, and F. G. Brickwedde. (Price 40 cents)	379
1933.	Chemical durability, specular gloss, and transmittance of optical glasses. Donald Hubbard and Gerald F. Rynders. (Price 10 cents)	477
1934.	Bending tests of large welded-steel box girders at different temperatures. Ambrose H. Stang and Bernard S. Jaffe. (Price 10 cents)	483
1935.	Standards for low values of direct capacitance. Charles Moon and C. Matilda Sparks. (Price 10 cents)	497
1936.	Experimental verification of theory of landing impact. Walter Ramberg and Albert E. McPherson. (Price 10 cents)	509
1937.	Copolymerization. Robert Simha and Leo A. Wall. (Price 15 cents)	521

For sale by the Superintendent of Documents, U. S. Government Printing Office, Washington 25, D. C. - Price $1.00
$4.50 per year on subscription

UNITED STATES GOVERNMENT PRINTING OFFICE, WASHINGTON : 1948

U. S. Department of Commerce
National Bureau of Standards

Research Paper RP1930
Volume 41, November 1948

Part of the Journal of Research of the National Bureau of Standards

Calibration of Accelerometers

By Samuel Levy, Albert E. McPherson, and Edward V. Hobbs

This paper describes three accelerometer calibrators. These calibrators were developed to provide a convenient means for calibrating lightweight accelerometers of the types used for measuring accelerations on airplanes in flight. The first calibrator is a shaking table having a sinusoidal motion with frequencies of 20 to 110 cycles per second and accelerations up to 80 gravity; the second is a portable calibrator producing a known pulse of acceleration with a peak value between 1 and 20 gravity; and the third is a centrifuge, which develops a maximum steady acceleration of about 1,000 gravity.

I. Introduction

Accelerometers of the types used to measure accelerations on airplanes in flight consist of a mass mounted on springs inside a case. Damping is frequently used to limit the response of the accelerometer at its resonant frequency. The mass is usually guided to make the instrument sensitive to accelerations along one line only. The output of the accelerometer is recorded mechanically for some of the larger instruments. For most of the smaller instruments the output is in the form of changes in an electric circuit, which are recorded on an oscillograph, an oscilloscope, or a pen-and-ink recorder. In the working range, the indicated response of the accelerometer is nearly proportional to the applied acceleration. The factor of proportionality is defined as the calibration factor.

Errors can arise in the accelerometer indication from several sources. The primary source of error is variation in the output with the frequency of the applied accelerations. This may be due to frequency effects in either the accelerometer itself or in the associated recording circuits. Secondary sources of errors are (1) nonlinearity of output with variation of applied acceleration at a fixed frequency due to "stops" that are not properly set or faulty design, and (2) response to accelerations applied in a direction transverse to the axis of the accelerometer due to misalinement of the instrument or inherent design characteristics.

The calibrators described in this paper were developed for the Bureau of Aeronautics, Navy Department, to give information on the calibration factors and on the magnitude of errors in accelerometers intended for airplane use.

II. Sinusoidal "Shaking Table"

The "shaking table" calibrator was intended to determine errors in calibration factor due to frequency effects. For this purpose it was essential that the table have a nearly pure sinusoidal motion with a minimum of harmonic distortion over a wide frequency band.

FIGURE 1. *Sinusoidal shaking table for calibration of accelerometers.*

The shaking table is shown in figure 1. It consists of the carriage, *A*, to which the accelerometer is fastened, and means for shaking the carriage, which includes an eccentric disk, *B*, riding with the carriage and a 1/2-hp 8,000-rpm 115-v a-c–d-c series motor, *C*, for rotating the disk over a wide range of speeds.

The carriage, *A*, weighing about 1.2 lb, is guided in a nearly straight line in a horizontal direction by flexure plates, *D*. The stiffness of these flexure plates determines the natural frequency of vibration of the table and, therefore, sets a lower limit to the speed range of the table. The natural frequency of the flexure plates, considered as plates clamped at both ends, determines an upper limit to the speed range of the table, beyond which undesirable high-frequency vibrations appear in the acceleration output. Four pairs of flexure plates are provided for operating the table over four speed ranges. The table is driven well above its natural frequency in order to make the amplitude insensitive to small variations in the speed of the driving motor. Extraneous high-frequency accelerations due to bearing noise are minimized by holding the eccentric disk, *B*, in a relatively long plain sleeve bearing having a clearance of the order of 0.0003 in. in preference to any multipieced bearing. Ball bearings previously used in similar equipment were found to introduce high-frequency accelerations corresponding to the passage of each ball.

The table is isolated from building vibration by 1½-in. rubber shock mounts, *E*, and from vibration of the driving motor by a ½-in.-thick sponge-rubber shock mount, *F*. In order to prevent coupling between the vibration of the carriage and any nearby flexibly supported masses, the mass of the supports, *M*, was made much larger than the mass of the carriage, *A*, and the shock mounts were chosen to make the natural frequency of the supports *M* less than 5 c/s. Pieces of sponge rubber, *G*, are used to keep the assembly in balance. Figure 2 is an assembly drawing of the shaking table.

The drive belt, *H*, between the pulley, *I*, and the disk, *B*, figure 1, is a taut single strand of No. 30 cotton thread. It was found that the small knot in this thread had no noticeable effect on the acceleration applied by the table.

FIGURE 2. *Assembly sheet, shaking table.*
Part numbers refer to shop detail drawings (detail drawings available from National Bureau of Standards upon request).

The eccentric masses, *J*, figure 1, are standard ½-in. bolt-nut combinations when large amplitudes are required and are replaced by specially made small masses when low amplitude is required. The masses are attached to disk *B* without set screws, since they show no tendency to vibrate loose on the rotating disk, *B*.

1. Operation

The accelerometer to be calibrated is attached to the carriage, *A*, figure 1, with its center line on the center line of the carriage.

The maximum acceleration of the carriage, *A*,

and the accelerometer attached to it is computed from the formula for harmonic motion,

$$a = 14.2g\left(\frac{S}{1{,}000}\right)^2 D, \qquad (1)$$

where

a = peak acceleration
g = acceleration of gravity
S = frequency in cycles per minute
D = double amplitude in inches.

The frequency of vibration, S, is measured with a stroboscopic tachometer. The double amplitude, D, is measured by observing the extreme positions of a bright spot on the carriage through a stationary telescope having a reticule graduated to 0.01 in. Excellent definition of the extreme positions of motion was obtained by observing a bright 0.001-in. wire, K, figure 1, illuminated from the side. Good contrast was obtained by placing this wire across the narrow slit in the dull-black-paper box shown at L, figure 1, and illuminating the wire from a point to the side and slightly below the slit. This measuring system permitted measurement of the double amplitude to ± 0.001 in.

The amplitude of vibration of the carriage is changed by changing the magnitude of the eccentric J, in disk, B. This is done either by bolting a single mass of suitable size through a hole in the disk or by bolting a pair of equal masses, M, through a pair of holes in the disk. The effective unbalanced mass, m, of such a pair of masses depends on the angle, θ, subtended by them at the center of the disk and is given by

$$m = 2M \cos\frac{\theta}{2}. \qquad (2)$$

The bearing in disk B is lubricated with light spindle oil applied to the felt washers at the ends of the disk bearing before each calibration run. Large accelerations at high speeds must not be applied to the carriage, A, for too long a period, as they may overheat the bearing, with resulting permanent damage to the close fit of the bearing.

The building up of excessive amplitudes at resonance is avoided either by holding the carriage by hand at the resonant speed or by passing quickly through the resonant speed.

A continuous calibration as a function of frequency is obtained conveniently by recording the accelerometer output on an oscillograph equipped with a time trace. The output of the accelerometer being calibrated is recorded as the shaking table is allowed to coast down from an initial frequency, S_0, and double amplitude, D_0. In this case, the frequency, S, while coasting, is obtained directly from the record, whereas the corresponding double amplitude D is computed from

$$D = D_0\frac{1 - S_r^2/S_0^2}{1 - S_r^2/S^2}, \qquad (3)$$

where S_r is the resonant speed of the table. The peak acceleration at any speed, S, is then computed by substituting S and D in eq. 1.

2. Range

The double amplitudes obtained during calibration of various instruments with the table are given in figure 3 for each of the four sets of flexure plates and for two or three effective eccentric weights, m, in each case. It will be noted that the amplitude with a given set of flexure plates is not exactly proportional to the eccentric weight, m, used. The reason for this is that the basic weight of 1.2 lb of the table is substantially increased by the masses, m. The increase is greater when a pair of equal masses, M (eq 2), is used to give the effective mass, m, than when a single mass is used. The effective eccentric weight used for a given double amplitude varied also with the weight of the instrument being calibrated and with the frequency. The largest double amplitude obtained was 0.44 in., figure 3,a; the highest frequency was 117 c/s, figure 3,c.

The curves of double amplitude versus frequency in figure 3 were converted into the curves of peak acceleration versus frequency, figure 4, by substitution in eq 1. The largest acceleration obtained was 81 g, figure 4,b.

A typical record of acceleration of the carriage as a function of time, obtained with a Statham accelerometer, is shown in figure 5,a, and with an NBS vacuum-tube accelerometer,[1] is shown in figure 5,b. It is evident that the curve of acceleration versus time is nearly sinusoidal.

The acceleration-time curves were practically sinusoidal for all test points shown in figures 3

[1] Walter Ramberg, J. Research NBS **37**, 391 (1946) RP1754.

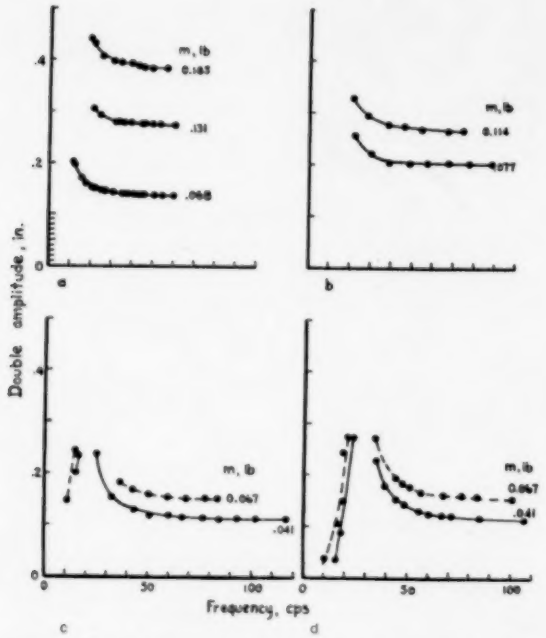

FIGURE 3. *Displacement amplitude vs. frequency for sinusoidal shaking table* (m = *effective eccentric weight*).

a, 0.030-in. flexure plates; b, 0.037-in. flexure plates; c, 0.053-in. flexure plates; d, 0.064-in. flexure plates.

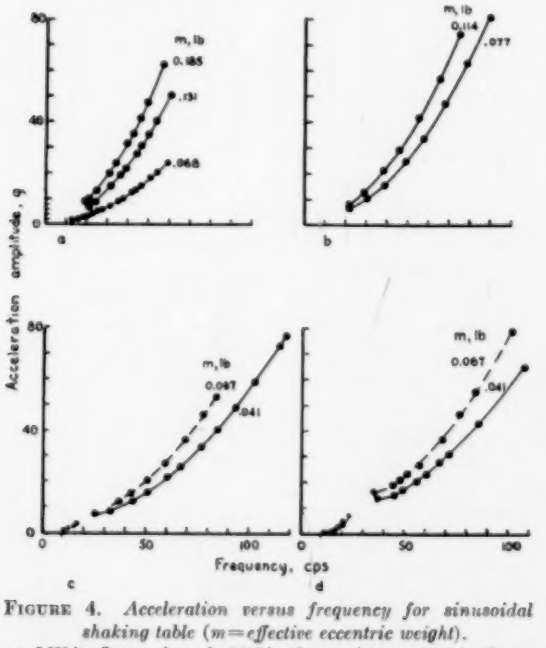

FIGURE 4. *Acceleration versus frequency for sinusoidal shaking table* (m = *effective eccentric weight*).

a, 0.030-in. flexure plates; b, 0.037-in. flexure plates; c, 0.053-in. flexure plates; d, 0.064-in. flexure plates.

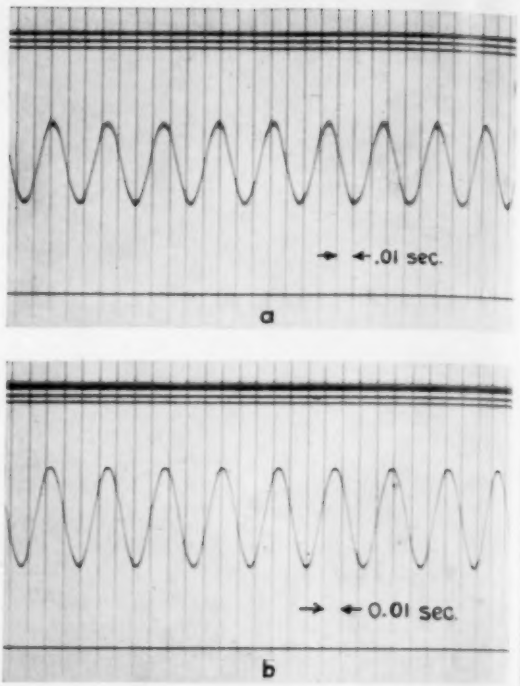

FIGURE 5. *Typical records from accelerometers on sinusoidal shaking table.*

a, Statham accelerometer, frequency 31 c/s, acceleration amplitude 5.6 g. b, NBS vacuum-tube acceleration pickup, frequency 31 c/s, acceleration amplitude 6.2 g.

and 4. It was concluded that the shaking table was capable of applying sinusoidal accelerations to accelerometers weighing up to 0.5 lb over a band of frequencies between 20 and 110 c/s.

III. Portable Calibrator of "Pulse" Type

The portable calibrator of the "pulse" type was designed for use in the field, where it might be necessary to determine the calibration factor for an accelerometer and its associated electrical circuits just before or after a test. A single spring-mass combination is sometimes used for this purpose; however, it has the disadvantage of subjecting the instrument to a suddenly applied acceleration, which tends to produce resonant response in the instrument and thus prevents it from indicating satisfactorily. In the portable calibrator of the pulse type, the acceleration increases gradually from zero to its maximum value.

The calibrator, figure 6, is essentially a three-mass system consisting of a relatively heavy mass, M_1, and two relatively light masses, M_2 and M_3.

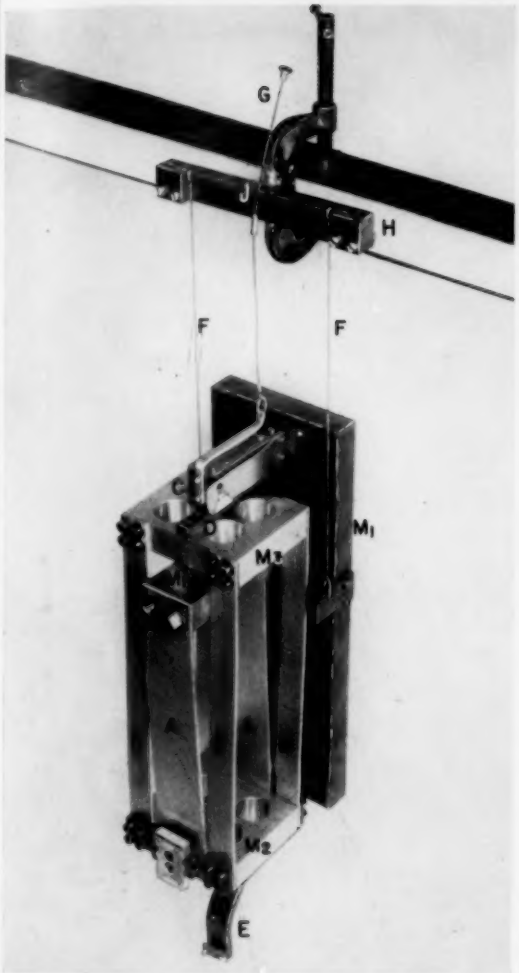

FIGURE 6. *Portable calibrator of "pulse" type for high-frequency accelerometer.*

The light mass, M_2, is flexibly supported by mass M_1, and mass M_3 is flexibly supported from M_2. The acceleration pickups are attached to mass M_2. They are subjected to a definite pulse of acceleration, rising smoothly from zero when mass M_3 is suddenly released from a deflected position.

The three masses are connected by double flexure plates A and B. Double, rather than single, flexure plates are used, since they prevent rotation of mass M_2, thereby subjecting all accelerometers on M_2 to the same pulse of acceleration. The position of M_3 relative to M_1, before release, is controlled by the point of engagement of the pawl, C, with the seven-position ratchet, D. The cable support, E, is provided to secure all except the last few inches of accelerometer cable to the heavy mass, M_1. The whole calibrator is suspended on the wires, F, which provide an effective shock mount with negligible damping.

Mass M_3 is released by drawing the pawl, C, with the release wire, G, which is guided to minimize its effect on the motion immediately after release.

An assembly drawing of the calibrator is given in figure 7. The calibrator was originally built for the calibration of vacuum-tube acceleration pickups (see footnote 1), and it is equipped with special clamps for mounting the unmounted pickups on mass M_2. It has an additional mounting table, figure 7, part 25, for attaching other pickups.

In assembling the calibrator, all bolts are tightened as much as possible to reduce mechanical damping to a minimum and to insure that no joint will lift clear during vibration, thus causing nonlinear behavior.

Distance A, figure 7, is chosen so that the release pawl engages the lowest tooth on the ratchet when the calibrator is hanging vertically and the springs are not bent. This distance is about 3.0 in.

Distance B, figure 7, is chosen so that the release pawl fully engages the highest tooth on the ratchet when the flexure springs, part 14, are not bent. This distance is about 3.3 in.

Distance C, figure 7, is chosen so that the hole in the trigger lock, part 15, engages a No. 6–32 filister-head screw in the side of the upper trigger block, part 13, in such a way as to hold the pawl out of contact with the ratchet during vibration of the calibrator. A thin piece of rubber is placed between the trigger lock and the upper trigger block to cushion the closing of the lock and thus prevent the setting up of undesirable high-frequency vibrations. The offset distance, C, between the center of the hole in the trigger lock and the center of the filister-head screw in the upper trigger block is about 0.1 in. when the pawl engages the lowest tooth of the ratchet.

Distance D, figure 7, is chosen so that the base of the calibrator hangs vertically from the support wires when the release pawl engages the lowest tooth of the ratchet. This distance is about 0.5 in.

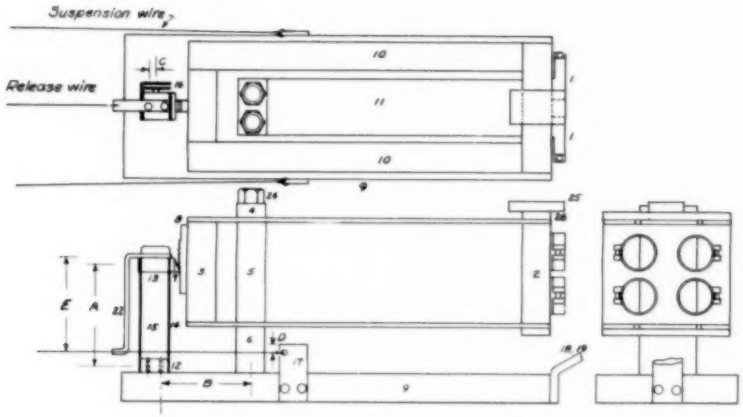

FIGURE 7. *Assembly sheet, pulse calibrator.*
Part numbers refer to shop detail drawings (detail drawings available from National Bureau of Standards).

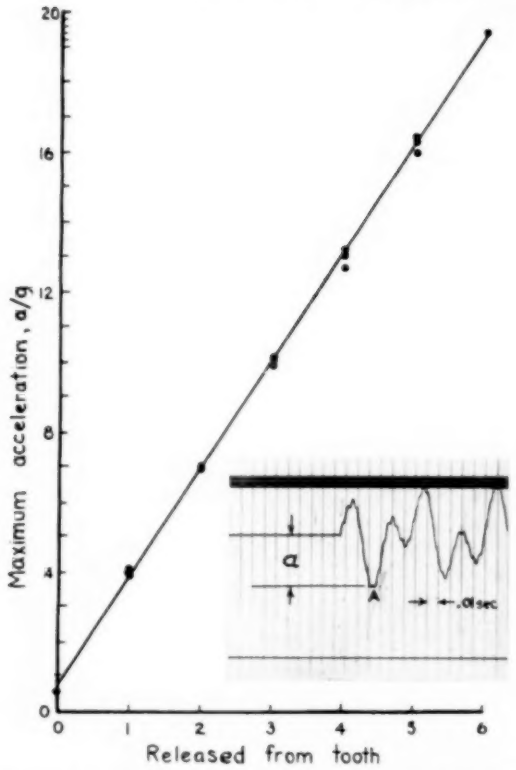

FIGURE 8. *Calibration of pulse-type calibrator using vacuum-tube accelerometer.*

Distance E, figure 7, is chosen so that the line of action of the trigger release wire is in the same plane as the support wires. This distance is about 3.1 in.

1. Operation

A convenient method of using the pulse calibrator is as follows.

Attach support bracket H, figure 6, to edge of table by means of the C-clamp and suspend calibrator by inserting bar J in the bracket as shown. After checking that the calibrator hangs vertically and clear of obstructions, it is removed from the support bracket so that the accelerometers may be more readily attached to mass M_2. Any cable connections to the accelerometers are attached to the clamp, E, figure 6, about 6 in. from the instrument. The calibrator is again suspended and "cocked" to the desired notch. When the calibrator has come to rest, the pulse can be initiated by means of the trigger wire, G.

A typical acceleration-time curve for the calibrator is shown in the insert in figure 8. Most of the acceleration is produced by vibration of the calibrator in its two principal flexural modes at frequencies of about 12 and 30 c/s. In addition, there is a small superimposed acceleration at about 250 c/s due to vibration of the springs in their fundamental mode as bars clamped at their ends in the masses, M_1, M_2, and M_3.

The nominal pulse of acceleration is taken as that produced by the two low-frequency modes only. It is obtained from the trace of acceleration versus time by fairing a curve through the mean points of the high-frequency oscillation. It was decided to remove the high-frequency component in this manner as the calibrator is designed primarily to check accelerometers, which should

record accelerations with a frequency up to 100 cycles per second but need not record accelerations with a frequency as high as 250 c/s.

The second peak of the acceleration-time curve (A, fig. 8 insert) is taken as the calibrating acceleration. Calculation of the motion of M_2 on the assumption that M_1 is much larger than M_2 or M_3, and that the spring joining M_1 and M_2 has the same stiffness, k, as the spring joining M_2 and M_3, shows that the acceleration of M_2 is given by

$$a=d\frac{k}{\sqrt{4M_3^2+M_2^2}}(\cos At-\cos Bt), \qquad (4)$$

where

a = acceleration of M_2

d = initial deflection of M_3

$$A^2=\frac{k}{2M_2M_3}(M_2+2M_3)+\sqrt{M_2^2+4M_3^2}$$

$$B^2=\frac{k}{2M_2M_3}(M_2+2M_3)-\sqrt{M_2^2+4M_3^2}.$$

When M_2 and M_3 are nearly equal, eq 4 shows that for the second peak, the phase relation of the two principal modes is such that a small change in the mass of M_2, corresponding to a change in the mass of the instrument being calibrated, causes a change in the peak acceleration, which can usually be neglected.

2. Calibration of Calibrator

The acceleration of M_2 at the second peak in the acceleration-time curve for release from a given tooth on the trigger ratchet may be determined with a vacuum-tube accelerometer (see footnote 1) as a secondary standard, using the following procedure:

1. The accelerometer is subjected to a 1-g change in acceleration by attaching it to a heavy mass, which is then suddenly released. The output for three consecutive releases of the heavy mass is recorded.

2. Using the same recording equipment, the accelerometer is then moved to the calibrator, and the output for release from each of the ratchet teeth is recorded.

3. Step 1 is repeated.

4. The acceleration of M_2 at the second peak in the acceleration-time curve, for release from a given tooth on the trigger ratchet, is determined on the assumption that the accelerometer output increases linearly with the applied acceleration and that the output per gram is the average of the six readings obtained in steps 1 and 3.

Three calibrations of a calibrator were made by using this procedure. The observed accelerations are shown as points in figure 8, together with a line faired through the points. Only two of the 21 measured points differ from this line by more than 0.2 g. The line indicates a maximum acceleration, corresponding to release from tooth 6, of 19.5 g and a minimum acceleration, for release from tooth 0, of 0.8 g.

The change in maximum acceleration applied by the calibrator, due to a change in the weight of the instrument being calibrated, was measured for the calibrator used above by successively adding 0.1-, 0.3-, and 0.5-lb weights to M_2 and repeating the calibrations as before. These calibrations were carried out only for release from tooth 2 and tooth 5 of the ratchet. The results are shown in figure 9

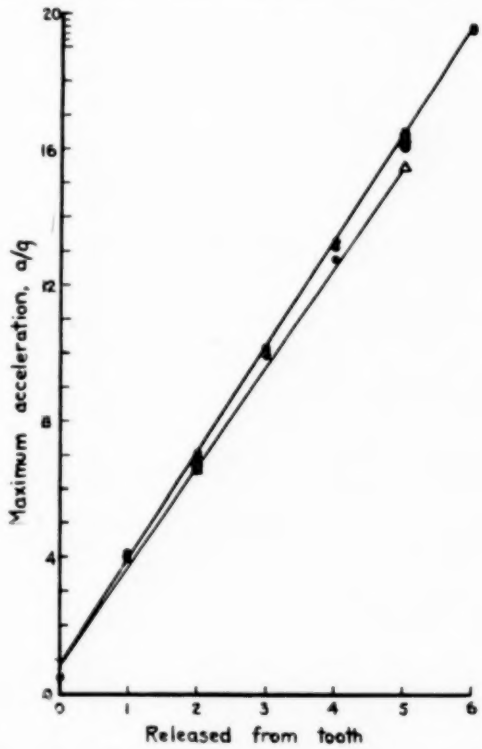

FIGURE 9. *Effect of added weight on output of pulse calibrator.*

Added weight in pounds—●, 0; ○, 0.1; □, 0.3; △, 0.5

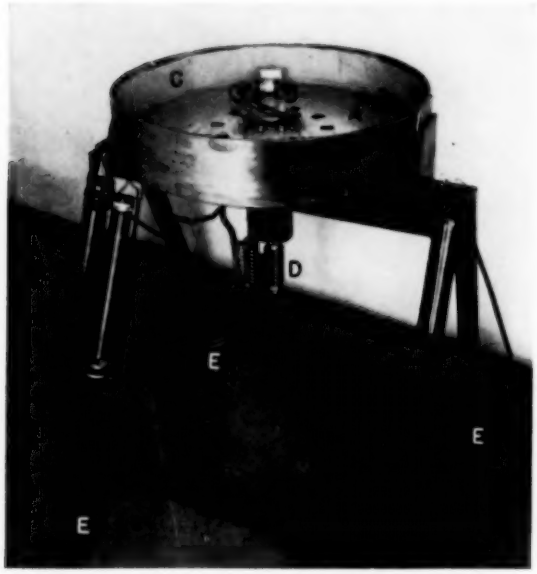

FIGURE 10. *Centrifuge for calibration of accelerometers.*

together with points taken from figure 8. The addition of weight to M_2 caused a decrease in maximum acceleration of the order of 1 percent per 0.1 lb of added weight.

It may be concluded that the portable calibrator of the pulse type may be used in the field for calibration of accelerometers weighing 0.5 lb or less, with a flat response up to at least 30 c/s and with a range up to about 20 g.

IV. Centrifuge

The centrifuge was designed for use in the laboratory to give an accurate measure of the calibration factor and to check the linearity between applied acceleration and response up to high sustained accelerations. The centrifuge is shown in figure 10. It consists of a horizontal disk, A, which is rigidly attached to a vertical spindle mounted on preloaded ball bearings. The assembly of the spindle is made clear by the sectioned drawing in figure 11.

The spindle is driven with a ½-in. V-belt connected to a ¼-hp. variable-speed motor (not visible in figure 11). The accelerometer is fastened to disk A at B. Electrical connection to the accelerometer is made through the slip rings, D. Dynamic balance is maintained by fastening a balance weight an equal distance from the axis of the table opposite B. Protection against rupture during test is provided by surrounding disk A with a guard ring, C, which is lined with oil-base modeling clay.

The centrifuge is mounted on sponge rubber pads, E, to give it a low critical speed, about 5 rps. Disk A will then rotate about its own center of gravity at the operating speeds, well above the critical speed, regardless of deviation from perfect balance.

The table was designed for operation at speeds up to 30 rps. This corresponds to a centripetal acceleration up to 1,000 g at the periphery of of disk A. With suitable attachments, accelerometers weighing 1 lb may be accommodated.

The ball bearings used are Ford part No. B–7065. In assembling the spindle, the bearings are preloaded to the point of slightly restricted rotation by shimming between the inner race of the bearing and the shoulder on the spindle or between the outer race of the bearing and the shoulder on the housing. The bearings must be entirely clean of abrasive matter and lightly oiled.

The slip rings are made of copper, and their brushes are made of copper-graphite, National 543. Both must be kept clean and dry. No lubricant is used on the slip rings.

1. Operation

The accelerometer to be calibrated is attached to disk A, and a counterweight of equal mass is attached diametrically opposite and equidistant from the center of the spindle.

The acceleration is computed from the formula,

$$a = 14.2\, g \left(\frac{S}{1{,}000}\right)^2 D, \tag{5}$$

where

a = acceleration.
g = acceleration of gravity.
S = speed in revolutions per minute.
D = diameter, in inches, of circle traversed by the center of gravity of the active element of the accelerometer.

The speed of rotation of disk A is measured with a stroboscopic tachometer. It was found helpful to place 10 marks on disk A, spaced at equal intervals around the disk. Nine all-black marks and one black with a white line through it

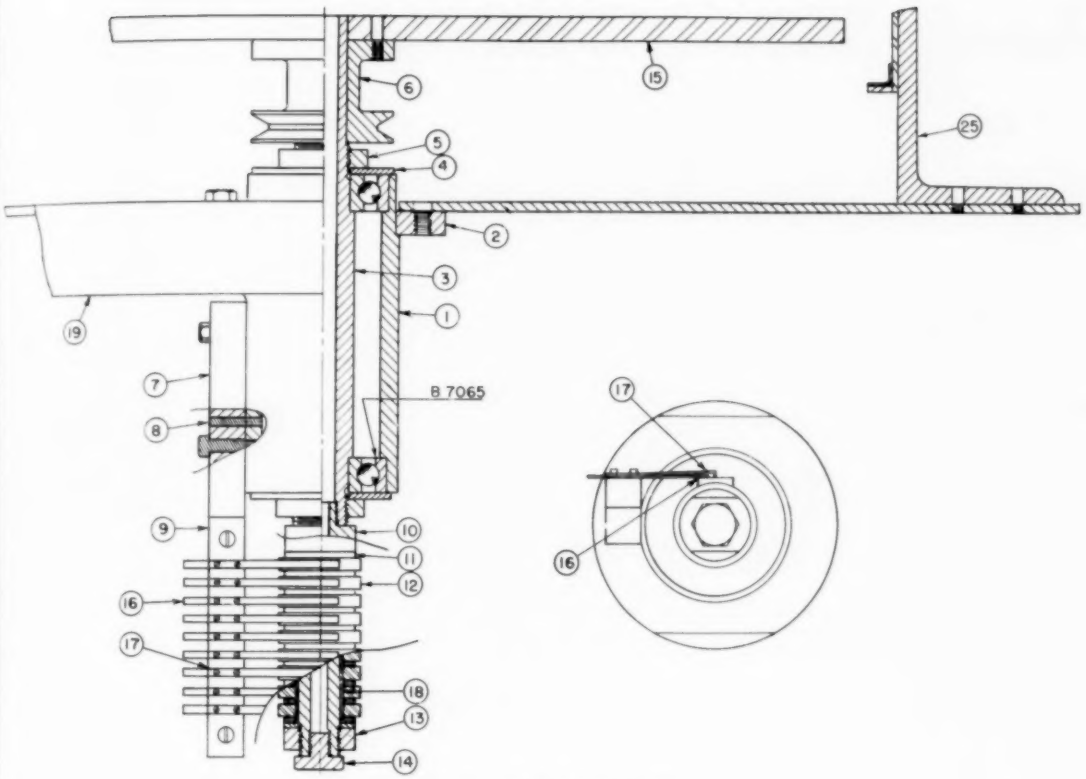

FIGURE 11. *Centrifuge assembly.*
Part numbers refer to shop detail drawings (detail drawings available from National Bureau of Standards upon request).

aided in making accurate measurements of the speed of rotation of disk A.

V. Comparison of Results

The performance of the pulse-type calibrator was compared with that of the sinusoidal shaking table by calibrating the accelerometers, A and B, figure 12, on both devices.

Accelerometer A is an accelerometer of the vacuum-tube type described in the reference given in footnote 1. It is undamped and has a natural frequency of about 800 cycles per second. Accelerometer B is a Statham accelerometer. It is damped and has a natural frequency of about 450 cycles per second.

The circuits used in each test and the results of the calibration are given in figure 13 for the vacuum-tube accelerometer and in figure 14 for the Statham accelerometer. Inspection of these figures shows that the measured accelerations

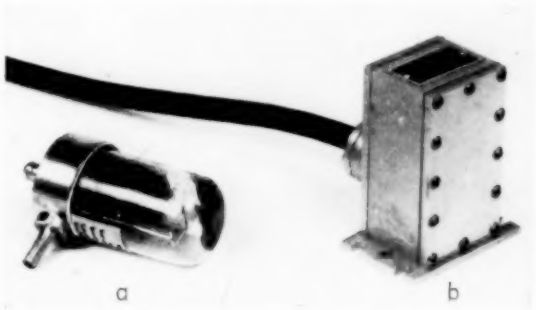

FIGURE 12. *Accelerometers.*
a, NBS vacuum-tube accelerometer; b, Statham 12-g accelerometer.

differed less than ± 0.5 g from a common straight line faired through the points.

1. Check of Calibration Methods

The procedure for calibrating under steady acceleration on the centrifuge was checked by comparing the recorded output for a vacuum-

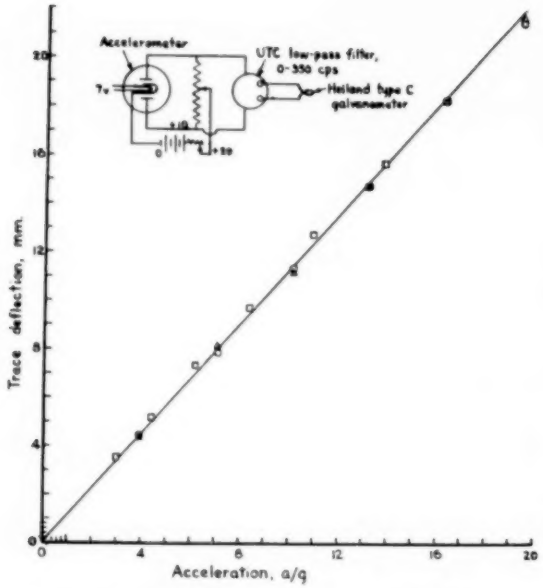

FIGURE 13. *Calibration of vacuum-tube accelerometer.*
○, Pulse (first calibration); □, shaking table (second calibration) △, pulse (third calibration).

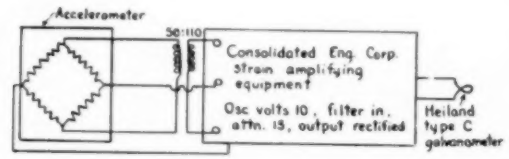
Accelerometer
Consolidated Eng. Corp. strain amplifying equipment
Osc volts 10, filter in, attn. 15, output rectified
Heiland type C galvanometer

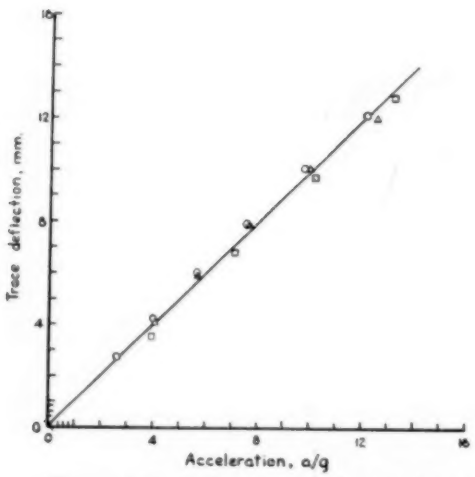

FIGURE 14. *Calibration of Statham accelerometer.*
○, shaking table (first calibration); □, pulse (second calibration); △, shaking table (third calibration).

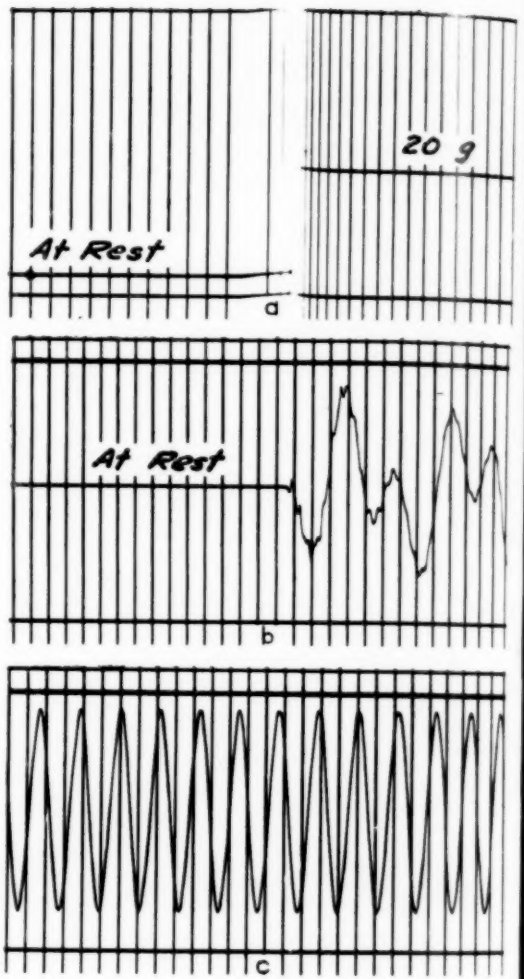

FIGURE 15. *Galvanometer records.*
a, Centrifuge, 20 *g*, 0.805 mm/g; b, pulse calibrator, 19.2 *g*, 0.788 mm/g; sinusoidal calibrator, 19.3 *g*, 0.784 mm/g.

tube accelerometer subjected to about 20 *g* on the centrifuge with that obtained on the shaking table and on the pulse-type calibrator. The output was measured with an electric circuit [2] by using a recorder with a galvanometer of 300 c/s natural frequency. The records are reproduced in figure 15. It may be seen that the output for 1 *g* deviated less than 2 percent from the average value for the three methods.

[2] Shown in figure 4 of "The measurement of acceleration with a vacuum tube," AIEE Transactions **66** (1947) by Walter Ramberg.

VI. Conclusions

The sinusoidal calibrator may be used to calibrate accelerometers weighing up to 0.5 lb, over a band of frequencies between 20 and 110 c/s. Amplitudes up to 0.4 in. may be applied at the low end of the frequency band. Accelerations up to 80 g may be applied at the high end.

The portable calibrator of the pulse type may be used to check accelerometers with a weight up to 0.5 lb for recording accelerations with a frequency up to at least 30 c/s. The calibrator applies to the accelerometer a known pulse of acceleration with a peak value that may be adjusted in six steps between about 1 and 20 g.

The centrifuge may be used to calibrate accelerometers weighing up to 1 lb with steady acceleration up to 1,000 g.

Acknowledgment is due the Bureau of Aeronautics, Navy Department, whose research projects on acceleration pick-ups have provided the impetus and the necessary financial support for the work presented in this paper. The authors take this opportunity to acknowledge also the assistance of members of the Engineering Mechanics Section of the National Bureau of Standards.

WASHINGTON, May 10, 1948.

U. S. Department of Commerce
National Bureau of Standards

Research Paper RP1931
Volume 41, November 1948

Part of the Journal of Research of the National Bureau of Standards

Studies of the Mattson Shot Classifier

By Raymond L. Blaine and Harold J. Valis

The size and distribution of peening and cleaning shot and sand particles of various shape characteristics were determined by use of a new apparatus and with a microscope and by microweighings. Tests indicated that the Mattson apparatus enabled a rapid visual evaluation to be made of size and distribution of shot and sand particles. A more precise evaluation can be made with the apparatus by determining the actual size distribution of the shot or other particles. This apparatus tends to determine the smallest dimension of particles that are irregular in shape and, when used with closely sized sieve fractions, makes possible an evaluation of the shape characteristics of the particles.

I. Introduction

In shot-peening, the energy with which the shot strikes the metal being treated must be carefully controlled. It is necessary to have the shot of uniform size, since differences in size or mass of the individual shot cause difficulties in regulating the intensities with which the shot strikes the metal part and unevenness in the peening operation.

The determination of particle size and the size distribution of materials have long been made with the aid of screens or sieves. When the sample contains a fairly wide range of sizes, the use of a series of closely sized sieves makes possible the determination of the size distribution of particles. However, when the particles are of nearly the same size, as with the peening shot, the information obtained from a series of sieves is inadequate to determine the size distribution. Another factor that is often important in measurements of granular materials is that of the shape of the particle. Some specifications (as for example ASTM D693–44, D694–44, D–556–40T, D557–40T, and D692–42T) require certain particle shape characteristics but do not offer adequate apparatus or methods for evaluating this shape factor.

R. L. Mattson of General Motors Research Laboratory has developed an apparatus for rapidly determining the size and size distribution of peening shot. Although the apparatus offered a very rapid visual evaluation of both the size and distribution, information was desired as to the precision of the apparatus and the significance of the results. The simplicity of the apparatus and the principle on which it is based have suggested the possibility of its use for materials other than the peening and cleaning shot for which it was designed.

II. Description of Apparatus

The Mattson apparatus (see fig. 1) consists essentially of two plane sheets of glass separated at the two vertical edges by accurately ground metal wedges. Particles dropped into the space between the glass plates lodge at a point where the effective diameter of the particle and the distance between the plates are the same. An additional feature of the apparatus is a sample splitter, which is needed to reduce the sample to a suitable size.

The apparatus used in these studies consisted of 8- by 10-in. glass plates. The back plate was ½ in. thick and reported by the manufacturer to be plane within 0.0005 in. The front plate was made of 3/16-in. plate glass. The ground metal wedges, cemented to the front plate and separating the plates, were tapered at 0.010 cm/cm. The space between the plates was 0.25 mm at the bottom of the scale and 2.00 mm at the top, corresponding to the nominal openings of the No. 60 and the No. 10 sieves,[1] respectively.

In order to remove the sample, a special cam arrangement was provided to separate the plates after the test. The spacings between the plates were indicated by a scale consisting of ruled hori-

[1] Federal Specification RR-S-366a.

FIGURE 1. *Mattson apparatus for determining size and distribution of peening shot.*

zontal lines on the front plate. However, for these tests, an auxiliary transparent plate, ruled every 2 mm, was attached to the front plate of the apparatus. The back plate was held against the wedges by springs.

The sample splitter consisted of a tilting table from which half of the sample could be removed into a container behind the apparatus. The sample can be halved as many times as necessary to obtain the required amount of material. Tilting the table forward prepared the remaining sample for the next division or for dropping the grains into the wedge-shaped space of the apparatus.

III. Materials

The samples of peening and cleaning shot that were furnished by the General Motors Corporation consisted of spherical iron particles of sizes commonly used in peening and metal-cleaning operations.

The three sands used in this study were chosen on the basis of their shape characteristics. The sands were separated by sieves, and the portion passing a No. 20 and retained on a No. 30 sieve was used. The Ottawa sand was that commonly used in testing portland cement (Federal Specification SS–C–158b). The river sand consisted of particles that had been worn smooth but were not as equidimensional as the Ottawa sand. The crushed limestone particles were angular and somewhat flaky.

IV. Scope

In order to determine the characteristics of the Mattson apparatus, measurements were made of the apparent diameter of individual peening shot and sand particles, the reproducibility of results obtained in retesting the same particles, the effect of the size of sample on particle interference, and the effectiveness of the sample splitter. The apparatus was used for size measurements of a number of samples of peening and cleaning shot. Microscopic measurements were made, and weights were determined of individual particles in order to compare the diameter values determined by different methods. Tests were made by means of the Mattson apparatus on samples of two sands and a crushed limestone passing a No. 20 and retained on a No. 30 screen in order to evaluate the shape factor of these materials.

V. Tests and Test Results

1. Measurements of Individual Particles

(a) Mattson Apparatus

Measurements were made to the nearest ½ mm of the position of individual particles dropped into the apparatus a number of times. From the position in the apparatus, the apparent or effective diameter of the peening shot or sand particle was determined to the nearest 0.005 mm. Twenty separate determinations were made on each of the 12 peening shot and 8 sand grains illustrated in figure 2.

(b) Microscopic Measurements

Microscopic measurements were also made of the maximum and minimum diameters of the particles. Each particle was shifted with a probe after each pair of measurements. The maximum and minimum values of the series of 10 measurements on each particle are reported.

(c) Microweighings

The weights of the individual particles were determined by means of a microbalance and were reported to 0.001 mg. The calculated diameters (assuming a spherical shape) are based on the specific gravity of larger quantities of materials determined by a picnometer method. The results of measurements and calculations are presented in table 1.

TABLE 1. *Diameters of individual particles as determined by the Mattson apparatus, microscope, and as calculated from the weights*

Identification	Mattson apparatus					Microscope [2]		Diameter calculated from weight
	Average diameter	Maximum diameter	Minimum diameter	Standard deviation	Coefficient of variation [1]	Maximum diameter	Minimum diameter [2]	
	mm	*mm*	*mm*	*mm*	*%*	*mm*	*mm*	*mm*
P46 1	1.314	1.335	1.295	0.0134	1.0	1.314	1.398	1.316
2	1.312	1.325	1.295	.0078	0.6	1.305	1.280	1.307
3	1.222	1.375	1.100	.0466	3.8	1.377	1.245	1.284
4	1.261	1.340	1.235	.0226	1.8	1.335	1.242	1.275
5	1.208	1.310	1.180	.0292	2.4	1.624	1.272	1.359
P28 1	0.776	0.800	0.755	.0124	1.6	0.837	0.734	0.796
2	.836	.860	.815	.0134	1.6	.873	.843	.845
3	.746	.765	.735	.0109	1.5	.785	.748	.766
4	.815	.830	.795	.0097	1.2	.835	.818	.825
5	.852	.860	.835	.0071	0.8	.898	.852	.861
P19 1	.530	.550	.515	.0109	2.1	.555	.549	.553
2	.518	.540	.500	.0087	1.7	.615	.570	.578
SS 1	.707	.770	.650	.0489	6.9	.940	.660	.773
2	.725	.735	.715	.0062	0.9	.960	.878	.861
3	.732	.760	.720	.0136	1.9	.895	.773	.787
RS 1	.992	1.160	.975	.0400	4.0	1.520	1.067	1.129
2	.954	1.340	.920	.0909	9.5	1.800	1.295	1.220
3	1.121	1.135	1.105	.0071	0.6	2.095	1.109	1.357
4	1.004	1.070	0.960	.0162	1.6	2.280	1.248	1.276
5	0.846	0.855	.840	.0043	0.5	1.360	1.128	1.029

[1] Based on 20 measurements of each particle.

[2] Based on 10 measurements of each particle.

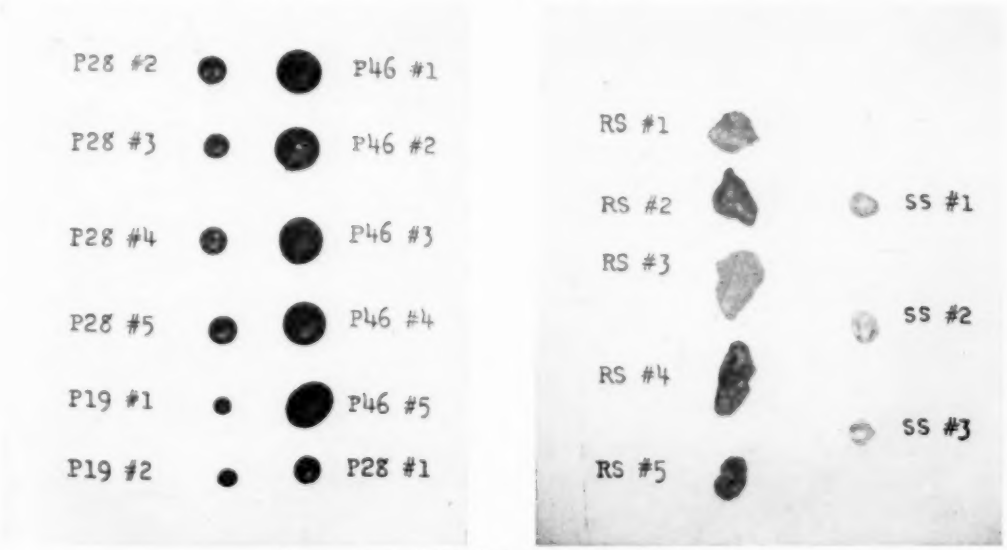

FIGURE 2. *Individual shot and sand particles.*

2. Repeated Tests on Same Materials

(a) Peening Shot

Approximately 90 P46 peening shot were separated from a larger sample with the sample splitter. The shot were then dropped into the wedge-shaped space and measurements made to the nearest ½ mm of the positions of the individual particles. The shot were recovered and the test repeated a total of 10 times. The average diameter ($\Sigma nd/\Sigma n$) and the number of shot smaller than or larger than certain arbitrary sizes were determined for each set of measurements and are presented in table 2.

TABLE 2. *Repeated tests on the same sample of 90 P46 shot*

	Average diameter	Number of shot larger than—			Number of shot smaller than—		
		1.350 mm	1.325 mm	1.300 mm	1.175 mm	1.200 mm	1.225 mm
	mm						
	1.270	4	14	27	1	13	18
	1.268	7	17	31	0	8	18
	1.267	3	14	27	1	16	23
	1.266	4	15	25	1	16	22
	1.262	4	13	21	1	14	21
	1.274	5	18	30	1	9	19
	1.266	6	12	24	3	14	23
	1.266	5	13	30	1	10	20
	1.267	3	16	28	1	17	26
	1.264	5	12	27	1	17	24
Average	1.267	4.6	14.4	27	1.1	13.4	21.4
Standard deviation	0.0033	1.3	2.1	3.1	0.54	3.3	2.7
Coefficient of variation (%)	.3	28	15	11	49	25	13

(b) Ottowa Sand

A similar series of tests was made on a sample of the Ottawa sand. A 20-g sample was split seven times, and the particle-size distribution was determined. The test was repeated a total of 10 times, a new sample being used for each test. The average diameter and number of particles larger and smaller than certain arbitrary diameters are presented in table 3.

3. Interference of Particles

Tests were made to study the possible interference of particles with each other in dropping to their positions in the wedge. Fifty-gram samples of P46 shot were split four, five, six, and seven times, giving a considerable range in the number of particles measured in the different tests. The particle-size distribution was determined as in previous tests. Each of the values presented in table 4 is the average of two determinations.

TABLE 3. *Ten samples of 20 g of Standard Ottawa sand (20 to 30 mesh), split 7 times*

	Average diameter	Number of particles	Number of particles greater than—		Number of particles smaller than—	
			0.750 mm	0.650 mm	0.450 mm	0.550 mm
	mm					
	0.643	261	24	130	3	33
	.644	265	27	130	1	33
	.643	243	17	116	2	22
	.641	237	27	113	4	37
	.638	248	22	111	2	32
	.647	223	21	112	1	29
	.644	239	21	119	2	30
	.639	241	26	108	5	31
	.640	256	25	121	4	42
	.642	245	16	124	3	31
Average	.642	246	22.6	118	2.7	32
Standard deviation	.003	11.5	3.9	7.8	1.3	5.2
Coefficient of variation (%)	.4	4.7	17	7	48	16

TABLE 4. *Effect of size of sample on average effective diameter of shot*

Number of times sample was split	Number of particles	Average diameter	Difference from grand average
		mm	*mm*
4	373	1.280	+0.006
5	190	1.271	−.003
6	114	1.267	−.007
7	50	1.280	+.006

4. Tests of Peening and Cleaning Shot

The particle-size distribution of a number of samples of peening and cleaning shot of a number of grades was determined. The size distributions are presented in figure 3. The various statistical diameters computed from the size-distribution values are presented in table 5, together with the diameters computed from the weight of lots of 1,000 shot, assuming spherical shape.

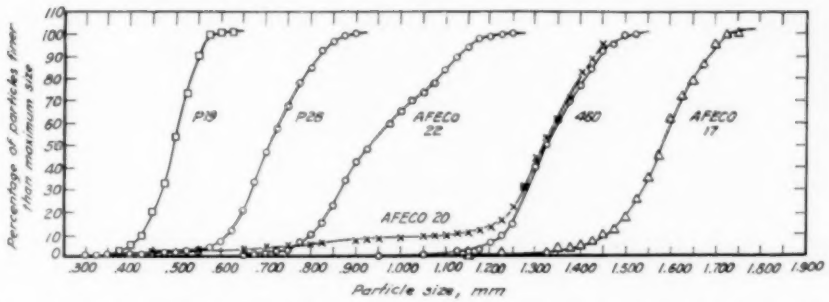

FIGURE 3. *Percentage of particles of different samples of peening and cleaning shot finer than given sizes.*

Determinations made by means of Mattson apparatus.

TABLE 5. *Shape factor and diameter of peening shot as calculated by various formulas*

Identification	Specific gravity	Average diameter from weight	$^1d_{ao}$	^2d_s	^3d_s	^4d_w	Shape factor [5]
	g/ml	*mm*	*mm*	*mm*	*mm*	*mm*	
P28	7.54	0.776	0.714	0.723	0.740	0.740	0.604
P46	7.48	1.308	1.307	1.242	1.274	1.279	.567
No. 460	7.11	1.348	1.375	1.301	1.338	1.345	.534
No. 20	7.16	1.350	1.274	1.305	1.309	1.323	.576
No. 22	7.56	1.005	0.952	0.969	0.970	1.002	.582
No. 19	7.46	0.555	.482	.488	.488	0.499	.766
No. 17	7.53	1.615	1.574	1.597	1.545	1.732	.600

[1] $d_{ao}=\Sigma nd/\Sigma n$.
[2] $d_s=\Sigma nd^2/\Sigma nd$.
[3] $d_s=\sqrt{\Sigma nd^3/\Sigma n}$.
[4] $d_w=\Sigma nd^4/\Sigma nd^3$.
[5] Shape factor $=1/\rho N d_s^3$.

n = number of particles per group.
d = mean of limits of group.
ρ = specific gravity, g/ml.
N = number of particles per gram.

5. Shape Factor

Tests were made of the apparent size-frequency distribution of materials of different shape factors. The P28 shot, Ottawa sand, river sand, and crushed limestone all passed the No. 20 sieve (0.84 mm) and were retained on the No. 30 sieve (0.59 mm). Of these materials, the peening shot were most nearly spherical; the Ottawa sand was rather rough but fairly well rounded. The river sand had some rather flat, semirounded particles, whereas the crushed limestone had sharp edges and corners and was composed mostly of flat particles. The size-frequency distribution curves are presented in figure 4, and the various statistical diameters are presented in table 6.

TABLE 6. *Shape factors and diameter of particles as calculated by various formulas*

Identification	Specific gravity	Average diameter calculated from weight	$^1d_{ao}$	d_s	d_s	d_w	Shape factor
	g/ml	*mm*	*mm*	*mm*	*mm*	*mm*	
P28 shot	7.54	0.776	0.714	0.723	0.740	0.740	0.604
Ottawa sand	2.65	.807	.642	.652	.652	.672	.992
River sand	2.62	.752	.551	.570	.570	.608	1.21
Limestone	2.70	.801	.482	.524	.521	.593	1.90

[1] See table 5 for symbol notation.

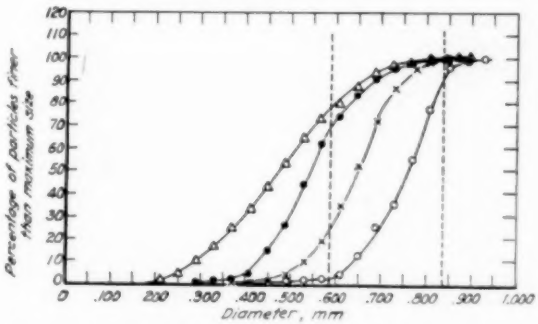

FIGURE 4. *Particle-size distribution as determined by the Mattson apparatus of 20- to 30-mesh shot, Ottawa sand, river sand, and crushed limestone.*

Dashed lines indicate nominal openings of No. 20 and No. 30 sieves. ○, P28 shot; ×, 20 to 30 Ottawa sand; ●, river sand; △, screened limestone, 20 to 30.

6. Sample Splitter

A series of tests were made in which a sample of P46 shot was split six times and tested in the Mattson apparatus. The weight of the final sample was compared with the weight of the sample before splitting. The remaining portion

of the sample from the first test was used for the second test and the remainder from the second, for the third, etc. This process was repeated for 10 successive determinations. The average diameter of the 10 successive determinations, together with the percentage by weight of each sample remaining after splitting six times, is presented in table 7. Other tests were made in which the number of particles remaining after splitting a definite number of times was counted. These also served to indicate the efficiency of the sample splitter. Where the weight was not determined directly, the weight of 1,000 particles was used to compute the average weight per particle, and the weight of the split sample was computed from this value.

TABLE 7. *Average diameter of particles and percentage by weight of particles remaining after splitting six times*

Each test was made on the material remaining after previous tests.

Test number	Average diameter	Percentage by weight of particles remaining after splitting 6 times
	mm	
1	1.271	2.02
2	1.269	1.92
3	1.270	2.02
4	1.265	1.97
5	1.276	1.84
6	1.283	2.10
7	1.261	1.76
8	1.274	1.63
9	1.265	1.61
10	1.265	1.75

VI. Discussion

1. Size of Particles Determined by Different Methods

The shape of the particles measured and the method of measurement usually influence the final results. For example, in microscopic measurements, irregularly shaped or flat particles tend to assume their most stable position when placed on a microscope slide and the two larger of their three dimensions are observed. Repeated measurements made according to the methods of Feret or Martin of the diameter of an irregularly shaped particle adjusted to a new position before each measurement would yield a variety of values with a calculable (statistical) mean and standard deviation. Similarly, individual particles dropped into the wedge-shaped space of the Mattson apparatus do not always exhibit the same effective diameter. It may be noted in table 1 that the standard deviation values of the measured diameters of individual particles were quite large, and

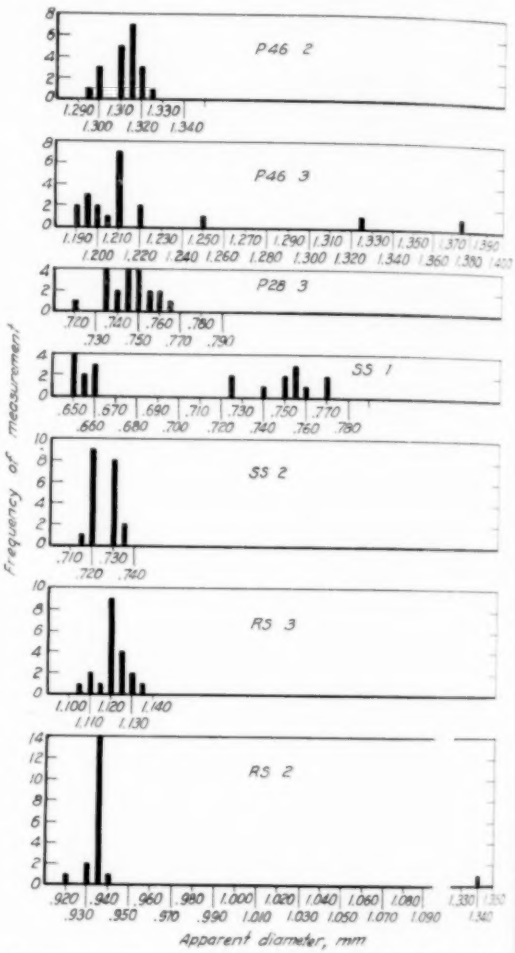

FIGURE 5. *Effective diameter values of individual particles tested 20 times with the Mattson apparatus.*

these values differed for different particles. The nature of these variations may also be noted in figure 5, which shows the measurement-distribution patterns of some typical particles. As may be noted, the patterns range from a rather close distribution diagram as in RS 2, to a skewed distribution as in P46 3, and to a bimodal distribution for SS 1. The average values for the ratio of the

mean microscopic diameter to the average diameter determined by the Mattson apparatus were 1.05, 1.16, and 1.52 for the peening shot, Ottawa sand, and river sand, respectively.

It is considered significant that the coefficient of variation values of the peening shot were approximately the same as the majority of the values for the Ottawa-sand and river-sand particles, which are not so equidimensional. It may be noted in table 1 and figure 6 that the average diameters of the individual particles determined by the Mattson apparatus were usually smaller than those calculated from the microweighings of the individual particles. This was more apparent with the sands than with the peening shot. The average of mean diameters of peening shot as determined by the Mattson apparatus was 96.6 percent of that determined by microweighings, whereas for Ottawa sand the value was 89.6 percent and for river sand, 84.1 percent. The diameter calculated from the microweighings was usually between the maximum- and minimum-diameter values determined by the microscope. However, for the sand particles it was smaller for three of the eight particles measured.

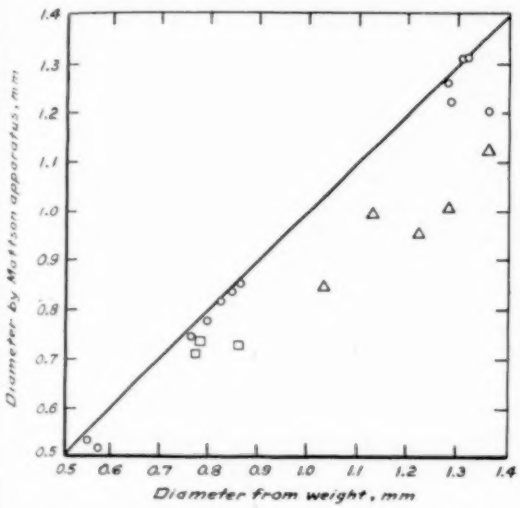

FIGURE 6. *Relation of average diameter as determined by the Mattson apparatus to that determined from microweights of individual particles.*

○, Shot; □, Ottawa sand; △, river sand.

The arithmetic mean diameter of a sample of irregularly shaped particles is not the same as the mean diameter based on volume or weight. Perrott and Kinney,[2] Green,[3] and Dalla Valle [4] have indicated the necessity for giving proper weight to the various sizes in a sample and have presented formulas for calculating the "mean volume diameter" and "weight mean diameter" from the measured diameters. These formulas and the calculated diameters are given in tables 5 and 6.

2. Shape Factors

Dalla Valle (see footnote 4) has shown that a value for the shape of the particles may be calculated from the mean volume diameter, the number of particles per unit weight, and the density, as given in the formula in tables 5 and 6.

The fact that the Mattson apparatus tends to indicate the smaller of three dimensions of flat- or disk-shaped particles makes possible an evaluation of the shape factor of particles when used in conjunction with sieves. The effect of the shape of the particles when testing four different 20- to 30-mesh materials with the Mattson apparatus is evident in figure 4. The factor calculated from the number of particles per gram, the specific gravity, and the average volume diameter, d_v, according to the Dalla Valle formula (see footnote 4), results in values ranging from 0.534 for one sample of shot to 1.90 for the crushed limestone. It has been shown by Martin [5] that this value is less than $\pi/6$, or 0.524, when computed from microscopic measurements. The shape factors of the peening shot were all slightly larger than $\pi/6$, or 0.524, but not as large as the values for Ottawa sand, river sand, or the crushed limestone. Microscopic examination and the measurements listed in table 1 indicated that the shot were not perfect spheres.

3. Variations in Effective Diameter

The variations of the effective diameter of individual particles may be expected to cause variations in the calculated average diameter of groups of particles. The standard-deviation values of the individual P46 shot in table 1 were from 2 to 14 times as great as the value for the group of 90 shot of table 2. For the Ottawa sand,

[2] G. Perrott and S. P. Kinney, J. Am. Ceram. Soc. **6**, 417 (1923).
[3] H. Green, J. Franklin Inst. **204**, 713 (1927).
[4] J. M. Dalla Valle, Micromerities, 2d ed. (Pitman Pub. Co., New York, N. Y., 1943).
[5] Martin, Trans. Brit. Ceram. Soc. **23**, 61 (1923).

the individual values in table 1 were from 2 to 16 times the group values in table 3.

The determination of the size distribution of a large number of particles in a sample is somewhat tedious. The possibility of starting with a definite weight sample, splitting a given number of times, and counting only the number of particles larger or smaller than certain limits was considered as a specification test. The number of particles per group varied more at the ends of the distribution curves than in the center, as indicated by the coefficient of variation values in tables 2 and 3.

4. Variations Due to Sample Splitter

Certain variations also occurred in splitting the sample, as indicated in table 7. Theoretically, 1.56 percent of the particles should remain after splitting six times, but the data in table 7 indicate that as much as 2.10 percent of the particle remained. Other indications of the variations of the sample splitter were obtained from counts of particles of duplicate tests on the same material. The computed weight of the test sample was usually 10 to 20 percent greater than it should have been. This was probably caused by the design or construction of the sample splitter itself and could possibly be remedied by placing the separators symetrically, by increasing the number of separating fins, or by proper placing of baffles.

There was no evidence, however, that any particular size of particles was removed. For example, as shown in table 4, the average diameter determined in any one test does not differ from the grand average by as much as three times the standard deviation, commonly considered significant. The data in this table indicate that a rather wide range of sample size may be used in the calculations of the average diameter. The smaller sample of 50 shot appears to define satisfactorily the average size and is about the minimum required to indicate the type of distribution of a sample of shot. It would be preferable to use a sample of this size in order to reduce the number of measurements.

5. Limitations of Testing Smaller Sizes

The determination of the particle-size distribution of the smaller sizes, such as the P19 shot, was more difficult than with the larger sizes. Even with the use of a reading glass it was difficult to count the particles in any size group when the particles were from 0.25 to 0.50 mm in diameter.

VII. Conclusions

The Mattson apparatus offers a rapid, visual method of determining the size and distribution of closely sized particles, such as peening shot, cleaning shot, and sand. More accurate evaluation of the average size and variations about this average can be made by determining the number of particles of each size grouping. The average diameter values calculated from these distributions are quite reproducible.

The diameter of irregular or flat particles as determined with the Mattson apparatus is a "statistical" diameter that is usually less than that determined by a microscope. This feature enables a determination of the shape factor of particles to be made when the apparatus is used with closely sized sieve fractions.

Washington, June 3, 1948.

U.S. Department of Commerce
National Bureau of Standards

Research Paper RP1932
Volume 41, November 1948

Part of the Journal of Research of the National Bureau of Standards

Compilation of Thermal Properties of Hydrogen in Its Various Isotopic and Ortho-Para Modifications

By Harold W. Woolley, Russell B. Scott, and F. G. Brickwedde

New developments in science and industry are aided by accurate knowledge of the behavior of important substances. The great abundance of chemical processes and compounds in which hydrogen is involved make it of particular interest. The experimental and derived data presented here for hydrogen extend over a large range of temperature. Low temperatures are required for the liquid and solid, and moderate and high temperatures occur in chemical reactions.

The available thermal data for H_2, HD, and D_2 in solid, liquid, and gaseous states have been brought together, including the distinctive properties of ortho and para forms of H_2 and D_2. Some data not previously published have been added. The thermal data include thermodynamic functions for the ideal gas state, equilibrium constants, data of state, viscosity, and thermal conductivity with dependence on the pressure, vapor pressure, solid-liquid equilibria, specific heats, and latent heats. Values of state derivatives useful in thermodynamic calculations have been given for normal hydrogen, and the related differences between thermodynamic functions for real and ideal gas states have been evaluated. A temperature entropy diagram for normal H_2 in the range of experimental data is also given. The compiled thermal properties of hydrogen are presented in 38 tables, 33 graphs, and numerous equations. The sources of the data have been given in an extensive bibliography.

I. Introduction

It was recommended by the National Research Council Committee on Thermal Data for Chemical Industries [1, 2] and by others that the thermal data on substances of industrial importance should be reexamined with the intention of preparing consistent tables of thermal data of especial interest to chemical engineers and investigators.

In this paper thermal data on hydrogen in its various isotopic and ortho-para modifications are compiled and correlated. Data on properties of the gaseous, liquid, and solid states are presented in tables and graphs, and by use of formulas. Thermodynamic properties are given for the ideal gas state. In addition, tables based on the PVT data for the real gas furnish the additional information required for the calculation of the thermodynamic properties of the real gas. For the condensed phases, directly observable properties are given. Because of the industrial importance of flow and heat-transfer problems, correlations of viscosity and of thermal conductivity are included and their dependence upon pressure discussed briefly. A number of topics are discussed in detail to explain the fundamental principles involved. Most of the data included were taken from published papers. However, a small proportion are based on unpublished measurements made at the Bureau.

The following are the symbols and values of physical constants and conversion factors used in this paper.

1. Symbols

Many symbols that are not used extensively in this paper have been omitted from this list.

A, constant in an equation for a PVT isotherm.

B, second virial coefficient in equation of state of gas.

B_e, rotational spectroscopic constant.

[1] Division of Chemistry and Chemical Technology, National Research Council.

[2] F. Russell Bichowsky, Chairman, 1938 to 1947.

b, b, constant in an equation for a PVT isotherm; also, a constant in an equation of state.

C, C, constant in an equation for a PVT isotherm; also, the Sutherland constant in a viscosity formula.

C', constant in an equation for a PVT isotherm.

C_p°, molar heat capacity (molar specific heat) at constant pressure for ideal gas.

C_s, molar heat capacity (molar specific heat) along a saturation curve.

C_v°, molar heat capacity (molar specific heat) at constant volume for ideal gas.

c, c, velocity of light; also a constant in an equation for a PVT isotherm.

c_2, radiation constant hc/k.

D_v, rotational spectroscopic constant.

E, a thermodynamic function, internal energy per mole.

E°, E for a substance in the ideal gaseous state.

E_0°, E° at the absolute zero of temperature when for each molecule the energy associated with internal degrees of freedom is at its lowest quantized value.

F, a thermodynamic function, molar free energy $F=E+PV-TS$.

F°, F for a substance in the ideal gaseous state at a pressure of 1 atmosphere.

F_v, rotational spectroscopic constant.

$F_{v,J}$, or F, term value.

f, a thermodynamic function, fugacity.

G_v, vibrational term value.

g, statistical weight of a quantum level.

H, a thermodynamic function, molar heat content or enthalpy, $H=E+PV$.

H°, H for a substance in the ideal gaseous state.

H_v, rotational spectroscopic constant.

h, Planck's constant.

i, nuclear spin.

J, rotational quantum number.

K, equilibrium constant.

k, k, Boltzmann constant; also, thermal conductivity.

L_v, latent heat of vaporization.

M, molecular weight.

m, reduced mass for molecule.

N, total number of molecules considered.

N_j, number of molecules in a given quantum level.

N_0, Avogadro's number.

P, pressure.

P_c, pressure at the critical point.

P_0, pressure of 1 standard atmosphere, 1.01325×10^6 dynes cm^{-2} by definition.

p, momentum corresponding to generalized coordinate q.

q, a generalized coordinate.

R, molar gas constant.

r, atomic separation.

r_e, atomic separation r for minimum potential energy.

S, a thermodynamic function, molar entropy.

S°, S for a substance in the ideal gaseous state at a pressure of 1 atmosphere.

T, absolute temperature on the Kelvin scale.

T_c, temperature T at critical point.

T_0, Kelvin temperature T of the ice point, that is, of 0° C.

U, intramolecular potential energy.

U_{11}, ratio of mean free path lengths for diffusion and viscosity.

V, molar volume.

V_c, molar volume at the critical point.

V_0, molar volume of gas at 1-atmosphere pressure and the ice point.

v_0, molar volume of liquid at zero pressure.

v, vibrational quantum number.

Z, abbreviation for PV/RT.

γ, ratio of specific heats, C_p/C_v.

ϵ, energy for a quantum state.

η, viscosity.

Θ, a characteristic Kelvin temperature for a crystal lattice in Debye's theory of specific heats.

Λ, length of mean free path.

μ, Joule-Thomson coefficient.

ξ, fractional increase in atomic separation beyond that for minimum potential energy.

ρ, density in Amagat units.

σ, a correlation function for PVT data.

χ, a function in one equation of state.

φ, a correlation function for PVT data.

2. Values Used for Some Physical Constants and Conversion Factors

(Numbers in parentheses refer to the references given below)

c (velocity of light $=2.99776\times10^{10}$ cm sec^{-1} (1).

c_2 (radiation constant $=\frac{hc}{k}=\frac{N_0hc}{R}=1.4384$ cm deg (2).

h (Planck's constant $=6.624\times10^{-27}$ cm sec (1).

N_0 (Avogadro number $=6.0228\times10^{23}$ mole^{-1} (1).

P_0 (pressure of standard atmosphere) $= 1.01325 \times 10^6$ dynes cm^{-2} (3).

R (molar gas constant) $= N_0 k = 8.3144 \times 10^7$ erg mole^{-1} deg^{-1} (1).
$= 1.98714$ thermochemical cal mole^{-1} deg^{-1} (4).

T_0 (Kelvin temperature of ice point) $= 273.16°$ K (5).

Atomic weight of hydrogen (H^1) on chemical scale $= 1.000786$ (1).

Atomic weight of deuterium (D or H^2) on chemical scale $= 2.01418$ (1).

1 thermochemical calorie $= 4.1833$ international joules (5).

1 international joule (NBS) $= 1.000165$ absolute joules (6).

(1) Raymond T. Birge, Rev. Modern Phys. **13,** 233 (1941).

(2) Birge's value (Rev. Modern Phys. **13,** 233 (1941)) adjusted for later NBS value of the ratio international coulomb/absolute coulomb $= 0.99985$; see also reference (7).

(3) Definition.

(4) Birge's value (Rev. Modern Phys. **13,** 233 (1941)) adjusted to thermochemical calorie and NBS value for ratio international joule/absolute joule.

(5) Definition.

(6) NBS Technical News Bulletin **31,** 49 (1947).

(7) R. W. Curtis, R. L. Driscoll, and C. L. Critchfield, J. Research NBS **28,** 133 (1942).

II. Thermodynamic Properties for the Hydrogens in the Ideal Gas State

1. General Principles of Calculation

For a gas in a state of extreme rarefaction the energy of interaction between molecules forms a minute part of the total energy of the gas. At such low pressures the thermodynamic properties of the gas may be calculated from the spectroscopically determined energies of the single molecules and the general physical constants without considering the energy of interaction of one molecule with another. Some thermodynamic properties, as for example molar entropy and free energy, do not approach a definite value as the pressure of the gas goes to zero. For this reason, values of thermodynamic functions of a gas at low pressure are often indicated by giving values for a pressure of 1 atm for a fictitious ideal gas having in the limit of low pressure the same thermodynamic functions as the actual gas. The result is then said to be for the gas at a pressure of 1 atmosphere in the hypothetical ideal gas state. Data of state may be used to calculate the differences between properties in the real and ideal gas states.

The procedure for calculating the thermodynamic properties of a substance in the ideal gas state has been discussed by many writers [3, 30, 31, 32].[3]

In outline, it involves the following ideas: The average number n_1 of molecules in a quantum state of energy ϵ_1 is related to the average number, n_2 of molecules in another state of energy ϵ_2 by the Boltzmann distribution law

$$n_1/n_2 = e^{-\epsilon_1/kT}/e^{-\epsilon_2/kT} = e^{-(\epsilon_1-\epsilon_2)/kT}, \qquad (2.1)$$

where k is the Boltzmann constant, and T is the absolute temperature.

As there are often several states having the same energy, the number of molecules in a given energy level [4] is also proportional to the number of states, g. If N_1, N_2, N_3, . . . are the numbers of molecules in the levels ϵ_1, ϵ_2, ϵ_3, . . ., respectively, the number of molecules in any one level is

$$N_i = \frac{Ng_i e^{-\epsilon_i/kT}}{g_1 e^{-\epsilon_1/kT} + g_2 e^{-\epsilon_2/kT} + \ldots} = \frac{Ng_i e^{-\epsilon_i/kT}}{\sum_i g_i e^{-\epsilon_i/kT}}, \qquad (2.2)$$

where N, the total number of molecules being considered, is equal to ΣN_i. If properties are to be expressed on the basis of 1 mole, N is taken equal to Avogadro's number, N_0.

The quantum states are specified by means of quantum numbers, the integer values which certain natural variables have when a molecule has a stationary value of energy. The magnitude of the energy is generally expressed in terms of these numbers. In diatomic molecules, the quantum numbers of interest are J, the rotational quantum number, K, the rotational quantum number apart from spin, and v, the vibrational quantum number. The electronic state is also similarly quantized, and quantum numbers appropriate to it may likewise be assigned. The nuclear spins of the two constituent atoms are designated by i_1 and i_2. In terms of these numbers, the statistical weight, g, of a level of a diatomic molecule composed of unlike atoms, as for example HD, is $g_e(2i_1+1)(2i_2+1)(2J+1)$, where g_e is the weight of the electronic level of the mole-

[3] Figures in brackets indicate the literature references at the end of this paper.

[4] The term *state* is used in the sense that two states differ if any of *all* the quantum numbers associated with the states are different. The term level is used to express the idea that the energy has a definite value. The statistical weight, g, of a level is the number of states having the energy which define the level. A level with more than one state is said to be degenerate.

cule. The ground electronic level of HD, and of H_2 and D_2, also, is a singlet state, and accordingly g_e is 1.

The proton and deuetron spins are ½ and 1, respectively. For diatomic molecules composed of like atoms, as for example, H_2 and D_2, there is a division of the rotational levels of the molecule into two groups referred to as the ortho and para series, one of which is composed of the even numbered and the other of the odd numbered rotational levels. Ordinarily, transitions between ortho and para levels are relatively rare, so that the gas can be considered as a mixture of two distinct components. The high temperature equilibrium mixture of the two forms is called the normal mixture, and the more abundant component of the normal mixture is called the ortho component. The statistical weights of the two series depends upon the quantum statistics applicable to the nuclei. For H_2 it is the Fermi-Dirac statistics, for D_2 the Bose-Einstein statistics.

Fermi-Dirac statistics:

$$\left.\begin{array}{l} g \text{ (para series, even } J\text{'s)} = \\ g_e\,(2i+1)i(2J+1) \\ \\ g \text{ (ortho series, odd } J\text{'s)} = \\ g_e\,(2i+1)(i+1)(2J+1) \end{array}\right\} \quad (2.3)$$

Bose-Einstein statistics:

$$\left.\begin{array}{l} g \text{ (ortho series, even } J\text{'s)} = \\ g_e\,(2i+1)(i+1)(2J+1) \\ \\ g \text{ (para series, odd } J\text{'s)} \quad = \\ g_e\,(2i+1)i(2J+1) \end{array}\right\} \quad (2.4)$$

The energy per mole due to molecular rotation and intramolecular vibration is

$$E_{v+r}=\Sigma N_j\epsilon_j=\frac{N_0\Sigma g_j\epsilon_j e^{-\epsilon_j/kT}}{\Sigma g_j e^{-\epsilon_j/kT}}, \quad (2.5)$$

where the ϵ's are the energies of the rotational-vibrational levels relative to the lowest energy level of the molecule. The translational energy, 3/2 N_0kT or 3/2 RT, is added to this to get $E^\circ-E_0^\circ$, the total internal energy per mole for the ideal gas above the chosen zero in which there would be no translational energy and each molecule would be in the lowest energy state available to any form of the molecule.[5]

$$E^\circ-E_0^\circ=3/2\ RT+N_0\frac{\sum\limits_j g_j\epsilon_j e^{-\epsilon_j/kT}}{\sum\limits_j g_j e^{-\epsilon_j/kT}}. \quad (2.6)$$

The superscript zero is used to indicate the ideal gas state.

The enthalpy H°, the specific heats C_v° and C_p°, the entropy S°, and the free energy F° for the ideal gas state are derivable in accordance with familiar methods of thermodynamics from (1) the internal energy $E^\circ-E_0^\circ$, (2) the equation of state $PV=RT$, and (3) the *translational* entropy S_t° of an ideal gas of molecular weight M. The equations for these properties as functions of (ϵ_j/kT) are

$$\frac{E^\circ-E_0^\circ}{RT}=\frac{\sum\limits_j g_j(\epsilon_j/kT)e^{-\epsilon_j/kT}}{\sum\limits_j g_j e^{-\epsilon_j/kT}}+\frac{3}{2}. \quad (2.7)$$

$$\frac{H^\circ-E_0^\circ}{RT}=\frac{E^\circ-E_0^\circ}{RT}+1. \quad (2.8)$$

$$\frac{C_v^\circ}{R}=\frac{\sum\limits_j g_j(\epsilon_j/kT)^2e^{-\epsilon_j/kT}}{\sum\limits_j g_j e^{-\epsilon_j/kT}}-\left(\frac{\sum\limits_j g_j(\epsilon_j/kT)e^{-\epsilon_j/kT}}{\sum\limits_j g_j e^{-\epsilon_j/kT}}\right)^2+\frac{3}{2}. \quad (2.9)$$

$$\frac{C_p^\circ}{R}=\frac{C_v^\circ}{R}+1. \quad (2.10)$$

$$\frac{S^\circ}{R}=\ln\sum_j g_j e^{-\epsilon_j/kT}+\frac{\sum\limits_j g_j(\epsilon_j/kT)e^{-\epsilon_j/kT}}{\sum\limits_j g_j e^{-\epsilon_j/kT}}+\frac{S_t^\circ}{R}. \quad (2.11)$$

$$\frac{S_t^\circ}{R}=\frac{5}{2}\ln T+3/2\ln M-\ln(P/P_0)+\ln\frac{(2\pi)^{3/2}R^{5/2}}{h^3N_0^4P_0}+\frac{5}{2} \quad (2.12)$$

$$\frac{S_t^\circ}{R}=\frac{3}{2}\ln T+3/2\ln M+\ln V+\ln\frac{(2\pi R)^{3/2}}{h^3N_0^4}+\frac{5}{2}. \quad (2.13)$$

$$\frac{F^\circ-E_0^\circ}{RT}=\frac{H^\circ-E_0^\circ-TS^\circ}{RT}=-\ln\sum_j g_j e^{-\epsilon_j/kT}+\frac{5}{2}-\frac{S_t^\circ}{R}. \quad (2.14)$$

[5] Accordingly for orthohydrogen and paradeuterium E_0° is not the internal energy at 0° K. For these substances at 0° K the internal energy above the chosen zero ($J=0$, $v=0$) is the rotational energy per mole of molecules in the rotational level $J=1$. At 0° K internal energies of normal hydrogen and normal deuterium are respectively three-fourths the internal energy of orthohydrogen and one-third the internal energy of paradeuterium.

In eq 2.12, P and P_0 are the pressure of the gas and standard atmospheric pressure, respectively, with both expressed in dynes cm^{-2}. The ratio P/P_0 is the pressure expressed in atmospheres.

For a monatomic gas in which the ground state is so far below the others in energy that it alone makes appreciable contribution to the state-sum, $\Sigma_j g_j \varepsilon^{-\epsilon_j/kT}$, eq 2.7 to 2.14 are simplified considerably. With ϵ_1, the energy of the ground state, taken as zero, the state-sum reduces to the constant g_1

As a result, $(E^\circ - E_0^\circ)/RT = 3/2$; $(H^\circ - E_0^\circ)/RT = 5/2$; $C_v^\circ/R = 3/2$; $C_p^\circ/R = 5/2$; $S^\circ/R = \ln g_1 + S_t^\circ/R$, and $(F^\circ - E_0^\circ)/RT = -\ln g_1 + 5/2 - S_t^\circ/R$. When the nuclear spin is included, g_1 contains $(2i+1)$ as a factor.

Normal hydrogen is a mixture 75 percent of orthohydrogen and 25 percent of parahydrogen, and normal deuterium 66⅔ percent of orthodeuterium, and 33⅓ percent of paradeuterium. The molar entropy and free energy of a mixture of ideal gases present in the mole fractions x_1, x_2, . . . are

$$S_{\text{mixture}} = \sum_j x_j S^\circ{}_j - R \sum_j x_j \ln x_j \qquad (2.15)$$

$$F_{\text{mixture}} = \sum_j x_j F^\circ{}_j + RT \sum_j x_j \ln x_j, \qquad (2.16)$$

where $S^\circ{}_j$ and $F^\circ{}_j$, the molar entropy and free energy of the ideal gas j in a pure state at the pressure of the mixture, are given by eq 2.11 and 2.14, using eq 2.12 for the evaluation of $S^\circ{}_t$. The summation $-R\Sigma x_j \ln x_j$ is called the entropy of mixing. Using eq 2.13 for the evaluation of S_t and setting V equal to the molar volume of the constituent, that is, the volume of the mixture divided by the moles of constituent present, is equivalent to using partial pressures in eq 2.12, in which case the entropy and free energy of the mixture are equal simply to $\Sigma x_j S^\circ{}_j$ and $\Sigma x_j F^\circ{}_j$.

2. Energy Values From Spectroscopic Data

The values of ϵ_j to be used in evaluating the equations of the preceding section are derived from analysis of molecular spectra. In general, banded electronic absorption and emission spectra, infrared, rotation-vibration absorption spectra, and Raman spectra are considered. But as the H_2 and D_2 molecules have no electric dipole moments in their normal states, they have no rotation-vibration absorption spectra. Similarly, no such spectra have been observed for HD, although lack of symmetry permits it to have a very weak dipole moment.

The spectroscopic energy level data for hydrogen are represented by a series in which the energies of the levels relative to the ground level, $v=0$, $J=0$, divided by hc are expressed as a function of the rotational and vibrational quantum numbers J and v, see eq 2.17. The quantity ϵ_j/hc is called the *term value* of the level and is designated by the symbol F. Term values are determined experimentally from differences between the wave numbers of spectrum lines and are expressed in terms of reciprocal centimeters as a unit. Here $F_{v,J}$ is the term value for the level v, J; $F_{0,0}$ for the ground state being zero.

Up to 25,000 cm^{-1}, the term values on which tables 4, 7, and 8 are based, can be represented by

$$F_{v,J} = G_v - G_0 + B_v J(J+1) + D_v J^2(J+1)^2 + F_v J^3(J+1)^3 + H_v J^4(J+1)^4 + \frac{(H_v J^4(J+1)^4)^2}{F_v J^3(J+1)^3 - H_v J^4(J+1)^4}, \qquad (2.17)$$

where the subscripts used indicate the quantum numbers on which the different symbols depend for their values.

The functions G_v, B_v, D_v, F_v, and H_v for H_2, HD and D_2 are as follows:

For H_2:

$$\left.\begin{aligned} G_v &= 4405.3(v+\tfrac{1}{2}) - 125.325(v+\tfrac{1}{2})^2 + 1.9473(v+\tfrac{1}{2})^3 - 0.11265(v+\tfrac{1}{2})^4 \\ B_v &= 60.8483 - 3.06635(v+\tfrac{1}{2}) + 0.068361(v+\tfrac{1}{2})^2 - 0.0065(v+\tfrac{1}{2})^3 \\ D_v &= -0.046435 + 0.0014904(v+\tfrac{1}{2}) - 0.000063648(v+\tfrac{1}{2})^2 \\ F_v &= 4.93203\times10^{-5} + 0.02800\times10^{-5}(v+\tfrac{1}{2}) \\ H_v &= -6.7217\times10^{-8} \end{aligned}\right\} 2.18$$

For HD:

$$\left.\begin{aligned} G_v &= 3817.09(v+\tfrac{1}{2}) - 94.958(v+\tfrac{1}{2})^2 + 1.4569(v+\tfrac{1}{2})^3 - 0.07665(v+\tfrac{1}{2})^4 \\ B_v &= 45.6549 - 1.992721(v+\tfrac{1}{2}) + 0.038482(v+\tfrac{1}{2})^2 - 0.00316885(v+\tfrac{1}{2})^3 \\ D_v &= -0.026136 + 0.00072661(v+\tfrac{1}{2}) - 0.0000268773(v+\tfrac{1}{2})^2 \\ F_v &= 2.0827\times10^{-5} + 0.01024\times10^{-5}(v+\tfrac{1}{2}) \\ H_v &= -2.1295\times10^{-8} \end{aligned}\right\} \quad 2.19$$

For D_2:

$$\left.\begin{aligned} G_v &= 3118.46(v+\tfrac{1}{2}) - 64.10(v+\tfrac{1}{2})^2 + 1.2514(v+\tfrac{1}{2})^3 - 0.10612(v+\tfrac{1}{2})^4 + 0.00034(v+\tfrac{1}{2})^5 \\ B_v &= 30.4286 - 1.04917(v+\tfrac{1}{2}) + 0.0057934(v+\tfrac{1}{2})^2 - 0.00027486(v+\tfrac{1}{2})^3 \\ D_v &= -0.011586 + 0.000151(v+\tfrac{1}{2}) + 0.000058(v+\tfrac{1}{2})^2 \\ F_v &= 6.22\times10^{-6} + 0.105\times10^{-6}(v+\tfrac{1}{2}) \\ H_v &= -0.442\times10^{-8} \end{aligned}\right\} \quad 2.20$$

The numerical values of the coefficients in eq 2.18 to 2.20 are based on the latest available spectroscopic measurements due principally to Rasetti [2], Hyman [5, 6], Jeppesen [6, 7, 12, 15, 24], Beutler [20, 21], and Teal and Mac Wood [22]. The data of Fujioka and Wada [23] were not used and the data of Mie [16] on HD only through its influence on the formula for G_v. The equations G_v for H_2 and HD are those given by Teal and Mac Wood [22], and that for D_2 by Jeppesen [24]. The equations for B_v are essentially Jeppesen's [12, 24] equations expressed for use with $J(J+1)$. The constants in the equations for D_v, F_v, and H_v were obtained from theory using the equations for G_v and B_v and the formulas of Dunham [10] without his correction terms.

In the case of hydrogen as for many other substances, extrapolations of spectroscopic formulas have to be made into regions of large rotational quantum numbers for which no wavelength measurements are available in order to obtain values for the energies ϵ_j of the higher quantum states. The energy values for large rotational and vibrational quantum numbers are influenced by the law of internuclear force of the molecule for large separations of the nuclei. Special consideration has been given to this point in the present work and two methods were developed whereby more reliable values of the energies of the unobserved higher rotational levels were obtained.

The first improvement was the addition of the final term in eq 2.17, $[H_vJ^3(J+1)^3]^2/[(F_vJ^2(J+1)^2 - H_vJ^3(J+1)^3)]$. Without the final term, eq 2.17 is of the form in which spectroscopic data have heretofore been represented, but in that form it is not a good approximation for large values of J. The third, fourth, fifth, and sixth terms of eq 2.17 are of alternate sign and for H_2 the third, fourth, and fifth terms are approximately equal for $J=28$. This suggested that the series be extended with successive terms in constant ratio. The final term of eq 2.17 is the sum of the geometric series of added terms in which the term to term ratio is that between the fifth and sixth terms of eq 2.17.

This change in the formula for the energies of the rotational-vibrational levels of the normal ($1s^1\Sigma$) electronic state of hydrogen has only a small effect on the energy values of the observed spectrum lines. Thus the mean difference between Jeppesen's [12] observed and calculated term values for the $2p^1\Sigma - 1s^1\Sigma$ band for H_2 was 1.032 cm^{-1}, whereas using eq 2.17 in place of Jeppesen's equation for the $1s^1\Sigma$ state the mean difference between observed and calculated values is 1.030 cm^{-1}.

As a second improvement, for the calculation of thermodynamic properties above 2,000° K, an alternative determination of the highest rotational levels was made. Instead of using the power series eq 2.17, the energies corresponding to any degree of rotation and vibration were determined from the potential energy. This was

carried out in effect by (1) determining the potential energy U of the nonrotating H_2 molecule as a function of the internuclear separation, (2) adding the rotational energy $h^2J(J+1)/8\pi^2I_e(r/r_e)^2$ to U to obtain an effective potential energy, U', for a molecule with rotational quantum number J, and (3) using the quantum condition $\oint pdq=\int(2m)^{1/2}(\epsilon_{v,J}-U')^{1/2}dr=(v+1/2)h$ to determine the energy $\epsilon_{v,J}$ of the quantum state v, J.

The coefficients of a power series used to represent the molecular potential energy were evaluated for the H_2 molecule using Dunham's [10] theoretical relations and the rotational and vibrational data for H_2:

$$U=79734\xi^2(1-1.6082\xi+1.8598\xi^2-1.8882\xi^3+1.7118\xi^4-1.450\xi^5+1.421\xi^6), \quad (2.21)$$

where ξ is $(r-r_e)/r_e$, r_e being the equilibrium value of the internuclear separation, and U is expressed in reciprocal centimeters. Although this series is a poor representation of U for internuclear separations twice the equilibrium value (i. e., at $\xi=1$), it is very good for small values of ξ. Therefore, this series was not used for the potential energy function finally accepted for internuclear separations much greater than the equilibrium value, but it was used for internuclear separations less than the equilibrium value. At dissociation the minimum value of r for classical motion is more than half of r_e (i. e., $|\xi|<0.5$), and the series determines the inner portion of the potential energy curve with sufficient reliability for the present purposes.

The ranges of internuclear oscillation, $\xi_{max}-\xi_{min}$, for different values of the energy needed to fix the outer portion of the potential energy curve, were determined from (1) the vibrational levels of the nonrotating molecule, symbolized by G_v in eq 2.17 to eq 2.20, which have been accurately measured to within 140 cm^{-1} of dissociation [5, 12, 20, 21] and (2) the quantum condition.

$$\oint pdq=(2mr_e^2hc)^{1/2}\oint(G_v-U)^{1/2}d\xi=(v+1/2)h. \quad (2.22)$$

The method used to obtain $(\xi_{max}-\xi_{min})$ by satisfying eq 2.22 was essentially that of Rydberg [8] and Klein [9]. Calculated values of the potential energy U in wave numbers are given in table 1.

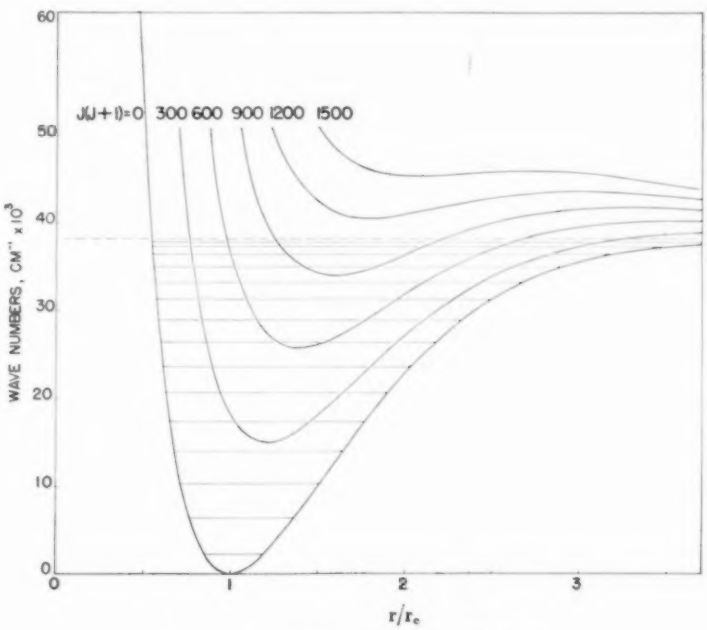

FIGURE 1. *Potential-energy curves for* H_2.

TABLE 1. *Molecular potential energy U for H_2 as a function of $\xi=(r-r_e)/r_e$, the change in internuclear separation*

ξ	U	ξ	U	ξ	U
	cm^{-1}		cm^{-1}		cm^{-1}
−0.5	53,648	0.9	20,540	2.3	36,828
−.4	27,150	1.0	22,822	2.4	37,100
−.3	12,338	1.1	24,915	2.5	37,322
−.2	4,511	1.2	26,810	2.6	37,503
−.1	942	1.3	28,505	2.7	37,650
0	0	1.4	30,009	2.8	37,770
.1	683	1.5	31,329	2.9	37,867
.2	2,360	1.6	32,472	3.0	37,946
.3	4,628	1.7	33,454	3.1	38,009
.4	7,223	1.8	34,292	3.2	38,061
.5	9,968	1.9	35,001	3.3	38,102
.6	12,744	2.0	35,599	3.4	38,136
.7	15,466	2.1	36,092	3.5	38,163
.8	18,079	2.2	36,496	∞	38,286

$r_e=0.7414\times10^{-8}$cm

The effective potential energy curves for rotating molecules obtained by adding to U for the nonrotating molecule the energy of rotation, $J(J+1)B_e/(1+\xi)^2$, in cm^{-1}, are illustrated in figure 1. By applying the quantum integral,

$$\oint pdq=(2mr_e^2hc)^{1/2}\oint (F-U')^{1/2}d\xi=(v+1/2)h, \tag{2.23}$$

to the effective potential energy curves, U', a set of corresponding values of energy (F) and vibrational quantum number was determined for each

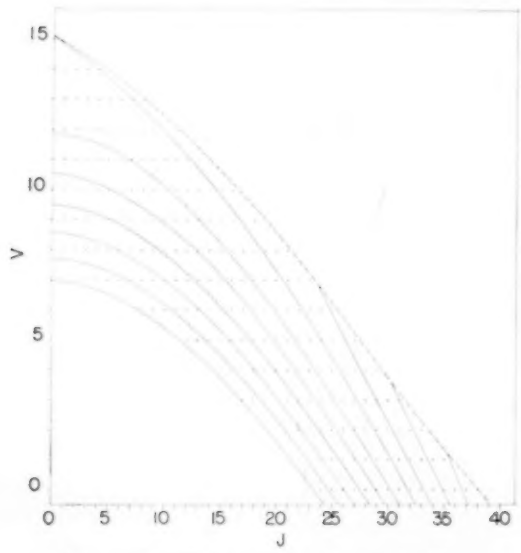

FIGURE 2. *Energy contour diagram for H_2.*

of a few large values of the rotational quantum number. In table 2 these corresponding values are given together with the maximum and minimum values of the energy (F) for different values of $J(J+1)$. The data were used to determine the constant energy lines in the v versus J diagram in figure 2.

TABLE 2. *Corresponding values of v, $J(J+1)$, and F obtained by evaluating $\oint pdq=(v+1/2)h$*

[The values of v and J are not integral and so do not represent stationary states, yet the table values indicate how F depends on v and J over a range including many stationary states.]

F (above U at $\xi=0$)	$J(J+1)$	v
cm^{-1}		
38,269	300	8.8483
34,269	300	6.2874
30,269	300	4.5015
26,269	300	2.9881
22,269	300	1.6461
38,269	600	4.8378
34,269	600	2.7292
30,269	600	1.0757
38,269	900	1.4032
42,269	1,200	0.4845
Maximum values of F and v for given values of $J(J+1)$		
38,288	0	15.053
39,098	300	9.919
40,323	600	6.615
41,858	900	3.929
43,712	1,200	1.703
45,989	1,500	−0.072
Minimum values of F and v for given values of $J(J+1)$		
0	0	−0.5
15,027	300	−.5
25,847	600	−.5
34,111	900	−.5
40,606	1,200	−.5
45,601	1,500	−.5

Table 3 shows that over a wide range of J values the results of the numerical integration just described are in good agreement with the rotational energy formula (eq 2.17) when the last term, corresponding to a geometric series continuation, is included. For the larger values of J there are appreciable differences; yet, when it

is observed how large the final term of eq 2.17 is in these cases, it seems surprising that the discrepancies between F (table 2) and F (eq 2.17 are as small as they are. In another publication [27] a more rapidly converging series representing $J(J+1)$ as a function of the rotational energy has been suggested.

TABLE 3. *Comparison of rotational-vibrational energies F from table 2 and from equation 2.17*

$J(J+1)$	v	F (table 2)	F (table 2) $-F$ (eq 2.17)	Final term of eq 2.17
		cm^{-1}	cm^{-1}	cm^{-1}
300	4.5015	30,269	−54	155
300	6.2874	34,269	−34	154
600	1.0757	30,269	−78	3,904
900	1.4032	38,269	−300	24,192
1,200	0.4845	42,269	761	86,345

3. Details of the Calculations and Results

In the evaluation of the series of section II, 1 for the calculation of the thermal properties, direct summation was employed for temperatures below 2,000° K. The resulting values to 2,000° K for the various thermodynamic functions $S°$, $H°-E_0°$, $-(F°-E_0°)/T$, and $C_p°$ for the ideal gas state at one atmosphere pressure are tabulated in tables 4, 5, and 6, for H_2, HD, and D_2. For n-H_2 for temperatures above 2,000° K, the contributions due to levels below 25,000 cm^{-1} were calculated by direct summation, whereas for levels above 25,000 cm^{-1} a less laborious method was used involving the determination of the number of levels within successive equal steps of 2,000 cm^{-1} in the rotational vibrational energy, using the results of the calculations of the last section which led to figures 1 and 2. For these

TABLE 4. *Thermodynamic functions for* H_2 *in the ideal gaseous state*

Values for $S°$ and $-(F°-E_0°)/T$ include nuclear spin

Temperature	$S°$, cal mole^{-1} deg^{-1}			$H°-E_0°$, cal mole^{-1}			$-\frac{F°-E_0°}{T}$, cal mole^{-1} deg^{-1}			$C_p°$ cal mole^{-1} deg^{-1}		
	p-H_2	o-H_2	n-H_2	p-H_2	o-H_2	n-H_2	p-H_2	o-H_2	n-H_2	p-H_2	o-H_2	n-H_2
°K												
10	11.215	15.581	15.607	49.6785	388.327	393.665	6.247	−23.252	−14.760	4.968	4.968	4.968
20	14.658	19.024	19.050	99.357	438.006	353.344	9.690	−2.876	1.382	4.968	4.968	4.968
20.39	14.754	19.120	19.146	101.295	439.943	355.281	9.786	−2.457	1.721	4.968	4.968	4.968
30	16.672	21.039	21.064	149.036	487.684	403.022	11.705	4.783	7.630	4.968	4.968	4.968
33.1	17.161	21.527	21.553	164.437	503.085	418.423	12.193	6.328	8.911	4.968	4.968	4.968
40	18.102	22.468	22.494	198.729	537.363	452.705	13.134	9.034	11.176	4.973	4.968	4.969
50	19.214	23.576	23.603	248.581	587.041	502.426	14.243	11.836	13.554	5.007	4.968	4.978
60	20.135	24.492	24.513	299.106	636.722	552.318	15.150	13.870	15.307	5.115	4.969	5.005
70	20.938	25.248	25.288	351.222	686.422	602.622	15.921	15.442	16.679	5.330	4.972	5.061
80	21.669	25.913	25.969	406.015	736.179	653.638	16.594	16.710	17.799	5.646	5.982	5.148
90	22.356	26.500	26.581	464.385	786.085	705.660	17.197	17.766	18.741	6.036	5.003	5.261
100	23.014	27.029	27.142	526.837	836.277	758.916	17.745	18.667	19.554	6.455	5.039	5.393
120	24.259	27.959	28.151	663.752	938.227	869.609	18.729	20.140	20.904	7.204	5.170	5.678
150	25.945	29.143	29.461	890.605	1,097.78	1,045.99	20.007	21.825	22.488	7.807	5.487	6.067
200	28.202	30.808	31.275	1,282.70	1,387.90	1,361.61	21.788	23.869	24.466	7.742	6.110	6.518
250	29.889	32.225	32.758	1,660.49	1,705.80	1,694.47	23.246	25.402	25.981	7.380	6.565	6.770
298.16	31.168	33.404	33.963	2,009.99	2,028.34	2,023.75	24.426	26.602	27.175	7.158	6.803	6.891
300	31.212	33.446	34.005	2,023.16	2,040.87	2,036.44	24.468	26.643	27.217	7.152	6.809	6.894
350	32.306	34.505	35.073	2,377.84	2,384.39	2,382.75	25.512	27.693	28.265	7.049	6.917	6.951
400	33.244	35.432	36.003	2,729.19	2,731.54	2,730.95	26.421	28.603	29.175	7.010	6.963	6.975
500	34.806	36.990	37.561	3,429.24	3,429.53	3,429.46	27.948	30.131	30.702	6.998	6.992	6.993
600	36.083	38.266	38.838	4,129.48	4,129.52	4,129.51	29.200	31.383	31.955	7.010	7.009	7.009
700	37.165	39.348	39.920	4,831.65	4,831.66	4,831.66	30.263	32.446	33.018	7.037	7.036	7.036
1,000	39.701	41.884	42.455	.....	.....	6,966.23	32.735	34.918	35.490	.....	.....	7.219
1,500	42.720	44.903	45.475	.....	.....	10,697.20	35.589	37.770	38.343	.....	.....	7.720
2,000	45.007	47.190	47.762	.....	.....	14,679.2	37.668	39.851	40.422	.....	.....	8.195
3,000	.....	.....	51.221	.....	.....	23,230.9	.....	.....	43.478	.....	.....	8.859
4,000	.....	.....	53.839	.....	.....	32,345.	.....	.....	45.753	.....	.....	9.342
5,000	.....	.....	55.969	.....	.....	41,895.	.....	.....	47.590	.....	.....	9.748

TABLE 5. *Thermodynamic functions for HD in the ideal gas state*

Values for S° and $-(F^\circ-E_0^\circ)/T$ include nuclear spin

Temperature	S_0	$H^\circ-E_0^\circ$	$-\frac{F^\circ-E_0^\circ}{T}$	C_p°
°K	*cal mole*$^{-1}$ *deg*$^{-1}$	*cal mole*$^{-1}$	*cal mole*$^{-1}$ *deg*$^{-1}$	*cal mol*$^{-1}$ *deg*$^{-1}$
10	15.982	49.681	11.014	4.971
20	19.497	100.600	14.468	5.365
22.13	20.050	112.234	14.979	5.564
30	21.861	159.230	16.553	6.367
40	23.792	226.510	18.129	6.991
50	25.375	297.472	19.425	7.149
60	26.680	368.910	20.531	7.126
70	27.772	439.914	21.488	7.076
80	28.714	510.464	22.333	7.037
90	29.542	580.708	23.089	7.013
100	30.279	650.733	23.772	6.999
120	31.554	790.592	24.966	6.985
150	33.112	1,002.02	26.445	6.978
200	35.119	1,348.82	28.375	6.975
250	36.676	1,697.62	29.885	6.977
298.16	37.905	2,033.66	31.084	6.979
300	37.948	2,046.50	31.126	6.979
400	39.957	2,744.72	33.095	6.986
500	41.517	3,443.85	34.629	6.999
600	42.795	4,144.90	35.886	7.025
700	43.881	4,849.60	36.953	7.072
1,000	46.443	7,007.50	39.436	7.339
1,500	49.527	10,821.2	42.313	7.909
2,000	51.871	14,898.4	44.421	8.376

higher levels having characteristic temperatures above 36,000° K, the exact placement of each individual level is not important for calculations up to 5,000° K.

Figure 1 shows that the effective potential energy curves for rotational quantum numbers other than 0 have broad potential energy barriers above the minimum dissociation energy, 38,296 cm^{-1}, for $J=0$. As a result there are above 38,296 cm^{-1}, the minimum dissociation energy, quantized rotational-vibrational levels belonging to the sequences of levels below 38,296 cm^{-1}. These states are represented by the points in figure 2 between the dashed curve and the full line dissociation energy curve passing through ($J=0$, $v=15.1$) and ($J=32.5$, $v=-\frac{1}{2}$).

It seemed proper to include in the calculations of the thermal properties of hydrogen above 2,000° K these quantized or partially quantized rotational-vibrational states. The values of the thermodynamic functions for n-H_2 from 2,000° to 5,000° K in table 4 are based on this convention.

The effect of the quantized rotational-vibrational levels above the minimum dissociation energy of H_2 on the most sensitive of the functions calculated, namely the molecular heat capacity, is represented in figure 3. Curve A represents the

TABLE 6. *Thermodynamic functions for D_2 in the ideal gaseous state*

Values for S° and $-(F^\circ-E_0^\circ)/T$ include nuclear spin

Temperature	S°, cal mole^{-1} deg^{-1}			$H^\circ-E_0^\circ$, cal mole^{-1}			$-\frac{F^\circ-E_0^\circ}{T}$, cal mole^{-1} deg^{-1}			C_p°, cal mole^{-1} deg^{-1}		
	p-D_2	o-D_2	e-D_2	p-D_2	e-D_2	n-D_2	p-D_2	o-D_2	n-D_2	p-D_2	o-D_2	n-D_2
°K												
10	17.645	16.839	18.372	220.505	49.679	106.621	−4.406	11.871	7.710	4.968	4.968	4.968
20	21.088	20.283	21.816	270.183	99.364	156.303	7.579	15.315	14.001	4.998	4.972	4.971
23.57	21.904	21.101	22.633	287.918	117.139	174.065	9.689	16.131	15.248	4.968	4.989	4.982
30	23.102	22.315	23.842	319.863	149.514	206.297	12.440	17.331	16.965	4.968	5.105	5.039
40	24.533	23.843	25.338	360.584	202.775	258.378	15.293	18.774	18.879	4.980	5.617	5.404
50	25.649	25.180	26.600	419.599	262.811	315.048	17.257	19.923	20.299	5.033	6.412	5.952
60	26.576	26.418	27.736	470.480	330.843	377.389	18.734	20.904	21.446	5.156	7.163	6.495
70	27.384	27.563	28.768	522.948	405.192	444.444	19.913	21.775	22.419	5.348	7.656	6.887
80	28.114	28.601	29.704	577.589	482.997	514.528	20.893	22.564	23.272	5.586	7.862	7.103
90	28.786	29.527	30.545	634.706	561.671	586.016	21.734	23.287	24.035	5.838	7.860	7.187
100	29.414	30.353	31.304	694.306	639.875	658.018	22.471	23.954	24.724	6.079	7.751	7.190
120	30.559	31.739	32.611	819.996	791.908	801.270	23.725	25.139	25.933	6.466	7.454	7.127
150	32.041	33.366	34.189	1,019.52	1,010.37	1,013.42	25.244	26.629	27.432	6.790	7.149	7.029
200	34.023	35.395	36.202	1,364.06	1,362.90	1,363.29	27.202	28.580	29.386	6.947	6.996	6.980
298.16	36.805	38.182	38.988	2,048.10	2,048.08	2,048.09	29.936	31.313	32.119	6.977	6.978	6.978
300	36.848	38.225	39.031	2,060.93	2,060.92	2,060.92	29.978	31.355	32.161	6.977	6.978	6.978
400	38.857	40.234	41.040	.....	.....	2,759.18	31.959	33.336	34.142	.....	.....	6.989
500	40.419	41.796	42.602	.....	.....	3,459.38	33.500	34.877	35.683	.....	.....	7.019
600	41.704	43.081	43.887	.....	.....	4,164.03	34.763	36.141	36.946	.....	.....	7.059
700	42.802	44.179	44.985	.....	.....	4,876.39	35.835	37.212	38.018	.....	.....	7.103
1,000	45.422	46.800	47.605	.....	.....	7,084.30	38.338	39.716	40.521	.....	.....	7.262
1,500	48.611	49.989	50.794	.....	.....	11,027.3	41.259	42.637	43.442	.....	.....	8.178
2,000	51.027	52.405	53.210	.....	.....	15,229	43.411	44.789	45.594	.....	.....	8.598

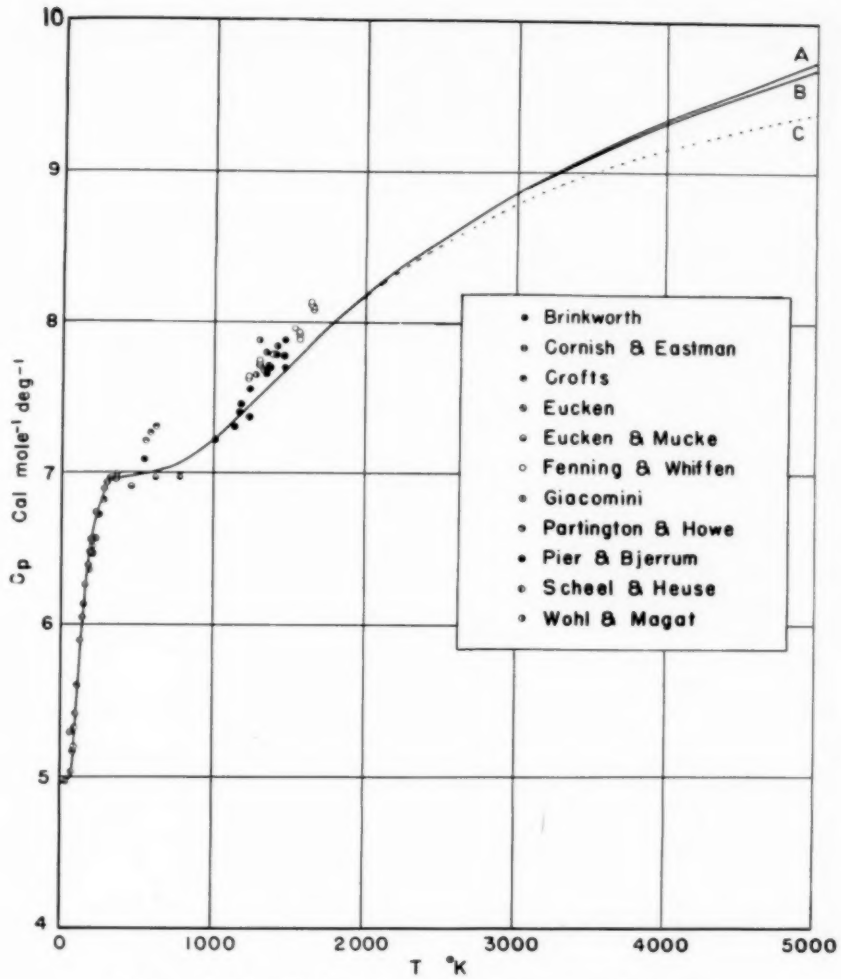

FIGURE 3. *Specific heat of normal hydrogen at constant pressure.*

TABLE 7. *Thermodynamic functions for* H_2 *in ideal gaseous state*

[Based only on levels below minimum dissociation energy]

T	Entropy	Enthalpy	$-\frac{F^\circ-E_0^\circ}{T}$	Specific heat
°K	*cal mole⁻¹ deg⁻¹*	*cal mole⁻¹*	*cal mole⁻¹ deg⁻¹*	*cal mole⁻¹ deg⁻¹*
3,000	51.221	23,230.8	43.478	8.859
4,000	53.838	32,341	45.753	9.341
5,000	55.960	41,854	47.589	9.675

molecular heat capacity if the quantized rotational-vibrational levels above the minimum dissociation energy are included as molecular levels, and curve B represents the molecular heat capacity if the molecular levels are regarded as extending only up to the minimum dissociation energy. In table 7 are tabulated the values of the thermodynamic functions for n-H_2 based on calculations involving only energy levels below the minimum dissociation energy.

For convenience in the calculation of the thermodynamic functions of the real gas n-H_2, values for n-H_2 in the ideal gas state at all temperatures for which there are entries in the tables of PVT data were obtained from table 4 by interpolation and are tabulated in table 8. The interpolated values of S°, $-(F^\circ-E_0^\circ)/T$, and C_p° agree to within ± 0.001 with values that would have been ob-

807127—48——3

tained by direct summation. In the case of $H^\circ - E_0^\circ$, the agreement is within three in the last digit carried.

TABLE 8. *Thermodynamic functions for normal* H_2 *in the ideal gaseous state*

Values for S° and $-(F^\circ - E_0^\circ)/T$ include nuclear spin

T	S°	$H^\circ - E_0^\circ$	$-\frac{F^\circ - E_0^\circ}{T}$	C_p°
° K	cal mole^{-1} deg^{-1}	cal mole^{-1}	cal mole^{-1} deg^{-1}	cal mole^{-1} deg^{-1}
16	17.942	333.473	−2.900	4.968
18	18.527	343.408	−0.551	4.968
20	19.050	353.344	1.382	4.968
22	19.524	363.280	3.011	4.968
24	19.956	373.215	4.405	4.968
26	20.353	383.151	5.616	4.968
28	20.722	393.087	6.683	4.968
30	21.064	403.022	7.630	4.968
32	21.385	412.959	8.480	4.968
34	21.686	422.896	9.248	4.968
36	21.970	432.832	9.947	4.968
38	22.239	442.767	10.587	4.968
40	22.494	452.705	11.176	4.969
42	22.737	462.643	11.722	4.970
44	22.968	472.583	12.227	4.971
46	23.189	482.527	12.699	4.973
48	23.400	492.474	13.140	4.975
50	23.603	502.426	13.554	4.978
52	23.798	512.384	13.944	4.982
54	23.986	522.351	14.313	4.986
56	24.168	532.327	14.662	4.991
58	24.343	542.315	14.993	4.998
60	24.513	552.318	15.307	5.005
65	24.915	577.309	16.032	5.029
70	25.288	602.622	16.679	5.061
75	25.639	628.022	17.265	5.101
80	25.969	653.638	17.799	5.148
85	26.283	679.507	18.289	5.202
90	26.581	705.660	18.741	5.261
95	26.868	732.122	19.161	5.325
100	27.142	758.916	19.554	5.393
105	27.408	786.056	19.922	5.463
110	27.664	813.549	20.268	5.534
115	27.911	841.400	20.595	5.606
120	28.151	869.609	20.904	5.678
125	28.384	898.175	21.198	5.748
130	28.610	927.086	21.479	5.816
135	28.831	956.335	21.747	5.883
140	29.047	985.91	22.005	5.947
145	29.257	1,015.80	22.251	6.008
150	29.461	1,045.99	22.488	6.067
155	29.661	1,076.47	22.716	6.123
160	29.856	1,107.22	22.936	6.177
165	30.047	1,138.23	23.149	6.228
170	30.234	1,169.49	23.355	6.276
180	30.595	1,232.71	23.747	6.366
190	30.942	1,296.78	24.116	6.446
200	31.275	1,361.61	24.466	6.518
210	31.594	1,427.10	24.798	6.581
220	31.901	1,493.20	25.114	6.638

TABLE 8. *Thermodynamic functions for normal* H_2 *in the ideal gaseous state*—Continued

T	S°	$H^\circ - E_0^\circ$	$-\frac{F^\circ - E_0^\circ}{T}$	C_p°
° K	cal mole^{-1} deg^{-1}	cal mole^{-1}	cal mole^{-1} deg^{-1}	cal mole^{-1} deg^{-1}
230	32.197	1,559.85	25.415	6.688
240	32.483	1,626.96	25.704	6.731
250	32.758	1,694.47	25.981	6.770
260	33.024	1,762.33	26.246	6.803
270	33.282	1,830.49	26.502	6.831
280	33.531	1,898.92	26.749	6.856
300	34.005	2,036.44	27.217	6.894
320	34.452	2,174.63	27.656	6.922
340	34.872	2,313.28	28.068	6.943
360	35.269	2,452.29	28.457	6.957
380	35.646	2,591.53	28.826	6.968
400	36.003	2,730.95	29.175	6.975
420	36.344	2,870.51	29.509	6.980
440	36.668	3,010.14	29.826	6.984
460	36.979	3,149.85	30.131	6.987
480	37.276	3,289.62	30.422	6.990
500	37.561	3,429.46	30.702	6.993
520	37.837	3,569.34	30.973	6.996
540	38.100	3,709.28	31.231	6.999
560	38.355	3,849.30	31.481	7.002
580	38.600	3,989.36	31.722	7.005
600	38.838	4,129.51	31.955	7.009
650	39.399	4,480.19	32.506	7.021

The contributions to the entropy and to the related free energy functions arising from (1) the nuclear spins, (2) the triple degeneracy of the lowest rotational state of *o*-H_2 and *p*-D_2, and (3) the mixing of the ortho and para varieties in *n*-H_2 and *n*-D_2 have been included through eq 2.3, 2.4, 2.15, and 2.16 in all the tables. A comparison of the entropies and free energies of hydrogen and deuterium calculated from calorimetric data with values in the tables must take into account the degeneracies existing in the solid state at the lowest temperature of the calorimetric measurements. There must accordingly be added to the calorimetric values of entropy calculated from data extending from 10° K to higher temperatures, the entropies of table 9. In calculations concerning chemical reactions above room temperature nuclear spin entropies are customarily omitted for all components of the reactions.

To obtain entropies of *n*-H_2, HD, and *n*-D_2 suitable for such use above room temperature, there should be subtracted from table values of the entropies $R \ln (2i_1+1)(2i_2+2)$ where i_1 and i_2 are the two nuclear spins within the molecule [14]. For *n*-H_2 this is equal to $R \ln 4 = 2.75$

TABLE 9. *Low-temperature (10° K) entropy contributions arising from rotational and nuclear-spin degeneracies*

	H_2		HD	D_2	
Variety	Para	Ortho	Only 1	Ortho	Para
Values of J	Even	Odd	Both odd and even	Even	Odd
Weight of lowest rotational level $(2J+1)$.	1	3	1	1	3
Nuclear spin weight, see eq 2.3 and 2.4.	1	3	6	6	3
Total added entropy	0	R ln 9=4.366 cal mole^{-1}deg^{-1}.	R ln 6=3.560 cal mole^{-1}deg^{-1}.	R ln 6=3.560 cal mole^{-1}deg^{-1}.	R ln 9=4.366 cal mole^{-1}deg^{-1}.

	n-H_2	n-D_2
$-R(x_o \ln x_o + x_p \ln x_p)$	$R(\ln 4 - \frac{3}{4} \ln 3) = 1.117$ cal mole^{-1} deg^{-1}	$R(\ln 3 - \frac{2}{3} \ln 2) = 1.265$ cal mole^{-1} deg^{-1}
$x_o s_o + x_p s_p$	$\frac{3}{4} R \ln 9 = 3.275$ cal mole^{-1} deg^{-1}	$R(\frac{2}{3} \ln 3 + \frac{2}{3} \ln 2) = 3.829$ cal mole^{-1} deg^{-1}
Total added entropy $(x_i s_i - R x_i \ln x_i)$	$R(\ln 4 + \frac{3}{4} \ln 3) = 4.392$ cal mole^{-1}deg^{-1}	$\frac{7}{3} R \ln 3 = 5.094$ cal mole^{-1}deg^{-1}

cal mole^{-1} deg^{-1}; for HD, $R\ ln\ 6 = 3.560$ cal mole^{-1} deg^{-1}, and for n-D_2, $R\ ln\ 9 = 4.366$ cal mole^{-1} deg^{-1}.

The reliability to be expected in thermodynamic functions for the ideal gas state calculated from spectroscopic data has been considered by earlier writers on the basis of the reliability of spectroscopic constants and the gas constant R. The former estimate of one or two hundredths of a calorie mole^{-1} deg^{-1} for the probable error in the free energy function, specific heat and entropy, appears reasonable. Over much of the temperature range it is probably a more liberal estimate than necessary, as more recent and presumably better spectroscopic data and values for the physical constants have been used. A larger allowance may be necessary for the higher temperatures, however, possibly twice as much at 5,000° K.

The results of the present calculations below 2,000° K are in fairly close agreement with those of Giauque [4], Johnston and Long [18], Davis and Johnston [17], and Wagman, et al. [28]. Above 2,000° K the effect of the new calculations of the high rotational levels of H_2 is apparent.

This can be seen in figure 3 in which the results of Davis and Johnston (curve C) for the specific heat of hydrogen, the most sensitive property calculated, are compared with table values of this paper (curves A and B). Curve A, corresponding to table 4, is based on the inclusion of the quantized rotational-vibrational levels above the minimum dissociation energy as molecular levels, and curve B, corresponding to table 7, is based only on levels below the minimum dissociation energy.

In figure 3 are plotted also a large number of scattered points representing the experimental observations of many investigators. [33 to 37, 40 to 46, 50, 51, 56]. In cases where mean specific heats were reported, they have been plotted for the mean temperatures of the experimental intervals. At room temperatures and below, the theoretical and experimental specific heats are in good agreement, as has been the case since the correct treatment of the ortho and para forms by Dennison [1] in 1927. Above 1,200° K the observations obtained by the explosion method lie above the theoretical curve. The difficulties of the explosion method are great and the accuracy not high [53], consequently the authors feel that the calculated curve and table are more reliable.

At atmospheric pressure and a temperature of 2,000° K, there is a small but perceptible dissociation of H_2, HD, and D_2. As the heat of dissociation of hydrogen is large there are significant differences between the calculated properties of molecular H_2, HD, and D_2, tables 4 to 6, and the properties of the dissociating gases. At 2,000° K the table value of C_p for molecular H_2 is 8.195 cal mole^{-1} deg^{-1}, whereas for an ideal gas mixture of molecular and atomic hydrogen in equilibrium at atmospheric pressure the value is 8.797, a difference of 0.60 cal mole^{-1} deg^{-1}. For HD and D_2 the differences between the two specific heats are 0.41 and 0.57 cal mole^{-1} deg^{-1}, respectively. The effect of pressure upon the specific heat of dissociating hydrogen is illustrated in figure 4 and discussed in section III. At temperatures where there is appreciable dissociation of HD, equilibrium mixtures of H_2, HD, and D_2, are established.

III. Equilibrium Constants for Dissociation, Isotopic Exchange, and Ortho-Para Conversion

The equilibrium constant K of a gaseous reaction

$$\alpha_1 A_1+\alpha_2 A_2+\alpha_3 A_3\ldots=\beta_1 B_1+\beta_2 B_2+\beta_3 B_3\ldots, \quad (3.1)$$

in which each of the participating gases $A_1, A_2, \ldots, B_1, B_2, \ldots$ has the equation of state $PV=RT$, is related to the partial pressures of the gases and to their free energies, F^*, at unit pressure by the equation

$$RT\ln\frac{P_{B_1}^{\beta_1}P_{B_2}^{\beta_2}P_{B_3}^{\beta_3}\cdots}{P_{A_1}^{\alpha_1}P_{A_2}^{\alpha_2}P_{A_3}^{\alpha_3}\cdots}=RT\ln K=-(\Sigma\beta_j F_{B_j}^*-\Sigma\alpha_j F_{A_j}^*)=-\Delta F^*. \quad (3.2)$$

Equilibrium constants for dissociation, isotopic exchange,[6] and ortho-para conversion of hydrogen may be calculated by using the $-(F^\circ-E_0^\circ)/T$ values of tables 4, 5, and 6. E_0° is the internal energy per mole of molecules without translational motion in the lowest energy level $J=0$, $v=0$ and in the ideal gas state, and F° is for the ideal gas state and a pressure of 1 atm: Using $-(F^\circ-E_0^\circ)/T$ instead of F^*,

$$R\ln K=\Delta\frac{-(F^\circ-E_0^\circ)}{T}-\frac{\Delta E_0^\circ}{T}. \quad (3.3)$$

The values of ΔE_0° for the reactions considered in this section are given by the spectroscopic data used in the previous section. Using free energy values as given in the tables of this paper, the atmosphere is the unit of pressure for K and P in the mass action law,

$$\frac{P_{B_1}^{\beta_1}P_{B_2}^{\beta_2}P_{B_3}^{\beta_3}\cdots}{P_{A_1}^{\alpha_1}P_{A_2}^{\alpha_2}P_{A_3}^{\alpha_3}\cdots}=K. \quad (3.4)$$

Deviations from the laws of ideal gases can be taken into account by use of fugacities or activities in place of partial pressures and the forms of eq 3.2, 3.3, and 3.4 for K are retained. When fugacities or activities are substituted for partial pressures, F^* becomes the free energy at unit fugacity or activity. For a fuller discussion of the use of fugacities and activities the reader is referred to references [29 to 32].

The entropies of monatomic H and D (see p. 383) must include the nuclear and electron spin entropies besides the entropy of translation, eq

[6] Equilibrium H_2 and D_2.

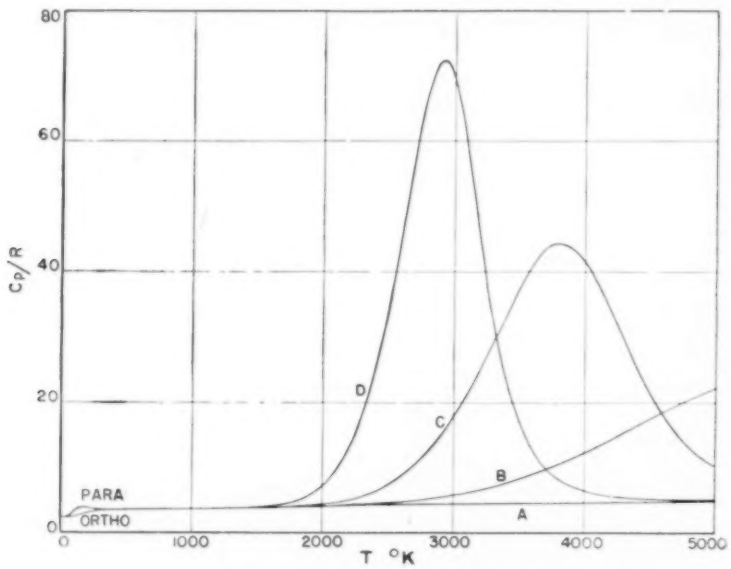

FIGURE 4. *Curves showing effect of dissociation on specific heat of* H_2.

2.12, when used with table values of the entropy and free energy of molecular H_2, HD, and D_2, in the calculation of equilibrium constants for dissociation. Accordingly for H,

$$-\frac{F^\circ - E_0^\circ}{RT} = \frac{5}{2} \ln T - 2.2663 \text{ and } \frac{S^\circ}{R} = \frac{5}{2} \ln T + 0.2337, \quad (3.5)$$

and for D,

$$-\frac{F^\circ - E_0^\circ}{RT} = \frac{5}{2} \ln T - 0.8223 \text{ and } \frac{S^\circ}{R} = \frac{5}{2} \ln T + 1.6777 \quad (3.6)$$

in the ideal gas state at a pressure of 1 atm for the range of temperatures covered by the tables.

1. Dissociation of H_2, D_2, and HD

The chemical equations for dissociation and the corresponding mass action equations are

$$\text{(a) } H_2 \rightleftarrows 2H; \quad \frac{P_H^2}{P_{H_2}} = K_{H_2}. \quad (3.7)$$

$$\text{(b) } D_2 \rightleftarrows 2D; \quad \frac{P_D^2}{P_{D_2}} = K_{D_2}. \quad (3.8)$$

$$\text{(c) } HD \rightleftarrows H + D; \quad \frac{P_H P_D}{P_{HD}} = K_{HD}. \quad (3.9)$$

For these reactions, ΔE_0° of eq 3.3 is the difference between the internal energy of 2 moles of dissociated atoms and 1 mole of molecules in the rotational-vibrational state $J=0$, $v=0$. Beutler's value [21], $36{,}116 \pm 6$ cm^{-1}, was accepted for the dissociation of H_2 from its ground state. Assuming that the total depth of the potential energy curve is the same for H_2, HD, and D_2, the dissociation energies of HD and D_2 were obtained from the zero-point vibrational energies. These zero point energies were calculated by adding to G_0 (see eq 2.17), the term which Dunham [10] included in the energy of the ground state relative to the bottom of the potential energy curve and designated Y_{00} in his system. The values thus obtained for the zero point energies of H_2, HD, and D_2 were respectively 2,179.6, 1,891.0, 1,546.6 cm^{-1}, and the corresponding energies of dissociation for HD and D_2 from the ground state $36{,}404._6$ and $36{,}749._0$ cm^{-1}, respectively.

The heats of dissociation of H_2, HD, and D_2 in the ideal gas state at temperature T are equal to $\Delta E_0^\circ + 5RT - (H^\circ - E_0^\circ)$, where $(H^\circ - E_0^\circ)$ is the table value of the enthalpy at temperature T. The heats of dissociation at 0° and 298.16° K are given in table 11. The theoretical value for the heat of dissociation of n-H_2 at 298° K agrees well with the calorimetric value $105{,}000 \pm 3{,}500$ cal mole^{-1} obtained by Bichowsky and Copeland [47].

On the assumption that the atomic and molecular forms of hydrogen and deuterium are individually ideal gases, the fraction of the originally totally nondissociated hydrogen which has dissociated is $\sqrt{K/(K+4P)}$, where K is the dissociation constant and P is the total pressure in atmospheres.

The dissociation constants K and fractions of originally undissociated diatomic molecules, dissociated at 1-atmosphere pressure, are given in table 10 for H_2, HD, and D_2.

The experimental values of the equilibrium dissociation constants of H_2 as determined by Langmuir and Mackay [32], and by Langmuir [39], are in agreement with the theoretical values of table 10. Langmuir's x-values are 0.17 percent at

TABLE 10. *Dissociation constants, K, and fraction dissociated, x, at 1-atm pressure*

T°K	K	x
	atm	
For $H_2 \rightleftarrows 2H$		
300	18.39×10^{-72}	21.44×10^{-37}
500	4.939×10^{-41}	3.514×10^{-21}
1,000	5.174×10^{-18}	1.137×10^{-9}
1,500	3.100×10^{-10}	8.675×10^{-6}
2,000	2.641×10^{-6}	8.125×10^{-4}
3,000	2.480×10^{-2}	0.07850
4,000	2.5236	.6220
5,000	41.038	.9546
For $HD \rightleftarrows H + D$		
300	2.732×10^{-72}	8.264×10^{-37}
500	1.265×10^{-41}	1.779×10^{-21}
1,000	1.987×10^{-18}	7.048×10^{-10}
1,500	1.350×10^{-10}	5.810×10^{-6}
2,000	1.215×10^{-6}	5.512×10^{-4}
For $D_2 \rightleftarrows 2D$		
300	1.319×10^{-72}	5.742×10^{-37}
500	1.171×10^{-41}	1.711×10^{-21}
1,000	2.972×10^{-18}	8.620×10^{-10}
1,500	2.330×10^{-10}	7.632×10^{-6}
2,000	2.227×10^{-6}	7.462×10^{-4}

2,000° K, 1.6 percent at 2,500° K, 7.2 percent at 3,000° K, and 21 percent at 3,500° K.

TABLE 11. *Heats of dissociation of* H_2, HD, *and* D_2 *in cal mole*$^{-1}$

T	p-H_2	o-H_2	n-H_2	HD	o-D_2	p-D_2	n-D_2
°K							
0	103, 239	102, 900	102, 985	104, 064	105, 048	104, 877	104, 991
298.16	104, 191	104, 173	104, 177	104, 992	105, 962	105, 962	105, 962

An equation of state for 1 mole of molecular H_2, HD, or D_2 capable of forming 2 moles of atoms when completely dissociated, assuming as before that atoms and molecules individually behave as ideal gases, is

$$\frac{PV}{RT}=1+\sqrt{\frac{K}{K+4P}} \tag{3.10}$$

or

$$\frac{PV}{RT}=1-\frac{KV}{8RT}\left(1-\sqrt{1+16\,\frac{RT}{KV}}\right), \tag{3.11}$$

where K is a function of T determined by eq 3.3 and V is the volume per $2N_0$ atoms uncombined or combined as molecules.

The thermodynamic properties of an equilibrium mixture of atomic and molecular hydrogen in the ideal gas state can in principle be calculated from the properties of atomic hydrogen at low pressures and the equation of state (eq 3.10) or (eq. 3.11). It is simpler, however, to determine the properties of the mixture from the properties of the atomic and molecular varieties and the fraction dissociated.

The equation given by Epstein [30] for the heat capacity of a reacting gas mixture, when applied to the heat capacity of an equilibrium mixture of atomic and molecular hydrogen, is

$$\frac{(C_p^\circ)_{\text{mixture}}}{R}=2x\,\frac{(C_p^\circ)_{\text{atomic}}}{R}+(1-x)\,\frac{(C_p^\circ)_{\text{molecular}}}{R}+\frac{(1-x^2)x}{2}\left[2\,\frac{(H^\circ)_{\text{atomic}}}{RT}-\frac{(H^\circ)_{\text{molecular}}}{RT}\right]^2, \tag{3.12}$$

where x is the fraction of the originally totally nondissociated hydrogen that has dissociated, $(C_p^\circ)_{\text{atomic}}$ and $(C_p^\circ)_{\text{molecular}}$ are heat capacities per mole of atoms and molecules respectively in the ideal gas state, and $(C_p^\circ)_{\text{mixture}}$ is for a mixture containing $2N_0$ of atoms combined or uncombined, the components being in the ideal gas state. $(C_p^\circ)_{\text{mixture}}$ is a function of P as well as T since x is a function of P. In figure 4, curves D, C, and B show the variation of $(C_p^\circ/R)_{\text{mixture}}$ for H_2 with temperature for pressures of 0.01, 1, and 100 atmospheres, respectively. Curve A drawn for comparison is the heat capacity of 1 mole of undissociated H_2, that is, $(C_p^\circ/R)_{\text{molecular}}$. It appears from these curves that when dissociation has its greatest importance, thermal effects originating in other ways are likely to be dwarfed by comparison. Wildt [19] has calculated the ratio of specific heats of hydrogen at high temperatures using principles similar to those employed here. The results obtained have application to stellar atmospheres.

2. Ortho-Para Equilibrium

$$o\text{-}H_2 \leftrightarrows p\text{-}H_2,\ \frac{P_{p\text{-}H_2}}{P_{o\text{-}H_2}}=\left(\frac{p\text{-}H_2}{o\text{-}H_2}\right)=K_1 \tag{3.13}$$

$$p\text{-}D_2 \leftrightarrows o\text{-}D_2,\ \frac{P_{o\text{-}D_2}}{P_{p\text{-}D_2}}=\left(\frac{o\text{-}D_2}{p\text{-}D_2}\right)=K_2 \tag{3.14}$$

The equilibrium constants of the ortho-para conversion of H_2 and D_2 in the ideal gas state are independent of P. Accordingly, pressure does not appreciably change the ortho-para ratio under equilibrium conditions. Although the lowest rotational levels of the ortho and para varieties differ, ΔE_0° for the two reactions (eq 3.13 and eq 3.14) is zero, because in the calculations for both the ortho and para varieties the ground state of the molecule, $J=0$ and $v=0$, was arbitrarily selected as the origin of energies.

In table 12 are given values of the percentage para composition in the ideal gas state of equilibrium mixtures of ortho-para varieties calculated from the state-sums, $\Sigma g_j \epsilon^{-\epsilon_j/kT}$, see eq 2.2 and eq 2.14. These values are in close agreement with earlier values obtained by Harkness and Deming [11] and are in agreement with the variations in the relative intensities of the ortho-para spectral lines and with estimates of the ortho-para compositions based on measurements of thermal conduction from heated wires. The success in explaining the heat capacity of gaseous hydrogen at moderate and low temperatures is also corroborating evidence for table 12 [48].

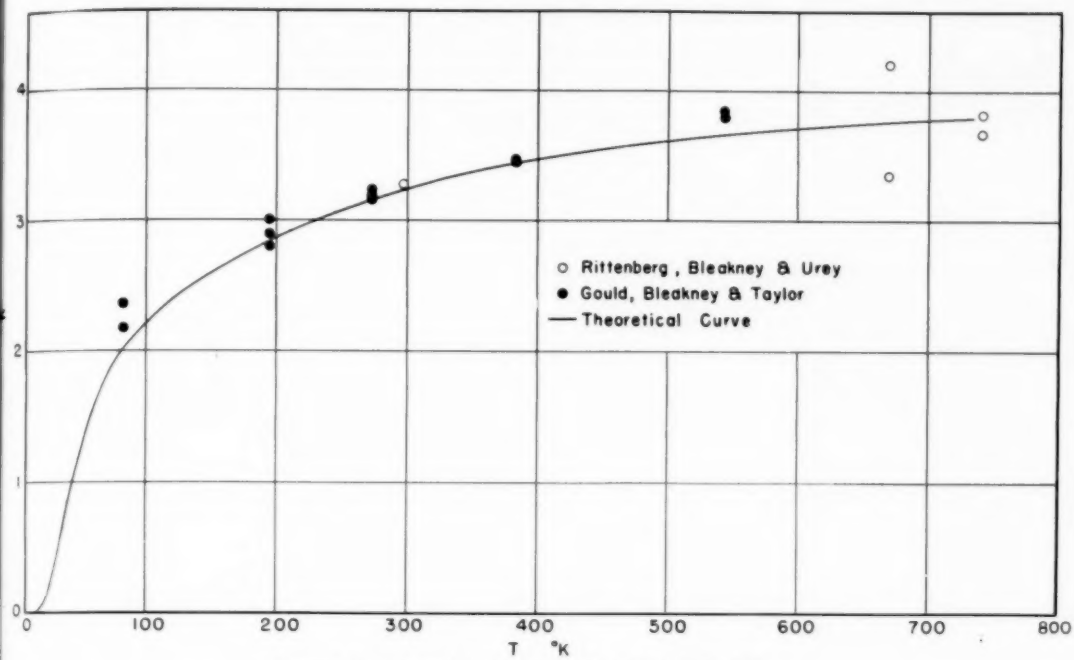

FIGURE 5. *The equilibrium constant for* $H_2+D_2 \rightleftarrows 2HD$.

TABLE 12. *Ortho-para composition at equilibrium*

T	Percentage in para form for H_2	Percentage in para form for D_2
°K		
10	99.9999	0.0277
20	99.821	1.998
20.39	99.789	.....
23.57	.....	3.761
30	97.021	7.864
33.19	95.034	.....
40	88.727	14.784
50	77.054	20.718
60	65.569	25.131
70	55.991	28.162
80	48.537	30.141
90	42.882	31.395
100	38.620	32.164
120	32.959	32.916
150	28.603	33.246
200	25.974	33.327
250	25.264	.....
298.16	25.075	33.333
300	25.072	33.333
350	25.019	.....
400	25.005	.....
500	25.000	.....

3. Isotopic Exchange

The chemical and mass action equations for isotopic exchange are

$$H_2+D_2 \rightleftarrows 2HD; \quad \frac{P_{HD}^2}{P_{H_2}P_{D_2}} = \frac{(HD)^2}{(H_2)(D_2)} = K_{ex}. \qquad (3.15)$$

The equilibrium constant K_{ex} of the isotopic exchange reaction (eq 3.15) is related to the dissociation constants K of eq 3.7, 3.8, and 3.9 by the equation

$$K_{ex} = \frac{K_{H_2}K_{D_2}}{K_{HD}^2}. \qquad (3.16)$$

The equilibrium constant K_{ex} for isotopic exchange in the ideal gas state is independent of P, and accordingly the relative equilibrium concentrations of H_2, HD, and D_2 are also independent of pressure in the ideal gas state. For this reaction the ΔE_0° of eq 3.3, the difference between twice the energy of the ground state of HD minus the sum of the energies of the ground states of H_2 and D_2, is equal to twice the zero-point vibrational energy of HD minus the sum of the zero-point vibrational energies of H_2 and D_2. Using the values given in section III, 1 for the zero point energies, ΔE_0° is 159.5 cal for the formation of 2 moles of HD.

In figure 5 are plotted experimental values of K_{ex}, whereas the curve was derived from spectroscopic data as has been indicated. The data of Rittenberg, Bleakney, and Urey [54] were obtained from measurements on hydrogen-deuterium mixtures prepared by the decomposition of mix-

tures of HI and DI, and those of Gould, Bleakney, and Taylor [55] were obtained with mixtures of hydrogen and deuterium that had been adsorbed on various catalysts or had been diffused through palladium. Some of the observations of Gould, Bleakney, and Taylor plotted in figure 5 were not plotted by them in their published article.

Although the theoretical curve of figure 5 is thought to be more reliable than the experimental data, it is to be pointed out that the uncertainties in the zero-point energies of H_2, HD, and D_2 can give rise to perceptible shifts in the curve. Thus a change in ΔE_0° of 3 cal mole^{-1}, which is equivalent to about 1 cm^{-1} in $2(G_0)_{HD}-(G_0)_{H_2}-(G_0)_{D_2}$, changes K_{ex} by about 1.5 percent at 100° K. It seems doubtful that ΔE_0° is known better than to a very few calories per mole, for while it is plausible, it is apparently not certain that D_e, the dissociation energy above the minimum of the potential energy curve, is so nearly the same for H_2, HD, and D_2 [25]. The theoretical values of Urey and Rittenberg [13] are, therefore, practically as reliable as the newly calculated ones.

IV. PVT Data and Relations for Hydrogen and Deuterium

In order to calculate the thermodynamic properties of gaseous hydrogen at high densities (in principle at any densities other than very low) from values of the properties for the hypothetical ideal gaseous state, it is necessary to have information concerning the relations between pressure, volume, and temperature for each temperature in question extending from very low to high densities.

1. Hydrogen

The available PVT data for hydrogen fall between 14° and 700° K. They consist, in general, of measurements of volume of known amounts of gas at several different pressures along selected isotherms. The quantities usually reported are values of PV or PV/P_0V_0 at the measured pressures or densities. In this report this information is presented in the form of tables in which integral values of the variables of state are spaced closely enough to allow accurate interpolation.

The dependent variable Z appearing in the tables is PV/RT. Through the definition of Z this quantity has the value 1 at extremely low densities, and it is of the same order of magnitude over a very extended range of densities. The independent variables chosen are T, the Kelvin temperature, and ρ, the Amagat density, which is defined as the ratio of the observed density to the density at standard conditions (0°C and 1 atmosphere). Density was chosen as an independent variable of state in preference to pressure because this resulted in simpler representation of the PV/RT isotherms. The Amagat density is also the ratio of the volume V_0 of the gas at standard conditions to its observed volume.

$$=\frac{\text{observed density}}{\text{density at standard conditions}}=\frac{V_0}{V}. \quad (4.1)$$

The best value for V_0, the molar volume of hydrogen at standard conditions, is 22.4279 liters or 22428.5 cm^3, according to the values of RT obtained by Cragoe [90] and the value of PV/RT for hydrogen at standard conditions as given by Cragoe and the present correlation. The density of hydrogen at standard conditions is 0.089885 gram liter^{-1}.

Values of PV/RT, or Z for n-H_2 are given in table 13 for different values of T and ρ. Corresponding values of P and of the derivatives $(dZ/dT)_\rho$, $(d^2Z/dT^2)_\rho$ and $(dZ/d\rho)_T$ needed for the calculation of some of the more important thermal properties of the real gas from ideal gas values (see section V) are given as functions of the same variables of state ρ and T in tables 14, 15, 16, and 17, respectively. The temperature intervals used are of graduated size, being as small as 2 degrees at low temperatures and as much as 20 deg above 0° C. The density intervals, except for entries at $\rho=1$, 2, 3, 6, and 10, are uniformly equal to 20 Amagats from $\rho=0$ to $\rho=500$.

TABLE 13. *Values of $Z = PV/RT$ for hydrogen at integral values of T, the absolute temperature, and ρ, the density in Amagat units*

Temperature	$\rho=1$	2	3	6	10	20	40	60	80	100	120	140	160	180	200
°K															
16	0.906004	0.081826	0.972765												
18	.992269	.984612	.976940	0.95401											
20	.993573	.986758	.980157	.96043	0.93430										
22	.994225	.988160	.982708	.96552	.94274										
24	.994917	.989846	.984783	.96965	.94962	0.90021									
26	.995492	.990894	.986505	.97309	.95532	.91150	.8265								
28	.995977	.991862	.987955	.97598	.96012	.92100	.8452	0.7724							
30	.996389	.992784	.989187	.97844	.96420	.92910	.8610	.7958	0.7334	0.6739					
32	.996742	.993499	.990245	.98055	.96771	.93606	.8747	.8159	.7698	.7092	0.6551	0.6067	0.5699	0.5176	
34	.997048	.994102	.991162	.98238	.97075	.94209	.8866	.8334	.7826	.7342	.6882	.6446	.6033	.5644	0.5279
36	.997315	.994636	.991962	.98397	.97340	.94735	.8969	.8487	.8025	.7587	.7171	.6777	.6404	.6054	.5726
38	.997550	.995104	.992664	.98537	.97573	.95197	.90598	.8620	.8201	.7803	.7426	.7089	.6732	.6415	.6119
40	.997758	.995520	.993287	.98692	.97779	.95606	.91403	.8739	.8357	.7995	.7652	.7328	.7023	.6737	.6470
42	.997943	.995892	.993844	.98773	.97964	.95972	.92125	.8846	.8497	.8166	.7854	.7560	.7284	.7026	.6786
	$\rho=220$	240	260	280	300	320	340	360	380	400	420	440	460	480	500
34	0.4937	0.4619	.434327	0.4062	0.3825	0.3613	0.3425	0.3259	0.3115	0.2992	0.2880	0.2808	0.2768	0.2717	0.2724
36	.5419	.5135	.4875	.4639	.4428	.4239	.4071	.3924	.3800	.3700	.3624	.3573	.3547	.3550	.3590
38	.5844	.5391	.5090	.5151	.4866	.4709	.4652	.4525	.4421	.4343	.4292	.4268	.4272	.4305	.4374
40	.6224	.5998	.5704	.5610	.5446	.5302	.5178	.5073	.4990	.4933	.4905	.4904	.4933	.4992	.5085
42	.6565	.6364	.6183	.6021	.5880	.5758	.5657	.5574	.5512	.5476	.5468	.5488	.5537	.5617	.5730
	$\rho=520$	540	560	580	600	620	640	660	680	700					
34	0.2775	0.2878	0.3038	0.3258	0.3544	0.3913	0.4385	0.4971	0.5678	0.6512					
36	.3675	.3809	.3995	.4242	.4557	.4944	.5406	.5947							
38	.4489	.4657	.4882	.5167	.5520										
40	.5225	.5421	.5682												
42	.5890	.6110													

TABLE 13. *Values of $Z=PV/RT$ for hydrogen at integral values of T, the absolute temperature, and ρ, the density in Amagat units*—Continued

Temperature	$\rho=1$	2	3	6	10	20	40	60	80	100	120	140	160	180	200
°K															
42	0.997943	0.995892	0.993844	0.98773	0.97964	0.95972	0.92125	0.8846	0.8497	0.8166	0.7854	0.7560	0.7284	0.7026	0.6786
44	.998116	.996226	.994344	.98873	.98130	.96302	.92775	.8942	.8623	.8321	.8037	.7770	.7520	.7287	.7071
46	.998261	.996528	.994798	.98963	.98280	.96601	.93364	.90288	.8737	.8462	.8204	.7961	.7734	.7524	.7330
48	.998399	.996802	.995209	.990453	.98417	.96872	.93898	.91079	.8841	.8560	.8355	.8135	.7929	.7740	.7567
50	.998524	.997052	.995583	.991199	.98541	.97118	.94384	.91798	.8936	.8707	.8493	.8293	.8108	.7938	.7783
52	.998638	.997280	.995925	.991881	.98654	.97342	.94827	.92455	.90224	8814	.8619	.8438	.8272	.8120	.7982
54	.998743	.997488	.996238	.992507	.98758	.97549	.95235	.93060	.91018	.8911	.8735	.8572	.8422	.8287	.8165
56	.998839	.997682	.996528	.993086	.98854	.97742	.95615	.93620	.91755	.90020	.8842	.8695	.8560	.8440	.8334
58	.998930	.997863	.996800	.993628	.98944	.97920	.95966	.94138	.92436	.90859	.8941	.8808	.8688	.8582	.8490
60	.999013	.998030	.997049	.994125	.99027	.98084	.96289	.94615	.93062	.91631	.90323	.8914	.8808	.8715	.8636
65	.999196	.998394	.997595	.995214	.99208	.98443	.96998	.95669	.94454	.93351	.92363	.91492	.90736	.90102	.8960
70	.999348	.998699	.998053	.996129	.99360	.98746	.97597	.96555	.95619	.94793	.94077	.93473	.92983	.92613	.9237
75	.999479	.998960	.998444	.996910	.99490	.99004	.98106	.97308	.96611	.96020	.95537	.95163	.94904	.94764	.9475
80	.999590	.999182	.998776	.997573	.99600	.99224	.98543	.97958	.97470	.97082	.96798	.96623	.96561	.96617	.9680
85	.999686	.999374	.999065	.998151	.99696	.99415	.98923	.98523	.98217	.98007	.97899	.97895	.98002	.98225	.9857
90	.999770	.999542	.999318	.998656	.99780	.99583	.99255	.99017	.98871	.98819	.98865	.99011	.99266	.99635	1.0012
95	.999844	.999690	.999539	.999098	.99854	.99730	.99548	.99454	.99449	.99536	.99719	.99999	1.00386	1.00884	1.0150
100	.999909	.999821	.999735	.999489	.99919	.99860	.99807	.99841	.99962	1.00173	1.00477	1.00878	1.01385	1.02004	1.0274
105	.999968	.999940	.999911	.999841	.99978	.99977	1.00038	1.00186	1.00420	1.00741	1.01154	1.01665	1.02280	1.03006	1.0385
110	1.000021	1.000046	1.000070	1.000158	1.00031	1.00082	1.00246	1.00495	1.00830	1.01250	1.01762	1.02371	1.03084	1.03905	1.0484
115	1.000068	1.000141	1.000212	1.000442	1.00078	1.00176	1.00434	1.00775	1.01200	1.01710	1.02311	1.03009	1.03808	1.04713	1.0573
120	1.000112	1.000228	1.000343	1.000703	1.00121	1.00262	1.00604	1.01028	1.01535	1.02127	1.02809	1.03586	1.04464	1.05445	1.0653
125	1.000152	1.000307	1.000463	1.000943	1.00161	1.00341	1.00760	1.01260	1.01842	1.02509	1.03265	1.04114	1.05062	1.06113	1.0727
130	1.000188	1.000379	1.000572	1.001160	1.00197	1.00413	1.00903	1.01473	1.02124	1.02860	1.03684	1.04599	1.05610	1.06725	1.0794
135	1.000221	1.000444	1.000672	1.001356	1.00230	1.00479	1.01035	1.01668	1.02383	1.03183	1.04069	1.05044	1.06113	1.07285	1.0856
140	1.000252	1.000505	1.000763	1.001542	1.00261	1.00540	1.01155	1.01847	1.02621	1.03479	1.04422	1.05453	1.06578	1.07797	1.0912
145	1.000280	1.000562	1.000847	1.001710	1.00289	1.00596	1.01267	1.02014	1.02842	1.03753	1.04748	1.05830	1.07002	1.08269	1.0964
150	1.000307	1.000615	1.000926	1.001868	1.00315	1.00648	1.01370	1.02168	1.03047	1.04007	1.05050	1.06179	1.07396	1.08707	1.1012
155	1.000332	1.000665	1.001000	1.002016	1.00340	1.00697	1.01467	1.02312	1.03237	1.04242	1.05330	1.06502	1.07762	1.09114	1.1057
160	1.000355	1.000711	1.001069	1.002154	1.00363	1.00743	1.01558	1.02447	1.03413	1.04469	1.05590	1.06803	1.08102	1.09492	1.1098
165	1.000376	1.000754	1.001133	1.002282	1.00384	1.00785	1.01641	1.02571	1.03577	1.04693	1.05831	1.07082	1.08417	1.09841	1.1136
170	1.000396	1.000793	1.001192	1.002398	1.00403	1.00823	1.01716	1.02684	1.03728	1.04850	1.06052	1.07338	1.08710	1.1016	1.1172
180	1.000430	1.000862	1.001296	1.002607	1.00438	1.00893	1.01856	1.02891	1.04001	1.05186	1.06451	1.07797	1.09226	1.1074	1.1235
190	1.000462	1.000925	1.001390	1.002795	1.00469	1.00955	1.01978	1.03072	1.04238	1.05478	1.06796	1.08193	1.09671	1.1124	1.1289
200	1.000490	1.000981	1.001474	1.002962	1.00497	1.01010	1.02085	1.03231	1.04447	1.05735	1.07100	1.08541	1.1006	1.1167	1.1336
210	1.000515	1.001031	1.001548	1.003108	1.00521	1.01058	1.02181	1.03372	1.04632	1.05964	1.07370	1.08850	1.1041	1.1205	1.1378
220	1.000537	1.001075	1.001614	1.003240	1.00543	1.01102	1.02267	1.03499	1.04798	1.06167	1.07610	1.09125	1.1072	1.1239	1.1415
230	1.000556	1.001113	1.001673	1.003358	1.00563	1.01141	1.02344	1.03611	1.04945	1.06348	1.07823	1.09370	1.1099	1.1270	1.1448
240	1.000573	1.001147	1.001725	1.003463	1.00580	1.01175	1.02411	1.03710	1.05076	1.06508	1.08011	1.09587	1.1124	1.1297	1.1477
250	1.000589	1.001178	1.001771	1.003555	1.00596	1.01205	1.02470	1.03798	1.05191	1.06649	1.08177	1.09777	1.11451	1.1320	1.1502
260	1.000602	1.001206	1.001812	1.003637	1.00609	1.01232	1.02523	1.03877	1.05293	1.06775	1.08325	1.09945	1.11638	1.1341	1.1525
270	1.000614	1.001231	1.001848	1.003709	1.00621	1.01257	1.02572	1.03948	1.05386	1.06889	1.08459	1.10100	1.11815	1.1360	1.1546

260	1.000612	1.001206	1.001812	1.003637	1.00600	1.01252	1.02523	1.03877	1.05283	1.06775	1.08325	1.09945	1.11638	1.1341	1.1525
270	1.000614	1.001231	1.001848	1.003709	1.006211	1.01257	1.02572	1.03948	1.05386	1.06889	1.08459	1.10098	1.11809	1.13594	1.15455
0° C	1.000618	1.001238	1.001859	1.003731	1.006247	1.01264	1.02586	1.03969	1.05414	1.06923	1.08499	1.10143	1.11859	1.13648	1.15514
280	1.000626	1.001254	1.001882	1.003777	1.006324	1.01279	1.02616	1.04012	1.05471	1.06992	1.08580	1.10255	1.11961	1.13760	1.15635
37.5° C	1.000644	1.001290	1.001936	1.003886	1.006508	1.01315	1.02685	1.04114	1.05603	1.07154	1.08768	1.10449	1.12199	1.14019	1.15913
300	1.000646	1.001293	1.001942	1.003896	1.006520	1.01318	1.02692	1.04124	1.05615	1.07169	1.08786	1.10469	1.12220	1.14043	1.15938
320	1.000652	1.001326	1.001991	1.003994	1.006683	1.01350	1.02755	1.04215	1.05734	1.07313	1.08953	1.10658	1.12429	1.14269	1.16179
340	1.000676	1.001354	1.002032	1.004076	1.006819	1.01377	1.02807	1.04291	1.05832	1.07431	1.09091	1.10812	1.12598	1.14451	1.16373
360	1.000688	1.001377	1.002067	1.004145	1.006934	1.01400	1.02851	1.04355	1.05914	1.07529	1.09204	1.10938	1.12736	1.14598	1.16527
100° C	1.000694	1.001390	1.002086	1.004183	1.006999	1.01412	1.02875	1.04390	1.05960	1.07584	1.09267	1.11000	1.12812	1.14679	1.16611
380	1.000697	1.001396	1.002096	1.004203	1.007030	1.01418	1.02887	1.04407	1.05981	1.07610	1.09297	1.11042	1.12848	1.14716	1.16650
400	1.000706	1.001413	1.002121	1.004253	1.007112	1.01434	1.02918	1.04452	1.06038	1.07678	1.09373	1.11126	1.12938	1.14812	1.16748
420	1.000713	1.001427	1.002142	1.004294	1.007181	1.01448	1.02944	1.04489	1.06085	1.07734	1.09436	1.11195	1.13012	1.14888	1.16826
440	1.000719	1.001439	1.002160	1.004336	1.007240	1.01459	1.02966	1.04520	1.06124	1.07780	1.09488	1.11251	1.13071	1.14948	1.16886
460	1.000724	1.001449	1.002175	1.004360	1.007290	1.01469	1.02984	1.04546	1.06157	1.07818	1.09531	1.11297	1.13118	1.14996	1.16932
480	1.000728	1.001458	1.002188	1.004385	1.007332	1.01477	1.03000	1.04568	1.06184	1.07849	1.09565	1.11333	1.13155	1.15032	1.16966
500	1.000732	1.001465	1.002199	1.004408	1.007367	1.01484	1.03013	1.04586	1.06206	1.07875	1.09593	1.11361	1.13183	1.15059	1.16991
520	1.000735	1.001471	1.002208	1.004426	1.007397	1.01490	1.03023	1.04601	1.06225	1.07895	1.09614	1.11383	1.13204	1.15078	1.17006
540	1.000737	1.001476	1.002216	1.004441	1.007423	1.01495	1.03032	1.04613	1.06239	1.07911	1.09631	1.11399	1.13219	1.15090	1.17015
560	1.000740	1.001481	1.002222	1.004454	1.007444	1.01499	1.03040	1.04623	1.06251	1.07924	1.09643	1.11411	1.13228	1.15096	1.17017
580	1.000741	1.001484	1.002228	1.004465	1.007462	1.01502	1.03046	1.04631	1.06260	1.07933	1.09652	1.11418	1.13233	1.15098	1.17014
600	1.000743	1.001487	1.002232	1.004474	1.007476	1.01505	1.03050	1.04637	1.06266	1.07939	1.09657	1.11421	1.13233	1.15095	1.17006

TABLE 13. *Values of $Z = PV/RT$ for hydrogen at integral values of T, the absolute temperature, and ρ, the density in Amagat units*—Continued

Temperature	ρ=220	240	260	280	300	320	340	360	380	400	420	440	460	480	500
°K															
42	0.6565	0.6364	0.6183	0.6021	0.5880	0.5758	0.5657	0.5574	0.5512	0.5476	0.5468	0.5488	0.5537	0.5617	0.5730
44	.6874	.6695	.6535	.6394	.6274	.6174	.6094	.6033	.5992	.5976	.5987	.6025	.6091	.6187	.6315
46	.7154	.6996	.6856	.6734	.6633	.6553	.6494	.6454	.6433	.6435	.6464	.6518	.6599	.6707	.6846
48	.7410	.7270	.7149	.7046	.6962	.6901	.6861	.6840	.6837	.6857	.6902	.6971	.7064	.7183	.7331
50	.7644	.7522	.7417	.7332	.7265	.7220	.7198	.7194	.7208	.7244	.7304	.7386	.7490	.7620	.7777
52	.7860	.7754	.7665	.7594	.7544	.7515	.7507	.7518	.7547	.7598	.7672	.7766	.7882	.8022	.8188
54	.8059	.7968	.7894	.7838	.7802	.7787	.7791	.7815	.7858	.7922	.8008	.8114	.8242	.8392	.8568
56	.8242	.8166	.8106	.8064	.8041	.8037	.8053	.8088	.8143	.8219	.8316	.8433	.8572	.8733	.8919
58	.8412	.8350	.8303	.8273	.8262	.8269	.8296	.8342	.8408	.8494	.8601	.8729	.8878	.9049	.9245
60	.8572	.8522	.8488	.8470	.8470	.8488	.8525	.8582	.8658	.8754	.8871	.9008	.9167	.9348	.9552
65	.8925	.8906	.8902	.8912	.8938	.8982	.9043	.9123	.9223	.9342	.9482	.9643	.9826	1.0032	1.0262
70	.9228	.9234	.9254	.9289	.9339	.9406	.9489	.9591	.9712	.9852	1.0012	1.0194	1.0397	1.0623	1.0874
75	.9488	.9515	.9556	.9611	.9681	.9768	.9872	.9994	1.0133	1.0291	1.0469	1.0668	1.0889	1.1132	1.1400
80	.9711	.9756	.9815	.9888	.9976	1.0080	1.0201	1.0339	1.0495	1.0669	1.0861	1.1075	1.1311	1.1568	1.1850
85	.9904	.9965	1.0040	1.0128	1.0232	1.0350	1.0485	1.0635	1.0806	1.0994	1.1199	1.1425	1.1672	1.1941	1.2234
90	1.0074	1.0148	1.0236	1.0339	1.0456	1.0587	1.0733	1.0896	1.1077	1.1275	1.1493	1.1730	1.1986	1.2265	1.2568
95	1.0224	1.0311	1.0411	1.0525	1.0653	1.0795	1.0953	1.1127	1.1317	1.1525	1.1752	1.1999	1.2264	1.2551	1.2863
100	1.0359	1.0457	1.0567	1.0691	1.0829	1.0981	1.1148	1.1332	1.1531	1.1748	1.1983	1.2238	1.2511	1.2806	1.3125
105	1.0481	1.0588	1.0707	1.0840	1.0987	1.1148	1.1323	1.1514	1.1722	1.1947	1.2189	1.2450	1.2732	1.3034	1.3358
110	1.0589	1.0705	1.0833	1.0974	1.1128	1.1297	1.1480	1.1678	1.1893	1.2124	1.2373	1.2640	1.2929	1.3236	1.3565
115	1.0686	1.0810	1.0946	1.1094	1.1256	1.1431	1.1620	1.1825	1.2046	1.2283	1.2538	1.2811	1.3104	1.3416	1.3750
120	1.0773	1.0905	1.1048	1.1203	1.1371	1.1552	1.1747	1.1957	1.2184	1.2427	1.2687	1.2965	1.3262	1.3579	1.3916
125	1.0854	1.0991	1.1140	1.1302	1.1475	1.1662	1.1862	1.2077	1.2309	1.2557	1.2821	1.3103	1.3404	1.3725	1.4065
130	1.0927	1.1070	1.1224	1.1391	1.1570	1.1762	1.1967	1.2187	1.2423	1.2675	1.2943	1.3228	1.3533	1.3856	1.4199
135	1.0994	1.1142	1.1301	1.1473	1.1656	1.1853	1.2063	1.2287	1.2527	1.2782	1.3053	1.3341	1.3648	1.3974	1.4319
140	1.1055	1.1208	1.1372	1.1548	1.1736	1.1936	1.2150	1.2378	1.2621	1.2879	1.3153	1.3444	1.3753	1.4081	1.4428
145	1.1111	1.1269	1.1438	1.1618	1.1810	1.2014	1.2231	1.2462	1.2707	1.2968	1.3245	1.3539	1.3850	1.4179	1.4527
150	1.1163	1.1325	1.1498	1.1681	1.1877	1.2085	1.2305	1.2539	1.2787	1.3051	1.3330	1.3626	1.3939	1.4269	1.4618
155	1.1212	1.1377	1.1553	1.1740	1.1939	1.2150	1.2373	1.2610	1.2861	1.3127	1.3408	1.3705	1.4019	1.4351	1.4701
160	1.1257	1.1426	1.1605	1.1795	1.1997	1.2211	1.2436	1.2675	1.2928	1.3195	1.3478	1.3776	1.4091	1.4424	1.4776
165	1.1299	1.1471	1.1653	1.1846	1.2050	1.2267	1.2495	1.2737	1.2992	1.3260	1.3542	1.3841	1.4157	1.4490	1.4841
170	1.1337	1.1512	1.1697	1.1892	1.2098	1.2316	1.2547	1.2790	1.3046	1.3316	1.3601	1.3901	1.4216	1.4548	1.4899
180	1.1405	1.1585	1.1774	1.1974	1.2184	1.2406	1.2640	1.2886	1.3145	1.3418	1.3705	1.4007	1.4323	1.4655	1.5005
190	1.1463	1.1647	1.1840	1.2044	1.2258	1.2483	1.2720	1.2969	1.3230	1.3505	1.3794	1.4097	1.4414	1.4747	1.5097
200	1.1514	1.1701	1.1898	1.2105	1.2322	1.2550	1.2790	1.3041	1.3305	1.3581	1.3871	1.4175	1.4493	1.4827	1.5177
210	1.1559	1.1749	1.1949	1.2159	1.2379	1.2610	1.2852	1.3105	1.3370	1.3648	1.3939	1.4244	1.4563	1.4897	1.5247
220	1.1599	1.1793	1.1995	1.2207	1.2430	1.2663	1.2906	1.3161	1.3428	1.3707	1.3999	1.4304	1.4624	1.4958	1.5307
230	1.1635	1.1831	1.2036	1.2250	1.2474	1.2709	1.2954	1.3210	1.3478	1.3758	1.4051	1.4357	1.4676	1.5010	1.5359
240	1.1666	1.1864	1.2071	1.2287	1.2512	1.2749	1.2996	1.3253	1.3522	1.3802	1.4096	1.4402	1.4721	1.5055	1.5403
250	1.1693	1.1893	1.2102	1.2319	1.2546	1.2784	1.3031	1.3288	1.3559	1.3840	1.4134	1.4440	1.4759	1.5092	1.5440
260	1.1718	1.1919	1.2129	1.2348	1.2576	1.2814	1.3062	1.3321	1.3591	1.3872	1.4166	1.4472	1.4790	1.5122	1.5469
270	1.17397	1.19420	1.21530	1.23728	1.26020	1.28407	1.30894	1.33486	1.36185	1.38998	1.41927	1.44980	1.48160	1.51473	1.54925
0°C	1.17560	1.19587	1.21701	1.23903	1.26194	1.28583	1.31070	1.33660	1.36357	1.39165	1.42088	1.45130	1.48295	1.51589	1.55016
280	1.17688	1.19723	1.21841	1.24048	1.26343	1.28737	1.31229	1.33819	1.36518	1.39327	1.42252	1.45296	1.48466	1.51769	1.55203
20°C	1.17883	1.19932	1.22053	1.24279	1.26583	1.28979	1.31470	1.34060	1.36752	1.39552	1.42465	1.45499	1.48658	1.51913	1.55316

20° C.																		
200	1.17883	1.19022	1.22063	1.24279	1.26583	1.29079	1.31479	1.34093	1.36752	1.39552	1.42463	1.45499	1.48638	1.51911	1.55316			
220	1.17910	1.19091	1.22092	1.24308	1.26613	1.29089	1.31500	1.34089	1.36781	1.39579	1.42485	1.45514	1.48659	1.51939	1.55331			
240	1.17954	1.19224	1.22204	1.24395	1.26692	1.29287	1.31774	1.34356	1.37036	1.39829	1.42710	1.45711	1.48826	1.52095	1.55478			
260	1.18007	1.19432	1.22576	1.24708	1.27044	1.29494	1.31953	1.34544	1.37211	1.39976	1.42843	1.45820	1.48936	1.52189	1.55633			
300	1.18125	1.20305	1.22740	1.24961	1.27262	1.29645	1.32134	1.34672	1.37323	1.40069	1.42944	1.45892	1.48917	1.52084	1.55595			
100° C.																		
320	1.18612	1.20862	1.22826	1.25045	1.27342	1.29720	1.32182	1.34731	1.37370	1.40102	1.42932	1.45852	1.48897	1.52040	1.55286			
340	1.18651	1.20722	1.22865	1.25083	1.27378	1.29753	1.32210	1.34754	1.37387	1.40112	1.42934	1.45854	1.48878	1.52019	1.55272			
400	1.18751	1.20820	1.22969	1.25173	1.27460	1.29825	1.32270	1.34799	1.37414	1.40118	1.42915	1.45809	1.48801	1.51898	1.55101			
420	1.18827	1.20895	1.23031	1.25235	1.27515	1.29869	1.32302	1.34815	1.37411	1.40095	1.42868	1.45734	1.48686	1.51758	1.54923			
440	1.18886	1.20950	1.23080	1.25279	1.27549	1.29892	1.32310	1.34807	1.37386	1.40048	1.42797	1.45636	1.48568	1.51598	1.54727			
460	1.18930	1.20989	1.23113	1.25304	1.27564	1.29896	1.32301	1.34782	1.37342	1.39983	1.42709	1.45522	1.48426	1.51422	1.54516			
480	1.18960	1.21015	1.23132	1.25315	1.27565	1.29884	1.32276	1.34741	1.37283	1.39904	1.42607	1.45394	1.48270	1.51236	1.54286			
500	1.18980	1.21029	1.23140	1.25314	1.27554	1.29861	1.32228	1.34688	1.37212	1.39813	1.42494	1.45257	1.48105	1.51041	1.54048			
520	1.18991	1.21034	1.23138	1.25303	1.27533	1.29828	1.32191	1.34625	1.37132	1.39714	1.42373	1.45112	1.47934	1.50841	1.53837			
540	1.18995	1.21032	1.23127	1.25284	1.27503	1.29786	1.32136	1.34555	1.37044	1.39607	1.42245	1.44961	1.47758	1.50638	1.53603			
560	1.18992	1.21022	1.23110	1.25258	1.27466	1.29738	1.32074	1.34478	1.36951	1.39495	1.42113	1.44807	1.47579	1.50432	1.53369			
580	1.18983	1.21007	1.23088	1.25226	1.27424	1.29684	1.32008	1.34397	1.36853	1.39379	1.41977	1.44650	1.47398	1.50226	1.53135			
600	1.18970	1.20987	1.23060	1.25189	1.27377	1.29626	1.31936	1.34311	1.36751	1.39260	1.41839	1.44490	1.47216	1.50019	1.52902			

TABLE 14. *Pressure (in atmospheres) at integral values of T, the absolute temperature, and ρ, the density in Amagat units*

Temperature	ρ=1	2	3	6	10	20	40	60	80	100	120	140	160	180	200
°K															
16	0.05800	0.11495	0.17083												
18	.06535	.13171	.19301	0.37696											
20	.07269	.14441	.21516	.42166	0.68364										
22	.08002	.15912	.23729	.46628	.75880										
24	.08736	.17383	.25941	.51085	.83382	1.58080									
26	.09469	.18853	.28152	.55538	.90873	1.73410	3.1448								
28	.10203	.20323	.30362	.59988	.98355	1.88695	3.4633	4.7475							
30	.10936	.21793	.32571	.64435	1.05828	2.03952	3.7805	5.2407	6.4397	7.3966					
32	.11669	.23262	.35800	.68879	1.13295	2.19178	4.0967	5.7313	7.1163	8.2678	9.2035	9.9441	10.507	10.908	
34	.12402	.24732	.36988	.73320	1.20754	2.34377	4.4114	6.2201	7.7879	9.1329	10.273	11.226	12.007	12.637	13.133
36	.13136	.28821	.39195	.77759	1.28206	2.4955	4.7252	6.7069	8.4557	9.9928	11.334	12.496	13.495	14.353	15.083
38	.13869	.27669	.41402	.82195	1.35652	2.6470	5.0382	7.1904	9.1212	10.848	12.389	13.759	14.975	16.053	17.014
40	.14602	.29138	.43608	.86632	1.43093	2.7983	5.3505	7.6734	9.7839	11.700	13.438	15.014	16.444	17.746	18.937
42	.15334	.30606	.45814	.91065	1.50532	2.9494	5.6624	8.1557	10.445	12.548	14.482	16.263	17.908	19.433	20.855
	ρ=220	240	260	280	300	320	340	360	380	400	420	440	460	480	500
34	13.511	13.790	13.994	14.148	14.274	14.382	14.485	14.594	14.724	14.887	15.099	15.369	15.724	16.223	16.942
36	15.702	16.232	16.694	17.108	17.496	17.866	18.230	18.606	19.019	19.493	20.047	20.706	21.490	22.443	23.642
38	17.874	18.655	19.375	20.051	20.708	21.350	21.990	22.647	23.356	24.152	25.061	26.108	27.320	28.728	30.405
40	20.039	21.066	22.046	22.988	23.910	24.829	25.764	26.726	27.750	28.876	30.148	31.577	33.208	35.066	37.208
42	22.193	23.470	24.702	25.905	27.106	28.313	29.555	30.834	32.185	33.658	35.289	37.105	39.138	41.429	44.024
	ρ=520	540	560	580	600	620	640	660	680	700					
34	17.950	19.332	21.162	23.506	26.451	30.179	34.909	40.811	48.028	56.703					
36	25.170	27.091	29.466	32.405	36.012	40.372	45.569	51.696							
38	32.453	34.962	38.009	41.664	46.046										
40	39.762	42.840	46.565												
42	47.063	50.699													
	ρ=1	2	3	6	10	20	40	60	80	100	120	140	160	180	200
42	0.15334	0.30606	0.45814	0.91065	1.50532	2.9494	5.6624	8.1557	10.445	12.548	14.482	16.263	17.908	19.433	20.855
44	.16067	.32074	.48020	.95498	1.57968	3.1005	5.9739	8.6368	11.105	13.395	15.525	17.511	19.369	21.115	22.766
46	.16800	.33542	.50226	.99930	1.65400	3.2515	6.2851	9.1170	11.763	14.241	16.568	18.757	20.826	22.792	24.672
48	.17533	.35010	.52431	1.04361	1.72832	3.4024	6.5959	9.5964	12.421	15.085	17.607	20.000	22.279	24.466	26.577
50	.18266	.36478	.54636	1.08792	1.80261	3.5531	6.9062	10.076	13.077	15.928	18.643	21.238	23.731	26.138	28.475
52	.18999	.37946	.56841	1.13221	1.87686	3.7038	7.2162	10.554	13.732	16.768	19.677	22.527	25.180	27.806	30.371
54	.19732	.39414	.59046	1.17650	1.95110	3.8544	7.5260	11.031	14.385	17.605	20.709	23.709	26.622	29.470	32.262
56	.20464	.40881	.61251	1.22079	2.02533	4.0051	7.8359	11.509	15.039	18.443	21.739	24.940	28.060	31.126	34.150
58	.21197	.42349	.63456	1.26508	2.09957	4.1557	8.1455	11.986	15.692	19.280	22.767	26.167	29.497	32.780	36.031
60	.21930	.43817	.65660	1.30935	2.17380	4.3062	8.4548	12.462	16.343	20.114	23.793	27.395	30.936	34.435	37.915
65	.23762	.47485	.71171	1.42002	2.35925	4.6821	9.2268	13.651	17.970	22.280	26.358	30.461	34.524	38.569	42.615
70	.25593	.51154	.76681	1.53066	2.54462	5.0578	9.9979	14.837	19.589	24.277	28.912	33.514	38.101	42.693	47.312
75	.27425	.54822	.82190	1.64128	2.72995	5.4332	10.768	16.020	21.208	26.347	31.458	36.557	41.666	46.805	51.988
80	.29257	.58490	.87699	1.75186	2.91519	5.80 84	11.537	17.203	22.823	28.415	33.998	39.592	45.220	50.903	56.664

65	23702	47485	71171	1.42092	2.85925	5.6821	9.2268	13.953	17.970	22.280	26.378	30.461	34.524	38.569	42.615
70	25703	51154	76683	1.53086	2.94362	5.8578	9.5079	14.347	19.580	23.277	28.012	33.513	38.101	42.693	47.312
75	.27425	.54822	.82190	1.64128	2.72685	5.4332	10.768	16.020	21.208	26.347	31.478	36.557	41.666	46.805	51.998
80	.29257	.58490	.87689	1.75186	2.91546	5.80 83	11.537	17.203	22.823	28.415	33.998	39.592	45.229	50.901	56.664
85	.31088	.62157	.93207	1.86243	3.10035	6.1832	12.305	18.383	24.435	30.478	36.534	42.021	48.763	54.983	61.307
90	.32920	.65824	.98715	1.97298	3.28549	6.5580	13.073	19.562	26.044	32.538	39.064	45.642	52.297	59.053	65.934
95	.34751	.69492	1.04222	2.08352	3.47059	6.9326	13.840	20.740	27.652	34.595	41.591	48.659	55.825	63.115	70.556
100	.36583	.73159	1.09729	2.19403	3.65563	7.3069	14.606	21.917	29.258	36.649	44.112	51.670	59.348	67.174	75.177
105	.38414	.76826	1.15235	2.30454	3.84067	7.6813	15.372	23.092	30.861	38.700	46.630	54.677	62.866	71.226	79.788
110	.40245	.80493	1.20742	2.41505	4.05570	8.0555	16.137	24.266	32.463	40.748	49.144	57.678	66.377	75.269	84.385
115	.42077	.84159	1.26248	2.52554	4.21066	8.4296	16.903	25.440	34.063	42.793	51.655	60.676	69.882	79.302	88.969
120	.43908	.87826	1.31754	2.63604	4.39562	8.8036	17.667	26.613	35.662	44.837	54.164	63.668	73.381	83.328	93.540
125	.45739	.91493	1.37261	2.74653	4.5806	9.1777	18.432	27.785	37.260	46.880	56.671	66.659	76.876	87.350	98.114
130	.47571	.95159	1.42767	2.85701	4.7655	9.5516	19.196	28.957	38.858	48.922	59.177	69.649	80.368	91.368	102.676
135	.49402	.98826	1.48272	2.96748	4.9505	9.9255	19.961	30.129	40.454	50.963	61.681	72.635	83.856	95.380	107.238
140	.51233	1.02492	1.53778	3.07795	5.1354	10.2993	20.725	31.300	42.050	53.002	64.182	75.619	87.343	99.385	111.783
145	.53064	1.06159	1.59284	3.18842	5.3203	10.6731	21.489	32.471	43.646	55.040	66.682	78.599	90.823	103.385	116.327
150	.54896	1.09825	1.64789	3.29888	5.5052	11.0469	22.252	33.641	45.241	57.078	69.180	81.501	94.300	107.383	120.865
155	.56727	1.13492	1.70295	3.40935	5.6901	11.4207	23.016	34.812	46.835	59.114	71.677	84.553	97.776	111.378	125.404
160	.58558	1.17158	1.75800	3.51981	5.8750	11.7945	23.780	35.982	48.428	61.148	74.172	87.528	101.248	115.369	129.939
165	.60389	1.20824	1.81305	3.63027	6.0599	12.1681	24.543	37.151	50.021	63.182	76.664	90.499	104.716	119.353	134.449
170	.62221	1.24491	1.86810	3.74071	6.2447	12.5416	25.305	38.319	51.612	65.212	79.152	93.464	108.181	123.327	138.971
180	.65883	1.31823	1.97820	3.96158	6.6143	13.2885	26.831	40.655	54.792	69.270	84.123	99.385	115.089	131.27	147.98
190	.69545	1.39155	2.08830	4.18245	6.9839	14.0354	28.355	42.989	57.967	73.321	89.085	105.292	121.977	139.19	156.95
200	.73208	1.46487	2.19839	4.40331	7.3535	14.7822	29.879	45.322	61.141	77.368	94.041	111.190	128.85	147.08	165.90
210	.76870	1.53819	2.30848	4.62415	7.7231	15.5286	31.402	47.653	64.311	81.413	98.991	117.082	135.72	154.96	174.84
220	.80532	1.61151	2.41857	4.84499	8.0926	16.2752	32.9255	49.983	67.481	85.453	103.937	122.967	142.59	162.83	183.76
230	.841944	1.68482	2.52865	5.06581	8.46213	17.0215	34.4480	52.312	70.647	89.489	108.876	128.845	149.43	170.70	192.66
240	.878565	1.75814	2.63873	5.28661	8.83154	17.7676	35.9693	54.638	73.811	93.521	113.808	134.714	156.28	178.55	201.55
250	.915186	1.83145	2.74880	5.50739	9.20069	18.5134	37.4896	56.963	76.970	97.546	118.733	140.570	163.101	186.37	210.41
260	.951806	1.90476	2.85887	5.72816	9.57026	19.2591	39.0093	59.287	80.127	101.568	123.651	146.417	169.910	194.18	219.26
270	.988428	1.97807	2.96894	5.94891	9.93956	20.0048	40.5291	61.6092	83.2820	105.5872	128.5657	152.260	176.716	201.979	228.098
0° C	1.000000	2.00124	3.00372	6.01867	10.05625	20.2403	41.0060	62.3428	84.2791	106.857	130.118	154.105	178.864	204.440	230.885
280	1.02505	2.05138	3.07901	6.16966	10.3089	20.7502	42.0482	63.9304	86.4362	109.603	133.476	158.096	183.510	209.766	236.915
25° C	1.09155	2.18451	3.27888	6 57052	10.9795	22.1038	44.8054	68.1434	92.1574	116.889	142.379	168.676	195.827	223.879	252.887
300	1.08829	2 19800	3 29913	6.61113	11.0474	22.2409	45.0850	68.5706	92.7366	117.626	143.281	169.748	197.072	225.308	254.502
320	1.17153	2.34461	3.51924	7.05258	11.7858	23.7311	48.1202	73.2059	99.0306	125.637	153.068	181.374	210.602	240.805	272.033
340	1.24476	2.49121	3.73935	7.49396	12.5240	25.2210	51.1536	77.8380	105.318	133.636	162.841	192.978	224.101	256.263	289.518
360	1.31800	2.63782	3.95945	7.93532	13.2623	26.7107	54.1858	82.4672	111.599	141.626	172.598	204.562	237.574	271.686	306.954
100° C	1.36619	2.73428	4.10427	8.22572	13.7480	27.6904	56.1797	85.5106	115.729	146.878	179.011	212.176	246.425	281.816	318.404
380	1.39124	2.78441	4.17954	8.37665	14.0004	28.1996	57.2161	87.0921	117.873	149.607	182.342	216.129	251.022	287.074	324.349
400	1.46447	2.93101	4.39963	8.81797	14.7385	29.6885	60.2456	91.7154	124.144	157.580	192.073	227.676	264.444	302.436	341.707
420	1.53771	3.07761	4.61970	9.25925	15.4764	31.1772	63.2739	96.3353	130.409	165.545	201.793	239.209	277.849	317.768	359.032
440	1.61094	3.22420	4.83978	9.70051	16.2144	32.6654	66.3011	100.952	136.669	173.502	211.502	250.726	291.232	333.074	376.322
460	1.68417	3.37079	5.05984	10.14175	16.9522	34.1535	69.3270	105.568	142.926	181.453	221.203	262.231	304.596	348.359	393.582
480	1.75740	3.51737	5.27990	10.5830	17.6900	35.6413	72.3524	110.181	149.178	189.396	230.892	273.721	317.943	363.619	410.814
500	1.83064	3.66396	5.49996	11.0242	18.4277	37.1289	75.3766	114.791	155.426	197.336	240.574	285.197	331.273	378.859	428.023
520	1.90387	3.81054	5.72001	11.4653	19.1654	38.6163	78.3993	119.400	161.672	205.267	250.245	296.664	344.588	394.078	445.201
540	1.97710	3.95712	5.94006	11.9065	19.9031	40.1036	81.4217	124.007	167.912	213.194	259.910	308.118	357.888	409.278	462.359
560	2.05033	4.10370	6.16010	12.3476	20.6407	41.5905	84.4439	128.612	174.151	221.116	269.566	319.565	371.173	424.459	479.492
580	2.12356	4.25027	6.38014	12.7888	21.3782	43.0772	87.4649	133.215	180.386	229.032	279.216	330.998	384.446	439.625	496.604
600	2.19679	4.39684	6.60017	13.2299	22.1157	44.5639	90.4844	137.817	186.617	236.943	288.857	342.421	397.703	454.773	513.693

TABLE 14. *Pressure (in atmospheres) at integral values of T, the absolute temperature, and ρ, the density in Amagat units*—Continued

Temperature	ρ=220	240	260	280	300	320	340	360	380	400	420	440	460	480	500
42	22.193	23.470	24.702	25.905	27.106	28.313	29.555	30.834	32.185	33.658	35.289	37.105	39.138	41.429	44.024
44	24.344	25.866	27.352	28.820	30.299	31.804	33.354	34.962	36.654	38.480	40.479	42.675	45.104	47.806	50.829
46	26.488	28.257	30.000	31.732	33.489	35.291	37.159	39.102	41.140	43.319	45.690	48.266	51.087	54.180	57.607
48	28.628	30.641	32.642	34.646	36.678	38.781	40.966	43.243	45.625	48.167	50.907	53.864	57.064	60.548	64.371
50	30.763	33.024	35.276	37.555	39.869	42.264	44.769	47.376	50.105	53.006	56.117	59.449	63.027	66.908	71.132
52	32.897	35.404	37.914	40.452	43.057	45.751	48.558	51.490	54.560	57.820	61.302	65.008	68.978	73.256	77.887
54	35.028	37.780	40.549	43.358	46.242	49.230	52.333	55.583	58.993	62.604	66.448	70.534	74.903	79.582	84.636
56	37.150	40.154	43.180	46.260	49.423	52.692	56.097	59.655	63.397	67.357	71.559	76.022	80.787	85.883	91.367
58	39.270	42.524	45.809	49.154	52.595	56.149	59.854	63.726	67.798	72.096	76.655	81.500	86.659	92.169	98.089
60	41.397	44.897	48.444	52.060	55.779	59.624	63.626	67.820	72.222	76.866	81.787	87.005	92.566	98.497	104.84
65	46.694	50.830	55.041	59.342	63.766	68.352	73.117	78.103	83.346	88.864	94.706	100.90	107.49	114.51	122.02
70	51.993	56.756	61.619	66.610	71.752	77.084	82.625	88.425	94.516	100.92	107.69	114.87	122.48	130.59	139.24
75	57.276	62.661	68.175	73.842	79.692	85.769	92.100	98.723	105.66	112.95	120.65	128.80	137.44	146.62	156.40
80	62.530	68.531	74.691	81.035	87.596	94.409	101.51	108.94	116.73	124.91	133.51	142.63	152.29	162.52	173.42
85	67.759	74.374	81.178	88.189	95.458	103.00	110.86	119.07	127.70	136.76	146.27	156.33	166.97	178.24	190.23
90	72.976	80.195	87.631	95.322	103.29	111.55	120.16	129.16	138.69	148.50	158.94	169.94	181.55	193.85	206.92
95	78.177	86.010	94.081	102.43	111.08	120.06	129.43	139.22	149.47	160.23	171.55	183.50	196.08	209.39	223.54
100	83.378	91.819	100.52	109.52	118.86	128.56	138.67	149.25	160.31	171.92	184.13	197.00	210.55	224.89	240.10
105	88.579	97.618	106.94	116.60	126.62	137.04	147.89	159.23	171.12	183.58	196.66	210.44	224.99	240.34	256.58
110	93.753	103.40	113.35	123.66	134.35	145.48	157.08	169.19	181.88	195.17	209.14	223.82	239.35	255.68	272.95
115	98.912	109.16	119.74	130.70	142.08	153.90	166.22	179.11	192.59	206.72	221.56	237.16	253.61	270.94	289.26
120	104.05	114.90	126.11	137.72	149.77	162.29	175.35	188.98	203.27	218.23	233.94	250.45	267.83	286.16	305.48
125	109.20	120.64	132.46	144.72	157.43	170.67	184.44	198.83	213.91	229.70	246.26	263.66	281.98	301.28	321.61
130	114.34	126.36	138.80	151.70	165.09	179.01	193.52	208.67	224.53	241.14	258.55	276.82	296.08	316.33	337.66
135	119.46	132.08	145.12	158.67	172.71	187.34	202.57	218.47	235.11	252.53	270.77	289.93	310.08	331.29	353.62
140	124.57	137.78	151.44	165.62	180.34	195.64	211.59	228.24	245.65	263.87	282.95	302.99	324.04	346.19	369.50
145	129.68	143.48	157.76	172.57	187.95	203.95	220.61	238.00	256.16	275.18	295.11	316.02	337.98	361.05	385.32
150	134.78	149.16	164.06	179.49	195.54	212.23	229.60	247.72	266.66	286.49	307.24	329.02	351.88	375.87	401.11
155	139.88	154.84	170.34	186.41	203.11	220.48	238.56	257.43	277.14	297.76	319.34	341.96	365.70	390.63	416.83
160	144.97	160.52	176.62	193.33	210.68	228.74	247.51	267.11	287.57	308.96	331.37	354.82	379.43	405.29	432.47
165	150.06	166.19	182.90	200.23	218.23	236.97	256.46	276.80	298.03	320.19	343.34	367.64	393.12	419.86	447.80
170	155.13	171.84	189.15	207.10	225.73	245.12	265.33	286.38	308.34	331.28	355.29	380.42	406.72	434.32	463.33
180	165.24	183.10	201.60	220.79	240.71	261.44	283.02	305.50	328.95	353.45	379.07	405.87	433.89	463.25	494.07
190	175.30	194.31	213.99	234.42	255.63	277.68	300.63	324.55	349.47	375.51	402.72	431.17	460.90	492.05	524.72
200	185.35	205.48	226.36	248.01	270.49	293.86	318.20	343.52	369.95	397.50	426.29	456.37	487.82	520.76	555.26
210	195.38	216.64	238.69	261.57	285.32	310.02	335.72	362.47	390.34	419.43	449.79	481.52	514.68	549.38	585.72
220	205.39	227.81	251.02	275.11	300.14	326.15	353.19	381.36	410.71	441.30	473.24	506.58	541.45	577.90	616.02
230	215.39	238.93	263.33	288.63	314.90	342.22	370.62	400.17	430.97	463.08	496.59	531.57	568.08	606.27	646.21
240	225.36	250.02	275.58	302.08	329.59	358.22	387.98	418.93	451.18	484.76	519.84	556.42	594.59	634.52	676.24
250	235.29	261.07	287.80	315.49	344.26	374.17	405.24	437.60	471.26	506.35	542.96	581.13	620.97	662.58	706.11
260	245.22	272.11	299.98	328.88	358.88	390.05	422.45	456.17	491.27	527.82	565.96	605.72	647.16	690.16	735.73
270	255.128	283.117	312.130	342.219	373.456	405.898	439.629	474.697	511.280	549.220	588.834	630.143	673.239	718.215	765.191
280	265.008	294.102	324.252	355.585	387.979	421.685	456.743	493.138	531.241	570.569	611.610	654.455	699.141	745.765	794.443
290	274.862	305.066	336.353	368.931	402.450	437.418	473.797	511.492	551.139	591.869	634.294	678.677	724.977	773.265	823.680
300	284.714	315.997	348.415	382.026	416.903	453.112	490.727	529.824	570.986	612.986	656.850	702.738	750.559	800.425	852.440
310	294.543	326.907	360.457	395.104	431.340	468.787	507.636	548.134	590.811	634.083	679.387	726.781	776.124	827.572	881.200
320	304.350	337.795	372.480	408.165	445.760	484.444	524.525	566.423	610.615	655.161	701.907	750.807	801.675	854.707	910.000
330	314.135	348.662	384.484	421.210	460.165	500.084	541.395	584.693	630.398	676.221	724.410	774.817	827.214	881.830	938.840
340	323.899	359.508	396.469	434.239	474.554	515.708	558.247	602.945	650.161	697.264	746.896	798.811	852.743	908.943	967.720
350	333.642	370.334	408.436	447.253	488.928	531.316	575.081	621.179	669.906	718.291	769.366	822.790	878.263	936.049	996.640
360	343.365	381.140	420.385	460.252	503.288	546.909	591.898	639.396	689.634	739.303	791.821	846.755	903.775	963.148	1025.60
370	353.068	391.926	432.317	473.236	517.634	562.488	608.699	657.597	709.346	760.301	814.263	870.707	929.281	990.243	1054.62
380	362.752	402.693	444.232	486.206	531.966	578.053	625.484	675.783	729.043	781.286	836.693	894.647	954.782	1017.34	1083.70
390	372.417	413.442	456.131	499.162	546.286	593.606	642.254	693.955	748.726	802.259	859.113	918.576	980.280	1044.44	1112.84
400	382.064	424.173	468.014	512.105	560.594	609.147	659.010	712.114	768.396	823.221	881.525	942.496	1005.78	1071.55	1142.05
410	391.694	434.887	479.882	525.035	574.890	624.677	675.753	730.261	788.054	844.174	903.931	966.409	1031.28	1098.67	1171.34
420	401.307	445.585	491.736	537.953	589.176	640.197	692.485	748.398	807.702	865.119	926.332	990.317	1056.79	1125.80	1200.72
430	410.904	456.268	503.576	550.860	603.451	655.708	709.208	766.527	827.342	886.057	948.729	1014.22	1082.31	1153.00	1230.21
440	420.486	466.936	515.403	563.756	617.716	671.211	725.923	784.650	846.975	906.990	971.124	1038.12	1107.85	1180.27	1259.80
450	430.053	477.590	527.218	576.642	631.972	686.706	742.631	802.768	866.603	927.919	993.518	1062.03	1133.42	1207.62	1289.50
460	439.606	488.230	539.021	589.518	646.219	702.193	759.333	820.882	886.227	948.846	1015.91	1085.95	1159.03	1235.07	1319.32
470	449.145	498.858	550.813	602.384	660.457	717.673	776.030	838.993	905.850	969.772	1038.31	1109.89	1184.68	1262.62	1349.26
480	458.671	509.474	562.594	615.241	674.687	733.146	792.724	857.102	925.473	990.698	1060.72	1133.86	1210.38	1290.27	1379.32
490	468.185	520.079	574.365	628.089	688.911	748.613	809.417	875.210	945.097	1011.63	1083.15	1157.87	1236.14	1317.99	1409.51
500	477.687	530.674	586.126	640.929	703.129	764.075	826.110	893.318	964.724	1032.57	1105.61	1181.92	1261.96	1345.79	1439.84

| | | |

TABLE 15. *Values of* $(dZ/dT)_\rho$ *at integral values of* T, *the*

Temperature	$\rho=1$	2	3	6	10	20
°K	°K^{-1}	°K^{-1}	°K^{-1}	°K^{-1}	°K^{-1}	°K^{-1}
16	8.04×10^{-4}	16.1×10^{-4}	24.1×10^{-4}			
18	6.07	12.1	18.2	36.2×10^{-4}		
20	4.76	9.50	14.2	28.4	47.1×10^{-4}	
22	3.82	7.64	11.4	22.8	37.9	
24	3.14	6.28	9.41	18.8	31.2	59.8×10^{-4}
26	2.62	5.24	7.86	15.7	26.0	51.1
28	2.21	4.43	6.65	13.3	22.0	43.7
30	1.90	3.80	5.69	11.3	18.8	37.5
32	1.64	3.28	4.91	9.79	16.3	32.3
34	1.43	2.85	4.27	8.51	14.2	28.1
36	1.25	2.50	3.74	7.46	12.4	24.6
38	1.10	2.20	3.30	6.59	10.9	21.7
40	0.982	1.96	2.94	5.87	9.73	19.4
42	.881	1.76	2.64	5.26	8.74	17.4
	220	240	260	280	300	320
34	256×10^{-4}	274×10^{-4}	291×10^{-4}	306×10^{-4}	320×10^{-4}	331×10^{-4}
36	226	242	257	271	284	296
38	200	215	229	242	254	266
40	180	193	205	217	228	240
42	162	174	185	196	207	218
	1	2	3	6	10	20
42	0.881×10^{-4}	1.76×10^{-4}	2.64×10^{-4}	5.26×10^{-4}	8.74×10^{-4}	17.4×10^{-4}
44	.794	1.59	2.38	4.75	7.89	15.7
46	.719	1.44	2.16	4.30	7.15	14.2
48	.653	1.30	1.96	3.91	6.49	12.9
50	.596	1.19	1.78	3.56	5.92	11.8
52	.546	1.09	1.63	3.26	5.43	10.8
54	.502	1.00	1.51	3.01	5.00	9.99
56	.466	0.931	1.40	2.79	4.64	9.24
58	.434	.867	1.30	2.59	4.30	8.53
60	.403	.803	1.20	2.39	3.97	7.84
65	.335	.669	1.00	2.00	3.32	6.59
70	.281	.561	0.841	1.68	2.79	5.56
75	.238	.473	.713	1.42	2.39	4.73
80	.205	.411	.616	1.23	2.07	4.09
85	.180	.360	.540	1.08	1.80	3.57
90	.159	.317	.475	0.949	1.58	3.14
95	.140	.279	.418	.836	1.39	2.77
100	.124	.247	.371	.742	1.24	2.46
105	.110	.220	.331	.662	1.10	2.20
110	.099	.198	.297	.593	0.991	1.98
115	.091	.182	.272	.544	.904	1.80
120	.083	.166	.248	.495	.824	1.64
125	.075	.151	.226	.452	.754	1.50
130	.069	.139	.208	.416	.692	1.38
135	.064	.128	.191	.383	.638	1.27
140	.059	.118	.177	.354	.588	1.17
145	.054	.108	.163	.328	.543	1.08
150	.051	.102	.153	.305	.508	1.01
155	.047	.095	.142	.284	.473	0.94
160	.044	.088	.133	.265	.442	.88

absolute temperature, and ρ, the density in Amagat units

40	60	80	100	120	140	160	180	200
°K⁻¹	°K⁻¹	°K⁻¹	°K⁻¹	°K⁻¹	°K⁻¹	°K⁻¹	°K⁻¹	°K⁻¹
100.5×10⁻⁴								
85.9	124.8×10⁻⁴							
73.6	108.0	141.5×10⁻⁴	173.3×10⁻⁴					
63.4	93.5	122.4	150.1	176.8×10⁻⁴	202.3×10⁻⁴	226.3×10⁻⁴	249.0×10⁻⁴	
55.1	81.3	106.5	130.8	154.2	176.6	197.7	217.8	237.1×10⁻⁴
48.3	71.2	93.4	114.8	135.4	155.1	173.9	191.7	208.8
42.7	63.0	82.7	101.6	119.7	137.2	154.0	170.1	185.5
38.1	56.2	73.7	90.5	106.6	122.4	137.5	152.1	166.1
34.2	50.4	66.1	81.3	95.9	110.2	123.8	137.1	149.8
340	360	380	400	420	440	460	480	500
340×10⁻⁴	349×10⁻⁴	358×10⁻⁴	370×10⁻⁴	384×10⁻⁴	401×10⁻⁴	419×10⁻⁴	437×10⁻⁴	455×10⁻⁴
306	315	325	336	349	364	380	396	412
276	287	297	308	320	332	346	360	373
251	262	272	283	294	304	316	328	338
229	240	250	260	270	280	289	298	307
40	60	80	100	120	140	160	180	200
34.2×10⁻⁴	50.4×10⁻⁴	66.1×10⁻⁴	81.3×10⁻⁴	95.9×10⁻⁴	110.2×10⁻⁴	123.8×10⁻⁴	137.1×10⁻⁴	149.8×10⁻⁴
30.9	45.5	59.8	76.6	87.0	99.9	112.2	124.2	135.7
28.0	41.3	54.4	67.0	79.2	90.9	102.1	113.0	123.5
25.4	37.6	49.6	61.1	72.2	82.9	93.2	103.2	113.0
23.2	34.4	45.3	55.9	66.0	75.8	85.4	94.5	103.7
21.3	31.6	41.5	51.2	60.5	69.5	78.3	86.8	95.3
19.7	29.1	38.2	47.1	55.7	63.9	72.0	79.8	87.7
18.2	26.9	35.3	43.5	51.4	59.0	66.5	73.8	81.1
16.8	24.9	32.7	40.3	47.7	54.8	61.8	68.7	75.6
15.5	23.0	30.4	37.5	44.5	51.3	57.9	64.4	70.8
13.0	19.3	25.4	31.3	37.2	43.0	48.7	54.3	59.9
11.0	16.3	21.5	26.5	31.5	36.5	41.5	46.4	51.2
9.40	13.9	18.4	22.8	27.1	31.4	35.6	39.8	44.0
8.13	12.1	16.0	19.8	23.5	27.2	30.8	34.4	38.0
7.09	10.6	14.0	17.3	20.6	23.8	26.9	30.0	33.1
6.23	9.30	12.3	15.3	18.2	21.0	23.7	26.5	29.2
5.50	8.20	10.9	13.5	16.1	18.6	21.1	23.6	26.1
4.89	7.30	9.69	12.0	14.3	16.6	18.9	21.2	23.4
4.38	6.53	8.66	10.7	12.8	14.9	17.0	19.0	21.0
3.95	5.88	7.78	9.63	11.5	13.4	15.3	17.1	18.9
3.57	5.32	7.04	8.73	10.4	12.1	13.8	15.4	17.0
3.25	4.84	6.42	7.97	9.50	11.0	12.5	14.0	15.4
2.98	4.44	5.89	7.32	8.71	10.1	11.5	12.8	14.1
2.74	4.08	5.41	6.73	8.00	9.24	10.4	11.7	12.9
2.52	3.75	4.98	6.19	7.36	8.51	9.58	10.7	11.8
2.32	3.46	4.60	5.71	6.79	7.85	8.84	9.84	10.8
2.15	3.21	4.26	5.28	6.28	7.25	8.18	9.10	9.99
2.00	2.98	3.95	4.89	5.81	6.71	7.57	8.43	9.26
1.86	2.77	3.66	4.53	5.38	6.21	7.02	7.82	8.59
1.74	2.58	3.40	4.20	4.99	5.76	6.51	7.25	7.96

TABLE 15. *Values of* $(dZ/dT)_p$ *at integral values of* T, *the absolute*

Temperature	1	2	3	6	10	20
°K	°K⁻¹	°K⁻¹	°K⁻¹	°K⁻¹	°K⁻¹	°K⁻¹
185	4.1×10^{-6}	8.3×10^{-6}	12.4×10^{-6}	24.8×10^{-6}	41.2×10^{-6}	82×10^{-6}
170	3.8	7.6	11.5	22.9	38.2	76
180	3.3	6.6	9.9	19.9	33.1	66
190	2.9	5.8	8.8	17.6	29.3	58
200	2.6	5.2	7.7	15.8	26.0	51
210	2.3	4.6	6.9	13.9	23.1	46
220	2.1	4.1	6.2	12.4	20.4	41
230	1.8	3.6	5.4	10.7	18.0	36
240	1.6	3.2	4.8	9.5	16.0	32
250	1.4	2.9	4.3	8.6	14.4	29
260	1.3	2.6	4.0	7.9	13.1	26
270	1.200	2.398	3.594	7.167	11.90	23.57
0°C	1.164	2.325	3.484	6.947	11.53	22.84
280	1.089	2.175	3.259	6.499	10.79	21.35
25°C	0.9109	1.832	2.744	5.470	9.075	17.94
300	.9014	1.801	2.698	5.377	8.921	17.64
320	.7517	1.502	2.249	4.482	7.431	14.67
340	.6306	1.259	1.886	3.757	6.226	12.27
360	.5315	1.061	1.590	3.164	5.241	10.32
100°C	.4759	0.9503	1.423	2.832	4.689	9.219
380	.4496	.8977	1.344	2.675	4.427	8.700
400	.3814	.7614	1.140	2.267	3.750	7.355
420	.3241	.6468	0.9683	1.925	3.181	6.227
440	.2756	.5500	.8231	1.635	2.700	5.274
460	.2344	.4676	.6996	1.389	2.291	4.464
480	.1990	.3970	.5939	1.178	1.941	3.771
500	.1687	.3363	.5029	0.9965	1.640	3.170
520	.1424	.2838	.4243	.8399	1.380	2.662
540	.1196	.2383	.3561	.7039	1.155	2.210
560	.0998	.1986	.2967	.5855	0.9583	1.828
580	.0824	.1639	.2447	.4819	.7867	1.489
600	.0675	.1335	.1991	.3911	.6361	1.196
	220	240	260	280	300	320
42	162×10^{-4}	174×10^{-4}	185×10^{-4}	196×10^{-4}	207×10^{-4}	218×10^{-4}
44	147	158	168	178	188	198
46	134	144	153	162	172	182
48	122	131	140	149	158	167
50	112	121	129	137	145	153
52	103	111	119	126	133	140
54	95.3	103	110	116	123	129
56	88.3	95.4	102	108	114	120
58	82.4	89.0	95.4	101	107	113
60	77.2	83.6	89.9	95.9	102	107
65	65.4	70.9	76.3	81.5	86.6	91.4
70	56.0	60.6	65.1	69.5	73.9	78.3
75	48.1	52.0	55.8	59.6	63.4	67.1
80	41.5	44.9	48.2	51.5	54.7	57.9
85	36.1	39.0	41.9	44.8	47.7	50.4
90	31.8	34.4	37.0	39.6	42.0	44.4
95	28.5	30.8	33.0	35.2	37.3	39.4
100	25.5	27.6	29.6	31.5	33.3	35.1
105	23.0	24.8	26.5	28.2	29.8	31.4
110	20.7	22.3	23.8	25.3	26.8	28.2
115	18.6	20.1	21.6	22.8	24.2	25.4
120	16.8	18.2	19.5	20.7	21.9	23.0

temperature, and ρ, the density in Amagat units—Continued

40	60	80	100	120	140	160	180	200
°K⁻¹	°K⁻¹	°K⁻¹	°K⁻¹	°K⁻¹	°K⁻¹	°K⁻¹	°K⁻¹	°K⁻¹
162×10⁻⁴	240×10⁻⁴	316×10⁻⁴	390×10⁻⁴	463×10⁻⁴	534×10⁻⁴	604×10⁻⁴	672×10⁻⁴	737×10⁻⁴
151	223	293	361	429	495	559	622	682
131	194	254	312	370	427	483	536	587
114	169	222	273	323	372	419	464	507
101	150	197	242	285	327	367	405	442
91	134	175	215	253	290	325	358	391
81	119	156	192	226	258	289	319	348
71	105	138	170	200	229	257	283	308
63	93	122	151	178	203	228	251	274
56	83	109	134	158	180	202	222	242
51	75	98	120	141	161	180	198	215
46.21	67.90	88.63	108.4	127.0	144.7	161.2	176.6	190.7
44.76	65.74	85.76	104.8	122.8	139.7	155.6	170.3	183.7
41.81	61.34	79.92	97.53	114.1	129.7	144.1	157.5	169.6
35.04	51.26	66.59	80.99	94.42	106.9	118.2	128.5	137.7
34.43	50.36	65.40	79.51	92.66	104.8	115.9	125.9	134.8
28.56	41.63	53.87	65.24	75.70	85.22	93.74	101.2	107.6
23.82	34.61	44.61	53.80	62.13	69.58	76.09	81.62	86.13
19.95	28.88	37.08	44.52	51.15	56.95	61.87	65.87	68.90
17.79	25.69	32.88	39.34	45.04	49.94	53.99	57.16	59.40
16.77	24.18	30.90	36.91	42.16	46.64	50.29	53.08	54.96
14.12	20.27	25.78	30.62	34.75	38.15	40.78	42.59	43.56
11.90	17.00	21.50	25.37	28.58	31.10	32.90	33.93	34.17
10.03	14.25	17.90	20.97	23.41	25.21	26.33	26.73	26.38
8.443	11.92	14.86	17.25	19.06	20.25	20.81	20.70	19.88
7.086	9.926	12.27	14.09	15.36	16.06	16.15	15.62	14.42
5.922	8.221	10.05	11.39	12.21	12.49	12.20	11.32	9.81
4.919	6.753	8.144	9.070	9.510	9.439	8.833	7.665	5.906
4.050	5.484	6.499	7.076	7.192	6.825	5.953	4.549	2.588
3.295	4.383	5.074	5.350	5.190	4.574	3.478	1.880	−0.246
2.636	3.423	3.834	3.852	3.456	2.627	1.345	−0.414	−2.673
2.059	2.585	2.754	2.549	1.951	0.943	−0.496	−2.387	−4.751
340	360	380	400	420	440	460	480	500
229×10⁻⁴	240×10⁻⁴	250×10⁻⁴	260×10⁻⁴	270×10⁻⁴	280×10⁻⁴	289×10⁻⁴	298×10⁻⁴	307×10⁻⁴
209	220	230	240	249	257	265	272	279
192	201	211	220	229	236	243	249	254
175	184	193	202	210	216	223	228	233
161	169	177	185	192	198	204	209	214
148	155	162	169	176	182	188	193	198
136	143	149	156	162	167	173	179	183
126	132	138	144	149	155	160	166	171
118	124	129	134	140	145	150	156	161
112	117	122	126	131	137	142	148	153
96.1	101	105	109	114	118	123	127	132
82.7	86.6	90.6	94.3	98.1	102	106	110	113
70.8	74.5	78.0	81.4	84.7	87.9	91.0	94.1	97.2
61.0	64.1	67.2	70.3	73.2	75.8	78.5	81.0	83.5
53.0	55.6	58.2	60.8	63.2	65.4	67.6	69.8	72.1
46.6	48.8	51.0	53.1	55.2	57.2	59.1	61.0	62.9
41.4	43.3	45.2	47.1	48.9	50.6	52.3	53.9	55.5
36.9	38.7	40.4	42.0	43.6	45.1	46.6	48.0	49.3
33.0	34.5	36.0	37.5	38.9	40.3	41.6	42.8	43.9
29.6	30.9	32.2	33.5	34.8	36.0	37.2	38.2	39.2
26.6	27.8	29.0	30.2	31.3	32.3	33.3	34.2	35.0
24.1	25.1	26.2	27.3	28.3	29.1	29.9	30.6	31.3

TABLE 15. *Values of* $(dZ/dT)_p$ *at integral values of* T, *the absolute*

Temperature	220	240	260	280	300	320
100° C	$°K^{-1}$	$°K^{-1}$	$°K^{-1}$	$°K^{-1}$	$°K^{-1}$	$°K^{-1}$
125	15.3×10^{-4}	16.5×10^{-4}	17.7×10^{-4}	18.8×10^{-4}	19.9×10^{-4}	20.9×10^{-4}
130	14.0	15.1	16.2	17.2	18.2	19.2
135	12.8	13.8	14.8	15.8	16.7	17.6
140	11.7	12.7	13.6	14.5	15.3	16.1
145	10.8	11.7	12.5	13.3	14.1	14.8
150	10.1	10.9	11.6	12.3	13.0	13.7
155	9.35	10.1	10.8	11.4	12.0	12.6
160	8.65	9.32	9.96	10.5	11.1	11.7
165	8.00	8.60	9.16	9.67	10.3	10.7
170	739×10^{-6}	792×10^{-6}	841×10^{-6}	887×10^{-6}	933×10^{-6}	980×10^{-6}
180	634	678	719	758	796	851
190	547	585	621	655	687	718
200	478	512	544	575	604	631
210	423	453	482	509	535	559
220	375	401	426	450	473	493
230	332	354	375	396	415	432
240	294	312	330	347	362	376
250	260	275	290	304	316	326
260	230	243	255	266	276	284
270	203.6	215.2	225.4	234.1	241.3	246.8
0° C	196.0	206.9	216.4	224.5	231.0	235.9
280	180.5	190.1	198.3	205.1	210.3	213.9
25° C	145.6	152.3	157.6	161.5	164.0	164.8
300	142.5	148.9	154.0	157.7	159.9	160.5
320	112.9	117.0	119.8	121.2	121.3	119.8
340	89.56	91.86	92.95	92.78	91.28	88.20
360	70.92	71.87	71.70	70.33	67.70	63.73
100° C	60.67	60.92	60.07	58.09	54.90	50.44
380	55.88	55.80	54.66	52.40	48.97	44.28
400	43.62	42.75	40.88	37.96	33.94	28.73
420	33.56	32.07	29.65	26.24	21.80	16.28
440	25.24	23.27	20.42	16.66	11.92	6.157
460	18.32	15.97	12.81	8.776	3.834	−2.069
480	12.52	9.885	6.479	2.260	−2.815	−8.792
500	7.644	4.786	1.201	−3.148	−8.303	−14.30
520	3.527	0.496	−3.220	−7.657	−12.85	−18.84
540	0.041	−3.122	−6.930	−11.42	−16.62	−22.38
560	−2.925	−6.186	−10.06	−14.57	−19.76	−25.99
580	−5.455	−8.789	−12.70	−17.22	−22.37	−28.20
600	−7.613	−11.00	−14.93	−19.43	−24.54	−30.28

temperature, and ρ, the density in Amagat units—Continued

340	360	380	400	420	440	460	480	500
$°K^{-1}$	$°K^{-1}$	$°K^{-1}$	$°K^{-1}$	$°K^{-1}$	$°K^{-1}$	$°K^{-1}$	$°K^{-1}$	$°K^{-1}$
21.9×10^{-4}	22.9×10^{-4}	23.9×10^{-4}	24.8×10^{-4}	25.6×10^{-4}	26.3×10^{-4}	27.0×10^{-4}	27.6×10^{-4}	28.1×10^{-4}
20.1	21.0	21.8	22.5	23.2	23.8	24.4	24.9	25.3
18.4	19.2	19.9	20.5	21.1	21.7	22.1	22.5	22.9
16.9	17.6	18.2	18.8	19.3	19.8	20.2	20.5	20.8
15.5	16.1	16.7	17.2	17.7	18.1	18.5	18.8	19.0
14.3	14.8	15.3	15.8	16.2	16.6	16.9	17.1	17.3
13.2	13.7	14.1	14.5	14.8	15.1	15.3	15.5	15.6
12.2	12.7	13.0	13.3	13.5	13.7	13.9	14.0	14.0
11.2	11.6	11.9	12.1	12.3	12.5	12.6	12.6	12.6
102×10^{-6}	$105_0\times10^{-6}$	$108_0\times10^{-6}$	$111_0\times10^{-6}$	$113_0\times10^{-6}$	$114_0\times10^{-6}$	$114_0\times10^{-6}$	$114_0\times10^{-6}$	$114_0\times10^{-6}$
863	892	918	940	958	971	980	986	988
746	771	792	810	825	837	846	852	854
656	678	696	711	722	730	736	741	744
580	598	613	625	634	640	644	646	647
511	527	539	548	554	558	560	561	560
447	460	470	476	480	482	482	481	479
389	399	406	410	412	412	410	407	402
336	344	348	350	350	348	343	337	329
290	295	297	297	294	290	283	273	262
250.6	252.6	252.6	250.5	246.1	239.5	230.2	218.3	203.5
220.0	240.3	239.7	237.0	232.0	224.7	214.9	202.4	187.0
215.7	215.8	213.9	210.0	203.8	195.3	184.3	170.7	154.2
164.0	161.4	157.0	150.5	142.0	131.1	117.9	102.1	83.59
159.5	156.7	152.0	145.4	136.6	125.6	112.2	96.25	77.58
116.8	112.1	105.6	97.22	86.85	74.34	59.57	42.39	22.64
83.95	77.96	70.30	60.85	49.52	36.19	20.73	3.011	−17.11
58.40	51.55	43.14	33.06	21.21	7.491	−8.216	−26.03	−46.08
44.64	37.40	28.67	18.34	6.314	−7.497	−23.21	−40.93	−60.78
38.29	30.90	22.03	11.61	−0.457	−14.28	−29.95	−47.58	−67.30
22.33	14.60	5.500	−5.058	−17.16	−30.88	−46.34	−63.61	−82.82
9.574	1.666	−7.529	−18.08	−30.08	−43.59	−58.70	−75.52	−94.14
−0.687	−8.670	−17.86	−28.31	−40.11	−53.33	−68.04	−84.33	−102.3
−8.984	−16.97	−26.08	−36.37	−47.92	−60.79	−75.06	−90.81	−108.1
−15.72	−23.64	−32.63	−42.72	−53.99	−66.49	−80.30	−95.48	−112.1
−21.20	−29.03	−37.85	−47.72	−58.68	−70.80	−84.14	−98.76	−114.7
−25.67	−33.38	−42.03	−51.65	−62.30	−74.03	−86.91	−101.0	−116.3
−29.32	−36.89	−45.34	−54.71	−65.04	−76.39	−88.82	−102.4	−117.1
−32.30	−39.72	−47.96	−57.08	−67.10	−75.08	−90.06	−103.1	−117.3
−34.72	−41.99	−50.03	−58.89	−68.60	−79.22	−90.78	−103.3	−116.9
−36.69	−43.79	−51.63	−60.24	−69.65	−79.92	−91.08	−103.2	−116.2

TABLE 16. *Values of* $(-d^2Z/dT^2)_\rho$ *at integral values of T,*

Temperature	$\rho=1$	2	3	6	10	20
°K	°K^{-2}	°K^{-2}	°K^{-2}	°K^{-2}	°K^{-2}	°K^{-2}
16	11.4×10^{-3}	22.6×10^{-3}	33.7×10^{-3}			
18	7.9	15.7	23.5	47.0×10^{-3}		
20	5.5	11.0	16.5	33.0	54.0×10^{-3}	
22	4.0	7.9	11.7	23.5	38.6	
24	3.0	5.9	8.8	17.4	29.2	48.5×10^{-3}
26	2.3	4.6	6.8	13.5	22.7	41.0
28	1.8	3.6	5.4	10.7	17.8	34.3
30	1.4	2.9	4.3	8.6	14.3	28.4
32	1.2	2.4	3.5	7.0	11.7	23.3
34	0.96	2.0	2.9	5.8	9.7	19.0
36	.79	1.7	2.4	4.8	8.0	15.5
38	.66	1.4	2.0	4.0	6.6	12.8
40	.55	1.1	1.7	3.3	5.5	10.7
42	.47	0.92	1.4	2.8	4.6	9.2
	220	240	260	280	300	320
34	167×10^{-5}	178×10^{-5}	186×10^{-5}	190×10^{-5}	190×10^{-5}	188×10^{-5}
36	138	146	154	160	162	161
38	114	121	128	135	138	138
40	96	102	108	114	118	119
42	82	87	92	97	101	103
	$\rho=1$	2	3	6	10	20
42	°K^{-2} 0.47×10^{-3}	°K^{-2} 0.92×10^{-3}	°K^{-2} 1.4×10^{-3}	°K^{-2} 2.8×10^{-3}	°K^{-2} 4.6×10^{-3}	°K^{-2} 9.2×10^{-3}
44	.40	.79	1.2	2.4	4.0	8.0
46	.35	.69	1.0	2.1	3.5	6.9
48	.31	.61	0.92	1.9	3.1	6.0
50	.27	.53	.80	1.6	2.7	5.2
52	.23	.46	.69	1.4	2.3	4.5
54	.20	.40	.60	1.2	2.0	4.0
56	.18	.35	.53	1.1	1.8	3.6
58	.16	.32	.48	0.96	1.7	3.3
60	.15	.30	.45	.90	1.5	3.0
65	.12	.24	.37	.74	1.2	2.4
70	.10	.19	.30	.60	0.96	1.9
75	.078	.15	.23	.48	.76	1.5
80	.063	.12	.18	.38	.61	1.2
85	.051	.10	.15	.31	.49	0.97
90	.042	.084	.13	.25	.41	.80
95	.036	.070	.11	.21	.35	.67
100	.030	.059	.091	.18	.29	.57
105	.025	.049	.075	.15	.24	.48
110	.020	.041	.062	.12	.20	.40
115	.017	.035	.052	.10	.17	.34
120	.015	.030	.045	.089	.15	.30
125	.013	.026	.039	.080	.13	.26
130	.012	.023	.035	.071	.12	.23
135	.011	.021	.032	.062	.11	.21
140	.0095	.019	.028	.055	.093	.19
145	.0082	.016	.024	.048	.081	.16
150	.0071	.014	.021	.043	.070	.14
155	.0063	.013	.019	.039	.062	.13
160	.0058	.012	.018	.036	.057	.12
165	.0054	.012	.017	.033	.054	.12
170	.0050	.011	.016	.031	.050	.11

60	80	100	120	140	160	180	200
$°K^{-1}$	$°K^{-2}$	$°K^{-2}$	$°K^{-2}$	$°K^{-2}$	$°K^{-2}$	$°K^{-2}$	$°K^{-2}$	$°K^{-2}$
79.8×10^{-5}							
67.1	99.0×10^{-5}						
55.8	81.9	106.2×10^{-5}	128.0×10^{-5}				
45.9	67.2	87.2	105.7	123.0×10^{-5}	139.6×10^{-5}	155.6×10^{-5}	171.0×10^{-5}	
37.5	55.1	71.9	87.8	102.8	116.9	130.1	142.9	155.2×10^{-5}
30.7	45.4	59.6	72.9	85.6	97.5	108.5	118.9	128.0
25.4	37.6	49.4	60.6	71.1	81.1	90.4	98.8	106.6
21.2	31.3	41.0	50.3	59.1	67.5	75.3	82.4	89.3
18.0	26.4	34.3	42.0	49.4	56.5	63.1	69.6	75.9

340	360	380	400	420	440	460	480	500
183×10^{-5}	178×10^{-5}	177×10^{-5}	181×10^{-5}	189×10^{-5}	199×10^{-5}	210×10^{-5}	220×10^{-5}	229×10^{-5}
158	154	152	154	160	170	182	193	204
137	134	132	133	138	147	159	171	183
119	118	117	118	122	130	141	153	165
104	105	106	108	112	118	127	137	148

40	60	80	100	120	140	160	180	200
$°K^{-2}$	$°K^{-2}$	$°K^{-2}$	$°K^{-2}$	$°K^{-2}$	$°K^{-2}$	$°K^{-2}$	$°K^{-2}$	$°K^{-2}$
18.0×10^{-5}	26.4×10^{-5}	34.3×10^{-5}	42.0×10^{-5}	49.4×10^{-5}	56.5×10^{-5}	63.1×10^{-5}	69.6×10^{-5}	75.9×10^{-5}
15.5	22.7	29.3	35.6	41.8	47.9	53.8	59.8	65.6
13.5	19.7	25.4	30.8	36.2	41.5	46.9	52.1	56.9
11.8	17.2	22.4	27.3	32.0	36.6	41.2	45.7	49.7
10.3	15.2	19.9	24.3	28.5	32.5	36.4	40.2	43.7
9.0	13.4	17.6	21.6	25.4	29.0	32.4	35.6	38.7
8.0	11.9	15.6	19.2	22.7	25.9	28.8	31.6	34.4
7.2	10.6	13.9	17.1	20.3	23.1	25.6	28.0	30.5
6.5	9.5	12.4	15.3	18.2	20.7	22.8	24.8	26.9
5.8	8.6	11.3	13.8	16.3	18.5	20.4	22.0	23.8
4.6	6.7	8.8	10.8	12.7	14.5	16.1	17.5	19.0
3.6	5.3	6.9	8.5	10.0	11.5	13.0	14.4	15.7
2.9	4.2	5.5	6.7	8.0	9.3	10.6	11.8	13.0
2.3	3.4	4.5	5.4	6.5	7.6	8.6	9.7	10.7
1.9	2.8	3.7	4.5	5.3	6.1	7.0	7.9	8.8
1.6	2.4	3.1	3.8	4.5	5.2	5.8	6.4	7.2
1.3	2.0	2.6	3.3	3.9	4.4	4.8	5.3	5.9
1.1	1.7	2.2	2.8	3.3	3.7	4.1	4.6	5.0
0.94	1.4	1.9	2.4	2.8	3.2	3.6	4.1	4.4
.80	1.2	1.6	2.0	2.4	2.8	3.2	3.6	3.9
.68	1.0	1.3	1.6	2.0	2.4	2.8	3.1	3.4
.58	0.87	1.1	1.4	1.7	2.0	2.4	2.6	2.9
.51	.77	1.0	1.2	1.5	1.7	2.1	2.3	2.5
.46	.69	0.93	1.1	1.3	1.5	1.8	2.0	2.2
.41	.61	.80	1.0	1.2	1.3	1.5	1.8	2.0
.37	.54	.72	0.91	1.1	1.2	1.4	1.6	1.8
.33	.48	.65	.82	0.97	1.1	1.3	1.4	1.6
.29	.44	.60	.75	.89	1.0	1.2	1.3	1.4
.26	.40	.55	.69	.82	0.93	1.1	1.2	1.3
.25	.37	.51	.63	.75	.87	1.0	1.1	1.2
.24	.35	.47	.58	.70	.81	0.91	1.0	1.1
.22	.32	.43	.53	.64	.74	.84	0.93	1.0

TABLE 16. *Values of* $(-d^2Z/dT^2)_\rho$ *at integral values of* T, *the*

Temperature	$\rho=1$	2	3	6	10	20
°K	$°K^{-2}$	$°K^{-2}$	$°K^{-2}$	$°K^{-2}$	$°K^{-2}$	$°K^{-2}$
170	0.50×10^{-7}	1.1×10^{-7}	1.6×10^{-7}	3.1×10^{-7}	5.0×10^{-7}	11×10^{-7}
180	.44	0.88	1.3	2.6	4.3	9.3
190	.38	.76	1.1	2.2	3.7	7.5
200	.33	.66	1.0	2.0	3.2	6.2
210	.29	.58	0.87	1.8	2.7	5.4
220	.26	.51	.78	1.6	2.4	4.7
230	.23	.45	.69	1.4	2.2	4.2
240	.20	.40	.60	1.2	2.0	3.7
250	.17	.34	.52	1.0	1.7	3.2
260	.14	.28	.43	0.86	1.4	2.8
270	.1185	.2370	.3554	.7101	1.182	2.356
0° C	.1140	.2280	.3419	.6830	1.137	2.271
280	.10501	.2100	.3148	.6289	1.047	2.086
25° C	.08510	.1701	.2551	.5094	0.8476	1.691
300	.08336	.1666	.2498	.4990	.8302	1.653
320	.06706	.1341	.2010	.4013	.6674	1.328
340	.05459	.1091	.1636	.3266	.5430	1.079
360	.04490	.08970	.1345	.2685	.4463	0.8896
100° C	.03960	.07932	.1189	.2373	.3945	.7857
380	.03727	.05448	.1116	.2228	.3702	.7350
400	.03119	.06233	.09342	.1864	.3097	.6143
420	.02629	.05254	.07875	.1571	.2609	.5173
440	.02231	.04458	.06682	.1333	.2213	.4385
460	.01905	.03806	.05703	.1137	.1888	.3739
480	.01635	.03266	.04894	.09758	.1620	.3205
500	.01410	.02817	.04221	.08414	.1396	.2761
520	.01221	.02440	.03660	.07286	.1209	.2389
540	.01062	.02122	.03180	.06336	.1051	.2076
560	.00928	.01853	.02776	.05530	.09169	.1810
580	.00812	.01623	.02431	.04842	.08027	.1583
600	.00714	.01426	.02136	.04254	.07049	.1390

	$\rho=220$	240	260	280	300	320
42	82×10^{-5}	87×10^{-5}	92×10^{-5}	97×10^{-5}	101×10^{-5}	103×10^{-5}
44	71	75	79	84	87	90
46	61	65	69	73	76	80
48	53	57	61	65	68	72
50	47	50	54	58	61	64
52	42	44	47	51	54	57
54	37	39	41	44	46	49
56	33	35	36	38	40	42
58	29	31	32	34	36	37
60	26	28	30	31	32	34
65	21	23	25	26	27	28
70	17	19	21	22	23	24
75	14	16	17	18	19	20
80	12	13	14	15	16	16
85	9.7	10	11	12	13	13
90	7.8	8.3	8.9	9.5	10	11
95	6.4	6.9	7.5	8.1	8.6	9.1
100	5.5	6.0	6.5	7.0	7.5	8.0
105	4.8	5.3	5.7	6.1	6.5	6.9
110	4.3	4.6	5.0	5.3	5.6	6.0
115	3.7	4.0	4.3	4.6	4.9	5.2
120	3.2	3.5	3.8	4.0	4.3	4.5
125	2.8	3.1	3.3	3.5	3.7	3.8
130	2.5	2.7	2.9	3.1	3.2	3.3
135	2.2	2.4	2.6	2.7	2.9	3.0
140	1.9	2.1	2.3	2.4	2.6	2.7

of T, the absolute temperature, and ρ, the density in Amagat units—Continued

40	60	80	100	120	140	160	180	200
$°K^{-2}$	$°K^{-2}$	$°K^{-2}$	$°K^{-2}$	$°K^{-2}$	$°K^{-2}$	$°K^{-2}$	$°K^{-2}$	$°K^{-2}$
22×10^{-7}	32×10^{-7}	43×10^{-7}	53×10^{-7}	64×10^{-7}	74×10^{-7}	84×10^{-7}	93×10^{-7}	100×10^{-7}
19	27	35	44	53	61	70	79	87
15	22	29	36	43	50	58	65	72
12	18	24	29	35	41	47	53	59
10	15	20	25	29	34	39	44	48
9.6	14	18	22	26	29	33	37	41
8.5	13	17	20	23	26	29	32	36
7.5	11	15	18	20	23	26	29	32
6.5	9.1	13	16	18	20	23	26	29
5.5	8.0	10	13	16	18	20	23	26
4.684	6.986	9.264	11.52	13.76	15.82	18.19	20.38	22.56
4.523	6.756	8.970	11.17	13.35	15.51	17.66	19.79	21.91
4.142	6.171	8.175	10.15	12.11	14.05	15.96	17.86	19.74
3.358	5.001	6.620	8.216	9.786	11.33	12.85	14.35	15.81
3.276	4.872	6.440	7.981	9.496	10.98	12.45	13.89	15.30
2.628	3.900	5.145	6.362	7.553	8.716	9.851	10.96	12.03
2.132	3.160	4.160	5.135	6.082	7.002	7.893	8.756	9.588
1.749	2.587	3.400	4.189	4.951	5.687	6.395	7.075	7.725
1.546	2.286	3.004	3.697	4.366	5.008	5.624	6.211	6.768
1.448	2.138	2.806	3.450	4.069	4.664	5.232	5.773	6.285
1.208	1.706	2.202	2.865	3.373	3.857	4.317	4.751	5.158
1.016	1.496	1.957	2.397	2.816	3.214	3.586	3.939	4.265
0.8402	1.265	1.651	2.019	2.368	2.696	3.004	3.289	3.550
.7325	1.075	1.402	1.711	2.003	2.276	2.529	2.762	2.973
.6271	0.9193	1.196	1.458	1.703	1.931	2.141	2.332	2.503
.5395	.7897	1.026	1.248	1.455	1.646	1.821	1.978	2.116
.4662	.6814	0.8839	1.073	1.249	1.410	1.555	1.685	1.797
.4045	.5903	.7645	0.9265	1.076	1.212	1.333	1.440	1.531
.3522	.5132	.6635	.8026	0.9299	1.045	1.147	1.235	1.309
.3067	.4466	.5777	.6975	.8063	0.9038	0.9892	1.062	1.121
.2686	.3916	.5045	.6078	.7011	.7838	.8554	0.9152	0.9626

340	360	380	400	420	440	460	480	500
104×10^{-5}	105×10^{-5}	106×10^{-5}	108×10^{-5}	112×10^{-5}	118×10^{-5}	127×10^{-5}	137×10^{-5}	148×10^{-5}
93	95	98	101	104	109	115	123	132
84	87	91	95	98	102	106	111	116
76	80	84	88	92	95	97	99	101
68	73	77	81	85	87	87	87	88
61	65	69	73	76	77	77	77	76
53	57	61	64	66	67	67	67	65
45	48	51	54	56	56	57	57	56
39	40	42	45	47	47	48	49	49
36	36	37	39	41	42	44	45	46
29	30	31	32	33	34	36	38	39
25	26	27	28	29	30	31	33	34
21	22	23	24	25	26	27	29	30
17	18	19	20	22	23	23	24	25
14	15	16	17	18	19	19	20	20
11	12	13	14	14	15	15	16	16
9.1	9.6	10	11	11	12	12	13	13
8.0	8.4	8.8	9.1	9.5	9.8	10	11	11
6.9	7.3	7.7	8.0	8.4	8.7	9.1	9.4	10	10
6.0	6.4	6.7	7.0	7.3	7.6	8.0	8.3	8.6	8.9
5.2	5.5	5.8	6.9	6.3	6.6	6.9	7.3	7.6	7.9
4.5	4.7	4.9	5.2	5.5	5.8	6.0	6.3	6.6	6.9
3.8	4.0	4.2	4.4	4.8	5.1	5.3	5.5	5.8	6.0
3.3	3.5	3.7	4.0	4.2	4.4	4.6	4.8	5.0	5.2
3.0	3.2	3.4	3.6	3.7	3.9	4.0	4.2	4.4	4.5
2.7	2.9	3.1	3.2	3.3	3.4	3.6	3.7	3.8	3.9

TABLE 16. *Values of* $(-d^2Z/dT^2)_\rho$ *at integral values of* T, *the*

Temperature	$\rho=220$	240	260	280	300	320
°K	°K^{-2}	°K^{-2}	°K^{-2}	°K^{-2}	°K^{-2}	°K^{-2}
145	1.7×10^{-5}	1.8×10^{-5}	2.0×10^{-5}	2.1×10^{-5}	2.3×10^{-5}	2.4×10^{-5}
150	1.5	1.6	1.8	1.9	2.1	2.2
155	1.4	1.5	1.6	1.8	1.9	2.0
160	1.3	1.4	1.5	1.7	1.8	1.9
165	1.3	1.4	1.5	1.6	1.6	1.8
170	110×10^{-7}	120×10^{-7}	130×10^{-7}	140×10^{-7}	150×10^{-7}	160×10^{-7}
180	96	100	110	120	120	130
190	78	83	87	91	96	99
200	63	67	70	73	78	81
210	52	56	59	63	66	69
220	45	49	53	56	59	62
230	40	44	48	51	53	56
240	36	40	43	46	48	51
250	32	35	38	40	43	46
260	29	31	33	35	37	40
270	24.73	26.89	29.03	31.17	33.30	35.42
0° C	24.01	26.09	28.15	30.20	32.23	34.24
280	21.60	23.44	25.26	27.07	28.85	30.62
25° C	17.25	18.66	20.04	21.38	22.69	23.96
300	16.68	18.04	19.37	20.67	21.94	23.17
320	15.08	14.09	15.08	16.02	16.93	17.80
340	10.39	11.16	11.89	12.58	13.24	13.90
360	8.343	8.929	9.480	9.994	10.47	10.96
100° C	7.293	7.785	8.242	8.662	9.043	9.383
380	6.767	7.218	7.635	8.017	8.360	8.663
400	5.536	5.885	6.202	6.485	6.733	6.942
420	4.564	4.834	5.076	5.285	5.461	5.601
440	3.787	3.998	4.181	4.335	4.458	4.547
460	3.161	3.325	3.464	3.575	3.658	3.709
480	2.653	2.780	2.884	2.962	3.014	3.038
500	2.236	2.334	2.411	2.464	2.493	2.499
520	1.892	1.967	2.022	2.056	2.067	2.055
540	1.606	1.663	1.701	1.720	1.718	1.695
560	1.367	1.409	1.434	1.441	1.429	1.396
580	1.166	1.196	1.211	1.208	1.188	1.149
600	0.997	1.018	1.023	1.014	0.988	0.944

TABLE 17. *Values of* $(dZ/d\rho)_T$ *at integral values of* T, *the*

Temperature	$\rho=0$	1	2	3	6	10	20
°K							
16	$-9,105\times10^{-6}$	$-9,087\times10^{-6}$	$-9,070\times10^{-6}$	$-9,052\times10^{-6}$			
18	−7,709	−7,694	−7,679	−7,664	$-7,620\times10^{-6}$		
20	−6,633	−6,621	−6,608	−6,595	−6,557	$-6,506\times10^{-6}$	
22	−5,781	−5,770	−5,759	−5,748	−5,714	−5,670	
24	−5,087	−5,077	−5,067	−5,058	−5,029	−4,990	$-4,892\times10^{-6}$
26	−4,512	−4,503	−4,494	−4,485	−4,460	−4,425	−4,338
28	−4,027	−4,019	−4,011	−4,003	−3,980	−3,948	−3,871
30	−3,615	−3,608	−3,601	−3,594	−3,572	−3,544	−3,474
32	−3,262	−3,255	−3,249	−3,242	−3,223	−3,197	−3,132
34	−2,955	−2,949	−2,943	−2,937	−2,919	−2,895	−2,836
36	−2,688	−2,682	−2,676	−2,671	−2,654	−2,632	−2,577
38	−2,453	−2,448	−2,443	−2,438	−2,422	−2,402	−2,350
40	−2,245	−2,240	−2,235	−2,230	−2,216	−2,197	−2,149
42	−2,059	−2,054	−2,050	−2,045	−2,032	−2,014	−1,968

absolute temperature, and ρ, the density in Amagat units—Continued

340	360	380	400	420	440	460	480	500
°K^{-2}	°K^{-2}	°K^{-2}	°K^{-2}	°K^{-2}	°K^{-2}	°K^{-2}	°K^{-2}	°K^{-2}
2.6×10^{-5}	2.8×10^{-5}	2.9×10^{-5}	3.0×10^{-5}	3.1×10^{-5}	3.3×10^{-5}	3.4×10^{-5}	3.4×10^{-5}	3.5×10^{-5}
2.3	2.5	2.6	2.7	2.9	3.0	3.2	3.2	3.3
2.1	2.2	2.3	2.5	2.7	2.8	3.0	3.1	3.2
2.0	2.1	2.2	2.4	2.5	2.6	2.7	2.9	3.0
2.0	2.1	2.2	2.3	2.4	2.5	2.5	2.6	2.7
170×10^{-7}	180×10^{-7}	180×10^{-7}	190×10^{-7}	190×10^{-7}	200×10^{-7}	200×10^{-7}	200×10^{-7}	210×10^{-7}
140	140	140	150	150	150	150	150	160
100	100	110	110	120	120	120	120	120
83	85	88	92	96	98	99	100	100
72	75	78	81	83	85	87	88	89
65	68	71	73	75	77	80	81	81
60	63	65	67	69	71	74	75	75
55	58	60	62	64	66	68	69	70
49	52	54	56	58	60	62	64	65
43	46	48	50	52	54	56	58	60
37.53	39.63	41.71	43.78	45.83	47.86	49.87	51.85	53.80
36.23	38.19	40.13	42.05	43.93	45.78	47.60	49.38	51.12
32.36	34.08	35.77	37.44	39.07	40.66	42.22	43.73	45.19
25.20	26.39	27.54	28.63	29.68	30.67	31.60	32.47	33.27
24.37	25.53	26.64	27.71	28.74	29.70	30.61	31.45	32.22
18.63	19.41	20.14	20.82	21.44	21.99	22.48	22.90	23.23
14.42	14.94	15.41	15.83	16.18	16.47	16.69	16.83	16.89
11.29	11.63	11.92	12.16	12.33	12.44	12.49	12.46	12.34
9.678	9.926	10.12	10.27	10.36	10.39	10.36	10.25	10.08
8.925	9.139	9.305	9.417	9.473	9.468	9.397	9.256	9.039
7.110	7.236	7.314	7.344	7.319	7.238	7.094	6.885	6.605
5.704	5.765	5.784	5.756	5.678	5.547	5.359	5.110	4.795
4.601	4.618	4.594	4.527	4.415	4.253	4.039	3.769	3.438
3.728	3.713	3.660	3.567	3.433	3.253	2.038	2.746	2.411
3.032	2.993	2.976	2.812	2.664	2.475	2.242	1.961	1.630
2.471	2.416	2.331	2.212	2.057	1.864	1.631	1.354	1.032
2.016	1.951	1.857	1.732	1.574	1.382	1.153	0.884	0.573
1.646	1.573	1.474	1.346	1.189	1.000	0.776	.517	.220
1.342	1.264	1.162	1.035	0.880	0.695	.480	.231	−.052
1.090	1.010	0.908	0.782	.630	.452	.245	.007	−.262
0.883	0.801	.700	.576	.428	.257	.059	−.167	−.422

absolute temperature, and ρ, the density in Amagat units

40	60	80	100	120	140	160	180	200
-4.165×10^{-6}								
−3.715	-3.559×10^{-6}							
−3.332	−3.191	-3.049×10^{-6}	-2.908×10^{-6}					
−3.003	−2.874	−2.745	−2.615	-2.486×10^{-6}	-2.357×10^{-6}	-2.228×10^{-6}	-2.098×10^{-6}	
−2.717	−2.598	−2.479	−2.360	−2.242	−2.123	−2.004	−1.885	-1.768×10^{-6}
−2.467	−2.357	−2.247	−2.137	−2.027	−1.917	−1.807	−1.697	−1.588
−2.248	−2.145	−2.043	−1.940	−1.838	−1.735	−1.633	−1.530	−1.428
−2.053	−1.957	−1.861	−1.765	−1.669	−1.573	−1.477	−1.381	−1.283
−1.878	−1.788	−1.698	−1.608	−1.517	−1.427	−1.337	−1.245	−1.151

TABLE 17. *Values of* $(dZ/d\rho)_T$ *at integral values of* T, *the absolute*

Temperature	$\rho=220$	240	260	280	300	320	340
°K							
34	$-1,650\times10^{-6}$	$-1,526\times10^{-6}$	$-1,392\times10^{-6}$	$-1,254\times10^{-6}$	$-1,121\times10^{-6}$	-998×10^{-6}	-884×10^{-6}
36	−1,477	−1,360	−1,239	−1,117	−1,001	−892	−788
38	−1,322	−1,210	−1,100	−989	−882	−782	−684
40	−1,181	−1,077	−973	−870	−768	−670	−573
42	−1,054	−956	−857	−758	−658	−558	−461
	$\rho=520$	540	560	580	600	620	640
34	387×10^{-6}	654×10^{-6}	941×10^{-6}	$1,255\times10^{-6}$	$1,627\times10^{-6}$	$2,090\times10^{-6}$	$2,638\times10^{-6}$
36	538	795	1,077	1,400	1,750	2,120	2,504
38	681	961	1,260	1,587			
40	812	1,135					
42	940						
	$\rho=0$	1	2	3	6	10	20
42	$-2,059\times10^{-6}$	$-2,054\times10^{-6}$	$-2,050\times10^{-6}$	$-2,045\times10^{-6}$	$-2,032\times10^{-6}$	$-2,014\times10^{-6}$	$-1,968\times10^{-6}$
44	−1,892	−1,887	−1,883	−1,879	−1,866	−1,849	−1,806
46	−1,740	−1,736	−1,732	−1,728	−1,716	−1,700	−1,659
48	−1,603	−1,599	−1,595	−1,591	−1,580	−1,564	−1,526
50	−1,478	−1,474	−1,470	−1,467	−1,456	−1,441	−1,404
52	−1,364	−1,360	−1,357	−1,353	−1,342	−1,328	−1,291
54	−1,259	−1,256	−1,252	−1,249	−1,239	−1,225	−1,191
56	−1,162	−1,159	−1,156	−1,152	−1,143	−1,129	−1,096
58	−1,072	−1,069	−1,066	−1,063	−1,053	−1,040	−1,009
60	−988	−985	−982	−979	−970	−958	−928
65	−807	−804	−801	−799	−790	−779	−751
70	−654	−651	−649	−646	−638	−628	−601
75	−524	−522	−519	−516	−509	−499	−474
80	−412	−410	−407	−405	−398	−388	−364
85	−315	−313	−310	−308	−301	−292	−269
90	−231	−229	−227	−224	−218	−209	−186
95	−157	−155	−153	−150	−144	−135	−113
100	−90	−88	−86	−84	−77	−69	−48
105	−34	−32	−30	−28	−21	−12	+9
110	+19	+21	+23	+25	+32	+40	61
115	67	69	71	73	79	87	108
120	111	113	115	117	123	131	151
125	151	153	155	157	139	171	190
130	187	189	191	193	199	206	226
135	221	223	225	227	232	240	259
140	252	254	256	258	263	271	289
145	281	283	285	286	292	297	317
150	307	309	311	312	318	325	343
155	331	333	335	336	342	349	367
160	353	355	357	358	364	371	389
165	373	375	377	378	384	391	409
170	393	395	397	398	404	411	429
180	429	431	433	434	439	446	464
190	460	462	463	465	470	477	494
200	489	490	491	493	498	504	521
210	512	514	516	517	522	529	545
220	534	536	538	539	544	550	566
230	553	555	557	558	563	569	585
240	571	573	574	576	580	586	602
250	587	589	590	592	596	602	617
260	602	604	605	606	610	616	631
270	613.9	615.3	616.8	618.2	622.5	628.3	642.8

340	360	380	400	420	440	460	480	500	
−884×10⁻⁶	−774×10⁻⁶	−667×10⁻⁶	−562×10⁻⁶	−460×10⁻⁶	−357×10⁻⁶	−234×10⁻⁶	−68×10⁻⁶	+148×10⁻⁶	
−788	−680	−564	−442	−318	−194	−62	+99	302	
−684	−577	−456	−324	−188	−51	+89	247	437	
−573	−467	−347	−213	−73	+69	218	374	550	
−461	−356	−241	−111	+29	173	321	475	639	
640	660	680							
2,638×10⁻⁶	3,227×10⁻⁶	3,848×10⁻⁶							
2,504									
20	40	60	80	100	120	140	160	180	200
1,908×10⁻⁶	−1,878×10⁻⁶	−1,788×10⁻⁶	−1,698×10⁻⁶	−1,608×10⁻⁶	−1,517×10⁻⁶	−1,427×10⁻	−1,337×10⁻⁶	−1,245×10⁻⁶	−1,151×10⁻⁶
1,806	−1,721	−1,636	−1,550	−1,465	−1,379	−1,294	−1,209	−1,122	−1,033
1,659	−1,578	−1,497	−1,416	−1,335	−1,254	−1,173	−1,092	−1,011	−926
1,526	−1,448	−1,371	−1,294	−1,216	−1,139	−1,062	−985	−908	−827
1,404	−1,330	−1,256	−1,182	−1,108	−1,034	−961	−887	−813	−736
1,293	−1,222	−1,151	−1,080	−1,009	−938	−868	−797	−726	−652
1,191	−1,123	−1,054	−986	−918	−849	−781	−713	−645	−573
1,098	−1,031	−965	−899	−834	−768	−702	−636	−570	−499
1,009	−946	−883	−820	−757	−693	−629	−565	−499	−428
928	−867	−807	−746	−685	−623	−561	−497	−431	−361
851	−794	−737	−680	−623	−565	−507	−446	−384	−321
781	−731	−680	−628	−576	−523	−465	−407	−346	−280
718	−674	−628	−581	−534	−486	−438	−386	−330	−273
664	−624	−581	−538	−495	−451	−407	−360	−309	−255
617	−580	−541	−501	−461	−420	−379	−336	−288	−238
577	−543	−507	−469	−432	−394	−355	−315	−270	−223
543	−512	−478	−443	−408	−372	−336	−298	−256	−211
514	−485	−453	−420	−387	−353	−319	−283	−243	−201
489	−462	−432	−401	−369	−337	−305	−271	−233	−193
468	−442	−414	−384	−354	−323	−292	−260	−224	−186
450	−425	−398	−370	−341	−312	−282	−251	−217	−180
435	−411	−385	−358	−330	−302	−273	−243	−210	−175
422	−399	−374	−348	−321	−294	−266	−237	−205	−171
411	−389	−365	−340	−314	−287	−260	−232	−201	−168
402	−381	−358	−333	−308	−282	−255	−227	−197	−165
395	−375	−352	−328	−304	−278	−252	−224	−195	−163
389	−370	−348	−325	−301	−276	−250	−223	−194	−162
385	−366	−345	−322	−299	−274	−249	−222	−193	−162
382	−364	−343	−321	−298	−274	−249	−222	−193	−162
381	−363	−342	−321	−298	−274	−249	−222	−193	−162
381	−363	−342	−321	−298	−274	−249	−222	−193	−162
382	−364	−343	−321	−298	−274	−249	−222	−193	−162
384	−365	−344	−322	−299	−275	−250	−223	−194	−163
387	−368	−346	−324	−301	−277	−252	−225	−196	−165
391	−371	−349	−327	−304	−280	−255	−228	−199	−168
396	−375	−353	−331	−308	−284	−259	−232	−203	−172
402	−380	−358	−336	−313	−289	−264	−237	−208	−177
408	−386	−364	−342	−319	−295	−270	−243	−214	−183
416	−393	−371	−349	−326	−302	−277	−250	−221	−190
424	−401	−379	−357	−334	−310	−285	−258	−229	−198
433	−410	−388	−366	−343	−319	−294	−267	−238	−207
443	−420	−398	−376	−353	−329	−304	−277	−248	−217
454	−431	−409	−387	−364	−340	−315	−288	−259	−228
466	−443	−421	−399	−376	−352	−327	−300	−271	−240
479	−456	−434	−412	−389	−365	−340	−313	−284	−253
493	−470	−448	−426	−403	−379	−354	−327	−298	−267
508	−485	−463	−441	−418	−394	−369	−342	−313	−282
524	−501	−479	−457	−434	−410	−385	−358	−329	−298
541	−518	−496	−474	−451	−427	−402	−375	−346	−315
559	−536	−514	−492	−469	−445	−420	−393	−364	−333
578	613	648	684	721	760	800	842	885	
599	633	667	703	739	777	816	857	900	
618	651	684	719	755	792	831	871	913	
634	666	699	734	770	806	844	884	925	
648	680	713	747	782	818	855	894	935	
661	692	725	758	792	828	865	903	943	
672.6	703.4	735.2	768.1	802.0	837.2	873.6	911.4	950.4	

Temperature	$\rho=0$	1	2	3	6	10	20
0° C	617.7×10⁻⁶	619.1×10⁻⁶	620.5×10⁻⁶	621.9×10⁻⁶	626.2×10⁻⁶	631.9×10⁻⁶	646.4×10⁻⁶
280	625.4	626.8	628.2	629.6	633.8	639.5	653.8
25° C	643.5	644.9	646.3	647.6	651.8	657.3	671.2
300	645.2	646.6	647.9	649.3	653.4	658.9	672.8
320	661.7	663.0	664.4	665.7	669.7	675.0	688.5
340	675.5	676.8	678.1	679.4	683.2	688.4	701.6
360	687.1	688.4	689.6	690.9	694.6	699.7	712.5
100° C	693.7	695.0	696.2	697.4	701.1	706.1	718.7
380	696.9	698.1	699.4	700.6	704.2	709.2	721.6
400	705.2	706.4	707.6	708.8	712.4	717.2	729.3
420	712.3	713.4	714.6	715.8	719.3	724.0	735.8
440	718.3	719.4	720.5	721.7	725.1	729.7	741.3
460	723.4	724.5	725.6	726.7	730.1	734.6	745.9
480	727.7	728.8	729.9	731.0	734.3	738.7	749.8
500	731.4	732.5	733.5	734.6	737.8	742.1	753.0
520	734.5	735.6	736.6	737.6	740.8	745.0	755.8
540	737.1	738.2	739.2	740.2	743.3	747.5	758.0
560	739.3	740.3	741.4	742.4	745.4	749.5	759.8
580	741.2	742.2	743.1	744.1	747.1	751.2	761.3
600	742.7	743.6	744.6	745.6	748.6	752.5	762.5

Temperature	$\rho=220$	240	260	280	300	320
42	−1,054×10⁻⁶	−956×10⁻⁶	−857×10⁻⁶	−758×10⁻⁶	−658×10⁻⁶	−558×10⁻⁶
44	−941	−847	−751	−653	−553	−452
46	−837	−747	−653	−555	−454	−351
48	−742	−654	−562	−464	−362	−258
50	−655	−569	−477	−380	−277	−174
52	−573	−489	−398	−301	−200	−98
54	−496	−413	−324	−229	−131	−31
56	−423	−342	−255	−163	−68	+30
58	−353	−274	−190	−102	−10	+86
60	−287	−211	−131	−46	+44	138
65	−137	−62	+15	+94	177	264
70	−9	+64	137	213	293	376
75	+99	169	241	316	393	475
80	191	260	331	403	480	560
85	270	338	408	480	555	633
90	340	406	475	546	620	696
95	402	467	534	604	676	751
100	457	520	586	655	725	798
105	507	568	632	699	768	840
110	552	611	673	739	807	878
115	592	650	711	775	841	911
120	628	685	745	807	872	941
125	660	716	775	836	900	968
130	689	744	802	862	925	992
135	716	770	827	886	948	1,014
140	740	794	850	908	970	1,034
145	762	816	871	930	990	1,053
150	783	836	891	948	1,008	1,070
155	802	854	908	965	1,024	1,087
160	819	871	924	980	1,038	1,099
165	835	886	938	993	1,051	1,111
170	849	899	951	1,005	1,062	1,121

absolute temperature, and ρ, the density in Amagat units—Continued

40	60	80	100	120	140	160	180	200
676.1×10⁻⁶	706.7×10⁻⁶	738.4×10⁻⁶	771.0×10⁻⁶	804.9×10⁻⁶	839.8×10⁻⁶	876.1×10⁻⁶	913.6×10⁻⁶	952.5×10⁻⁶
683.2	713.5	744.8	777.1	810.6	845.2	881.1	918.2	956.7
699.8	729.2	759.7	791.2	823.7	857.4	892.3	928.4	965.8
701.3	730.7	761.0	792.4	824.9	858.5	893.2	929.2	966.5
716.2	744.7	774.2	804.7	836.2	868.8	902.5	937.4	973.5
728.4	756.2	784.8	814.5	845.1	876.7	909.5	943.3	978.4
738.6	765.6	793.5	822.3	852.1	882.9	914.7	947.6	981.6
744.4	770.9	798.4	826.6	855.9	886.1	917.3	949.6	983.0
747.1	773.4	800.6	828.6	857.6	887.6	918.5	950.5	983.6
754.2	779.9	806.4	833.7	861.9	891.1	921.2	952.4	984.5
760.1	785.2	811.0	837.7	865.2	893.7	923.0	953.4	984.7
765.1	789.5	814.8	840.8	867.7	895.5	924.1	953.7	984.2
769.2	793.1	817.8	843.3	869.5	896.6	924.6	953.5	983.3
772.6	796.0	820.2	845.1	870.8	897.3	924.6	952.8	981.9
775.4	798.3	822.0	846.4	871.6	897.5	924.2	951.8	980.2
777.6	800.2	823.4	847.3	871.9	897.3	923.5	950.4	978.2
779.5	801.6	824.4	847.8	871.9	896.8	922.4	948.9	976.1
780.9	802.6	825.0	848.0	871.7	896.1	921.2	947.1	973.8
782.1	803.4	825.3	847.9	871.2	895.1	919.8	945.2	971.3
782.9	803.9	825.4	847.6	870.5	894.0	918.2	943.1	968.7

340	360	380	400	420	440	460	480	500
−461×10⁻⁶	−356×10⁻⁶	−241×10⁻⁶	−111×10⁻⁶	+29×10⁻⁶	173×10⁻⁶	321×10⁻⁶	475×10⁻⁶	639×10⁻⁶
−352	−249	−139	−15	+120	259	403	553	707
−250	−149	−42	+76	203	335	471	612	759
−157	−57	+48	162	281	404	531	664	804
−73	+27	130	240	353	468	588	715	849
+2	102	204	310	418	528	643	765	894
+68	168	270	373	478	585	697	815	939
128	228	329	431	534	640	750	864	984
183	282	382	484	587	692	800	913	1,031
234	332	431	532	635	740	848	961	1,079
355	450	547	647	752	861	973	1,089	1,210
464	556	652	751	855	963	1,075	1,191	1,312
561	651	745	842	944	1,050	1,160	1,274	1,394
644	733	824	919	1,018	1,122	1,231	1,345	1,465
715	802	892	984	1,081	1,183	1,291	1,405	1,526
776	860	948	1,039	1,134	1,234	1,340	1,454	1,576
829	911	997	1,086	1,180	1,279	1,384	1,496	1,616
875	956	1,041	1,129	1,221	1,319	1,422	1,531	1,646
916	996	1,080	1,167	1,258	1,355	1,456	1,561	1,670
953	1,032	1,115	1,201	1,291	1,387	1,486	1,587	1,693
985	1,064	1,146	1,231	1,320	1,414	1,511	1,611	1,715
1,014	1,092	1,173	1,257	1,345	1,437	1,533	1,633	1,736
1,041	1,117	1,197	1,280	1,366	1,457	1,552	1,652	1,754
1,064	1,140	1,218	1,299	1,384	1,473	1,567	1,667	1,768
1,085	1,159	1,236	1,316	1,399	1,487	1,580	1,678	1,779
1,103	1,176	1,252	1,331	1,413	1,500	1,591	1,686	1,785
1,120	1,191	1,266	1,345	1,426	1,511	1,600	1,693	1,790
1,136	1,205	1,278	1,356	1,436	1,520	1,607	1,699	1,795
1,150	1,218	1,290	1,366	1,444	1,526	1,612	1,704	1,799
1,162	1,229	1,300	1,374	1,451	1,531	1,616	1,707	1,801
1,173	1,240	1,309	1,381	1,457	1,536	1,619	1,707	1,800
1,183	1,248	1,317	1,388	1,462	1,539	1,620	1,706	1,797

897127—48——5

TABLE 17. *Values of* $(dZ/d_\rho)_T$ *at integral values of* T, *the absolute*

Temperature	ρ=220	240	260	280	300	320
180	874×10⁻⁶	922×10⁻⁶	972×10⁻⁶	1 025×10⁻⁶	1, 081×10⁻⁶	1, 140×10⁻⁶
190	895	943	992	1, 043	1, 098	1, 156
200	913	961	1, 009	1, 060	1, 113	1, 169
210	929	976	1, 024	1, 074	1, 126	1, 180
220	943	989	1, 037	1, 086	1, 137	1, 190
230	956	1, 001	1, 048	1, 096	1, 146	1, 198
240	967	1, 011	1, 057	1, 104	1, 154	1, 205
250	976	1, 020	1, 065	1, 111	1, 160	1, 211
260	984	1, 027	1, 072	1, 117	1, 165	1, 215
270	991. 0	1, 033. 1	1, 076. 8	1, 122. 1	1, 169. 3	1, 218. 3
0° C	992. 9	1, 034. 7	1, 078. 2	1, 123. 3	1, 170. 2	1, 219. 0
280	996. 6	1, 038. 0	1, 081. 0	1, 125. 6	1, 172. 0	1, 220. 2
25° C	1, 004. 5	1, 044. 7	1, 086. 4	1, 129. 7	1, 174. 7	1, 221. 4
300	1, 005. 2	1, 045. 3	1, 086. 8	1, 130. 0	1, 174. 8	1, 221. 4
320	1, 011. 0	1, 049. 8	1, 090. 1	1, 131. 8	1, 175. 1	1, 220. 1
340	1, 014. 7	1, 052. 3	1, 091. 3	1, 131. 7	1, 173. 6	1, 217. 1
360	1, 016. 9	1, 053. 4	1, 091. 2	1, 130. 3	1, 170. 9	1, 212. 9
100° C	1, 017. 6	1, 053. 4	1, 090. 4	1, 128. 8	1, 168. 5	1, 209. 7
380	1, 017. 8	1, 053. 2	1, 089. 9	1, 127. 9	1, 167. 2	1, 207. 9
400	1, 017. 8	1, 052. 2	1, 087. 8	1, 124. 7	1, 162. 9	1, 202. 4
420	1, 017. 1	1, 050. 6	1, 085. 2	1, 121. 0	1, 158. 0	1, 196. 4
440	1, 015. 8	1, 048. 4	1, 082. 1	1, 116. 9	1, 152. 9	1, 190. 2
460	1, 014. 0	1, 045. 8	1, 078. 6	1, 112. 6	1, 147. 6	1, 183. 8
480	1, 011. 9	1, 042. 9	1, 074. 9	1, 108. 0	1, 142. 1	1, 177. 4
500	1, 009. 5	1, 039. 8	1, 071. 0	1, 103. 3	1, 136. 6	1, 171. 0
520	1, 006. 9	1, 036. 5	1, 067. 0	1, 098. 5	1, 131. 0	1, 164. 6
540	1, 004. 2	1, 033. 1	1, 062. 9	1, 093. 7	1, 125. 4	1, 158. 2
560	1, 001. 2	1, 029. 6	1, 058. 7	1, 088. 8	1, 119. 9	1, 151. 9
580	998. 2	1, 026. 0	1, 054. 6	1, 084. 0	1, 114. 4	1, 145. 7
600	995. 1	1, 022. 3	1, 050. 3	1, 079. 2	1, 108. 9	1, 139. 7

temperature, and ρ, the density in Amagat units—Continued

340	360	380	400	420	440	460	480	500
1.201×10⁻⁶	1.264×10⁻⁶	1.330×10⁻⁶	1.399×10⁻⁶	1.471×10⁻⁶	1.545×10⁻⁶	1.623×10⁻⁶	1.706×10⁻⁶	1.794×10⁻⁶
1.215	1.276	1.341	1.408	1.478	1.550	1.626	1.707	1.792
1.227	1.287	1.350	1.416	1.484	1.550	1.629	1.708	1.790
1.237	1.296	1.358	1.422	1.489	1.559	1.632	1.708	1.788
1.246	1.304	1.365	1.428	1.493	1.561	1.633	1.708	1.787
1.253	1.310	1.370	1.432	1.496	1.562	1.633	1.708	1.786
1.259	1.315	1.373	1.434	1.497	1.563	1.633	1.706	1.783
1.264	1.319	1.376	1.436	1.498	1.563	1.631	1.702	1.778
1.267	1.321	1.378	1.436	1.497	1.561	1.628	1.697	1.771
1.269.3	1.322.4	1.377.6	1.435.2	1.495.1	1.557.6	1.622.8	1.690.8	1.761.8
1.269.7	1.322.5	1.377.4	1.434.6	1.494.2	1.556.3	1.621.1	1.688.6	1.759.1
1.270.3	1.322.4	1.376.6	1.433.1	1.491.9	1.553.2	1.617.1	1.683.7	1.753.1
1.269.9	1.320.3	1.372.8	1.427.3	1.484.1	1.543.3	1.604.8	1.669.0	1.735.8
1.269.7	1.320.0	1.372.3	1.426.6	1.483.2	1.542.2	1.603.5	1.667.4	1.734.0
1.266.8	1.315.3	1.365.7	1.418.1	1.472.5	1.529.2	1.588.1	1.649.5	1.713.4
1.262.2	1.309.0	1.357.7	1.408.2	1.460.6	1.515.1	1.571.8	1.630.8	1.692.0
1.256.6	1.301.8	1.348.8	1.397.5	1.448.0	1.500.6	1.555.1	1.611.8	1.670.7
1.252.4	1.296.7	1.342.6	1.390.2	1.439.6	1.490.9	1.544.1	1.599.4	1.656.8
1.250.2	1.293.9	1.339.3	1.386.4	1.435.2	1.485.8	1.538.4	1.593.0	1.649.7
1.243.3	1.285.6	1.329.6	1.375.1	1.422.3	1.471.2	1.521.9	1.574.6	1.629.2
1.236.1	1.277.2	1.319.7	1.363.8	1.409.4	1.456.7	1.505.8	1.556.6	1.609.3
1.228.7	1.268.6	1.309.9	1.352.6	1.396.8	1.442.6	1.490.0	1.539.2	1.590.1
1.221.3	1.260.1	1.300.1	1.341.6	1.384.5	1.428.9	1.474.8	1.522.4	1.571.6
1.213.9	1.251.6	1.290.5	1.330.8	1.372.4	1.415.5	1.460.1	1.506.2	1.553.9
1.206.5	1.243.2	1.281.1	1.320.2	1.360.7	1.402.6	1.445.8	1.490.6	1.536.9
1.199.2	1.234.9	1.271.8	1.310.0	1.349.4	1.390.1	1.432.1	1.475.6	1.520.5
1.192.0	1.226.8	1.262.8	1.300.0	1.338.4	1.378.0	1.418.9	1.461.2	1.504.8
1.184.9	1.218.9	1.254.0	1.290.3	1.327.7	1.366.3	1.406.2	1.447.3	1.489.8
1.177.9	1.211.2	1.245.5	1.280.9	1.317.4	1.355.0	1.393.9	1.434.0	1.475.4
1.171.1	1.203.6	1.237.2	1.271.7	1.307.4	1.344.1	1.382.0	1.421.2	1.461.5

Many thermodynamic equations involve derivatives in which P, V, and T are the variables of state. Applications of the tables of this paper in which the variables are Z, ρ, and T to calculations of properties involving derivatives in which the variables are P, V, and T may be facilitated by means of equations relating the P, V, T and the Z, ρ, T derivatives. The following are adequate for many ordinary uses:

$$\frac{T}{P}\left(\frac{dP}{dT}\right)_V=\frac{T}{P}\left(\frac{dP}{dT}\right)_\rho=\frac{T}{P}\left(\frac{dS}{dV}\right)_T=1+\frac{T}{Z}\left(\frac{dZ}{dT}\right)_\rho \tag{4.2}$$

$$-\frac{V}{P}\left(\frac{dP}{dV}\right)_T=\frac{\rho}{P}\left(\frac{dP}{d\rho}\right)_T=1+\frac{\rho}{Z}\left(\frac{dZ}{d\rho}\right)_T \tag{4.3}$$

$$-\frac{T}{V}\left(\frac{dV}{dT}\right)_P=\frac{T}{\rho}\left(\frac{d\rho}{dT}\right)_P=\frac{T}{V}\left(\frac{dS}{dP}\right)_T=\frac{1+\frac{T}{Z}\left(\frac{dZ}{dT}\right)_\rho}{1+\frac{\rho}{Z}\left(\frac{dZ}{d\rho}\right)_T}. \tag{4.4}$$

The Joule-Thomson coefficient μ may be utilized to illustrate the use of these formulas. Thus for purposes of calculations with the tables of this paper, the familiar equation

$$\mu=\left(\frac{dT}{dP}\right)_H=\frac{V}{C_p}\left[\frac{T}{V}\left(\frac{dV}{dT}\right)_P-1\right], \tag{4.5}$$

is put in the form

$$\mu=\left(\frac{dT}{dP}\right)_H=\frac{V_0}{\rho C_p}\left[\frac{1+\frac{T}{Z}\left(\frac{dZ}{dT}\right)_\rho}{1+\frac{\rho}{Z}\left(\frac{dZ}{d\rho}\right)_T}-1\right], \tag{4.6}$$

where V_0 is the molar volume of hydrogen at standard conditions and C_p is the molar heat capacity at the given conditions of T and P or T and ρ.

In correlating the PVT data for hydrogen the function

$$\sigma=\frac{T}{T_0}\frac{V}{V_0}\log_{10}\frac{PV}{RT} \tag{4.7}$$

was used, where T_0 is the Kelvin temperature of the ice point. Reported temperatures were reduced wherever possible to a thermodynamic scale having the ice point temperature 273.16°. All available data were considered in this work but only those appearing most reliable were used and these were weighted according to their apparent precision. The data used [59, 61, 63, 65, 66, 67, 70 to 74, 76, 79, 81, 85, 88, 91, 177] are plotted in figure 6 with the exception of a few observations at temperatures below 29° K and at densities lower than $\rho=10$, which were omitted because in these regions of low precision the scattering is so great that the points would be confusing.

A lower boundary to the σ versus ρ gas-liquid diagram in figure 6 is furnished by the vapor-liquid saturation line and the freezing curve. These are represented in figure 6 by dashed lines. The saturation line for the vapor rises steeply onto the diagram at low densities and with decreasing slope approaches tangency to the critical isotherm at the critical point which is indicated by an asterisk. The saturation line for liquid hydrogen is a nearly straight and horizontal line from a density somewhat greater than the critical to the triple point. The freezing curve, which represents the values of σ for liquid when for a given temperature the pressure is great enough to cause the liquid to freeze, rises nearly vertically from the triple point and bends towards higher densities.

The saturation curve on the vapor side was obtained with the help of the vapor pressure equation (eq 7.2) and the PVT representation given by eq 4.14 and table 19. On the liquid side it was obtained from the same vapor pressure equation and the volumes of the liquid at saturation pressure, given in table 31 and discussed in section VIII. The freezing curve was obtained from the melting point-pressure relations given in table 30 combined with extrapolations based on the higher density observations of Bartholomé for the isotherms of the liquid which are given in table 32.

The isothermal curves of figure 6 represent final table values. The curves are not necessarily the best fit for the experimental data for each individual isotherm inasmuch as the curves and table values are the result of correlating all the data and include the temperature dependence which, while it does not affect the relative position of points on one isotherm, may shift the whole isotherm somewhat. Isotherms that depended upon only a few individual observations and covered only a small range of densities were given less weight than others. For a given isotherm, data at higher densities, corresponding to larger deviations from the ideal gas law, were usually given

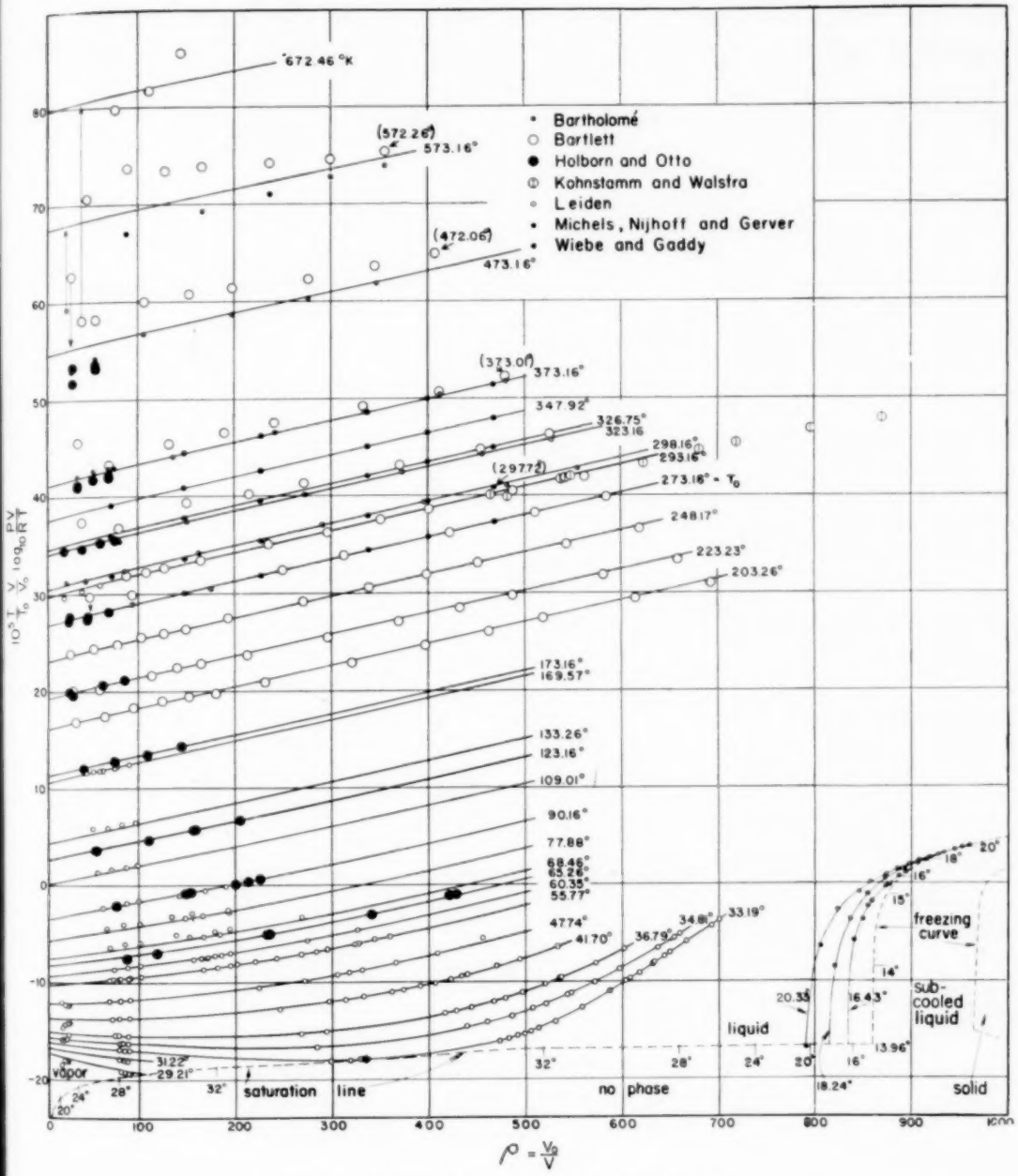

FIGURE 6. *Plot of PVT data for H_2 in the fluid states.*

greater weight than data at low densities. In fact in some instances the low density data were given zero weight. Data at the highest temperatures do not appear to be very reliable, probably because of penetration of the containers by hydrogen. At very low temperatures the deviations from the ideal gas law have not been measured very precisely because the pressure range over which

measurements can be made is limited by condensation.

Cragoe has shown that for densities up to $\rho=500$ the 0° C isotherm is fitted to within experimental accuracy by the equation $\sigma=b+c\rho$. Figure 6 shows that, although this linear relation between σ and ρ fails at low temperatures, it is valid within experimental error over a considerable range of temperatures above 200° K. This relation was made the basis for the correlation of the PVT data above 0° C. The different method used for correlating the data below 0° C is described under (b).

(a) Region Above 0° C

Above 0° C, equations of the form $\sigma=b+c\rho$ were fitted to the PVT data plotted in figure 6, and b and c, the intercept and slope of an isothermal line, were determined as functions of T. The quantity $Z=PV/RT$ thus obtained as a function of T and ρ,

$$PV/RT=\exp 2.30259\ \frac{T_0}{T}\ [b(T)\rho+c(T)\rho^2]=$$
$$\exp\ [B(T)\rho+C(T)\rho^2], \qquad (4.8)$$

was used for the calculation of the tables of Z, P, $(dZ/d\rho)_T$, $(dZ/dT)_\rho$, and $(d^2Z/dT^2)_\rho$.

Before fitting functions of T to b and c, small corrections were applied to some of the data. A constant error in T and constant factor errors along an isotherm in P, V, and the number of moles of gas, cause deviations from the true isotherm that are very nearly proportional to $1/\rho$. Such hyperbolic deviations from a straight line are most easily detected in data extending from low to high densities. A change in V by 0.2 percent is sufficient to considerably straighten the 573.16° K (300° C) isotherm of Wiebe and Gaddy, and raise the line drawn through their adjusted data so that it intersects the σ axis of figure 6 only 0.7 unit below the table line for 573.16° K and crosses the table line at $\rho=550$. Wiebe and Gaddy call attention in their paper to an estimated error of 0.05 to 0.10 percent in the volume of their high pressure steel pipette at 200° and 300° C. It would seem that some part of the 0.2-percent adjustment, which straightens the 300° C isotherm of Wiebe and Gaddy, might be attributed to small temperature and pressure errors and to some loss of hydrogen in the steel.

Hyperbolic adjustments proportional to $1/\rho$ of Bartlett's higher temperature data straighten the isotherms and improve their agreement with the lines representing the tables. A comparison of the observations of Michels, Nijhoff, and Gerver [79] at different temperatures for nearly constant values of ρ, revealed apparent small hyperbolic trends of the data for the separate isotherms superposed on one larger though small random pattern of scattering common to all their isotherms. Using their 0° C isotherm as a reference line, their other data were adjusted to remove the hyperbolic deviations. The points of figure 6 represent reported data adjusted only to the Kelvin scale having 273.16° at the ice point.

Least square determinations were made of the straight lines fitting the adjusted σ versus ρ isothermal data for the different observers separately. From these, values of intercept b and slope c were obtained for the different observers at each temperature of measurement. Holborn's data above 0° C, however, were used only for obtaining intercepts, the slopes of adjacent isotherms of other observers being used with his data.

Expanding the exponential of eq 4.8,

$$PV/RT=1+B\rho+[(1/2)B^2+C]\rho^2+[(1/6)B^3+BC]\rho^3$$
$$+[(1/24)B^4+(1/2)C^2+(1/2)B^2C]\rho^4+\ldots \qquad (4.9)$$

shows that $B\ (T)$ is the second virial coefficient and that a correlation of intercepts b of σ-isotherms is essentially a correlation of values of the second virial coefficients of hydrogen. Formulas expressing the dependence of the second virial coefficient on temperature have been derived theoretically on the assumption of simple laws of intermolecular forces. One of the most satisfactory formulas is based on a law of intermolecular force of the form $\lambda_n r^{-n}-\lambda_m r^{-m}$ and is due to Lennard-Jones. For $n=13$ and $m=7$, the Lennard-Jones formula for B is

$$B=B_1T^{-1/4}+B_2T^{-3/4}+B_3T^{-5/4}+\ldots, \qquad (4.10)$$

where all the coefficients B_i of this infinite series are determined by λ_n and λ_m. Following essentially a procedure used successfully by F. G. Keyes [89], we used only the first three terms of the series and selected values for B_1, B_2, and B_3 which resulted in the best fit of a three constant equation with the intercepts of the σ-isotherms. Our formula,

$$B=0.0055478T^{-1/4}-0.036877T^{-3/4}-0.22004T^{-5/4} \qquad (4.11)$$

intended for use above 0° C, passes through the intercept of the −50° C isotherm determined by the correlation below 0° C.

The slopes of the σ-isotherms were represented by a two term empirical formula without theoretical justification, except that it involves powers of T which make C go to zero as T grows very large.

$$C=0.004788T^{-3/2}-0.04053T^{-2}. \quad (4.12)$$

The exponents of T were chosen so as to simplify the temperature function coefficients in the power series in ρ of eq 4.9.

The tables from 270° to 600° K have been computed on the basis of these formulas, and in this temperature range the various derivatives tabulated have been calculated analytically.

It was not until considerably after the preparation of the tables on hydrogen that we were able to examine the data of Michels and Goudeket published in Physica 1941 [91]. Values of σ for these data on H_2 are shown as solid circles in figure 7 with the tables represented by the solid straight lines. The agreement for H_2 is not complete but seems fairly satisfactory at moderate densities. At low densities there are discrepancies, roughly hyperbolic, which have the appearance of the hyperbolic deviations resulting from small systematic errors discussed earlier in this section. If the hyperbolic deviation is attributed to a systematic error in the volume, the error amounts to 0.06 percent for the 100° C isotherm, and for the other isotherms it is of this approximate magnitude or smaller. At low densities the deviation for the 0° C isotherm does not appear to be systematic. On the other hand, it will be seen that there is a systematic deviation at densities greater than 500 with the experimental values for σ less than those obtained by linear extrapolation from the intermediate densities. This trend is supported by the high pressure data of Kohnstamm and Walstra [61, 81], also shown in the figure. If the representation of the σ isotherm by an equation is extended beyond $\rho=500$, it will be necessary to include a small quadratic term in the expression for σ.

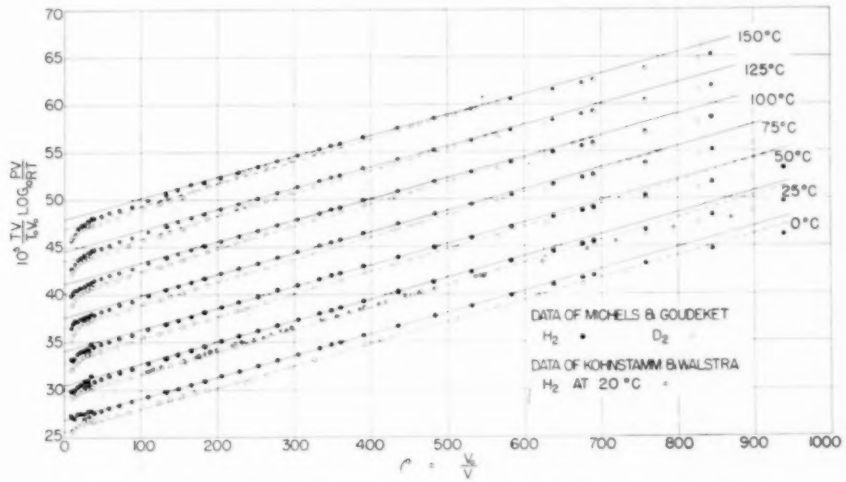

FIGURE 7. *A plot of part of the PVT data for* H_2 and D_2 *from* 0° *C to* 150° *C.*

(b) Region Below 0° C

At low temperatures the σ versus ρ isotherms are curved; making it difficult to decide how the isotherm should be drawn at low densities where the data were meager and the precision was low. Another function, $T^{3/2}V/V_0\left(1-\frac{PV}{RT}\right)$, plotted against $\rho=V_0/V$ as abscissa gave lines which appeared to be straight at low densities for temperatures below 56°K, though there is considerable curvature at high densities. In figure 8, $T^{3/2}V/V_0\left(1-\frac{PV}{RT}\right)+0.0006\rho=\psi$ is plotted against ρ, the term 0.0006ρ being added to make isotherms nearly horizontal at low densities and thus increase the scale of the plot. The sensitivity to

small changes of PV/RT at $\rho=200$ and $T=55°$ K is 18 times greater in figure 8 than in figure 6 and 14 times greater at $\rho=200$ and $T=33°$ K. The curves of figure 8 were drawn to fit the data for each particular isotherm considered independently, and though the curves do not represent the tables exactly they agree closely with them. Below 31°K the data were not sufficient and precise enough to determine consistent isothermal curves when the isotherms were considered independently. The data lower than 29°K were not plotted because the double valued nature of ψ causes the data below 29° K to fall in the same region on the diagram as is covered by the data above 29° K.

At first it appeared that the critical isotherm in figure 8 could be represented by a straight line from ρ equal to zero to ρ greater than the critical density. However, the conditions that $(dP/dV)_T$ and $(d^2P/dV^2)_T$ be zero at the critical point impose upon the slope and curvature of the isotherm at the critical point the conditions

$$\left.\begin{aligned}\left(\frac{d\psi}{d\rho}\right)_{T_c}&=\frac{T_c^{3.2}}{\rho_c^2}\left(2\,\frac{P_cV_c}{RT_c}-1\right)+0.0006,\\ \left(\frac{d^2\psi}{d\rho^2}\right)_{T_c}&=\frac{2T_c^{3.2}}{\rho_c^3}\left(1-3\,\frac{P_cV_c}{RT_c}\right).\end{aligned}\right\}\qquad(4.13)$$

In addition, values for the critical temperature and pressure should satisfy the vapor-pressure equation.

Only a single determination has been made of the critical temperature and pressure of hydrogen [62]. The critical isotherm was located somewhere between the 2 measured isotherms at 32.94° and 33.29° K, and was at the time (1917) considered to be 33.19° K with a certainty of about 0.1°, though in 1925 it was stated in a footnote to Leiden Communication 172a that T_c should be about 0.1° lower. The critical pressure inferred from the P versus V isotherms in 1917 was 12.8 atm. Later in 1917 [142] the vapor pressure equation of H_2 above the boiling point was determined and the value 12.75 atm deduced for P_c using $T_c=33.18°$ K (on basis of $T_0=273.09$). Two determinations [62] were made of the critical density based on the extrapolation of the rectilinear diameter. These gave $\rho_c=345$. The values reported in later Leiden Communications have not in all cases been the latest determined values. The most recently reported Leiden values [69] are

[7] Unless otherwise stated, temperatures are expressed on the Kelvin scale with $T_0=273.16°$.

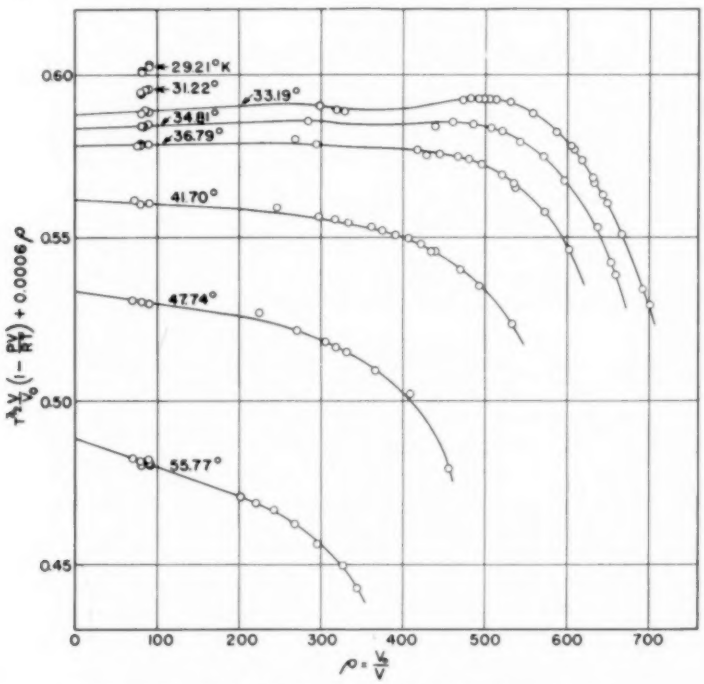

FIGURE 8. *Plot of PVT data for* H_2 *at low temperatures.*

T_c=33.19° K (on basis of T_0=273.16), P_c=12.751 atm and $1/\rho_c$=0.02909 or ρ_c=344. The lower critical temperature 33.1° K inferred from Leiden Communication 172a is supported by the agreement of the vapor pressure 12.81 atm, calculated from vapor pressure equation (eq 7.2) with the critical pressure determined in 1917 from the P versus V isotherms.

Difficulties are encountered in obtaining agreement with the experimental PVT data (fig. 8) on the basis of T_c=33.1° and P_c=12.81 atm, however, unless the critical density is inferred to be about 320, in Amagat units, instead of the reported values 345 or 344. This difference in critical density seemed too large on the basis of the probable precision of the density measurements. The adjustment has instead been so made and the critical isotherm in figure 8 so drawn that T_c=33.19°, P_c=12.98 atm, and ρ_c=335. This value of P_c is consistent with the PVT data and with vapor pressure equation (7.2). These critical constants are listed in table 18.

TABLE 18. *Critical constants of hydrogen*

T_c	P_c	$\rho_c=\frac{V_0}{V_c}$	V_c	$\frac{P_cV_c}{RT_c}$
°K	*atm*		*cm³mole⁻¹*	
33.19	12.98	335	66.95	0.3191

It seemed reasonable to assume that the isotherms of figure 8 are straight lines up to ρ=200. This assumption was used in correlating the observed data below the critical temperature where the data were scarce and the precision low. In figure 9 the intercepts A and the slopes C' of the isotherms of figure 8 are plotted as functions of the temperature. The curve for the slope was extrapolated smoothly to lower temperatures as slopes could not be obtained from the data below 33° K.

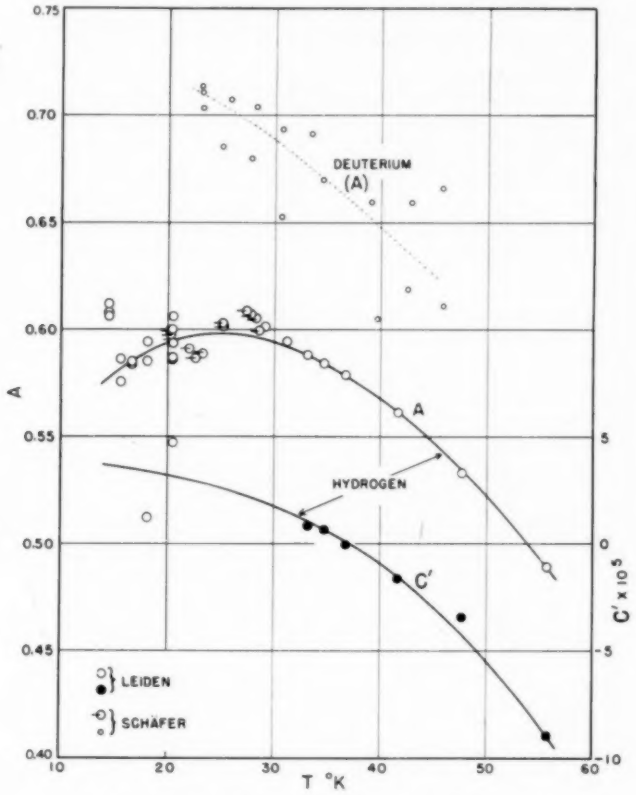

FIGURE 9. *Intercepts and slopes from figure 8.*

807127—48— —6

Also shown in figure 9 are values for A calculated from second virial coefficients determined experimentally by Schäfer [85]. Schäfer reported the results of his PVT measurements as virial coefficients $B'(T)=d(PV/RT)/dP$ at constant temperature and at $P=0$. The values of $A=-(RT^{5/2}/V_0)B'(T)$ obtained from Schäfer's results agree well with those obtained from data of the Leiden Laboratory as shown by figure 9. Schäfer observed no consistent difference between the second virial coefficients of para hydrogen, normal hydrogen, and a one to one mixture of ortho and para varieties.

The equation for the straight part of the ψ-isotherms of figure 8 may be written

$$\frac{T^{3/2}}{\rho}\left(1-\frac{PV}{RT}\right)=A+C\rho, \qquad (4.14)$$

where $C=C''-0.0006$, C' being the slopes plotted in figure 9 of the ψ-isotherms in figure 8. Values of A and C and their derivatives are given for hydrogen in table 19. The values of PV/RT from $\rho=0$ to $\rho=200$ and from $T=14°$ to $T=56°$ K in table 13 were calculated using eq 4.14 with table 19. Table 20, giving the pressure, density, and value of PV/RT for saturated H_2 vapor, was prepared similarly using the vapor pressure equation for n-H_2 (eq 7.2). For certain uses eq 4.14 with table 19 may be more convenient than the tables of PV/RT and its derivatives.

TABLE 19. *Hydrogen values of A and C (and derivatives) in the equation for isotherms*

$$T^{3/2}\frac{V}{V_0}\left(1-\frac{PV}{RT}\right)=A+C\rho$$

[Applicable at Amagat densities less than 200]

T	A	C	dA/dT	dC/dT
° K	° $K^{3/2}$	° $K^{3/2}$	° $K^{3/2}$	° $K^{3/2}$
14	0.5754	$-5,621\times10^{-7}$	0.03388	-75×10^{-5}
16	.5827	−5,636	.03330	−82
18	.5887	−5,653	.03264	−90
20	.5933	−5,672	.03192	−100
22	.5965	−5,693	.03116	−112
24	.5981	−5,716	.03040	−127
26	.5981	−5,743	−.02932	−145
28	.5966	−5,774	−.02797	−165
30	.5940	−5,809	−.02154	−187
32	.5904	−5,848	−.02202	−213
34	.5858	−5,892	−.02243	−245
36	.5805	−5,943	−.02280	−282
38	.5746	−6,003	−.03317	−320
40	.5679	−6,071	−.03356	−358
42	.5604	−6,146	−.03397	−396
44	.5521	−6,229	−.03438	−436
46	.5429	−6,320	−.03476	−478
48	.5330	−6,420	−.03509	−522
50	.5225	−6,529	−.03540	−565
52	.5114	−5,646	−.03572	−603
54	.4996	−6,770	−.03608	−636
56	.4871	−6,900	−.03650	−664

TABLE 20. *Pressure, density, and PV/RT for saturated H_2 vapor*

T	P	ρ	PV/RT
° K	*atm*	*Amagats*	
14	0.0728	1.445	0.9841
16	.2018	3.562	.9679
18	.4551	7.321	.9436
20	.8891	13.311	.9120
22	1.5645	22.235	.8749
24	2.5455	35.017	.8278
26	3.8986	53.02	.7728
28	5.695	78.55	.7078
30	8.010	116.33	.6272
32	10.933	180.94	.5159
33.19	12.98	335	.3191

For temperatures below 56° K and densities greater than $\rho=200$ where ψ could not be represented by a simple function of ρ, a table was made of values of ψ for each ρ and T entry in the Z-table. The ψ-values of this table were obtained from figure 8 by graphical interpolation. Large plots of ψ-isochores, 20 Amagat units apart, on ψ versus T graphs were made of values of ψ read from figure 8. Values of ψ at 2-degree intervals were read from the isochores. A $Z(\rho,T)$ table was calculated from the $\psi(\rho,T)$ table.

From 56° to 273° K, the σ-function rather than the ψ-function was used because above 56° K the σ-isotherms approach linear functions of the density. The method of graphical interpolation used below 56° K was used above, also, to obtain a table of σ-values for the ρ and T entries of the Z-table. The accuracy of graphical interpolation was improved by using more sensitive plots than figure 6 of modified σ-functions obtained by adding to σ simple functions of T and ρ, which brought the isotherms and isochores closer together so that they could be easily plotted to a large scale. Values of σ were obtained at densities as high as $\rho=500$, although between 70° and 200° K measurements were not available at densities this high. This region was filled in by extrapolation of σ curves to higher densities along isotherms and by interpolation along isochores between the upper

and lower temperature regions where there were data to determine the trend. From the $\sigma(\rho,T)$ table a $Z(\rho,T)$ table was obtained by calculation.

The $Z(\rho,T)$ table obtained through graphical interpolation of the ψ and σ isotherms as has just been described was smoothed along isotherms and along isochores by inspection of second differences. In general the Z-tables are smooth to one unit in the last digit.

The tables of $(dZ/dT)_\rho$ and $(dZ/d\rho)_T$ below 0° C were for the most part calculated from the smoothed Z table by the method of Rutledge [179] for the calculation of derivatives from smooth sets of tabular values of data.[8] In the region below 56° K and $\rho=200$, where the ψ versus ρ isotherms are straight lines, the following equations, obtained by differentiating eq 4.14, were used with table 19 to calculate the derivatives

$$\left(\frac{dZ}{dT}\right)_\rho = \frac{3}{2}\frac{(1-Z)}{T} - \frac{\rho}{T^{3/2}}\frac{dA}{dT} - \frac{\rho^2}{T^{3/2}}\frac{dC}{dT} \quad (4.15)$$

$$\left(\frac{dZ}{d\rho}\right)_T = -\frac{1}{T^{3/2}}[A+2(C'-0.0006)\rho]. \quad (4.16)$$

Where the derivatives could be obtained both by the method of Rutledge and by eq 4.15 and 4.16, the agreement was very satisfactory. The $(dZ/d\rho)_T$ and $(dZ/dT)_\rho$ tables were also smoothed along isotherms and isochores by inspection of second differences.

The $(d^2Z/dT^2)_\rho$ table below 0° C was obtained throughout by the method of Rutledge from the smoothed $(dZ/dT)_\rho$ table and was also smoothed. The equation for $(d^2Z/dT^2)_\rho$ corresponding to eq 4.15 for the first derivative was considered too involved for easy computation.

In general, the tables of derivatives are smooth to the last digit recorded.

(c) Reliability of Tables of PVT Data

By inspecting figures 6 to 8 it is possible to arrive at some general conclusions regarding the deviations of the observed data from the $Z(\rho,T)$ table. It may be noted that, except at low densities, the deviations of the observational values of σ from the curves representing the table are of about the same magnitude at different densities along a given isotherm up to $\rho=500$.[9] This means that deviations of $(PV/RT)-1$ along an isotherm are approximately proportional to the density. At low densities the deviations are large because the sensitivity of the σ and ψ plots approaches infinity as ρ approaches zero. It is difficult to make an estimate of the probable error in PV/RT based on the deviations because, as is seen, the greatest deviations are the systematic differences between the results of different observers and are not accidental errors as should be the case if error theory were to apply. The user of the tables can make an estimate of the mean difference between the observed and tabulated values of PV/RT, in any particular region of temperature and density by noting the deviations shown on the graph and from these calculating the corresponding deviations in PV/RT. For temperatures below 60° K it would be best to use figure 8 for this purpose as it is plotted to a larger scale than is figure 6.

In constructing the tables for the intermediate temperature regions where analytical equations of state were not used, just enough digits were retained so that changes made in smoothing would be confined to the last digit. As a considerable amount of smoothing resulted from the graphical methods used, many of the irregularities in the measured values were not apparent in the unsmoothed tables.

It is believed that throughout the table the values were carried out to at least as many significant figures as were at all justified by the data, and that the last digit recorded should be considered very uncertain. In that part of the table between 77° and 200° K which was filled in by interpolation and extrapolation the last two digits should be considered uncertain, the last recorded digit being retained to achieve continuity with the rest of the table.

The tables are thought to be most reliable for temperatures between 273° and 373° K (0° and 100° C), because at these temperatures the experimental difficulties encountered are not as great as at higher and lower temperatures. Also, as is shown by figure 6 the results of several different investigators are in agreement at these temperatures. Above 373° K the experimental data are not as self-consistent as at temperatures immediately below. As the values of PV/RT given in the tables for these higher temperatures are derived largely from an extrapolation based on the temperature region between 273° and 373° K,

[8] Assuming that differences of higher order than the fourth are negligible.
[9] For still greater densities larger deviations occur as shown by figure 7.

an estimate of reliability of the high temperature portion of the tables involves both the applicability of the correlating function, eq 4.8, and the precision of the experimental data. Considering the differences between the isothermal lines determined by different sets of experimental data of different observers and the same observer at different temperatures, it seems probable that the extrapolation is more reliable than the experimental data at temperatures above 473° K.

It is doubted that PV/RT is known to better than 0.2 percent for densities as high as 100 Amagats near 33° K, the critical temperature.

Below the critical temperature, the data are not very satisfactory. In addition to the difficulties of making measurements at low temperatures, there exists the circumstance that below the critical temperature the range of vapor densities that can be covered is limited by the density of saturated vapor. At low densities the deviations $(1-Z)$ from the ideal gas law are small and hence difficult to measure precisely.

There is another method of obtaining values of second virial coefficients which may be advantageous for the low temperature region. It involves the determination of the velocity of sound, which has been carried out for gaseous hydrogen at liquid-hydrogen temperatures and various pressures by van Itterbeek and Keesom [77], using a resonance method. The change of the velocity of sound with pressure at very low pressures is related to the value of the second virial coefficient and to its first and second derivatives. Because of this relationship, it is possible to determine the second virial coefficient from the velocity of sound if the second virial coefficient is already known in an adjacent range of temperature. Van Itterbeek and Keesom concluded that the agreement between their own measurements and the PVT data was "rather good", although for both types of data the scattering was quite appreciable.

In calculating the tables of derivatives by the method of Rutledge, the criterion for retaining significant figures in the recorded values was the same as that previously mentioned, namely, enough places were carried so that the changes resulting from the smoothing were in general confined to the last digit. As in the case of the tables of PV/RT, it is believed that the tabulated values of the derivatives are given to as many significant figures as are justified by the data.

2. Deuterium

The interesting features of the PVT data for deuterium are most evident when deuterium is compared with hydrogen. The difference between the second virial coefficients of H_2 and D_2 has been investigated theoretically [86, 87], though a complete treatment of the problem has not been made.

Assuming the same intermolecular forces for H_2 and D_2, classical mechanics and statistics lead to the same equation of state for H_2 and D_2. The quantum theory of virial coefficients leads to effective volumes of molecules and to second virial coefficients that are larger than the classical values, the differences being small at ordinary temperatures but becoming large at low temperatures.[10]

In table 21 are given ratios between quantum mechanical and classical values of second virial coefficients, for gases whose molecules are rigid nonattracting spheres. They may also be considered as ratios between apparent molecular volumes for the two treatments. These ratios are based on formulas derived by Uhlenbeck and Beth [84]. Columns 2 and 3 are for gases with molecular weights 2 and 4, respectively. The value of the ratio depends, among other things, upon the diameters of the rigid spheres. Here the size of the spheres was taken to be the same for the two

TABLE 21. *Ratio between quantum mechanical and classical second virial coefficients for nonattracting rigid spherical molecules* [a] *of molecular weight M*

T	$\frac{B \text{ quantum}}{B \text{ classical}}$ for $M=2$	$\frac{B \text{ quantum}}{B \text{ classical}}$ for $M=4$
° K		
600	1.21	1.15
300	1.30	1.21
100	1.52	1.37
25	2.7	2.0
5	4.6	2.6

[a] With diameters calculated from the van der Waals' b for hydrogen.

[10] The application of quantum mechanics instead of ordinary mechanics has as one effect for rigid spherical molecules the removal of the classical discontinuity in the calculated distribution of molecules for pair separations corresponding to contact between the spheres. As smaller separations are prevented by the impenetrability of the spheres, the continuity is established by a reduction of the molecular density for separations greater than that corresponding to contact. The effect is large for separations of sphere surfaces up to a considerable fraction of the de Broglie wavelength (for which $h/\sqrt{2mkT}$ is a representative value) and depends through this upon the temperature. This reduction of molecular density beyond the minimum separation could be represented roughly in a classical description as an increase of the volume from which 1 molecule causes the centers of other molecules to be excluded. In classical theory the second virial coefficient for nonattracting rigid spheres is proportional to the excluded volume.

gases and to be equal to the size calculated from the van der Waals b for H_2.

Although it would scarcely be expected that the results of calculations for rigid nonattracting spheres would apply to real H_2 and D_2 molecules, it would seem likely that qualitative indications would be correct, at least at higher temperatures where the excluded volume predominates over the intermolecular attractive forces in determining the magnitude of the second virial coefficient. This is borne out by experiment, the difference in second virial coefficients $(B_{H_2}-B_{D_2})$, being positive, though smaller than would be indicated by table 21 for rigid spheres by a factor of about 2.6 at 300° K. Uhlenbeck and Beth derived an approximate quantum mechanical representation for the second virial coefficient applicable at high

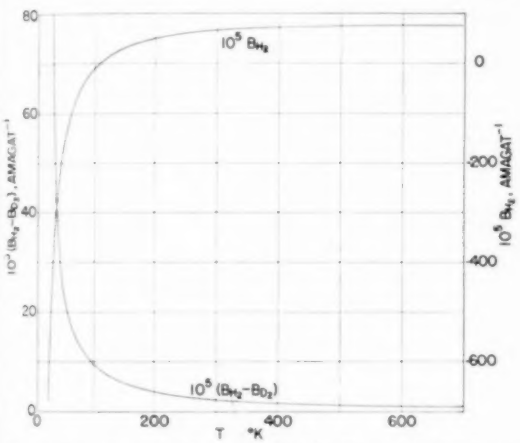

FIGURE 10. *Second virial coefficient for* H_2 *and the difference between second virial coefficients for* H_2 *and* D_2.

temperatures for molecules with radially symmetrical force fields. Their formulas were applied to hydrogen and deuterium by de Boer and Michels [87] upon the assumption that the intermolecular forces were the same for H_2 and D_2. They obtained differences between the virial coefficients for H_2 and D_2 represented by the upper temperature portion of one of the curves of figure 10. In a later paper by Michels and Goudeket [92] attention was called to the fact that the intermolecular forces of hydrogen and deuterium do differ a little because the mean internuclear separations of H_2 and D_2 molecules are different as a result of the different zero point vibrations of their nuclei.

The effect of the intermolecular attractive forces overbalances the effect of the excluded volume or the repulsive forces of the molecules in determining the magnitude of the second virial coefficient at low temperatures, and makes the coefficient negative. Nevertheless, at low temperatures, as at high temperatures, the difference in second virial coefficients $B_{H_2}-B_{D_2}$ is positive, partly for the reason already discussed in the case of high temperatures, namely the larger apparent quantum-mechanical volume of H_2 molecules, and partly for another reason. There is a closer spacing of the discrete negative energy states and smaller zero point energy for pairs of D_2 molecules than for pairs of H_2 molecules because of the mass difference, so that by reason of the Boltzmann factor, exp [−energy/kT], there is a greater degree of association or clustering together of D_2 molecules than of H_2 molecules. Without a consideration of the Boltzmann factors for these negative energy levels the effect of the difference of mass would be less clear, as the quantum treatment for the continuum would require that the spacing of the levels there be smaller for D_2 than for H_2 in essentially the same ratio as in the case of the discrete negative energy levels. With these or similar ideas in mind, Schäfer [86] derived a formula for the difference in second virial coefficients for H_2 and D_2 at low temperatures, which involved a constant whose magnitude he so chose as to obtain a fit with his experimental values for the difference in the second virial coefficients.

Figure 9 shows values of A in the equation of state (eq 4.14) calculated from the second virial coefficients of deuterium for the temperature range 23° to 45° determined experimentally by Schäfer [85].

$$A=-T^{3/2}(dZ/d\rho)_{T,\rho=0}=-T^{3/2}B_1, \quad (4.17)$$

where B_1 is the second virial coefficient in the equation of state $PV=RT\ (1+B_1\rho+B_2\rho^2+\ldots)$. The dashed line curve in figure 9 was obtained by adding to the A's for H_2 the differences between the A's calculated from the differences between the second virial coefficients of H_2 and D_2 which Schäfer determined partly theoretically and partly empirically. Schäfer's measurements were made on deuterium at low densities and hence do not give information on higher virial coefficients. Approximate values of PV for deuterium at low

temperatures may be found by using values of A from figure 9 in eq 4.14, and either neglecting the C term or preferably using the corresponding value of C for H_2.

Values of the function $\sigma=(TV/T_0V_0)\ \log_{10}(PV/RT)$ calculated from the data of Michels and Goudeket [92] for D_2 are shown as open circles in figure 7. The dashed straight lines for deuterium are obtainable from the equation

$$PV/RT=\exp[B(T)\rho+C(T)\rho^2], \qquad (4.18)$$

where

$$B(T)=0.0055298T^{-1/4}-0.036040T^{-3/4}-0.25878T^{-5/4}$$

and

$$C(T)=0.00580T^{-3/2}-0.0565T^{-2}.$$

The constants in the formula for B have been so chosen that the difference between D_2 and H_2 intercepts on the $\sigma-$axis is in close agreement with the theoretical result of de Boer and Michels [87] from 250° to 450° K.

In figure 10, a curve marked $10^5(B_{H_2}-B_{D_2})$ shows the trend of differences between second virial coefficients based on the theoretical calculations above 150° K and on the results of Schäfer below 50° K with an interpolation between. It may be inferred that the differences between the PVT data for H_2 and D_2 decrease rather rapidly with increase of temperature. For comparison, the curve marked $10^5\ B_{H_2}$, in figure 10, shows on a different scale the magnitude of the corresponding second virial coefficient for H_2 at the same temperatures.

If it is assumed that the σ or $(TV/T_0V_0)\ \log\ (PV/RT)$ isotherms for D_2 and H_2 are parallel, values of PV/RT for D_2 may be obtained from those tabulated for H_2 by (1) calculating the σ_{H_2} or σ for H_2, from the values of PV/RT, T and ρ, (2) subtracting the difference $(\sigma_{H_2}-\sigma_{D_2})_{\rho=0}$ to get σ_{D_2}, and then (3) calculating the corresponding value of PV/RT for D_2. A plot of the difference $10^5\ (\sigma_{H_2}-\sigma_{D_2})_{\rho=0}$ which may be used for this purpose is shown in figure 11. An alternative method based on the assumption that only the second term of the series expansion eq 4.9 for PV/RT is to be changed is as follows. 10^5 $(B_{H_2}-B_{D_2})$, obtained from figure 11 by multiplying $10^5\ (\sigma_{H_2}-\sigma_{D_2})_{\rho=0}$ by 2.302585 T_0/T or obtained directly from figure 10, is multiplied by 10^{-5} and the product subtracted from PV/RT for H_2 to give PV/RT for D_2. This alternative method is simpler than the other method and may be as reliable.

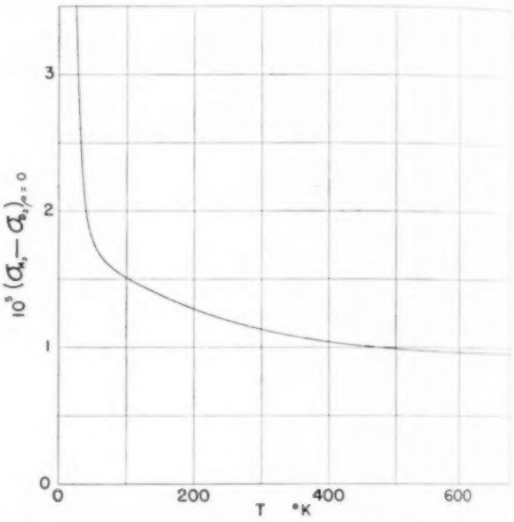

FIGURE 11. *Difference between intercepts of σ versus ρ isotherms for H_2 and D_2.*

V. Calculation of Thermal Properties of the Real Gas

The calculation of thermodynamic properties of a real gas from values of these properties for the ideal gas rests upon the principle that the difference between values of a thermodynamic function at different densities for the same temperature may be determined from data of state for the gas at the given temperature.

The entropy and free energy of a gas are dependent upon the pressure, even in the ideal state, and in tables 4 to 8 they are given for the hydrogens in the ideal gas state at a pressure of 1 standard atm. On the other hand, the internal energy, enthalpy, and specific heat in the ideal gas state are independent of density at constant temperature.

Equations 5.1 to 5.8 show how, using the data of state expressed in the form, $Z=Z(\rho,\ T)$, the thermodynamic properties of the real gas at a temperature T and an Amagat density ρ may be calculated from properties for the ideal gas state

at a pressure of 1 atm, given for the hydrogens in tables 4 to 8.

$$\frac{S_{\rho,\,T\,(\text{real gas})}}{R}=\frac{S^{\circ}_{p=1,\,T\,(\text{ideal})}}{R}+\ln\frac{P_0V_0}{RT_0}-\ln\frac{T}{T_0}-\ln\rho-\int_0^{\rho}[(Z-1)/\rho]d\rho-\int_0^{\rho}[T(dZ/dT)_{\rho}/\rho]d\rho \tag{5.1}$$

This can be expressed in a slightly different form by using the identity

$$\int_0^{\rho}[(Z-1)/\rho]d\rho+\int_0^{\rho}[T(dZ/dT)_{\rho}/\rho]d\rho=\left(d\left\{T\int_0^{\rho}[(Z-1)/\rho]d\rho\right\}/dT\right). \tag{5.2}$$

$$\frac{H_{\rho,\,T\,(\text{real gas})}}{RT}=\frac{H^{\circ}_{T\,(\text{ideal})}}{RT}-\int_0^{\rho}[T(dZ/dT)_{\rho}/\rho]d\rho+(Z-1). \tag{5.3}$$

$$\frac{F_{\rho,\,T\,(\text{real gas})}}{RT}=\frac{F^{\circ}_{p=1,\,T\,(\text{ideal})}}{RT}-\ln\frac{P_0V_0}{RT_0}+\ln\frac{T}{T_0}+\ln\rho+\int_0^{\rho}[(Z-1)/\rho]d\rho+(Z-1). \tag{5.4}$$

$$\ln[f\ (\text{fugacity of real gas})/P]=\int_0^{\rho}(Z-1)/\rho]d\rho-\ln Z+(Z-1). \tag{5.5}$$

$$\frac{E_{\rho,\,T\,(\text{real gas})}}{RT}=\frac{E^{\circ}_{T\,(\text{ideal})}}{RT}-[T(dZ/dT)_{\rho}/\rho]d\rho. \tag{5.6}$$

$$\frac{(C_v)_{\rho,\,T\,(\text{real gas})}}{R}=\frac{(C^{\circ}_v)_{T\,(\text{ideal})}}{R}-2\int_0^{\rho}[T(dZ/dT)_{\rho}/\rho]d\rho-\int_0^{\rho}[T^2(d^2Z/dT^2)_{\rho}/\rho]d\rho. \tag{5.7}$$

$$\frac{(C_P)_{\rho,\,T\,(\text{real gas})}}{R}=\frac{(C^{\circ}_P)_{T\,(\text{ideal})}}{R}-\left.\begin{aligned}&2\int_0^{\rho}[T(dZ/dT)_{\rho}/\rho]d\rho-\int_0^{\rho}[T^2(d^2Z/dT^2)_{\rho}/\rho]d\rho+\\&\{[Z+T(dZ/dT)_{\rho}]^2/[Z+\rho(dZ/d\rho)_T]\}-1.\end{aligned}\right\} \tag{5.8}$$

In order to facilitate the calculation of the thermodynamic properties of hydrogen in the real gas state, tables 22 and 23 were computed.[11] Lagrangian four point formulas [181] were used for the tabular integrations.

Table 22 is intended for use in the calculation of entropies. The values in the second column, headed $(S^{\circ}_{\rho=1}-S^{\circ}_{\rho=1})/R$, are for the difference between entropies of hydrogen in the ideal gas state at 1-atm pressure and at unit Amagat density, divided by R.

$$\frac{S^{\circ}_{p=1,\,T\,(\text{ideal})}-S^{\circ}_{p=1,\,T\,(\text{ideal})}}{R}=-\ln\frac{P_0V_0}{RT_0}+\ln\frac{T}{T_0}=-0.000618+\ln T/T_0 \tag{5.9}$$

The row at the bottom of the table, headed $(S^{\circ}_{\rho=1}-S^{\circ})/R$, is for the difference between entropies in the ideal gas states at Amagat densities one and ρ, divided by R.

$$\frac{S^{\circ}_{p=1,\,T\,(\text{ideal})}-S^{\circ}_{p,\,T\,(\text{ideal})}}{R}=\ln\rho \tag{5.10}$$

The other rows and columns of table 22 headed $(S^{\circ}-S)/R$ give the differences between the entropies in the ideal and real gas states at the same temperature and density, divided by R.

$$\frac{S^{\circ}_{\rho,\,T\,(\text{ideal})}-S_{\rho,\,T\,(\text{real})}}{R}=\int_0^{\rho}[(Z-1)/\rho]d\rho+\int_0^{\rho}[T(dZ/dT)_{\rho}/\rho]d\rho \tag{5.11}$$

In order, then, to get S/R for the real gas hydrogen at a temperature T and Amagat density ρ, one subtracts from S°/R, obtained from S° given in table 8, the sum of three numbers for the appropriate values of T and ρ to be obtained from table 22: one comes from the second column, headed $(S^{\circ}_{\rho=1}-S^{\circ}_{\rho=1})/R$; another from the bottom row of the table, headed $(S^{\circ}_{\rho=1}-S^{\circ})/R$; and the third from the rows and columns of the table headed $(S^{\circ}-S)/R$.

Table 23 is for the difference between the enthalpy of hydrogen in the ideal and real gas states at temperature T and Amagat density ρ, divided by RT.

$$\frac{H^{\circ}_{T\,(\text{ideal})}-H_{\rho,\,T\,(\text{real})}}{RT}=\int_0^{\rho}[T(dZ/dT)_{\rho}/\rho]d\rho-(Z-1). \tag{5.12}$$

Hence to obtain H/RT for hydrogen in the real gas state, one subtracts the appropriate value of $(H^{\circ}-H_{\rho})/RT$ in table 23 from the value of H°/RT obtained from H° given in table 8 for the deal gas state.

[11] For the calculation of these tables the authors are indebted to Messrs Roger E. Clapp, Kingsley Elder, Jr., and Robert Mann, who worked as student assistants at the National Bureau of Standards during the summer of 1941.

TABLE 22. *Entropy differences divided by R, for normal* H_2

$\frac{S^\circ - S}{R}$, Entropy of ideal gas minus entropy of real gas at same T and ρ, divided by R.

$\frac{S^\circ_{p=1} - S^\circ_{\rho=1}}{R}$, Entropy of ideal gas at pressure of 1 atmosphere minus entropy of ideal gas at density of 1 Amagat, divided by R.

$\frac{S^\circ_{\rho=1} - S^\circ}{R}$, Entropy of ideal gas at density of 1 Amagat minus entropy of ideal gas at density of ρ Amagats, divided by R.

Temperature	$\frac{S^\circ_{p=1} - S^\circ_{\rho=1}}{R}$	$\frac{S^\circ - S}{R}$														
		$\rho=1$ Amagat	2	3	6	10	20	40	60	80	100	120	140	160	180	200
°K																
16	−2.83809	0.00373	0.00745	0.01117												
18	−2.72030	.00323	.00645	.00968	0.01933											
20	−2.61494	.00288	.00576	.00864	.01724	0.0287										
22	−2.51963	.00264	.00529	.00792	.01583	.0263										
24	−2.43262	.00245	.00489	.00733	.01463	.0245	0.0488									
26	−2.35258	.00230	.00459	.00690	.01378	.0230	.0458	0.0915								
28	−2.27847	.00218	.00435	.00653	.01304	.0218	.0436	.0867	0.129							
30	−2.20948	.00208	.00415	.00623	.01245	.0208	.0416	.0827	.123	0.163	0.202					
32	−2.14494	.00198	.00396	.00595	.01189	.0198	.0396	.0787	.117	.155	.193	0.239	0.266	0.302	0.337	
34	−2.08432	.00190	.00379	.00569	.01137	.0190	.0379	.0753	.112	.148	.184	.229	.255	.290	.324	0.358
36	−2.02716	.00182	.00363	.00545	.01088	.0181	.0362	.0719	107	.142	.176	.211	.245	.278	.311	.344
38	−1.97309	.00175	.00349	.00524	.01047	.0174	.0347	.0692	.103	.137	.170	.203	.236	.268	.300	.332
40	−1.92180	.00169	.00338	.00508	.01014	.0169	.0337	.0672	.100	.133	.165	.198	.229	.261	.293	.324
42	−1.87301	.00165	.00329	.00494	.00988	.0165	.0329	.0655	.098	.130	.161	.193	.225	.256	.287	.317
44	−1.82649	.00160	.00320	.00480	.00960	.0160	.0320	.0640	.096	.128	.158	.190	.221	.252	.283	.313
46	−1.78204	.00156	.00313	.00469	.00938	.0156	.0313	.0626	.094	.125	.156	.186	.217	.248	.278	.308
48	−1.73948	.00153	.00306	.00460	.00919	.0153	.0306	.0613	.092	.122	.153	.183	.213	.244	.274	.303
50	−1.69865	.00150	.00300	.00451	.00902	.0150	.0301	.0601	.090	.120	.150	.180	.210	.240	.270	.299
52	−1.65943	.00148	.00295	.00443	.00886	.0148	.0295	.0591	.089	.118	.148	.177	.207	.237	.266	.295
54	−1.62169	.00146	.00291	.00436	.00873	.0146	.0291	.0582	.088	.117	.146	.175	.204	.234	.262	.291
56	−1.58532	.00144	.00287	.00431	.00862	.0144	.0287	.0575	.087	.116	.144	.173	.202	.231	.259	.288
58	−1.55023	.00142	.00284	.00426	.00851	.0142	.0284	.0568	.086	.114	.142	.171	.200	.228	.257	.285
60	−1.51633	.00140	.00280	.00420	.00840	.0140	.0280	.0560	.084	.112	.140	.168	.197	.225	.254	.283
65	−1.43629	.00135	.00270	.00405	.00810	.01352	.0271	.0540	.0812	.109	.136	.164	.192	.219	.248	.276
70	−1.36218	.00131	.00261	.00392	.00784	.01309	.0263	.0525	.0790	.106	.132	.159	.186	.213	.241	.269
75	−1.29319	.00127	.00254	.00381	.00762	.01271	.0254	.0510	.0768	.103	.129	.155	.182	.209	.236	.263
80	−1.22865	.00124	.00248	.00371	.00743	.01240	.0248	.0499	.0752	.101	.126	.152	.179	.205	.232	.259
85	−1.16802	.00121	.00242	.00364	.00728	.01214	.0244	.0490	.0739	.099	.124	.150	.176	.202	.228	.254
90	−1.11087	.00119	.00238	.00357	.00714	.01192	.0239	.0481	.0726	.097	.122	.148	.173	.199	.225	.251
95	−1.05680	.00117	.00234	.00351	.00702	.01171	.0234	.0472	.0712	.096	.120	.145	.170	.196	.221	.247
100	−1.00551	.00115	.00229	.00344	.00689	.01149	.0230	.0464	.0700	.094	.118	.143	.168	.193	.218	.244
105	−0.95672	.00113	.00226	.00339	.00679	.01133	.0227	.0458	.0691	.093	.117	.141	.165	.190	.215	.241
110	−.91020	.00112	.00224	.00335	.00671	.01120	.0224	.0452	.0683	.092	.115	.139	.163	.188	.213	.238
115	−.86574	.00111	.00222	.00333	.00665	.01111	.0222	.0448	.0677	.091	.114	.138	.162	.186	.211	.236
120	−.82318	.00110	.00220	.00331	.00661	.01104	.0221	.0445	.0672	.090	.113	.137	.161	.185	.209	.234
125	−.78236	.00109	.00219	.00329	.00658	.01098	.0220	.0442	.0667	.090	.113	.136	.160	.184	.208	.233
130	−.74314	.00109	.00218	.00327	.00653	.01092	.0219	.0440	.0664	.089	.112	.136	.159	.183	.207	.232

125	−.78250	.00109	.00219	.00329	.00438	.01093	.0220	.0442	.0667	.090	.113	.136	.160	.184	.208	.231
130	−.74314	.00109	.00218	.00327	.00435	.01092	.0219	.0440	.0664	.089	.112	.136	.159	.183	.207	.232
135	−.70540	.00109	.00217	.00325	.00650	.01086	.0218	.0438	.0662	.089	.112	.135	.158	.182	.206	.230
140	−.66903	.00108	.00215	.00323	.00647	.01080	.0216	.0435	.0656	.088	.111	.134	.157	.181	.205	.229
145	−.63394	.00107	.00214	.00321	.00643	.01074	.0215	.0433	.0653	.088	.110	.133	.157	.180	.204	.228
150	−.60004	.00107	.00213	.00320	.00639	.01068	.0214	.0430	.0649	.087	.110	.133	.156	.179	.203	.227
155	−.56725	.00106	.00212	.00318	.00636	.01062	.0213	.0428	.0646	.087	.109	.132	.155	.178	.202	.225
160	−.53550	.00106	.00211	.00316	.00632	.01056	.0212	.0426	.0642	.087	.109	.131	.154	.177	.201	.224
165	−.50473	.00105	.00210	.00315	.00629	.01051	.0211	.0424	.0639	.086	.108	.130	.153	.176	.199	.222
170	−.47488	.00104	.00209	.00313	.00626	.01046	.0210	.0422	.0636	.085	.107	.129	.152	.174	.197	.220
180	−.41772	.00103	.00207	.00310	.00620	.01033	.0208	.0418	.0629	.0843	.1059	.127	.149	.172	.194	.217
190	−.36365	.00102	.00204	.00307	.00613	.01021	.0205	.0413	.0622	.0834	.1047	.126	.147	169	.191	.214
200	−.31236	.00100	.00202	.00303	.00606	.01007	.0203	.0408	.0615	.0824	.1035	.125	.146	.167	.189	211
210	−.26357	.00099	.00200	.00299	.00599	.01004	.0201	.0403	.0608	.0814	.1023	.124	.145	.166	.188	.210
220	−.21705	.00098	.00197	.00295	.00592	.00994	.0198	.0398	.0600	.0805	.1011	.122	.143	.165	.186	.208
230	−.17260	.00097	.00195	.00292	.00585	.00976	.0196	.0394	.0593	.0795	.1000	.120	.141	.162	.184	.205
240	−.13004	.00096	.00193	.00289	.00578	.00964	.0194	.0389	.0587	.0786	.0988	.119	.139	.160	.181	.203
250	−.08922	.00095	.00191	.00286	.00573	.00952	.0192	.0385	.0581	.0778	.0978	.118	.138	.158	.179	.200
260	−.04999	.00095	.00190	.00284	.00568	.00948	.0191	.0382	.0576	.0770	.0968	.117	.137	.157	.177	.198
270	−.01225	.000938	.001877	.002816	.005636	.009402	.01885	.03786	.05705	.07641	.09595	.1157	.1356	.1557	.1760	.1965
280	+.024114	.000931	.001861	.002793	.005589	.009323	.01869	.03754	.05656	.07574	.09510	.1146	.1344	.1543	.1743	.1946
300	+.093106	.000916	.001833	.002750	.005504	.009180	.01840	.03694	.05565	.07451	.09354	.1127	.1321	.1516	.1713	.1912
320	.157645	.000902	.001805	.002708	.005420	.009042	.01812	.03639	.05481	.07338	.09210	.1110	.1300	.1492	.1686	.1881
340	.218270	.000890	.001781	.002672	.005347	.008919	.01787	.03589	.05404	.07234	.09079	.1094	.1281	.1470	.1661	.1853
360	.275428	.000879	.001759	.002639	.005280	.008807	.01765	.03543	.05334	.07140	.08959	.1079	.1264	.1450	.1638	.1827
380	.329495	.000868	.001737	.002605	.005213	.008696	.01742	.03498	.05266	.07048	.08844	.1065	.1248	.1431	.1617	.1803
400	.38079	.00086	.00172	.00257	.00515	.00859	.0172	.0346	.0520	.0697	.0874	.1053	.1233	.1414	.1597	.1781
420	.42958	.00085	.00170	.00255	.00510	.00850	.0170	.0342	.0515	.0689	.0864	.1041	.1219	.1398	.1578	.1760
440	.47610	.00084	.00168	.00252	.00504	.00841	.0169	.0338	.0509	.0681	.0855	.1030	.1205	.1383	.1561	.1741
460	.52055	.00083	.00166	.00250	.00499	.00833	.0167	.0335	.0504	.0675	.0846	.1019	.1193	.1368	.1545	.1723
480	.56311	.00082	.00165	.00247	.00494	.00825	.0165	.0332	.0499	.0668	.0838	.1009	.1181	.1355	.1530	.1706
500	.60393	.00082	.00163	.00245	.00490	.00817	.0164	.0329	0495	0662	.0830	.1000	.1170	.1342	.1515	.1689
520	.64315	.00081	.00162	.00243	.00486	.00810	.0162	.0326	.0490	0656	.0823	.0990	.1160	.1330	.1501	.1674
540	.68089	00080	.00160	.00241	.00482	.00803	.0161	.0323	.0486	.0650	.0815	.0982	.1149	.1318	.1488	.1659
560	.71726	.00080	.00159	.00239	.00478	.00797	.0160	.0320	.0482	.0645	.0809	.0974	.1140	.1307	.1476	.1645
580	.75235	.00079	.00158	.00237	.00474	00790	.0158	.0318	.0478	.0640	.0802	.0966	.1131	.1297	.1464	.1632
600	.78625	.00078	.00157	.00235	.00470	00784	.0157	.0315	.0474	.0635	.0796	.0958	.1122	.1286	.1452	.1619
$\frac{S^\circ_{(T-1)}-S^\circ}{R}$		0	.69315	1.09861	1.79176	2.30259	2.9957	3.6889	4.0943	4.3820	4.6052	4.7875	4.9416	5.0752	5.1930	5.2983

TABLE 22. *Entropy differences divided by R, for normal* H_2—Continued

Temperature	$\frac{S^\circ_{(p-1)}-S^\circ_{(p=1)}}{R}$	$\frac{S^\circ-S}{R}$														
		$\rho=220$	240	260	280	300	320	340	360	380	400	420	440	460	480	500
16																
18																
20																
22																
24																
26																
28																
30																
32																
34	−2.0843	0.391	0.424	0.457	0.489	0.520	0.551	0.581	0.610	0.638	0.666	0.694	0.723	0.753	0.784	0.816
36	−2.0272	.376	.408	.441	.473	.504	.535	.565	.594	.623	.652	.682	.712	.742	.774	.807
38	−1.9731	.364	.395	.427	.458	.489	.519	.550	.580	.610	.640	.671	.701	.733	.766	.800
40	−1.9218	.355	.386	.417	.448	.478	.509	.539	.570	.601	.632	.664	.696	.728	.762	.796
42	−1.8730	.348	.379	.409	.439	.470	.500	.531	.563	.594	.626	.658	.691	.724	.758	.792
44	−1.8265	.343	.374	.404	.434	.465	.495	.526	.557	.589	.622	.655	.688	.721	.755	.789
46	−1.7820	.338	.368	.399	.428	.459	.489	.520	.551	.583	.616	.649	.682	.716	.750	.784
48	−1.7395	.333	.363	.393	.422	.453	.483	.514	.545	.577	.609	.642	.676	.710	.743	.777
50	−1.6987	.328	.358	.388	.417	.447	.478	.508	.539	.571	.603	.636	.669	.702	.736	.769
52	−1.6594	.325	.354	.383	.413	.443	.472	.503	.534	.565	.596	.629	.661	.694	.728	.762
54	−1.6217	.320	.350	.379	.408	.438	.467	.497	.528	.559	.590	.622	.654	.687	.720	.754
56	−1.5853	.317	.346	.375	.405	.434	.464	.494	.524	.554	.586	.617	.649	.682	.715	.749
58	−1.5502	.314	.343	.373	.402	.432	.462	.492	.523	.554	.585	.616	.648	.681	.715	.749
60	−1.5163	.312	.341	.371	.401	.431	461	.492	.523	.554	.586	.618	.650	.683	.717	.751
65	−1.4363	.305	.334	.363	.393	.424	.454	.485	.516	.548	.580	.613	.646	.679	.714	.749
70	−1.3622	.298	.326	.356	.385	.415	.445	.476	.507	.539	.571	.604	.637	.670	.705	.739
75	−1.2932	.291	.320	.348	.377	.407	.436	.467	.497	.529	.560	.593	.625	.659	.692	.727
80	−1.2286	.286	.314	.342	.370	.399	.428	.458	.488	.519	.550	.582	.614	.647	.680	.714
85	−1.1680	.281	.308	.336	.364	.392	.421	.450	.480	.510	.540	.571	.603	.635	.667	.700
90	−1.1109	.278	.304	.332	.359	.387	.416	.445	.474	.503	.534	.564	.595	.627	.659	.691
95	−1.0568	.274	.301	.328	.355	.383	.411	.440	.469	.498	.528	.558	.589	.620	.652	.684
100	−1.0055	.270	.297	.324	.351	.379	.407	.435	.464	.493	.522	.552	.583	.614	.645	.677
105	−0.9567	.267	.294	.320	.347	.375	.402	.430	.459	.487	.517	.546	.576	.607	.638	.670
110	−.9102	.264	.290	.317	.344	.371	.398	.426	.454	.482	.511	.540	.570	.600	.631	.662
115	−.8657	.262	.287	.313	.340	.367	.394	.421	.449	.477	.505	.534	.564	.594	.624	.655
120	−.8232	.259	.285	.311	.337	.364	.390	.418	.445	.473	.501	.530	.559	.589	.619	.649
125	−.7824	.258	.284	.309	.335	.361	.388	.415	.442	.470	.498	.526	.555	.584	.614	.644
130	−.7431	.257	.282	.307	.333	.359	.386	.412	.439	.467	.495	.523	.552	.580	.610	.640
135	−.7054	.255	.280	.305	.331	.357	.383	.409	.436	.463	.491	.519	.547	.576	.605	.634
140	−.6690	.253	.278	.303	.329	.354	.380	.407	.433	.460	.488	.515	.544	.572	.601	.630
145	−.6339	.252	.277	.301	.327	.352	.378	.404	.431	.457	.485	.512	.540	.568	.597	.626
150	−.6000	.251	.275	.300	.325	.351	.376	.402	.429	.455	.482	.509	.537	.565	.593	.622
155	−.5673	.249	.274	.298	.323	.349	.374	.400	.426	.453	.479	.506	.534	.561	.589	.617
160	−.5355	.248	.272	.297	.321	.346	.372	.397	.424	.450	.476	.503	.530	.557	.585	.613
165	−.5047	.246	.270	.294	.319	.344	.369	.395	.421	.447	.473	.500	.527	.554	.581	.609

150	−.5633	.249	.274	.298	.321	.349	.374	.399	.426	.453	.479	.506	.534	.564	.589	.617
160	−.5355	.248	.272	.297	.321	.346	.372	.397	.423	.450	.476	.503	.530	.557	.585	.615
165	−.5047	.246	.270	.294	.319	.344	.369	.394	.420	.446	.472	.498	.525	.552	.579	.607
170	−.4749	.244	.267	.291	.316	.340	.365	.390	.415	.441	.467	.493	.519	.546	.573	.600
180	−.4177	.240	.263	.287	.310	.334	.359	.383	.408	.433	.458	.484	.510	.537	.563	.590
190	−.3637	.237	.259	.282	.306	.329	.353	.378	.402	.427	.452	.477	.503	.529	.555	.582
200	−.3124	.234	.256	.279	.302	.326	.349	.373	.398	.422	.447	.472	.498	.523	.550	.576
210	−.2636	.232	.254	.277	.300	.323	.347	.370	.394	.419	.443	.468	.494	.519	.545	.571
220	−.2170	.230	.252	.274	.297	.320	.343	.367	.391	.415	.439	.464	.489	.514	.540	.566
230	−.1726	.227	.249	.271	.293	.316	.339	.362	.386	.410	.434	.458	.483	.508	.533	.559
240	−.1300	.224	.246	.268	.290	.3127	.335	.358	.381	.405	.428	.452	.477	.501	.526	.552
250	−.0892	.221	.243	.264	.286	.308	.331	.353	.376	.399	.423	.447	.471	.495	.519	.544
260	−.0500	.219	.240	.262	.283	.305	.327	.350	.372	.395	.418	.441	.465	.489	.513	.538
270	−.0123	.2172	.2381	.2593	.2806	.3022	.3240	.3460	.3683	.3908	.4136	.4366	.4598	.4833	.5071	.5311
280	+.0241	.2151	.2358	.2567	.2778	.2991	.3206	.3424	.3644	.3866	.4090	.4317	.4546	.4777	.5011	.5248
300	.0931	.2113	.2316	.2520	.2727	.2935	.3145	.3358	.3572	.3789	.4008	.4228	.4451	.4676	.4904	.5133
320	.1576	.2078	.2277	.2478	.2680	.2885	.3091	.3299	.3508	.3720	.3934	.4149	.4367	.4587	.4808	.5032
340	.2183	.2047	.2242	.2440	.2638	.2839	.3041	.3245	.3451	.3658	.3868	.4079	.4292	.4507	.4723	.4942
360	.2754	.2018	.2211	.2405	.2600	.2797	.2996	.3197	.3399	.3603	.3808	.4015	.4221	.4434	.4647	.4861
380	.3295	.1991	.2181	.2372	.2565	.2759	.2955	.3152	.3351	.3551	.3753	.3957	.4162	.4369	.4577	.4787
400	.3808	.197	.215	.234	.253	.272	.292	.311	.331	.350	.370	.390	.410	.431	.451	.472
420	.4296	.194	.213	.231	.250	.269	.288	.307	.327	.346	.366	.385	.405	.425	.445	.466
440	.4761	.192	.210	.229	.247	.266	.285	.304	.323	.342	.361	.381	.400	.420	.440	.460
460	.5206	.190	.208	.226	.245	.263	.282	.300	.319	.338	.357	.376	.396	.415	.435	.455
480	.5631	.188	.206	.224	.242	.260	.279	.297	.316	.335	.353	.372	.392	.411	.430	.450
500	.6039	.186	.204	.222	.240	.258	.276	.294	.313	.331	.350	.369	.388	.407	.426	.445
520	.6432	.185	.202	.220	.238	.255	.273	.291	.310	.328	.346	.365	384	.403	.421	.441
540	.6809	.183	.200	.218	.235	.253	.271	.289	.307	.325	.343	.362	.380	.399	.418	.436
560	.7173	.182	.199	.216	.233	.251	.269	.286	.304	.322	.340	.358	.377	.395	.414	.432
580	.7524	.180	.197	.214	.231	.249	.266	.284	.302	.319	.337	.355	.374	.392	.410	.429
600	.7863	.179	.195	.212	.230	.247	.264	.282	.299	.317	.335	.352	.370	.389	.407	.425
$\frac{S°_{(p=1)} - S°}{R}$		5.3936	5.4806	5.5607	5.6348	5.7038	5.7683	5.8289	5.8861	5.9402	5.9915	6.0403	6.0868	6.1312	6.1738	6.2146

TABLE 23. *Enthalpy of ideal gas minus enthalpy of real gas at the same T and ρ, divided by RT, for normal H_2*

Temperature	$\frac{H^\circ - H}{RT}$														
	ρ=1 Amagat	2	3	6	10	20	40	60	80	100	120	140	160	180	200
°K															
16	0.02193	0.04381	0.06568												
18	.01869	.03725	.05583	0.11144											
20	.01614	.03226	.04835	.09650	0.1604										
22	.01420	.02838	.04253	.08489	.1411										
24	.01263	.02524	.03783	.07551	.1255	0.2494									
26	.01132	.02260	.03388	.06765	.1125	.2237	0.4420								
28	.01023	.02045	.03063	.06116	.1017	.2023	.3994	0.591							
30	.00931	.01860	.02786	.05564	.0925	.1839	.3637	.538	0.708	0.872					
32	.00851	.01701	.02549	.05089	.0846	.1681	.3318	.491	.646	.797	0.943	1.085	1.222	1.355	
34	.00781	.01556	.02337	.04666	.0776	.1541	.3042	.451	.593	.731	.865	0.995	1.121	1.243	1.361
36	.00719	.01436	.02153	.04298	.0714	.1420	.2801	.414	.545	.673	.796	.916	1.032	1.145	1.253
38	.00665	.01329	.01991	.03976	.0661	.1313	.2592	.383	.504	.622	.736	.847	0.955	1.059	1.160
40	.00617	.01234	.01850	.03692	.0614	.1220	.2409	.357	.469	.578	.684	.787	.887	0.984	1.078
42	.00576	.01151	.01727	.03445	.0573	.1140	.2249	.333	.438	.539	.638	.734	.828	.918	1.007
44	.00538	.01077	.01615	.03223	.0536	.1067	.2104	.312	.410	.505	.598	.688	.775	.860	0.942
46	.00504	.01008	.01513	.03020	.0502	.1000	.1971	.292	.384	.473	.560	.645	.727	.806	.883
48	.00473	.00946	.01420	.02834	.0471	.0937	.1849	.274	.360	.444	.526	.605	.682	.757	.829
50	.00445	.00889	.01324	.02665	.0443	.0881	.1739	.257	.338	.417	.494	.569	.641	.711	.779
52	.00419	.00837	.01257	.02509	.0417	.0830	.1638	.243	.319	.394	.466	.537	.605	.671	.734
54	.00396	.00792	.01188	.02371	.0393	.0784	.1548	.229	.302	.373	.441	.507	.571	.632	.692
56	.00376	.00750	.01126	.02247	.0374	.0743	.1466	.217	.286	.353	.417	.479	.540	.598	.654
58	.00356	.00710	.01066	.02127	.0354	.0704	.1389	.206	.271	.333	.394	.453	.511	.566	.619
60	.00337	.00674	.01010	.02017	.0335	.0666	.1315	.194	.256	.315	.373	.429	.483	.536	.586
65	.00296	.00592	.00887	.01771	.02943	.0584	.1153	.1706	.2242	.276	.327	.376	.423	.469	.513
70	.00261	.00522	.00782	.01542	.02595	.0515	.1017	.1503	.1974	.243	.287	.330	.371	.411	.449
75	.00231	.00461	.00692	.01382	.02297	.0456	.0900	.1330	.1747	.215	.254	.291	.327	.362	.395
80	.00205	.00411	.00616	.01230	.02043	.0406	.0799	.1182	.1552	.191	.225	.258	.290	.320	.349
85	.00184	.00368	.00551	.01101	.01828	.0363	.0714	.1055	.1384	.170	.201	.230	.257	.283	.308
90	.00165	.00330	.00495	.00987	.01639	.0325	.0639	.0942	.1235	.152	.179	.204	.229	.252	.273
95	.00148	.00296	.00444	.00884	.01469	.0291	.0571	.0842	.1101	.135	.159	.181	.203	.223	.241
100	.00133	.00265	.00398	.00793	.01316	.0261	.0511	.0752	.0983	.120	.141	.161	.179	.197	.213
105	.00119	.00238	.00357	.00712	.01182	.0234	.0458	.0673	.0878	.107	.125	.143	.159	.174	.187
110	.00107	.00215	.00322	.00642	.01065	.0210	.0412	.0603	.0785	.095	.111	.126	.140	.153	.165
115	.00097	.00194	.00290	.00579	.00960	.0190	.0370	.0540	.0701	.085	.099	.112	.124	.135	.144
120	.00088	.00175	.00262	.00523	.00867	.0171	.0333	.0485	.0628	.076	.088	.099	.109	.118	.126
125	.00079	.00158	.00236	.00472	.00781	.0154	.0299	.0434	.0561	.068	.078	.088	.097	.104	.110
130	.00071	.00143	.00213	.00425	.00704	.0139	.0268	.0388	.0499	.060	.069	.077	.084	.090	.095
135	.00064	.00128	.00191	.00382	.00632	.0124	.0239	.0345	.0442	.053	.061	.067	.073	.078	.081
140	.00057	.00115	.00172	.00341	.00563	.0110	.0212	.0305	.0389	.046	.053	.058	.063	.066	.068
145	.00051	.00102	.00154	.00304	.00502	.0098	.0188	.0269	.0340	.040	.045	.050	.053	.055	.056
150	.00045	.00090	.00136	.00269	.00444	.0087	.0165	.0235	.0295	.035	.039	.042	.044	.045	.045
155	.00040	.00081	.00121	.00239	.00393	.0076	.0144	.0204	.0254	.029	.033	.035	.036	.036	.035
160	.00035	.00071	.00106	.00209	.00343	.0066	.0124	.0174	.0216	.024	.027	.028	.029	.028	.027

140	.00057	.00115	.00172	.00341	.00503	.0119	.0212	.0335	.0489	.046	.053	.058	.063	.066	.068
145	.00053	.00102	.00154	.00303	.00502	.0098	.0186	.0293	.0430	.040	.045	.050	.053	.055	.056
150	.00045	.00091	.00140	.00269	.00444	.0087	.0165	.0255	.035	.034	.038	.042	.044	.045	.045
155	.00040	.00081	.00121	.00239	.00391	.0076	.0144	.0204	.0254	.029	.033	.035	.036	.036	.035
160	.00035	.00071	.00106	.00209	.00341	.0067	.0125	.0174	.0214	.024	.027	.028	.028	.027	.025
165	.00031	.00061	.00092	.00180	.00295	.0057	.0105	.0145	.0176	.020	.021	.023	.020	.018	.015
170	.00026	.00052	.00076	.00152	.00248	.0047	.0087	.0117	.0139	.015	.015	.014	.012	.010	.006
180	.00017	.00034	.00050	.00100	.00161	.0030	.0052	.0066	.0070	.0065	.005	.003	−.001	−.005	−.011
190	.00010	.00019	.00028	.00053	.00085	.0015	.0022	.0021	.0011	−.0008	−.004	−.008	−.012	−.018	−.025
200	.00003	.00006	.00008	.00015	.00021	.0002	−.0003	−.0017	−.0059	−.0070	−.011	−.016	−.022	−.029	−.037
210	−.00003	−.00005	−.00009	−.00020	−.00037	−.0009	−.0026	−.0051	−.0084	−.0126	−.018	−.024	−.031	−.039	−.048
220	−.00008	−.00016	−.00024	−.00051	−.00091	−.0020	−.0047	−.0082	−.0126	−.0178	−.024	−.031	−.039	−.047	−.057
230	−.00013	−.00027	−.00041	−.00084	−.00143	−.0030	−.0068	−.0113	−.0166	−.0228	−.030	−.038	−.047	−.056	−.067
240	−.00018	−.00036	−.00056	−.00113	−.00192	−.0040	−.0088	−.0142	−.0204	−.0274	−.035	−.044	−.054	−.064	−.076
250	−.00023	−.00046	−.00068	−.00138	−.00233	−.0048	−.0104	−.0166	−.0236	−.0314	−.040	−.050	−.060	−.071	−.083
260	−.00026	−.00053	−.00078	−.00159	−.00268	−.0055	−.0118	−.0187	−.0265	−.0349	−.044	−.054	−.065	−.077	−.090
270	−.000280	−.000584	−.000877	−.001770	−.002985	−.00615	−.01299	−.02058	−.02891	−.03802	−.0479	−.0587	−.0703	−.0828	−.0962
280	−.000321	−.000645	−.000969	−.001953	−.003290	−.00675	−.01421	−.02238	−.03131	−.04099	−.0515	−.0628	−.0749	−.0879	−.1018
300	−.000375	−.000752	−.001131	−.002276	−.003827	−.00782	−.01634	−.02556	−.03549	−.04620	−.0577	−.0699	−.0830	−.0970	−.1118
320	−.000422	−.000845	−.001271	−.002556	−.004291	−.00875	−.01816	−.02826	−.03907	−.05062	−.0629	−.0760	−.0899	−.1046	−.1202
340	−.000462	−.000926	−.001390	−.002794	−.004688	−.00954	−.01973	−.03058	−.04213	−.05440	−.0674	−.0812	−.0957	−.1111	−.1273
360	−.000496	−.000994	−.001493	−.003000	−.005031	−.01022	−.02108	−.03259	−.04478	−.05766	−.0713	−.0856	−.1007	−.1166	−.1334
380	−.000526	−.001054	−.001584	−.003181	−.005332	−.01081	−.02226	−.03433	−.04707	−.06049	−.0746	−.0895	−.1051	−.1214	−.1386
400	−.00055	−.00111	−.00166	−.00334	−.00560	−.0113	−.0233	−.0359	−.0491	−.0630	−.0776	−.0928	−.1088	−.1256	−.1432
420	−.00058	−.00116	−.00174	−.00348	−.00583	−.0118	−.0242	−.0372	−.0509	−.0652	−.0801	−.0958	−.1121	−.1292	−.1471
440	−.00060	−.00120	−.00180	−.00360	−.00604	−.0122	−.0250	−.0384	−.0524	−.0671	−.0824	−.0984	−.1150	−.1324	−.1506
460	−.00062	−.00123	−.00185	−.00372	−.00622	−.0126	−.0257	−.0395	−.0538	−.0688	−.0844	−.1006	−.1176	−.1352	−.1536
480	−.00063	−.00127	−.00190	−.00382	−.00639	−.0129	−.0264	−.0404	−.0550	−.0703	−.0862	−.1027	−.1199	−.1377	−.1563
500	−.00065	−.00130	−.00195	−.00390	−.00653	−.0132	−.0270	−.0413	−.0562	−.0716	−.0877	−.1045	−.1218	−.1399	−.1587
520	−.00066	−.00132	−.00199	−.00398	−.00667	−.0135	−.0275	−.0420	−.0571	−.0728	−.0892	−.1061	−.1236	−.1419	−.1608
540	−.00067	−.00135	−.00202	−.00406	−.00679	−.0137	−.0279	−.0427	−.0580	−.0739	−.0904	−.1075	−.1252	−.1436	−.1627
560	−.00068	−.00137	−.00205	−.00412	−.00689	−.0139	−.0284	−.0433	−.0588	−.0749	−.0916	−.1088	−.1267	−.1452	−.1643
580	−.00069	−.00139	−.00208	−.00418	−.00699	−.0141	−.0287	−.0439	−.0596	−.0758	−.0926	−.1100	−.1280	−.1466	−.1658
600	−.00070	−.00141	−.00211	−.00424	−.00708	−.0143	−.0291	−.0444	−.0602	−.0766	−.0935	−.1110	−.1291	−.1478	−.1671

TABLE 23. *Enthalpy of ideal gas minus enthalpy of real gas at the same T and p, divided by RT, for normal H_2*—Continued

Temperature	$\frac{H°-H}{RT}$														
	ρ=220	240	260	280	300	320	340	360	380	400	420	440	460	480	500
°K															
16															
18															
20															
22															
24															
26															
28															
30															
32															
34	1.475	1.582	1.692	1.793	1.890	1.983	2.071	2.154	2.234	2.310	2.382	2.453	2.521	2.586	2.647
36	1.359	1.461	1.559	1.653	1.743	1.830	1.912	1.991	2.065	2.136	2.204	2.269	2.331	2.390	2.446
38	1.257	1.351	1.442	1.529	1.612	1.693	1.770	1.844	1.914	1.981	2.044	2.104	2.161	2.215	2.265
40	1.168	1.256	1.340	1.421	1.499	1.574	1.646	1.715	1.781	1.843	1.902	1.958	2.010	2.059	2.104
42	1.090	1.171	1.250	1.325	1.398	1.467	1.534	1.599	1.661	1.719	1.774	1.826	1.874	1.919	1.959
44	1.021	1.097	1.170	1.241	1.308	1.373	1.436	1.496	1.553	1.608	1.659	1.707	1.752	1.792	1.829
46	0.957	1.028	1.097	1.163	1.226	1.286	1.344	1.400	1.453	1.504	1.551	1.596	1.637	1.674	1.707
48	.898	0.965	1.029	1.091	1.150	1.206	1.260	1.311	1.361	1.407	1.451	1.492	1.530	1.564	1.594
50	.844	.907	0.968	1.025	1.081	1.133	1.183	1.231	1.276	1.319	1.359	1.396	1.430	1.461	1.489
52	.796	.855	.911	0.966	1.017	1.066	1.112	1.156	1.198	1.237	1.273	1.307	1.338	1.366	1.391
54	.750	.806	.859	.910	0.958	1.003	1.046	1.087	1.125	1.161	1.195	1.225	1.253	1.279	1.301
56	.708	.761	.811	.859	.904	0.947	0.987	1.025	1.060	1.093	1.123	1.151	1.177	1.200	1.219
58	.670	.720	.767	.812	.855	.896	.934	0.969	1.002	1.033	1.061	1.087	1.110	1.130	1.148
60	.635	.682	.727	.770	.811	.849	.886	.919	0.950	0.979	1.005	1.028	1.049	1.069	1.085
65	.555	.596	.634	.671	.706	.739	.770	.799	.825	.849	0.870	0.889	0.906	0.920	0.931
70	.486	.521	.554	.586	.615	.643	.669	.692	.714	.733	.750	.764	.776	.786	.793
75	.427	.457	.485	.511	.536	.559	.580	.599	.616	.631	.644	.654	.662	.667	.669
80	.376	.401	.425	.447	.468	.487	.503	.518	.531	.542	.551	.557	.561	.562	.561
85	.331	.353	.373	.391	.408	.423	.436	.448	.457	.464	.469	.472	.472	.470	.466
90	.293	.312	.328	.344	.357	.369	.380	.388	.394	.398	.400	.400	.398	.393	.385
95	.259	.274	.289	.301	.312	.322	.329	.335	.338	.340	.340	.337	.332	.325	.315
100	.228	.241	.253	.263	.272	.279	.284	.287	.288	.288	.285	.280	.274	.264	.252
105	.200	.211	.221	.229	.235	.240	.242	.244	.243	.240	.236	.229	.220	.208	.195
110	.175	.184	.191	.197	.202	.204	.205	.204	.202	.197	.191	.182	.171	.158	.142
115	.152	.159	.165	.169	.171	.172	.172	.169	.164	.158	.150	.140	.127	.112	.095
120	.132	.137	.141	.144	.144	.144	.141	.137	.131	.123	.114	.102	.088	.072	.052
125	.115	.118	.121	.121	.121	.118	.115	.109	.102	.093	.082	.068	.053	.036	.016
130	.098	.100	.101	.101	.099	.095	.090	.083	.075	.064	.052	.038	.021	.003	−.018
135	.083	.084	.083	.081	.078	.073	.067	.059	.049	.038	.024	.009	−.008	−.028	−.050
140	.068	.068	.066	.063	.059	.053	.046	.037	.026	.014	−.001	−.017	−.036	−.056	−.079
145	.056	.054	.051	.047	.041	.035	.026	.016	.005	−.009	−.024	−.042	−.061	−.082	−.106
150	.044	.041	.037	.032	.026	.018	.009	−.002	−.015	−.029	−.045	−.064	−.084	−.106	−.130
155	.032	.029	.024	.018	.011	.002	−.008	−.020	−.033	−.048	−.066	−.084	−.105	−.128	−.154

135	.083	.084	.083	.081	.078	.073	.067	.059	.049	.038	.024	.009	−.008	−.028	−.050
140	.068	.068	.066	.063	.059	.053	.046	.037	.026	.014	−.001	−.017	−.036	−.056	−.079
145	.056	.054	.051	.047	.041	.035	.026	.016	.005	−.009	−.024	−.042	−.061	−.082	−.106
150	.044	.041	.037	.032	.026	.018	.009	−.002	−.015	−.029	−.045	−.064	−.084	−.105	−.130
155	.032	.029	.024	.018	.011	.002	−.008	−.020	−.033	−.048	−.066	−.084	−.105	−.128	−.154
160	.022	.017	.012	.005	−.003	−.013	−.024	−.036	−.051	−.067	−.084	−.104	−.126	−.150	−.176
165	.011	.006	−.000	−.008	−.017	−.028	−.040	−.053	−.068	−.085	−.103	−.124	−.146	−.171	−.197
170	.001	−.005	−.013	−.021	−.031	−.042	−.055	−.070	−.085	−.103	−.122	−.143	−.166	−.191	−.218
180	−.017	−.025	−.034	−.044	−.055	−.068	−.082	−.098	−.115	−.134	−.154	−.176	−.200	−.225	−.253
190	−.033	−.042	−.052	−.063	−.076	−.090	−.105	−.122	−.140	−.160	−.181	−.204	−.228	−.255	−.283
200	−.046	−.056	−.068	−.080	−.093	−.108	−.125	−.142	−.161	−.181	−.203	−.227	−.252	−.279	−.308
210	−.057	−.068	−.081	−.094	−.108	−.124	−.141	−.159	−.179	−.200	−.223	−.247	−.273	−.300	−.330
220	−.068	−.080	−.093	−.107	−.122	−.139	−.156	−.175	−.196	−.218	−.241	−.266	−.292	−.320	−.350
230	−.079	−.091	−.105	−.120	−.136	−.153	−.172	−.191	−.212	−.235	−.259	−.284	−.311	−.340	−.370
240	−.088	−.101	−.116	−.132	−.148	−.166	−.185	−.206	−.227	−.250	−.275	−.301	−.328	−.358	−.388
250	−.096	−.111	−.126	−.142	−.159	−.178	−.198	−.219	−.241	−.265	−.290	−.316	−.344	−.374	−.405
260	−.104	−.119	−.134	−.151	−.169	−.188	−.209	−.230	−.253	−.277	−.303	−.330	−.358	−.388	−.420
270	−.1105	−.1258	−.1421	−.1595	−.1780	−.1976	−.2184	−.2405	−.2638	−.2884	−.3144	−.3419	−.3709	−.4014	−.4336
280	−.1167	−.1326	−.1494	−.1673	−.1862	−.2063	−.2276	−.2500	−.2738	−.2988	−.3252	−.3530	−.3824	−.4133	−.4458
300	−.1276	−.1443	−.1619	−.1806	−.2004	−.2212	−.2432	−.2664	−.2908	−.3165	−.3436	−.3719	−.4018	−.4332	−.4662
320	−.1367	−.1541	−.1724	−.1918	−.2122	−.2336	−.2562	−.2799	−.3048	−.3310	−.3585	−.3873	−.4175	−.4492	−.4824
340	−.1444	−.1624	−.1813	−.2012	−.2220	−.2440	−.2670	−.2911	−.3164	−.3429	−.3707	−.3998	−.4302	−.4621	−.4954
360	−.1510	−.1694	−.1888	−.2091	−.2304	−.2527	−.2760	−.3005	−.3261	−.3528	−.3808	−.4100	−.4406	−.4725	−.5059
380	−.1566	−.1755	−.1952	−.2159	−.2375	−.2601	−.2837	−.3084	−.3342	−.3611	−.3892	−.4186	−.4492	−.4811	−.5144
400	−.161	−.181	−.201	−.222	−.2435	−.266	−.290	−.315	−.341	−.368	−.396	−.426	−.456	−.488	−.521
420	−.166	−.185	−.206	−.227	−.249	−.272	−.296	−.321	−.347	−.374	−.402	−.432	−.462	−.494	−.527
440	−.169	−.189	−.210	−.231	−.253	−.277	−.301	−.326	−.352	−.379	−.407	−.437	−.467	−.499	−.532
460	−.173	−.193	−.213	−.235	−.257	−.281	−.305	−.330	−.356	−.383	−.411	−.441	−.471	−.503	−.536
480	−.176	−.196	−.217	−.238	−.261	−.284	−.308	−.334	−.360	−.387	−.415	−.444	−.475	−.506	−.539
500	−.178	−.198	−.219	−.241	−.264	−.287	−.311	−.337	−.363	−.390	−.418	−.447	−.477	−.509	−.541
520	−.180	−.201	−.222	−.244	−.266	−.290	−.314	−.339	−.365	−.393	−.421	−.450	−.480	−.511	−.543
540	−.182	−.203	−.224	−.246	−.269	−.292	−.316	−.342	−.368	−.395	−.423	−.452	−.482	−.513	−.545
560	−.184	−.205	−.226	−.248	−.271	−.294	−.319	−.344	−.370	−.397	−.425	−.453	−.483	−.514	−.546
580	−.186	−.206	−.228	−.250	−.272	−.296	−.320	−.345	−.371	−.398	−.426	−.455	−.485	−.515	−.547
600	−.187	−.208	−.229	−.251	−.274	−.298	−.322	−.347	−.373	−.400	−.427	−.456	−.486	−.516	−.548

Values of F/RT, E/RT, and $\ln(f/P)$ may be obtained rather simply from values of S/R and H/RT and the Z-table in accordance with the following equations:

$$F/RT=(H/RT)-(S/R) \tag{5.13}$$

$$\ln\frac{f}{P}=\frac{F_{\rho,T\,(\text{real})}-F^{\circ}_{\rho,T\,(\text{ideal})}}{RT}-\ln Z \tag{5.14}$$

$$E/RT=(H/RT)-Z. \tag{5.15}$$

The value of $[F^{\circ}_{\rho,T\,(\text{ideal})}-F_{\rho,T\,(\text{real})}/RT]$ may be obtained by subtracting $(S^{\circ}-S)/R$, given in table 22, from $(H^{\circ}-H)/RT$, given in table 23.

The calculation of the heat capacities of the real gas involves the evaluation of

$$\int_0^{\rho}[T^2(d^2Z/dT^2)_{\rho}/\rho]d\rho.$$

This may be carried out using the $(d^2Z/dT^2)_{\rho}$ table (table 16), and a method of tabular integration. Table 23 may be used to obtain $\int_0^{\rho}[T(dZ/dT)_{\rho}/\rho]d\rho$, since from eq 5.12 it follows that

$$\int_0^{\rho}[T(dZ/dT)_{\rho}/\rho]\,d\rho=\frac{H^{\circ}-H}{RT}\ (\text{from table 23})+(Z-1). \tag{5.16}$$

In the temperature and density ranges where Z may be represented by an analytic expression,[12] these two integrals may be evaluated by using series expansions for Z and its derivatives in the integrands. The difference between the specific heats at constant pressure for the real and ideal gas states may be calculated using the equation

$$[C_{p(\text{real gas})}-C^{\circ}_{p(\text{ideal})}]/R=T\left\{\left(\frac{d}{d\rho}\left[\frac{H^{\circ}-H}{RT}\right]\right)_T\left(\frac{dP}{dT}\right)_{\rho}\Big/\left(\frac{dP}{d\rho}\right)_T-\left(\frac{d}{dT}\left[\frac{H^{\circ}-H}{RT}\right]\right)_{\rho}\right\}-\frac{H^{\circ}-H}{RT} \tag{5.17}$$

$$=-T\left(\frac{d}{dT}\left[\frac{H^{\circ}-H}{RT}\right]\right)_{\rho}-\frac{H^{\circ}-H}{RT}+\left[Z+T\left(\frac{dZ}{dT}\right)_{\rho}\right]\left[T\left(\frac{dZ}{dT}\right)_{\rho}-\rho\left(\frac{dZ}{d\rho}\right)_T\right]\Big/\left[Z+\rho\left(\frac{dZ}{d\rho}\right)_T\right] \tag{5.17a}$$

The derivatives in eq 5.17 may be calculated from tables 14 and 23, using a method of tabular differentiation. Except for the first term, the derivatives in eq 5.17a are given in tables 15 and 17.

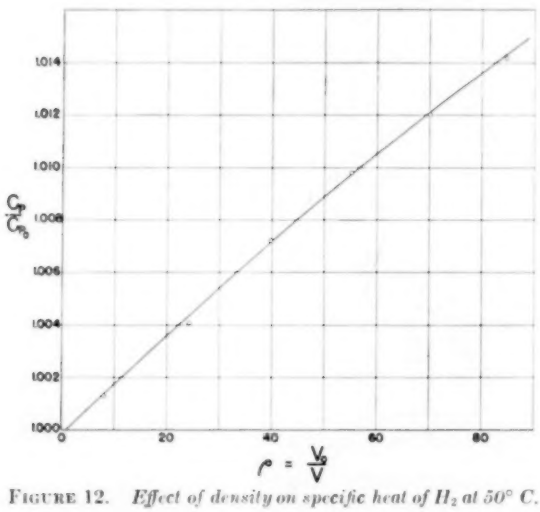

FIGURE 12. *Effect of density on specific heat of H_2 at 50° C.*

Figure 12 shows the dependence of the specific heat at constant pressure for hydrogen at 50° C upon the Amagat density ρ. The curve represents the results of the evaluation of formula 5.8, using the PVT correlation of this paper. The plotted points are observations by Workman [49]. No other direct experimental data on the effect of pressure upon the specific heat at constant pressure are available for hydrogen.

An indirect indication of the effect of pressure on the specific heat of hydrogen is found in the work of van Itterbeek [78], who used the results of van Itterbeek and Keesom [77] on the effect of pressure on the velocity of sound in hydrogen at liquid hydrogen temperatures. The results of van Itterbeek at a pressure of one-tenth of an atmosphere indicate that the increase of C_p with pressure above the zero-pressure value agrees with the PVT prediction within 3 percent at 17.5° K and at 19.0° K, but is lower by more than 30 percent at 20.5° K. At pressures above ½ atm at 20.5° K, this difference in heat capacity has become approximately 0.1 cal deg^{-1} mole^{-1}, but this discrepancy is reduced by roughly 50 percent if the data of van Itterbeek and Keesom are evaluated with values of C_p-C_v based on the PVT tables of this paper.

[12] Up to $\rho=500$ at temperatures above 0° C, the equation $Z=\exp(B\rho+C\rho^2)$ has been used. This is eq 4.8 and eq 4.9 is its series expansion. The symbols B and C stand for functions of T, which are given by eq 4.11 and 4.12.

From $\rho=0$ to $\rho=200$ and $T=14°$ to 56° K Z can be expressed by $Z=1+(A/T^{3/2})\rho-(C/T^{3/2})\rho^2$, which is equivalent to eq 4.14. The symbols A and C stand for functions of T, whose values are tabulated in table 18.

The specific heat of hydrogen at constant volume has been determined by Eucken [169] for various combinations of temperature and density in the ranges 35° to 110° K and 60 to 150 Amagats.

Joule-Thomson coefficients of hydrogen may be of interest. These may be calculated from eq 4.6. For this calculation there are required: the value of C_p which may be calculated using eq 5.8 or 5.17. Values of Z, $(dZ/dT)_\rho$, and $(dZ/d\rho)_T$ are given explicitly in tables 13, 15, and 17. By using values of C_p for H_2 at 50° C derived from figure 12, the following values of μ for 50° C were obtained by calculation: at $\rho=20$, $\mu=-0.0350$ deg atm^{-1}; $\rho=40, \mu=-0.0364$; $\rho=60, \mu=-0.0378$; $\rho=80$, $\mu=-0.0390$, and $\rho=100$, $\mu=-0.0402$. By extrapolation, one obtains for μ at $\rho=0$ the value -0.0335.

There are no accurate measured Joule-Thomson data for hydrogen for 50° C with which these calculated values of μ may be compared.

Results of measurements on Joule-Thomson effects in hydrogen and deuterium at liquid air and room temperatures have been published recently by Johnston and coworkers [57, 58], with curves showing calculated values for hydrogen based on the tables of this paper.* Considering that the Joule-Thomson coefficients are not obtained with great simplicity from the PVT data and depend sensitively on the trends of the representation, the agreement is considered fairly satisfactory.

The location of the inversion curve for the Joule-Thomson effect in hydrogen on a ρ-T graph may be determined from tables 15 and 17 by finding values of ρ and T for which $T(dZ/dT)_\rho = \rho(dZ/d\rho)_T$, in accordance with eq. 4.6.

An expression for μ in terms of derivatives of the enthalpy, H, is

$$\mu=\frac{(dH/d\rho)_T}{\left(\frac{dH}{d\rho}\right)_T\left(\frac{dP}{dT}\right)_\rho-\left(\frac{dH}{dT}\right)_\rho\left(\frac{dP}{d\rho}\right)_T}. \qquad (5.18)$$

In accordance with this equation the inversion curve may be determined by inspection of the $(H°-H)/RT$ table (table 23), since $\mu=0$ where

$$\left(\frac{d(H°-H)/RT}{d\rho}\right)_T=0. \qquad (5.19)$$

*The tables of this paper were completed before the papers by Johnston and coworkers [57, 58] on the Joule-Thomson coefficients of H_2 and D_2 appeared. The correlation of PVT data would doubtless have been better if these Joule-Thomson data had been available at the time the correlation was made.

The heavy curve in figure 13 is the inversion curve of hydrogen as given by the correlation of this paper. In locating it, values of P were determined with the help of table 14. For temperatures below 75° K some extrapolation beyond the limit of the tables was necessary. In this extrapolated region the σ versus ρ diagram, figure 6, was worked with, and the relation for the inversion curve on this diagram was used to get the extrapolated part of the inversion curve directly from the σ versus ρ diagram.

In a Joule-Thomson expansion of hydrogen at constant temperature from a high to a very low

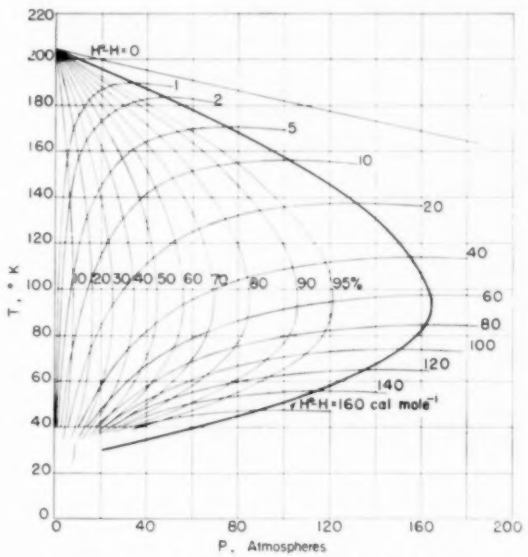

FIGURE 13. *Curves related to the Joule-Thomson cooling of H_2.*

density, approaching zero density, there is a change in enthalpy equal to $(H°-H)$. In figure 13 the curves that cross the inversion curve horizontally are curves of constant $H°-H$. As $H°$ is a function of temperature, these constant $(H°-H)$ curves are not isenthalpics.

The horizontal crossing of the inversion curve by the $(H°-H)$ curve is related to the fact that μ, which is zero along the inversion curve, is equal to $(dH/dP)_T/C_p$, which means that along the inversion curve $(dH/dP)_T$ is zero. The enthalpy change $(H°-H)$ is equal, very nearly, to the amount of refrigeration, per mole of gas, available for the liquefaction of hydrogen in a Hampson or Linde low pressure type of hydrogen liquefier in which a

continuous flow of gaseous hydrogen is allowed to expand from a high to a low pressure without doing work against an external force system. The fraction x of the high pressure hydrogen flow that might, theoretically, be liquefied is

$$x=\frac{H'-H}{H'-H_{liq}}=\frac{H'-H}{(H'-H_{vap})+L_v}, \quad (5.20)$$

where H and H' are the enthalpies of the compressed and expanded hydrogen at the temperature at which the compressed hydrogen leaves the precooler and enters the last stage interchanger before expansion; L_v is the heat of vaporization of liquid hydrogen at the boiling temperature determined by the pressure of the expanded hydrogen; and $(H_{vap}-H_{liq})=L_v$ is the difference in enthalpies of saturated vapor and liquid in equilibrium at the pressure of the expanded hydrogen. Only a relatively small error is made in x if in place of H' and H_{vap} for the real gas at atmospheric pressure one uses the enthalpies H° and H°_{vap} of hydrogen in the ideal gas state at the same temperatures as would be used for H' and H_{vap}.

$$x=\frac{H^\circ-H}{H^\circ-H^\circ_{vap}+L_v}. \quad (5.21)$$

For a temperature of precooling equal to 65° K, the error introduced by the approximation is about 0.5 percent.

The lines of figure 13 that are roughly parallel to the inversion curve and converge with it at the inversion point, 204.6° K, are lines showing the pressure at which $H^\circ-H$ has reached a given fraction of its maximum value for the given temperature. As the inversion curve is the line of maximum values of $(H^\circ-H)$ it is also the 100-percent line in this family of constant percentage lines.

In the free expansion of a continuous flow of gas not doing work against an external force system, the maximum refrigeration is obtained by expanding from the inversion pressure for the given temperature of the compressed gas. The curves of constant percentage of maximum values of $(H^\circ-H)$ are also curves of constant percentage of the maximum available refrigeration in an expansion to low pressure.

Figure 13 makes apparent how greatly the refrigeration and the fraction of hydrogen liquefied (eq 5.21) by a Hampson type liquefier are increased by lowering the temperature of the compressed hydrogen before it enters the final interchanger from which expansion of the hydrogen takes place. It is also seen that the condition of highest inversion pressure (92° K and 165 atm) is by no means the most favorable condition for liquefaction; a further cooling of the compressed hydrogen by 32 degrees nearly doubles the refrigeration produced and more than doubles the fraction liquefied. It is also seen from figure 13 that for the usual range of temperatures (55° to 90° K) to which compressed hydrogen is precooled before expansion in a Hampson-type liquefier, about 95 percent of the maximum refrigeration is obtained when the pressure of the compressed gas is only 75 percent of the inversion pressure.

VI. Viscosity and Thermal Conductivity

1. Viscosity and Thermal Conductivity of the Gas Near Atmospheric Pressure

(a) Hydrogen

Values for the viscosity of gaseous normal hydrogen at atmospheric pressure for temperatures above the boiling point and at saturation pressure for two temperatures below the boiling point are given in table 24. These were calculated using the empirical equation

$$\eta=85.558\times10^{-7}\frac{T^{3/2}}{T+19.55}\frac{T+650.39}{(T+1175.9)} \text{ poises} \quad (6.1)$$

for the viscosity at very low pressure,[13] together with values for the small differences between viscosities at atmospheric or saturation pressure and at very low pressure (see eq 6.17 and 6.16). The four constants of eq 6.1 were chosen on the basis of experimental data near 20°, 90°, 300°, and 685° K. The value used for the viscosity of hydrogen at 685° K was 0.55 percent larger than the experimental values of Trautz and Zink [99], as their value was based on Millikan's value for the viscosity of air which is now known to be low by about this amount.

In figure 14 are plotted deviations of recent experimental viscosity data from eq 6.1. No changes were made in the experimental data for

[13] This viscosity at very low pressure is a true or bulk viscosity. The pressure effect mentioned here is not the familiar low pressure effect on the apparent experimental viscosity involving the accommodation coefficient and the limited size of experimental apparatus.

TABLE 24. *Viscosity of gaseous hydrogen* (H_2)

T	η	T	η	T	η
°K	*Poises*	°K	*Poises*	°K	*Poises*
10	51.0×10^{-7}	260	813.6×10^{-7}	620	$1,461\times10^{-7}$
20	109.3	270	834.6	640	1,493
30	160.7	280	855.3	660	1,524
40	206.8	290	875.8	680	1,555
50	248.9	300	896.0	700	1,585
60	287.6	310	916.0	720	1,616
70	323.8	320	935.8	740	1,646
80	357.9	330	955.4	760	1,675
90	390.3	340	974.8	780	1,705
100	421.1	350	994.0	800	1,734
110	450.8	360	1,013	820	1,763
120	479.3	370	1,032	840	1,792
130	507.0	380	1,051	860	1,820
140	533.8	390	1,069	880	1,848
150	559.8	400	1,087	900	1,876
160	585.2	420	1,124	920	1,904
170	610.0	440	1,160	940	1,932
180	634.3	460	1,195	960	1,959
190	658.1	480	1,230	980	1,986
200	681.4	500	1,264	1,000	2,013
210	704.3	520	1,298	1,020	2,040
220	726.9	540	1,331	1,040	2,066
230	749.0	560	1,364	1,060	2,092
240	770.9	580	1,397	1,080	2,118
250	792.4	600	1,429	1,100	2,144

the differences in density. Deviations of table 24 values from eq 6.1 are represented in figure 14 by the peaked curve, which is appreciably above the zero line between 10° K and 100° K and in very close agreement with it at higher temperatures. This peaked curve represents the viscosity at atmospheric pressure above the boiling point and at saturation vapor pressure below the boiling point. Different reported values of viscosity at low temperatures are so poorly in agreement that their comparison does not indicate the magnitude of the peak, which has accordingly been obtained from theory, using data of state. To limit the crowding of experimental points in the figure, those plotted represent only data published since 1928, but a few data obtained after 1928 have been omitted. The data of Trautz and co-workers [94 to 102] would be in better agreement with the zero line if increased by about one half percent for the revision in the value for the viscosity of air.

It has been pointed out by others that the Sutherland formula

$$\eta=\eta'\left(\frac{T}{T'}\right)^{3/2}\frac{T'+C}{T+C} \tag{6.2}$$

does not fit the data for hydrogen over an extended range of temperature. This may be seen in figure 14 in which the deviations of the Sutherland formula from eq 6.1 are represented by the curve below the zero line. The constant C was evaluated at 300° K to represent the trend of the best data.

Values of the thermal conductivity of gaseous normal hydrogen are given in table 25.

TABLE 25. *Thermal conductivity of gaseous hydrogen at 1 atm*

T	K	T	K
°K	*cal cm⁻¹ sec⁻¹ °C⁻¹*	°K	*cal cm⁻¹ sec⁻¹ °C⁻¹*
10	14.3×10^{-6}	260	397.0×10^{-6}
20	34.6	270	409.7
30	53.5	280	422.1
40	70.7	290	434.2
50	86.5	300	446.3
60	101.4	320	469.8
70	116.1	340	492.8
80	130.8	360	515
90	145.9	380	537
100	161.3	400	559
110	177.0	420	580
120	192.9	440	601
130	208.8	460	622
140	224.6	480	643
150	240.4	500	664
160	256.0	520	684
170	271.4	540	705
180	286.5	560	725
190	301.1	580	745
200	315.4	600	766
210	329.6		
220	343.5		
230	357.2		
240	370.7		
250	384.0		

They were calculated from the equation

$$k=[1.8341-0.004458T+(1.1308+0.0008973T)C_v^\circ]\frac{\eta}{M}\frac{1}{\left(1+\frac{3.2}{T}\right)} \tag{6.3}$$

In principle, a correction from low pressure to one atmosphere would be applicable, but it has been omitted because the uncertainty of the experimental values is much greater. In eq 6.3, M is the molecular weight, η the viscosity given by eq 6.1, C_p° the specific heat in calories per mole per degree at constant pressure, and T the temperature in degrees Kelvin. This equation is an empirical representation of the data and was

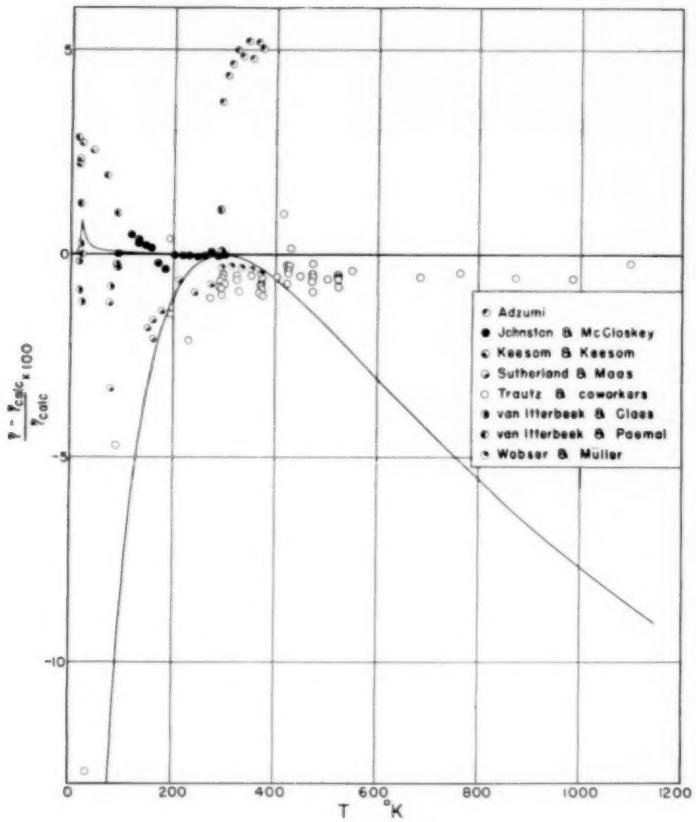

FIGURE 14. *Viscosity of hydrogen.*

obtained in several steps, which will be explained in the discussion that follows.

In figure 15, curve A represents eq 6.3, whereas curves B and C are theoretical and are given for comparison. Curve C is for Eucken's relation

$$k=(9\gamma-5)C_v^\circ\eta/(4M), \tag{6.4}$$

or its equivalent

$$k=(C_p^\circ+1.25R)\eta/M. \tag{6.5}$$

Chapman and Cowling [137] proposed the formula

$$k=\left[\frac{15}{4}(\gamma-1)+\frac{1}{2}U_{11}(5-3\gamma)\right]\eta C_v^\circ/M, \tag{6.6}$$

which is equivalent to

$$k=[U_{11}C_p^\circ+(3.75-2.5U_{11})R]\eta/M. \tag{6.7}$$

The transport of internal molecular energy of a gas is supposed to be represented better theoretically as a result of including the quantity U_{11}, which is the ratio of mean free path lengths for diffusion and viscosity.

U_{11} is a pure number whose value was determined theoretically for (1) smooth elastic spheres and (2) for molecules repelling as the inverse fifth power of the distance (Maxwellian molecules), the values being 1.204 and 1.55, respectively.

For U_{11} equal to 1, curve C is obtained, as eq 6.6 and 6.7 then reduce to eq 6.4 and 6.5. Curve B of figure 15 is a graph of eq 6.7 with $U_{11}=1.4$, a value indicated by a group of measurements of the conductivity near 300° K. It is evident that the main body of the experimental data is not consistent with a constant value of U_{11}. On the basis of a value of 1.4 for U_{11} near 300° K and a higher value at 700° K, as indicated by a curve representing the data, the relation

$$U_{11}=1.1308+0.0008973T \tag{6.8}$$

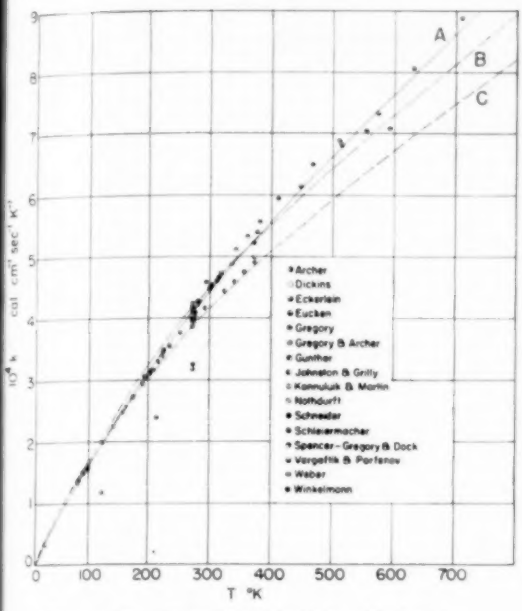

FIGURE 15. *Thermal conductivity of hydrogen.*

was adopted. It was found that the curve was not critically dependent on the functional form of U_{11} as a change to $U_{11}=a+b\sqrt{T}$ altered the final curve negligibly between 300° and 700° K.

At temperatures somewhat below 100° K, the ideal gas specific heat of hydrogen at constant pressure approaches the value $(5/2)R$ characteristic of a monatomic gas. For this value of C_p°, the U_{11} terms in eq 6.7 cancel and eq 6.4 to 6.7 reduce to

$$k=\frac{5}{2}\eta(C_v/M). \tag{6.9}$$

This equation has been derived exactly for a force that at all distances is repulsive and proportional to $1/r^5$. Enskog [132] has shown that for attracting rigid spheres (Sutherland molecules),

$$k=[2.522/1(1+0.03C/T)]\eta C_v/M,$$

where C is the Sutherland constant in eq 6.2. Thermal conductivities of hydrogen measured at liquid air temperatures are a few percent lower than equations 6.4 to 6.9 would indicate. No theoretical explanation of this is at hand, but the agreement of the three independent investigations in this region indicates that the lower value is to be accepted. To take account of this, a correction factor $1/(1+3.2/T)$ has been included, having a form suggested by Enskog's theoretical result for attracting rigid spheres but with the constant chosen to fit these experimental data. The inclusion of this factor also brings the final curve closer to Eucken's experimental value at 20.96° K, which is still almost 12 percent lower than the curve.

The curve as chosen to fit the thermal conductivity data is not regarded as completely satisfactory. In the temperature range 270° to 400° K, the experimental data appear to fall into two groups, one quite close to the curve adopted and the other lower by about 7 percent. The lower group includes the most recent data.

Equation 6.4 to 6.9 make it evident that at low-temperatures where the specific heats of ortho and para hydrogen differ, their thermal conductivities differ also. This difference in thermal conductivity was the basis of the method of ortho-para analysis used by Bonhoeffer and Harteck [121]. The temperature or electrical resistance of an electrically heated wire carrying a given current determines, after calibration, the ortho-para composition of the hydrogen that surrounds the wire in a tube externally thermostated at liquid air temperature. A small difference is to be expected in the viscosities of ortho and para hydrogen by reason of small differences in their intermolecular forces manifested by small differences in vapor pressure, and density of the condensed states.

This difference in viscosities is small and was not detected in the experiment undertaken by Harteck and Schmidt [122], in which an accuracy of 1 percent was attained. In later developments of the so-called thermal conductivity method of ortho-para analysis, the pressure of the gas was reduced to make the mean free path large compared with the diameter of the heated wire. For this condition the ordinary thermal conductivity is not the controlling factor.

(b) Deuterium

Several investigations have been made of the viscosity of deuterium at atmospheric pressure, the most recent being that of Van Itterbeek and Van Paemel [106, 107], published in 1940. Table 26, which gives values for the ratio between viscosities of deuterium and hydrogen for several temperatures, was taken from the paper by Van Itterbeek and Van Paemel.

TABLE 26. *Ratio of viscosities for gaseous* D_2 *and* H_2

T	$\eta(D_2)/\eta(H_2)$
° K	
293	1.40
90	1.38
80	1.37
70	1.36
20	1.24
15	1.24
12.5	1.24

The ratio of the thermal conductivity of deuterium at 0° C to the thermal conductivity of hydrogen also at 0° was determined by C. T. Archer [127] and by W. G. Kannuluik [130], who obtained respectively, the values 0.736_5 and 0.732_4. By using the mean of these values with appropriate values of C_p and η, one obtains for f_{11} in eq 6.7 for the thermal conductivity of D_2 at 0° C the value 1.55. Archer also measured the thermal conductivity of various equilibrium mixtures of H_2, HD, and D_2.

For two isotopic gases with identically the same intermolecular forces, the classical theory values for the ratio of their viscosities,and the ratio of their thermal conductivities at temperatures where their heat capacities are equal are

$$\eta_1/\eta_2 = \sqrt{M_1/M_2} \text{ and } k_1/k_2 = \sqrt{M_2/M_1} \quad (6.10)$$

For H_2 and D_2 these ratios have the values: $\eta_{D_2}/\eta_{H_2} = 1.414$ and $k_{D_2}/k_{H_2} = 0.707$, and are independent of the intermolecular force field so long as it is the same for the two isotopes. The difference between the rotational heat capacities of H_2 and D_2 at low temperatures by itself makes the ratio k_{D_2}/k_{H_2} larger and thus has an effect opposite to but less than that of the smaller mean velocity of D_2 molecules caused by the greater mass. Using Eucken's eq 6.4 for k and making allowance for the difference in heat capacities of H_2 and D_2, one obtains 0.718 for k_{D_2}/k_{H_2} at 0° C. The classical theory values for these ratios of thermal conductivities and viscosities are approached closely at room temperatures. The effect of quantum mechanical interaction in transport phenomena can be described in terms of increase in the apparent size of the molecules. In classical theory the size of the molecule plays an important role, the viscosity and thermal conductivity decreasing as the size increases. For hydrogen and deuterium, the quantum mechanical increase in apparent size is small at room temperature but becomes large at low temperature. The increase depends also upon the masses of the colliding molecules and is larger for H_2 than for D_2 at the same temperature. It was pointed out in the section on the PVT data for deuterium that the quantum theory of second virial coefficients includes an effect interpretable classically as an increase in apparent size of molecules, becoming very large at low temperatures. The quantum mechanically obtained increase in apparent size with lowering of temperature is not the same for viscosity as that associated with the second virial coefficient, however. This is not surprising when one considers that the increase in the mean de Broglie wave length with decreasing temperature increases the diffraction behind a scattering molecule; an effect that does not enter in the determination of the second virial coefficient, but which taken by itself would decrease the apparent size of a scattering molecule for viscosity.

2. Viscosity and Thermal Conductivity of the Gas at High Pressures

There are no experimental data on the thermal conductivity of gaseous H_2 at high pressures. For viscosity, however, experimental data obtained by Boyd [134] and Gibson [135] are available. Gibson's data, which are for 25° C, are more precise than those of Boyd and are plotted in figure 16. It will be seen that there is fairly good agreement between these better experimental data and the curve representing the theoretical formula due to Enskog. Differing approaches to the problem of relating viscosity and variables of state will be found elsewhere [133, 136].

In elementary theory, the viscosity and thermal conductivity for a given gas are proportional to the product of V, ρ, and Λ, where V is the mean molecular velocity, ρ is the density, and Λ is a suitable mean path length for the transfer of momentum or energy. Although Λ is often taken as identical with the ordinary free path of molecular motion, it is actually greater by a small distance of the order of magnitude of a molecular diameter, as at each collision the momenta and energies are transferred an additional distance related to the diameters of the molecules involved. Thus instead of Λ decreasing as $1/\rho$ when ρ is increased, which would make $\rho\Lambda$ independent of

ρ, Λ decreases a little less slowly so as to make $\rho\Lambda$ increase slightly as ρ is increased. Accordingly, both the thermal conductivity and the viscosity of a gas would be expected to increase with increasing density, particularly when multiple encounters between molecules occur frequently as in the case of high densities.

Enskog's theory was developed for a gas whose molecules were assumed to be mutually attracting rigid spheres, for which the equation of state has the form

$$P+a\rho^2=RT\rho(1+b\rho\chi), \tag{6.11}$$

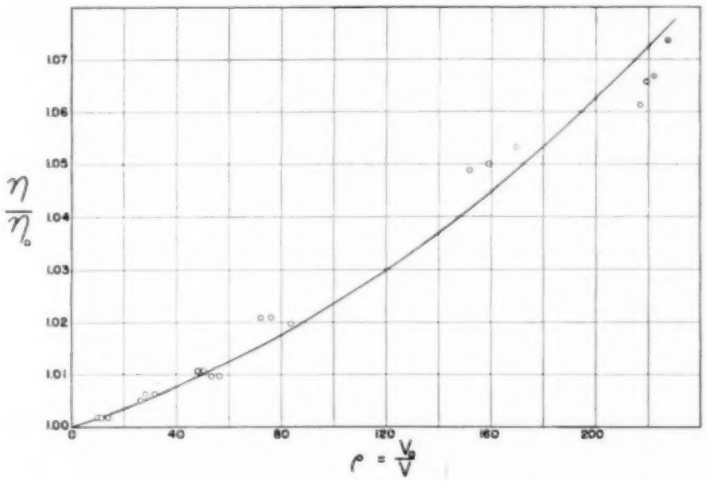

FIGURE 16. *Effect of density on viscosity of hydrogen at 25° C.*

where the constants a and b are assumed to be independent of T and ρ, and χ is a function of ρ expressed in the form of a power series in $b\rho$. The equation of state that was used is thus almost the same as the Van der Waals equation

$$P+a\rho^2=RT\rho(1-b\rho)^{-1}=RT\rho \\ [1+b\rho(1+b\rho+b^2\rho^2+\ldots)] \tag{6.12}$$

except for the details of the dependence of χ upon ρ. The Van der Waals equation is derived on the basis that simultaneous encounters of three or more molecules are rare enough to be neglected. Only at low pressures is this valid and under this condition terms of the second degree and higher in $b\rho$ are neglected in the derivation. The function

$$\chi=1+0.625b\rho+0.2869b^2\rho^2+\ldots. \tag{6.13}$$

used by Enskog takes account of simultaneous encounters of three and four molecules as treated by Boltzmann and Clausius.

According to Enskog's theory, the viscosity and thermal conductivity of a compressed gas are related to the viscosity η_0 and conductivity k_0 at low pressure by the equations

$$\eta/\eta_0=b\rho[1/(b\rho\chi)+0.8+0.7614b\rho\chi\ \ldots\ ] \tag{6.14}$$

and

$$k/k_0=b\rho[1/(b\rho\chi)+1.2+0.7574b\rho\chi\ \ldots\ ] \tag{6.15}$$

It follows from eq 6.11, the equation of state assumed for Enskog's theory, that

$$b\rho\chi=\frac{T}{P}\left(\frac{dP}{dT}\right)_\rho\left(\frac{PV}{RT}\right)-1=Z-1+T\left(\frac{dZ}{dT}\right)_\rho. \tag{6.16}$$

Thus, the value of $b\rho\chi$ may be calculated from the tables of Z and $(dZ/dT)_\rho$ and the value of $b\rho$ may then be found with the help of eq 6.13.

Over the range of Gibson's experimental viscosity data very little change is made in the values predicted if simple power series expansions in $b\rho\chi$, obtained from equations 6.14 and 6.15, are used:

$$\eta/\eta_0=1+0.175b\rho\chi+0.7557(b\rho\chi)^2-0.405(b\rho\chi)^3 \tag{6.17}$$

$$k/k_0=1+0.575b\rho\chi+0.5017(b\rho\chi)^2-0.204(b\rho\chi)^3 \tag{6.18}$$

The coefficient of the last term of each equation would be changed if higher order terms were added to eq 6.13, 6.14, and 6.15. Dropping the last term of eq 6.17 for η/η_0 does not significantly change the agreement with Gibson's experimental data.

In order to show the general magnitude of the theoretical effect of pressure on the viscosity and thermal conductivity of hydrogen the preceding equations have been evaluated for several additional combinations of temperature and pressure, using data from the PVT tables. Table 27 gives the values thus obtained. It is seen that the calculated relative change in η and k with pressure is much more pronounced at the lower temperatures, for which large deviations from the ideal gas law occur even at moderate pressures.

TABLE 27. *Effect of pressure on viscosity and thermal conductivity of hydrogen*

T	P	η/η_0	k/k_0
°K	*atm*		
18	0.455	1.0045	1.0138
20	.889	1.0077	1.0225
22	1.565	1.0126	1.0347
30	1	1.0037	1.0114
30	2.04	1.0086	1.0248
38	30.4	1.53	1.76
40	1	1.0021	1.0068
40	2.80	1.0067	1.0199
40	37.2	1.53	1.76
50	1	1.0015	1.0048
50	3.55	1.0060	1.0178
50	50	1.31	1.49
60	1	1.0012	1.0037
70	1	1.0009	1.0030
70	5.06	1.0051	1.0155
70	50	1.11	1.22
80	1	1.00075	1.0024
90	1	1.00065	1.0021
90	6.56	1.0047	1.0141
90	50.0	1.06	1.13
100	1	1.00056	1.0018
110	1	1.00049	1.0016
150	1	1.00034	1.0011
250	1	1.00018	1.0006
400	1	1.00010	1.0003
600	1	1.00006	1.0002

3. The Viscosity of Liquid Hydrogen

The first determination of the viscosity of liquid hydrogen was made in 1917 by Verschaffelt and Nicaise [138] from measurements of the logarithmic decrement of the oscillatory rotation of a sphere in liquid hydrogen at 20.36° K. Later, determinations were made of the viscosity of liquid hydrogen from 15° to 20° K, in 1938 by Keesom and Mac Wood [139] from measurements of the logarithmic decrement of an oscillating disc, and in 1939 by Johns [140], using the capillary flow method. The reported viscosities are shown in figure 17. The values obtained by Johns are roughly 10 percent greater than those of Keesom and Mac Wood except near the boiling point, 20.4° K. There seems to be no clear indication in the papers reporting the measurements that either of these two later sets is less dependable than the other. Accordingly a curve to represent the present most probable values of the viscosity of liquid hydrogen was drawn principally between the two sets. Near the boiling point the curve was drawn approximately parallel to that of Johns because it was felt that the lower value of Verschaffelt and Nicaise supported the more regular variation of viscosity with temperature as reported by Johns.

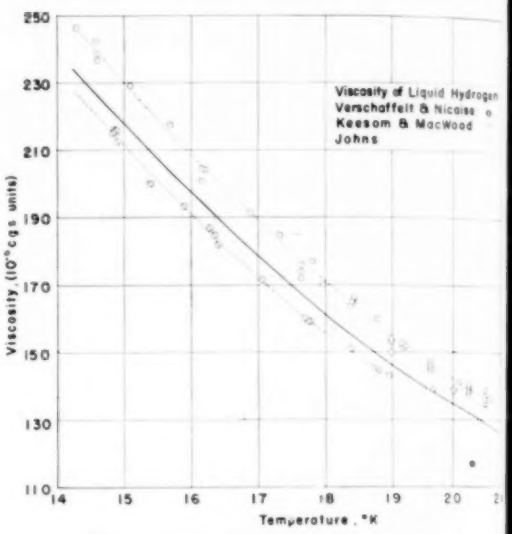

FIGURE 17. *Viscosity of liquid hydrogen.*

VII. Pressure Temperature Relations for Two-Phase Equilibria for H_2, HD, and D_2 as Single Components

In this section are presented data on (1) vapor pressures of solid and liquid H_2, HD, and D_2 with such derived constants as normal boiling temperatures and triple-point temperatures and pres-

ures; differences between the vapor pressures of different mixtures of *o*- and *p*-H_2; and changes in vapor pressures of ortho-para H_2 mixtures resulting from self conversion; (2) the pressure-temperature relations for the solid-liquid equilibrium of H_2, HD, and D_2. The data are presented in the form of equations, tables, and graphs.

1. Vapor Pressures, Boiling, and Triple Points [14]

The present vapor-pressure data on the hydrogens can be fitted with equations of the form

$$\log_{10}P = A + B/T + CT \qquad (7.1)$$

to within the accuracy of the experimental data. The millimeter of Hg at 0° C and standard gravity is used in this section as the unit of vapor pressure. Temperatures are on the Kelvin Scale.

In tables 28 and 29 the vapor pressures, boiling points, and triple points of the different isotopic and ortho-para modifications of hydrogen are compared.

(a) H_2

The differences between the hydrogen vapor-pressure data reported in the literature [143 to 146, 148] are the result, principally, of differences in the temperature scales used by different observers and of unknown differences in the ortho-para composition of the hydrogen.

The vapor-pressure data recently obtained [146] at the National Bureau of Standards are on the low-temperature scale established at the National Bureau of Standards and are for known ortho-

[14] Boiling-point and triple-point data from this section have been used in advance of publication in the "Tables of Selected Values of Chemical Thermodynamic Properties" prepared by the National Bureau of Standards in connection with the Office of Naval Research of the U. S. Navy Department.

TABLE 28. *Vapor pressures of the several isotopic varieties of hydrogen at integral temperatures and at their triple points and boiling points.*

[Values marked (*) were obtained by extrapolation of the vapor-pressure equation to temperatures at which no data were available. The *o*-H_2 table is based on an extrapolation with respect to composition.]

T	20.4° K Equilibrium hydrogen 0.21 percent *o*-H_2		Normal hydrogen 75 percent *o*-H_2		Orthohydrogen 100 percent *o*-H_2		Normal deuterium 66.67 percent *o*-D_2		20.4° K Equilibrium deuterium 97.8 percent *o*-D_2		Hydrogen deuteride	
	P	State	*P*	State	*P*	State	*P*	State	*P*	State	*P*	State
°K	*mm* Hg		*mm* Hg		*mm* Hg		*mm* Hg		*mm* Hg		*mm* Hg	
	1.93	Solid*	1.7$_1$	Solid*		Solid	0.05	Solid*	0.05	Solid*	0.28	Solid.*
	5.62	Solid	5.0$_9$	Solid		do	.20	do	.21	do	.99	Solid.
	13.9	do	12.7	do		do	.73	do	.75	do	2.94	Do.
	30.2	do	27.9	do		do	2.14	do	2.20	do	7.46	Do.
	52.8	Triple point.	49.1	do		do	4.61	do	4.73	do	14.6	Do.
	57.4	Liquid	54.0	Triple point		do	5.24	do	5.37	do	16.3	Do.
	58.8	do	55.4	Liquid		do	5.44	Solid	5.57	Solid	16.8	Do.
	60.5	do	57.0	do	55.1	Triple point*	5.68	do	5.82	do	17.5	Do.
	100.4	do	95.0	do	92.2	Liquid*	12.3	do	12.6	do	34.4	Do.
	161.2	do	153.3	do	149.1	do	25.4	do	26.0	do	65.2	Do.
	209.3	do	199.7	do	194.4	do	37.9	do	38.7	do	92.8	Triple point.
	246.2	do	235.2	do	229.2	do	48.6	do	49.6	do	112.5	Liquid.
	360.6	do	345.9	do	337.8	do	87.2	do	88.7	do	176.4	Do.
	459.8	do	442.0	do	432.3	do	126.3	do	128.5	Triple point	234.5	Do.
	464.9	do	446.9	do	437.1	do	128.5	Triple point	130.3	Liquid	237.5	Do.
	510.1	do	490.8	do	480.7	do	145.1	Liquid	147.2	do	264.7	Do.
	709.3	do	675.7	do	662.6	do	219.9	do	223.1	do	382.8	Do.
	760	do	733.9	do	720.0	do	244.9	do	248.4	do	420.9	Do.
	786.8	do	760	do	745.7	do	256.2	do	259.9	do	438.1	Do.
	801.7	Liquid*	774.4	Liquid*	760	do	262.5	Liquid*	266.2	Liquid*	447.7	Liquid.*
	937.0	do	906.4	do	890.6	do	322.2	do	326.9	do	536.2	Do.
	1226.6	do	1189.0	do	1170.4	do	458.5	do	465.1	do	730.5	Do.
	1269.4	do	1230.8	do	1211.8	do	479.6	do	486.5	do	760	Do.
	1574.9	do	1529.6	do	1508.4	do	636.2	do	645.3	do	972.0	Do.
	1784.4	do	1734.5	do	1712.2	do	749.3	do	760	do	1120.1	Do.
	1893.5	do	1753.3	do	1730.8	do	760	do	770.6	do	1133.8	Do.

TABLE 29. *Boiling points and triple points of the hydrogens*

	Boiling point	Triple point	
		T	P
	° K	° K	mm Hg
20.4° K equilibrium hydrogen (0.21% o-H_2)	20.27	13.81	52.8
38 percent o-H_2, 62 percent p-H_2	20.32	13.86	53.0
Normal hydrogen (75% o-H_2)	20.39	13.95	54.0
Orthohydrogen	20.45	14.05	55.1
Normal deuterium (66.67% o-D_2)	23.57	18.72	128.5
20.4° K equilibrium deuterium (97.8% o-D_2)	23.52	18.69	128.5
Paradeuterium	23.66	18.78	128.5
Hydrogen deuteride	22.13	16.60	92.8

para compositions. Only the NBS results are given here.

Normal hydrogen (75 percent o-H_2, 25 percent p-H_2):

$$\text{Liquid: } \log_{10}P(\text{mm Hg}) = 4.66687 - \frac{44.9569}{T} + 0.020537\,T. \tag{7.2}$$

$$\text{Solid: } \log_{10}P(\text{mm Hg}) = 4.56488 - \frac{47.2059}{T} + 0.03939\,T. \tag{7.3}$$

20.4°K-equilibrium hydrogen (99.79 percent p-H_2, 0.21 percent o-H_2:

$$\text{Liquid: } \log_{10}P(\text{mm Hg}) = 4.64392 - \frac{44.3450}{T} + 0.02093\,T. \tag{7.4}$$

$$\text{Solid: } \log_{10}P(\text{mm Hg}) = 4.62438 - \frac{47.0172}{T} + 0.03635\,T. \tag{7.5}$$

The triple-point temperatures and pressures were determined experimentally with a low-temperature calorimeter with a platinum resistance thermometer for the temperature measurements. Equations 7.2 to 7.5 were made to fit these triple points, and are based on vapor pressure data extending from 10.5° to 20.4° K. Although the equation for liquid normal H_2 is based only on National Bureau of Standards data below 20.4° K, the equation represents, within the limits of experimental accuracy, the Leiden data that extend nearly to the critical point, 33.19° K. As mentioned in section IV, the vapor-pressure equation for normal hydrogen was used in constructing the PVT relations for hydrogen. The experimentally determined triple-point temperatures and pressures for n-H_2 and e-H_2 are given in tables 2[illegible] and 29.

Figure 18 is a diagram of differences between the vapor pressures of a 20.4°K equilibrium mixture of o- and p-H_2 (0.21 percent o-H_2) and five different mixtures of o- and p-H_2 in the liquid state. The vapor pressure of the 20.4°K equilibrium mixture is denoted by $P_{(e-H_2)}$ and that of any other mixture by $P_{(\text{mixture})}$. Each curve of the graph is for a single mixture whose composition is indicated on the graph by its o-H_2 composition. The 75 percent curve is for normal hydrogen. The vapor pressure differences ΔP are plotted as a function of the vapor pressure of the 20.4°K equilibrium hydrogen. The circles represent the experimental data.

Figure 19 shows the vapor pressure differences of figure 18 extended into the solid range, for mixtures of 38 and 75 percent ortho composition. At the extreme right of the figure, these mixtures and the e-H_2 with which they are compared are all liquid. Passing to the left, the first sharp break encountered on either curve corresponds to the triple point of the mixture. The second sharp break corresponds to the triple point of e-H_2. To the left of the last break, both materials are solid. Between the two breaks on either curve, the mixture is solid but the e-H_2 is liquid.

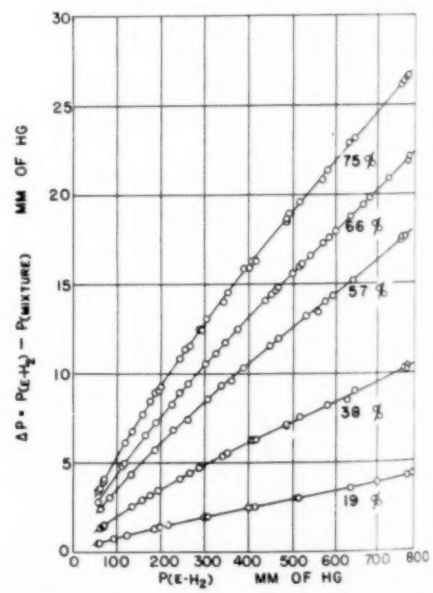

FIGURE 18. *Vapor pressure differences for liquid ortho-para H_2 mixtures.*

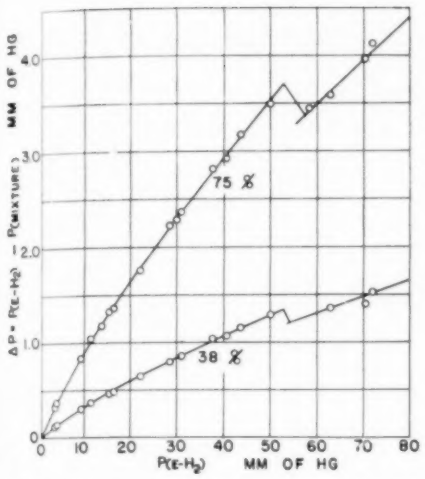

FIGURE 19. *Vapor pressure differences for solid ortho-para* H_2 *mixtures.*

A comparison of the ΔP's for different mixtures of o- and p-H_2 in figures 18 and 19 shows that the P's are not proportional to their corresponding differences in composition.

For ideal solutions the ratio $\Delta P/\Delta x$, where Δx is the difference in composition, is independent of the composition at constant temperature. In figure 20 this ratio is plotted for four temperatures, the circles representing the experimental vapor pressure data as given by points on the smooth curves of figure 18. Figure 20 shows that the vapor pressures of ortho-para mixtures differ greatly from ideal solution predictions.

The vapor pressure differences ($P_{\epsilon\text{-}H_2} - P_m$) for mixtures of o- and p-H_2 of any composition at 14.00°, 16.00°, 18.00° and 20.39° K may be calculated from the isotherms of figure 20. Other isotherms may be determined with the help of figures 18 and 19. By extending the isotherms of figure 20 to 100 percent o-H_2, the vapor pressure of pure liquid o-H_2 was determined. The following equation represents the vapor pressures of pure liquid o-H_2 obtained in this way:

$$\text{liquid: } \log_{10}P(\text{mm Hg}) = 4.65009 - \frac{45.0439}{T} + 0.021168T \qquad (7.6)$$

The triple-point temperature and pressure of H_2 were determined by a quadratic extrapolation of the triple point temperatures and pressures of ϵ-H_2(20.4° K), m-H_2(38 percent o-H_2) and n-H_2. The values thus obtained for o-H_2 were 14.05° K and 55.1 mm Hg. These are in agreement with eq 7.6 for the vapor pressure of liquid o-H_2.

If linear extrapolation is used, omitting the values for m-H_2, one obtains 14.00° K and 54.4 mm Hg as lower limiting values of the triple point constants for o-H_2. The triple point constants of m-H_2 were obtained by reading the values $P(\epsilon\text{-}H_2)$ and ΔP corresponding to the upper break in the 38 percent curve. The difference of these is the triple point pressure of m-H_2. By substituting $P(\epsilon\text{-}H_2)$ into the vapor pressure equation (eq 7.4) for liquid ϵ-H_2, the triple point temperature of m-H_2 is obtained. The uncertainties in these derived triple point constants of m-H_2 and o-H_2 are greater than for the experimentally determined values for ϵ-H_2 and n-H_2.

The vapor pressure of a nonequilibrium mixture of o- and p-H_2 changes slowly with time because of the slow conversion of a nonequilibrium mixture, liquid or solid, to the equilibrium composition. At its normal boiling point, the vapor pressure of n-H_2 changes at the rate of 0.23 mm Hg per hour [148]. Paramagnetic substances increase the rate of conversion. The rate of increase of the vapor pressure at 20.4° K of a sample of hydrogen containing 0.01 percent oxygen was about three times that for pure hydrogen.

The interconversion of ortho and parahydrogen in the absence of molecular dissociation is the result of an intra-molecular rearrangement of pro-

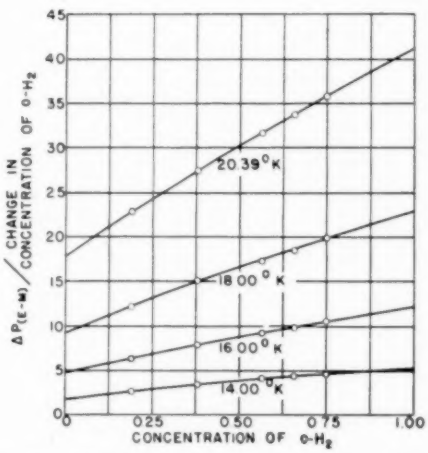

FIGURE 20. *Deviations of vapor pressure of ortho-para* H_2 *mixtures from law of ideal solutions.*

tons in the presence of a strong magnetic field, inhomogeneous on a scale of molecular dimensions.

As p-H_2 has no net nuclear magnetic moment, the self conversion of nonequilibrium mixtures results only from the interaction of o-H_2 molecules, which do have a nuclear magnetic moment, with each other and with p-H_2 molecules. Hence, the ortho-para conversion in liquid and solid H_2 is a bimolecular change.

$$-d[o\text{-}H_2]/dt = k_1[o\text{-}H_2]^2 - k_2[o\text{-}H_2]\,[p\text{-}H_2] \quad (7.7)$$

The velocity constant k_2 is much smaller than k_1 in accord with the small equilibrium proportion of o-H_2. At equilibrium, where $d[o\text{-}H_2]/dt$ is zero, $k_2/k_1 = [o\text{-}H_2]/[p\text{-}H_2]$. Values of equilibrium concentrations are given in table 12. For liquid hydrogen the velocity constant k_1 for conversion is 0.0114 per hour when concentrations are expressed in mole fractions. The value of k_1 for solid H_2, 0.019 hr^{-1} [147], is larger than for liquid H_2 but decreases with time due to the immobility of molecules in the solid. The initial value of k_1 is restored however by melting and freezing.

(b) D_2

The vapor pressures of normal and equilibrium deuterium were measured [149] relative to the vapor pressure of liquid n-H_2 from 14° to 20.4° K. As these measurements are independent of a temperature scale their functional relations are given. Vapor pressures are expressed in terms of mm of Hg at standard conditions.

Normal deuterium (66.67 percent o-D_2, 33.33 percent p-D_2):

$$\text{Liquid: } \log_{10} P(n\text{-}D_2) = -1.3376 + 1.3004 \log_{10} P\,(n\text{-}H_2). \quad (7.8)$$

$$\text{Solid: } \log_{10} P(n\text{-}D_2) = -1.9044 + 1.5143 \log_{10} P(n\text{-}H_2). \quad (7.9)$$

20.4K Equilibrium deuterium (97.8 percent o-D_2, 2.2 percent p-D_2):

$$\text{Liquid: } \log_{10} P(e\text{-}D_2) = -1.3302 + 1.3000 \log_{10} P\,(n\text{-}H_2). \quad (7.10)$$

$$\text{Solid: } \log_{10} P(e\text{-}D_2) = -1.8873 + 1.5106 \log_{10} P\,(n\text{-}H_2). \quad (7.11)$$

Substituting for $\log_{10} P(n\text{-}H_2)$ values given by eq. 7.2 for liquid n-H_2 the following equations for $\log_{10} P(D_2)$ are obtained:

Normal deuterium (66.67 percent o-D_2, 33.33 percent p-D_2):

$$\text{Liquid: } \log_{10} P(\text{mm Hg}) = 4.7312 - \frac{58.4619}{T} + 0.02671\,T. \quad (7.12)$$

$$\text{Solid: } \log_{10} P(\text{mm Hg}) = 5.1626 - \frac{68.0782}{T} + 0.03110\,T. \quad (7.13)$$

20.4°K equilibrium deuterium (97.8 percent o-D_2, 2.2 percent p-D_2)

$$\text{Liquid: } \log_{10} P(\text{mm Hg}) = 4.7367 - \frac{58.4440}{T} + 0.02670\,T. \quad (7.14)$$

$$\text{Solid: } \log_{10} P(\text{mm Hg}) = 5.1625 - \frac{67.9119}{T} + 0.03102\,T. \quad (7.15)$$

The triple-point temperatures and pressures for D_2 given in tables 28 and 29 were obtained by simultaneous solution of the vapor pressure equations for solid and liquid.

The self conversion of nonequilibrium mixtures of o- and p-D_2 proceeds at a very much slower rate than for H_2. Thus no increase in the vapor pressure of liquid n-D_2 resulting from self conversion was observed at 20.4° K over a period of 100 hours [149]. The estimated probable error of two observations extending over 100-hour periods was ±0.27 mm Hg. The small rate of self conversion of D_2, compared with H_2, is a result of the smaller magnetic moment of the deuteron compared with the proton. The ratio of nuclear magnetic moments D/H is 0.26. The relative rate of self conversion for the same displacements of D_2 and H_2 from the equilibrium ortho-para composition is proportional, *as to order of magnitude only*, to the fourth power of their relative magnetic moments, that is to 0.005. Allowing for the smaller displacement of n-D_2 from equilibrium composition and the smaller difference between the vapor pressures of the ortho and para varieties of D_2 the expected ratio of the rates of vapor pressure change, n-D_2 to n-H_2, is of the order of 10^{-7}. For a more detailed discussion see reference [149].

(c) HD

As the two nuclei of the HD molecule are dissimilar, hydrogen deuteride does not have ortho and para varieties. Measurements of the vapor

pressure of HD extend from 10.4° to 20.4° K [150]. The following vapor-pressure equations were made to fit the triple-point temperature 16.60$_4$° K measured with a platinum resistance thermometer in a calorimeter in which the solid and liquid phases were in equilibrium.

HD:

$$\text{Liquid: } \log_{10} P \text{ (mm Hg)} = 5.04964 - \frac{55.2495}{T} + 0.01479\,T \qquad (7.16)$$

$$\text{Solid: } \log_{10} P \text{ (mm Hg)} = 4.70260 - \frac{56.7154}{T} + 0.04101\,T \qquad (7.17)$$

The triple-point pressure of HD given in tables 28 and 29 can be obtained from either of these equations.

(d) HT and DT

Tritium, T, the hydrogen isotope of atomic weight 3 is radioactive and has a half-lifetime of 31 ±8 years [151]. Its disintegration products are a negative β-particle and He^3. Because of its comparatively short half-life, the natural abundance of T in hydrogen is extremely small. Libby and Barter [152] determined the vapor pressures of HT and DT using T made by the irradiation of a block of metallic Li with neutrons ($Li^6 + n \rightarrow He^4 + T^3$). The tritium held by the Li as LiT was liberated by the reaction of H_2O or D_2O with the Li block. Gaseous H_2 or D_2 with a trace of HT or DT was obtained. The gas was liquefied and then evaporated, and the radioactivity of the evaporated vapor was measured as a function of the volume of the remaining unevaporated liquid. From a comparison of the radioactivity of the vapor leaving the liquid during different periods of the evaporation, Libby and Barter calculated the vapor pressures of HT and DT, making use of ideal solution laws for this purpose. They obtained for the vapor pressures of HT and DT, 254 ±16 and 123 ±6 mm Hg, respectively, at the normal boiling temperature of hydrogen (20.39° K). By extrapolation, they estimated that the vapor pressure of T_2 at 20.39° K is 45 ±10 mm Hg.

2. Pressure-Temperature Relations for Solid-Liquid Equilibrium

The melting, or freezing pressures, of n-H_2, HD, and n-D_2 given in table 30 are based on smooth curves drawn through the experimental data (H_2, [153 to 157]; HD [150]; D_2 [174]) and cover the same ranges of pressure and temperature as the data. Figure 21 is a diagram of the deviations of the data for n-H_2 from the table. The dashed line shows a 1-percent deviation from the table and the full-line curve represents the deviation from the table of the equation

$$\log_{10}(237.1 + P) = 1.85904 \log_{10} T + 0.24731, \qquad (7.18),$$

where P is in kg cm^{-2}.

TABLE 30. *Melting temperature-pressure relations for n-H_2, HD, and n-D_2*

T	P		
	n-H_2	HD	n-D_2
°K	kg cm^{-2}	kg cm^{-2}	kg cm^{-2}
13.96	0.07	.....	.....
14	1.4	.....	.....
15	33.2	.....	.....
16	67.3	.....	.....
16.60	.....	0.13	.....
17	103.5	14.2	.....
18	142.3	52.6	.....
18.72	.....	.....	0.17
19	183.6	92.9	13.9
20	227.1	.....	56.0
21	272.3	.....	100.0
22	318.6	.....	.....
23	366.0	.....	.....
24	415.0	.....	.....
25	465.6	.....	.....
26	518	.....	.....
27	572	.....	.....
28	628	.....	.....
29	685	.....	.....
30	744	.....	.....
32	867	.....	.....
34	996	.....	.....
36	1,131	.....	.....
38	1,274	.....	.....
40	1,422	.....	.....
45	1,821	.....	.....
50	2,258	.....	.....
55	2,735	.....	.....
60	3,249	.....	.....
65	3,801	.....	.....
70	4,389	.....	.....
75	5,014	.....	.....
80	5,674	.....	.....

Figure 22 is intended to show the relation between the melting pressures of n-H_2, HD, and n-D_2. The curve for n-H_2 is a graph of table values. The curves through the experimental

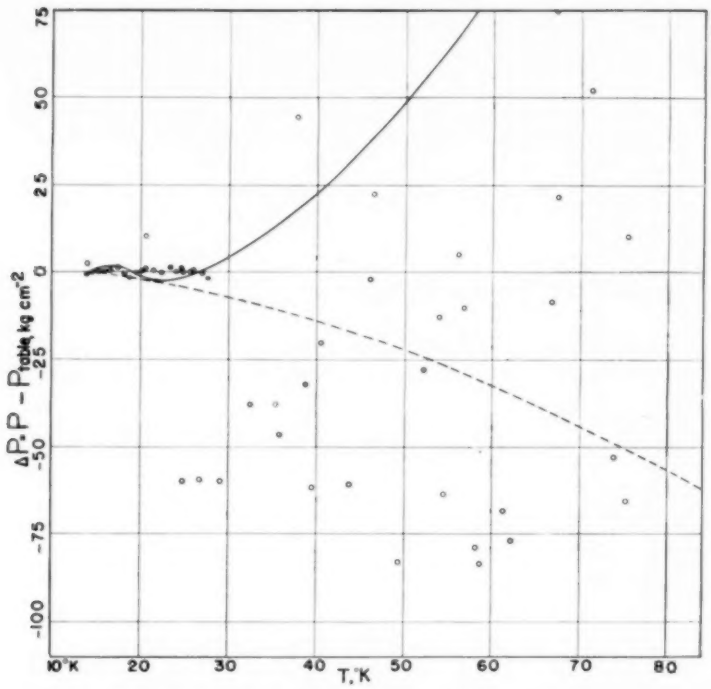

FIGURE 21. *Melting pressure of* n-H_2 *as a function of temperature.*

data for HD and D_2 were obtained by a simple vertical displacement of the H_2 curve and show that the differences in melting pressures of the three isotopic varieties are only slightly dependent upon the temperature. These differences in pressure are 89.6 kg cm^{-2} for H_2 and HD and 170.6 kg cm^{-2} for H_2 and D_2. As the change of melting pressure with temperature, dP/dT, has nearly the same value for H_2, HD, and D_2, if compared at the same temperature, it follows from the Clapeyron equations that $L_f/\delta V$, the ratio of the heat of fusion to the change in volume on melting, also has nearly the same value for the three isotopes when compared at the same value of T. A similar statement can be made for $S_f/\delta V$, the ratio of the entropy of fusion to the change in volume on melting.

The table values of melting pressure for HD and D_2 were obtained from curves drawn through the experimental data and not from the curves of figure 22.

VIII. PVT Data for the Condensed State

The available date of state for the condensed phases of H_2, HD, and D_2 are meager [158 to 16] and in general not accurate enough for the calculation of reliable values of thermodynamical properties. The data on the liquid, however, were used in the construction of the liquid regions of the σ versus ρ diagrams, figure 6, and the T versus diagram, figures 31, 32, and 33.

1. Liquid H_2, HD, and D_2

In table 31 are given the molar volumes of liquid n-H_2, p-H_2, HD, and n-D_2 in equilibrium

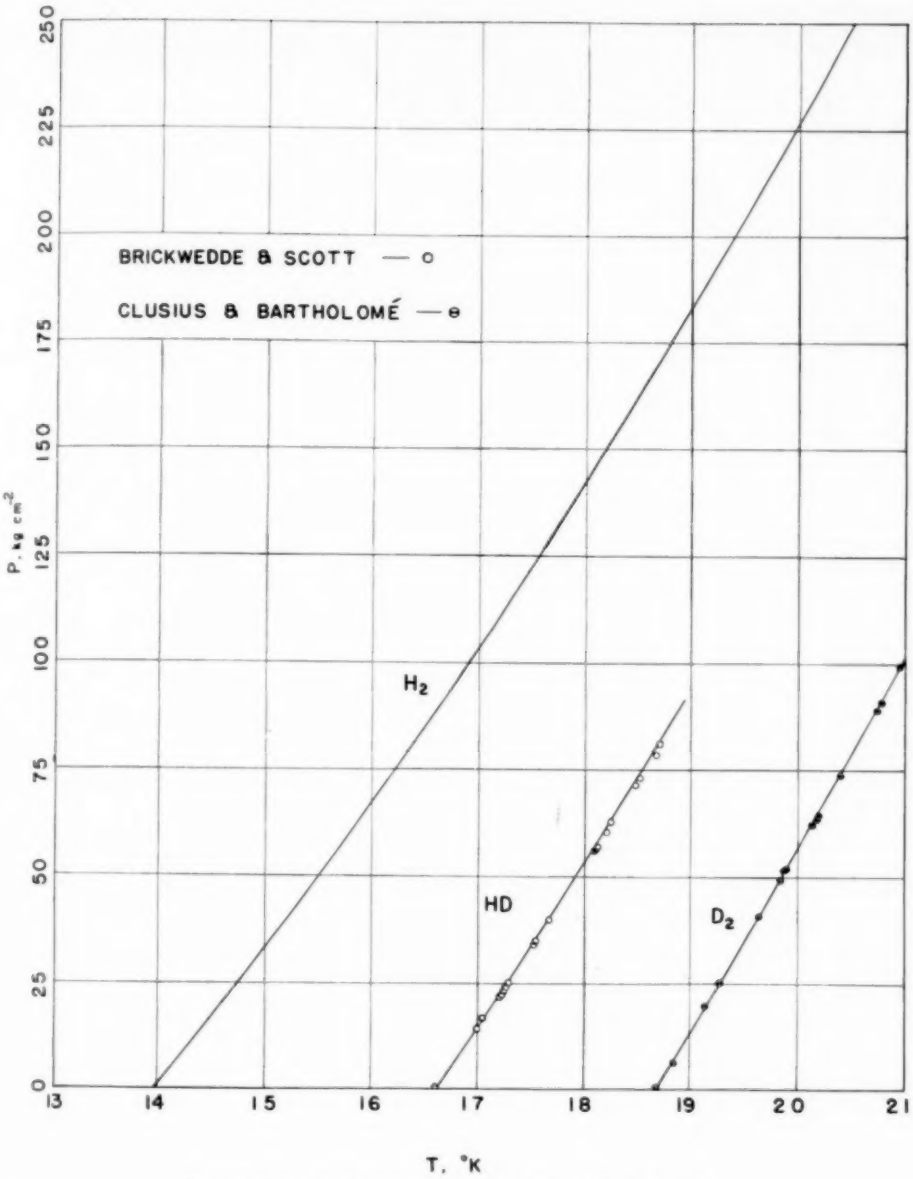

FIGURE 22. *Melting pressures of* n-H_2, HD, *and* n-D_2.

TABLE 31. *Molar volumes of normal hydrogen, parahydrogen, normal deuterium, and hydrogen deuteride, in the liquid state*

T	Volume of liquid at saturation pressure			
	n-H_2	p-H_2	n-D_2	HD
°K	$cm^3\ mole^{-1}$	$cm^3\ mole^{-1}$	$cm^3\ mole^{-1}$	$cm^3\ mole^{-1}$
13.813	.....	26.176	.....	.....
13.96	26.108	.....	.....	.....
14	26.119	26.227	.....	.....
15	26.407	26.518	.....	.....
16	26.721	26.836	.....	.....
16.604	.....	.....	.....	24.487
17	27.061	27.179	.....	24.594
18	27.426	27.549	.....	24.885
18.723	.....	.....	23.162	.....
19	27.816	27.945	23.237	25.211
20	28.232	28.368	23.525	25.572
20.39	28.401	.....	.....	.....
22	29.233	.....	.....	.....
24	30.451	.....	.....	.....
26	31.995	.....	.....	.....
28	34.079	.....	.....	.....
30	37.138	.....	.....	.....
32	43.211	.....	.....	.....
33.19	66.95	.....	.....	.....

with vapor from the triple point to the highest temperature of measurement. From the triple point to 20.4° K, these equilibrium molar volumes have been represented by the following equations, in which temperatures are on the Kelvin scale:

Normal hydrogen [163]:

$$V(\text{cm}^3\ \text{mole}^{-1}) = 24.747 - 0.08005T + 0.012716T^2. \quad (8.1)$$

Parahydrogen [163]:

$$V(\text{cm}^3\ \text{mole}^{-1}) = 24.902 - 0.0888T + 0.013104T^2. \quad (8.2)$$

Hydrogen deuteride [150]:

$$V(\text{cm}^3\ \text{mole}^{-1}) = 24.886 - 0.30911T + 0.01717T^2. \quad (8.3)$$

Normal deuterium [174]:

$$V(\text{cm}^3\ \text{mole}^{-1}) = 22.965 - 0.2460T + 0.0137T^2. \quad (8.4)$$

Table values at 20.39° K and lower were calculated from these equations. Values of the molar volume of liquid normal hydrogen above 20.4° K were obtained from the experimental data of Mathias, Crommelin, and Onnes [161] with the help of a sensitive interpolation method based upon the use of an empirical equation and a deviation graph. A change was made in the experimental data because the value used by Mathias, Crommelin and Onnes for the density of gaseous hydrogen at standard conditions differs from that recommended in this paper on page 396.

Bartholomé [177] measured the molar volumes of liquid n-H_2 and n-D_2 as a function of pressure at three temperatures between 16° and 21° K. The measurements extended from the vapor pressure to nearly the freezing pressure. Smoothed values of molar volumes are given in tables 32 and 33. Bartholomé showed that isothermal changes in volume to about 9 percent of the volume of "saturated" liquid can be represented to within the precision of his measurements, ±0.05 $cm^3\ mole^{-1}$ by Eucken's equation

$$\frac{1}{V^3} = \frac{1}{2}\left[\frac{1}{v_0^3} + \sqrt{\frac{1}{v_0^6} + aP}\right], \quad (8.5)$$

in which V, the molar volume of the liquid, is expressed as a function of the pressure P. v_0 is the molar volume extrapolated to zero pressure and a is an empirical constant dependent upon the temperature. Tables 32 and 33 include values of the molar volumes of liquid n-H_2 and n-D_2 at freezing pressure for the three temperatures of Bartholomé's measurements.

TABLE 32. *Molar volumes of liquid* n-H_2 *for various temperatures and pressures.*

Pressure	T=16.43° K	T=18.24° K	T=20.33° K
$kg\ cm^{-2}$	$cm^3\ mole^{-1}$	$cm^3\ mole^{-1}$	$cm^3\ mole^{-1}$
0[a]	26.87	27.54	28.[illegible]
10	26.59	27.18	27.[illegible]
25	26.20	26.72	27.[illegible]
50	25.66	26.10	26.[illegible]
75	25.20	25.59	25.[illegible]
82.6	25.08	.....	.....
100	.....	25.14	25.[illegible]
125	.....	24.71	24.[illegible]
150	.....	24.30	24.[illegible]
151.98	.....	24.27	.....
175	.....	.....	24.[illegible]
200	.....	.....	23.[illegible]
225	.....	.....	23.[illegible]
241.83	.....	.....	23.[illegible]
	$a=3.80\times10^{-11}\ \frac{\text{mole}^6}{\text{cm}^{18}\text{kg}}$	$a=3.93\times10^{-11}\ \frac{\text{mole}^6}{\text{cm}^{18}\text{kg}}$	$a=4.16\times10^{-11}\ \frac{\text{mole}^6}{\text{cm}^{18}\text{kg}}$

[a] The values at zero pressure were obtained by extrapolation consistent with the molar volumes at saturation vapor pressure given by eq. 8.1.

TABLE 33. *Molar volumes of liquid n-D_2 for various temperatures and pressures*

Pressure	T=19.70° K	T=20.31° K	T=20.97° K
kg cm^{-2}	cm^3 mole^{-1}	cm^3 mole^{-1}	cm^3 mole^{-1}
0[a]	23.44	23.63	23.84
10	23.24	23.37	23.59
20	23.06	23.16	23.35
30	22.89	22.97	23.14
40	22.74	22.79	22.95
43.18	22.70	.....	.....
50	.....	22.63	22.77
60	.....	22.49	22.60
70.46	.....	22.36	.....
70	.....	.....	22.45
80	.....	.....	22.30
90	.....	.....	22.16
96.67	.....	.....	22.05
	a=6.75×10^{-11} mole^4/cm^{16} kg	a=7.20×10^{-11} mole^4/cm^{16} kg	a=7.37×10^{-11} mole^6/cm^{16} kg

[a] The values at zero pressure were obtained by extrapolation consistent with the molar volumes at saturation vapor pressure given by eq 8.4.

2. Solid H_2, HD, and D_2

The crystal structure of solid hydrogen is thought to be hexagonal close-packed, on the basis of an X-ray investigation of solid parahydrogen by the Debye-Scherrer method at the temperature of liquid helium, conducted by Keesom, de Smedt, and Mooy [162].

Tables 34 and 35 contain all the available experimental data of state on solid H_2, HD, and D_2. Molar volumes at 0° K were obtained by calculation.

Molar volumes of the solid at the triple point given in table 34 were obtained by subtracting the volume changes on fusion from the triple point volumes of the liquid calculated from eq 8.1, 8.3, and 8.4. The volume changes on fusion, given in table 34, were calculated using the Clapeyron equation with the calorimetrically measured heats of fusion (section IX, 3), and dP/dT for the solid-liquid equilibrium at the triple point (section VII, 2).

Molar volumes of the solid in table 34 above the triple-point temperature were obtained from Bartholome's measurements of the change in volume on fusion at the temperatures given in table 34, and the volumes of the liquid at melting pressure given in tables 32 and 33.

The molar volumes of solid H_2 and D_2 at 4.2° K in table 34 were measured by Megaw [165] with a picnometer in which the solid H_2 or D_2 was surrounded with liquid helium, the volume of which had previously been measured as a function of pressure at this temperature. The compressibilities of solid H_2 and D_2 at 4.2° K, given in table 35, were calculated by Miss Megaw from the results of these measurements.

TABLE 34. *Molar volumes of solid n-H_2, HD and n-D_2 and volume changes upon fusion*

T	P	n-H_2		HD		n-D_2		Remarks
		Volume of solid	Volume change on fusion	Volume of solid	Volume change on fusion	Volume of solid	Volume change on fusion	
°K	kg/cm^2	cm^3/mole	cm^3/mole	cm^3/mole	cm^3/mole	cm^3/mole	cm^3/mole	
20.97	98.7	.....	.....	.....	.....	20.07	1.98	T and P for solid-liquid equilibrium.
20.31	69.5	.....	.....	.....	.....	20.20	2.16	T and P for solid-liquid equilibrium.
18.72	0.17$_5$	.....	.....	.....	.....	20.48	2.66	n-D_2 triple point.
16.60	.126	.....	.....	21.84	2.65	.....	.....	HD triple point.
18.24	152.0	22.24	2.03	.....	.....	.....	.....	T and P for solid-liquid equilibrium.
20.43	82.6	22.78	2.30	.....	.....	.....	.....	T and P for solid-liquid equilibrium.
12.96	0.07$_2$	23.25	2.85	.....	.....	.....	.....	n-H_2 triple point.
4.2	.....	22.65	.....	.....	.....	19.56	.....	Solid-vapor equilibrium.
4.2	0	22.65	.....	.....	.....	19.56	.....	Smoothed values based on direct experimental determination.
4.2	10	22.49	.....	.....	.....	19.50	.....	
4.2	25	22.30	.....	.....	.....	19.41	.....	
4.2	50	22.03	.....	.....	.....	19.28	.....	
4.2	75	21.80	.....	.....	.....	19.16	.....	
4.2	100	21.60	.....	.....	.....	19.06	.....	
0	0	22.57	.....	.....	.....	19.49	.....	By calculation.

807127—48——8

TABLE 35. *Experimentally determined compressibilities,* $\frac{1}{V}\left(\frac{dV}{dP}\right)_T$, *of solid* H_2 *and* D_2 *at 4.2° K*

Compressibility	H_2 compressibility	D_2 compressibility
	$kg^{-1}\ cm^2$	$kg^{-1}\ cm^2$
At pressure 0 kg cm^{-2}	$(6.8 \pm 1.5)\times10^{-4}$	$(4.5 \pm 2)\times10^{-4}$
At pressure 100 kg cm^{-2}	3.2×10^{-4}	2.1×10^{-4}
Average for range 0 to 100 kg cm^{-2}	$(5.0 \pm 0.5)\times10^{-4}$	$(3.3 \pm 0.7)\times10^{-4}$

Miss Megaw calculated the expansivities of solid H_2 and D_2 at 4.2° and 11° K, given in table 36, using the formula

$$C_p - C_v = TV\left(\frac{dV}{dT}\right)_P^2 \Big/ \left(\frac{dV}{dP}\right)_T, \qquad (8.6)$$

with the calorimetrically determined specific heats at constant pressure and volume, and the compressibility measured at 4.2° K (table 35).

TABLE 36. *Expansivities,* $\frac{1}{V}\left(\frac{dV}{dT}\right)_P$, *of solid* H_2 *and* D_2 *calculated from* $C_p - C_v$

T	H_2	D_2
° K	$°\ K^{-1}$	$°\ K^{-1}$
4.2	0.24×10^{-2}	0.17×10^{-2}
11	$.51\times10^{-2}$	$.37\times10^{-2}$

The compressibilities and expansivities of solid H_2 and D_2 are large when compared with values of these properties for other substances. This is ascribed to the zero-point vibrational energy of the lattice which for hydrogen is an unusually large fraction of the negative potential energy of the lattice. This accounts also for an unusually large variation in the compressibilities of H_2 and D_2 with pressure (see table 35), and for the variation with T and V of $d \ln \theta / d \ln V$, which derivative of the Debye θ is usually regarded as a constant for other solids [165].

IX. The Thermal Properties of the Condensed Phases

In this section are included the calorimetrically measured properties: specific heats and heats of fusion and vaporization.

1. Specific Heats of the Solids and Liquids

(a) Hydrogen

The specific heats at saturation pressure of solid and liquid hydrogen were measured (1923) by Simon and Lange [171] between 10° and 20° K, before the discovery of parahydrogen. Clusius and Hiller [172] measured (1929) the specific heats of solid and liquid parahydrogen over the same range of temperatures and obtained the same values, within experimental error, for the specific heats of parahydrogen as had been obtained by Simon and Lange for supposedly normal hydrogen. Mendelsohn, Ruhemann, and Simon [173] measured (1931) the specific heats of several mixtures of ortho- and parahydrogen between 2.5° and 11.5° K. Their results on pure parahydrogen were in agreement with the earlier measurements of Clusius and Hiller, the data from 2.5° to

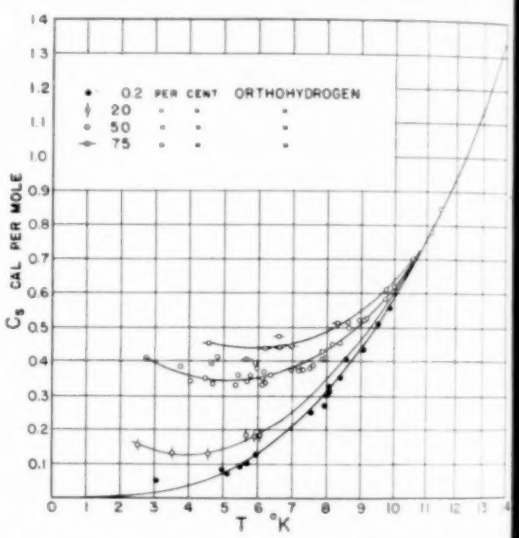

FIGURE 23. *Specific heat,* C_v, *of solid* H_2 *for various ortho-para compositions.*

14° K fitting rather closely a Debye function with $\Theta = 91°$ K.

The data of Mendelsohn, Ruhemann, and Simon are shown in figure 23. It is seen that, at temperatures below 11° K, the specific heats of mixtures containing orthohydrogen are larger than for pure parahydrogen. This difference in specific heats is connected with the multiplicity of states belonging to the lowest o-H_2 rotational level, $J=1$. The different states, three in number, correspond to three different orientations of the angular momentum vector of an o-H_2 molecule relative to the electric field in the hydrogen crystal. At 0° K, all o-H_2 molecules are in the orientation state of lowest energy. At tempera-

tures of the order of $\Delta E/k$, where ΔE is the difference in the energy of the states, the distribution of o-H_2 molecules over the three states changes rapidly with change of temperature. Along with this there is an absorption of energy and an increase in specific heat. As temperatures are approached that are high compared with $\Delta E/k$, the distribution of o-H_2 molecules becomes uniform over the three orientation states, and the specific heat of orientation approaches zero. It may be seen from figure 23 that 12° K is effectively a high temperature for this distribution, and that at temperatures above 12° K the distribution over the three $J=1$ states must be practically uniform.

The specific heats, C_s, of liquid and solid hydrogen along the saturated vapor lines are given in table 37. The C_s curves of figures 24, 25, and 26 for n-H_2 at temperatures above 11° K represent this table.

In figures 25 and 26 the heat capacity, C_v, of

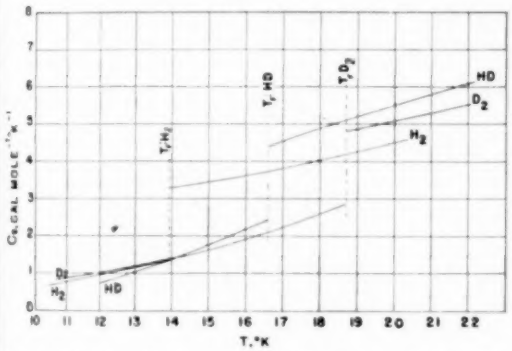

FIGURE 24. *Specific heat, C_s, of solid and liquid* H_2, HD, *and* D_2.

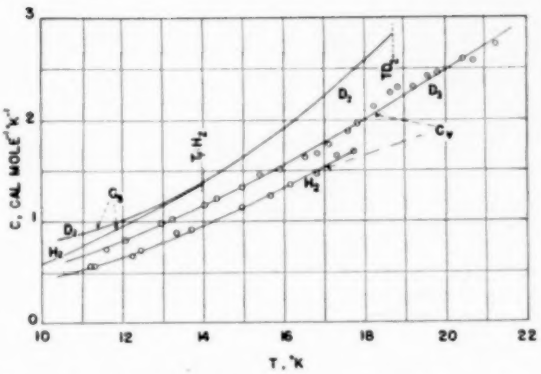

FIGURE 25. *Specific heats, C_s and C_v, of solid* H_2 *and* D_2.

solid and of liquid n-H_2 at constant specified values of the density are compared with the heat capacity, C_s, of solid and liquid n-H_2 in equilibrium with saturated vapor. It is to be noted that the C_v curves of these two figures are not for C_v of solid and liquid H_2 along a line of equilibrium of vapor and condensed phase. The C_v measurements on the solid were made by Bartholomé and Eucken [176] at the density of solid H_2 at a melting temperature of about 19° K. The C_v measurements for the liquid were made by Eucken [169] and by Bartholomé and Eucken at densities ranging from 0.034 to 0.077 g cm^{-3} (380 Amagats to 860 Amagats). The density of liquid n-H_2 at its normal boiling point is 0.07097 g cm^{-3} (789.7 Amagats).

The difference between C_v in figure 25 for the solid at constant density and C_v at densities of the solid along the solid-vapor equilibrium line is small. The corresponding difference for the liquid is larger and, at the critical temperature 33.19° K, is of the order of 1 or 2 cal mole^{-1} °K^{-1}

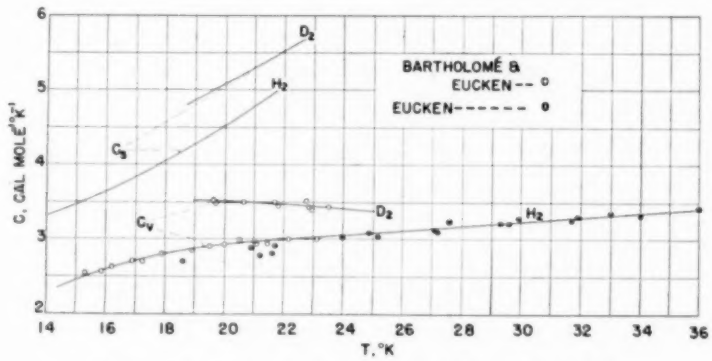

FIGURE 26. *Specific heats, C_s and C_v, of liquid* H_2 *and* D_2.

TABLE 37. *Specific heats at saturation pressure of normal hydrogen, normal deuterium, and hydrogen deuteride in the solid and liquid states*

T	Hydrogen		Deuterium		Hydrogen deuteride	
	C_s	State	C_s	State	C_s	State
° K	cal mole^{-1} deg^{-1}		cal mole^{-1} deg^{-1}		cal mole^{-1} deg^{-1}	
10	0.58	Solid				
11	.76	do	0.88	Solid		
12	.95	do	1.00	do	0.69	Solid
13	1.16	do	1.18	do	1.03	Do.
13.96	1.37	do				
13.96	3.31	Liquid				
14	3.31	do	1.39	do	1.39	Do.
15	3.46	do	1.63	do	1.76	Do.
16	3.63	do	1.90	do	2.17	Do.
16.60					2.42	Do.
16.60					4.40	Liquid
17	3.83	do	2.21	do	4.53	Do.
18	4.04	do	2.56	do	4.88	Do.
18.72			2.84	do		
18.72			4.80	Liquid		
19	4.27	do	4.86	do	5.20	Do.
20	4.50	do	5.08	do	5.49	Do.
21			5.30	do	5.79	Do.
22			5.52	do	6.09	Do.

C_v along the liquid-vapor line being greater [176].

The difference between C_s and C_v for hydrogen is large when compared with the differences for other substances having higher boiling temperatures. In general, $(C_s—C_v)$ is large for low-boiling substances because of their larger expansivities.

The Debye Θ in the Debye specific heat function that fits the C_v data on solid H_2 is 105° K. This may be compared with 91° K for C_v.

The specific heats at constant pressure of compressed liquid hydrogen and gaseous hydrogen were measured by Gutsche [178] for temperatures from 16° K to 38° K and for pressures of about 10, 25, 40, 60, 80, and 100 kg cm^{-2}, using a calorimeter so arranged that approximate constancy of pressure was maintained by manual operation of valves permitting fluid to pass from the calorimeter. As a result of this experimental procedure, the mass of hydrogen in the calorimeter was smaller at the higher temperatures, and consequently the accuracy of measurement is probably lower at the higher temperatures.

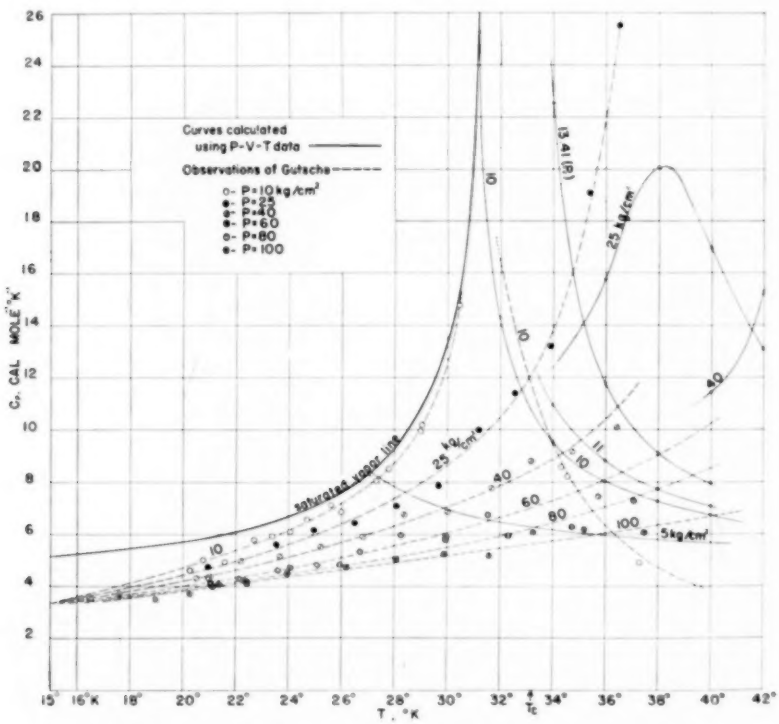

FIGURE 27. *Specific heat, C_v, of compressed liquid and gaseous* H_2.

In figure 27 are plotted Gutsche's experimental data with dotted curves as drawn by Gutsche in his paper to represent the experimental data. The full line curves apply only to the vapor and were obtained by calculation from the PVT correlations of preceding sections of the paper and specific heats in the ideal gas state, table 8. The heavy curve shows C_p for saturated vapor. The full-line curves beginning on this heavy curve, or saturated vapor line, sloping downward toward the right represent the specific heats, C_p, for the vapor at pressures of 5 and 10 kg cm^{-2}. Parts of similar curves also based on the PVT data are shown for 11 and for 13.41 kg cm^{-2}, the critical pressure.

For temperatures above the critical, the dashed curves of Gutsche for 10, 25, and 40 kg cm^{-2} are quite different from the full line curves based on PVT data. The dashed curve for the gas at 10 kg cm^{-2} is certainly incorrect at the highest temperatures, as the actual deviation from the ideal gas law for hydrogen is such as to increase C_p above the approximately 5 cal deg^{-1} mole^{-1} of the ideal gas at these temperatures.

It is seen in figure 27 that Gutsche's experimental values for the liquid scatter considerably. It is believed that Gutsche's recommended values of C_p for liquid hydrogen, represented by the dashed lines in figure 27, are too high. In figure 30 are shown two sets of isobars, E and E', on a temperature-entropy diagram for liquid hydrogen. The full-line curves, E, were calculated from Gutsche's C_p data; the dashed curves, E', are the best fit for all the thermal and state data on liquid hydrogen and are the ones used in the construction of the temperature-entropy diagram. As $(dS/dT)_P=C_p/T$, the two sets of isobars, E and E', imply different C_p's and show that Gutsche's values of C_p are too high to be consistent with the other data on liquid hydrogen. The differences are of the order of 15 percent in the C_p's of liquid hydrogen. The ratio C_p/C_v for liquid hydrogen in equilibrium with vapor was calculated from the velocity of sound in liquid hydrogen, and C_p was obtained by combining this calculated value of the ratio (C_p/C_v), with C_v from figure 26. Pitt and Jackson [175] obtained the value 1,127 m sec^{-1} for the velocity of sound in liquid hydrogen at 20.46° K. Using this with a value of (dV/dP) extrapolated from Bartholomé's data (VIII), one obtains a value of 5.07 cal deg^{-1} mole^{-1} for C_p for liquid hydrogen in equilibrium with vapor (~1 atm) at 20.46° K.

This is slightly lower than would probably be obtained by extrapolating Gutsche's curves to 1 atm.

(b) D_2 and HD

In figure 24 the specific heats C_s at saturation pressure of liquid and solid n-D_2 and HD are compared with C_s for H_2. The D_2 measurements were made by Clusius and Bartholomé [174] and the HD measurements by Brickwedde and Scott [150]. The solid D_2 data are fitted, within experimental accuracy, by a Debye function with $\Theta=89°$. The data on solid HD, however, can not be fitted over the range of measurement with a single value of Θ. Thus Θ for C_s of HD at 16.3° K is 79°, whereas for 12.5° K, Θ is 98°. As the Debye function is intended to represent C_v, this failure to fit the C_s data is not surprising.

In figures 25 and 26 the specific heat C_v at constant volume of solid and liquid D_2 is compared with C_s for D_2 and C_v for H_2. A Debye function with $\Theta=97°$ fits within experimental accuracy the C_v data for solid D_2. This value of Θ for solid D_2 may be compared with 105° for solid H_2. According to the simple theory of lattice vibrations, which assumes simple harmonic restoring forces in the lattice, Θ would be proportional to $1/\sqrt{M}$ and the Θ's for H_2 and D_2 would be in the ratio $\sqrt{4/2}=1.41$. The ratio of the experimental values however, is 1.08. This is evidence that the lattice restoring forces in solid H_2 and D_2 are strongly anharmonic.

2. Latent Heats of Vaporization

(a) Normal Hydrogen

Simon and Lange [171] measured the heat of vaporization of normal hydrogen at several temperatures between the triple point and the boiling point. They found that heat of vaporization, in calories per mole, was given by

$$L_v=219.7-0.27\ (T-16.6)^2, \qquad (9.1)$$

where T is the Kelvin temperature.

(b) Mixtures of o-H_2 and p-H_2

As orthohydrogen and parahydrogen are very closely related, it might be expected that their mixtures would have properties related very simply to those of the pure components. Never-

theless, the H_2 vapor-pressure data of Brickwedde and Scott [146] given by the equations and graphs of Section 7 show that the ortho-para H_2 mixtures do not follow Raoult's law for ideal solutions. A simple application of the Clapeyron equation in the form applying to a pure substance indicates that the latent heat of vaporization and the internal energy of the liquid and solid do not follow a linear, but rather an approximately quadratic dependence upon the composition. This same qualitative result is obtained when account is taken of change of composition by fractionation during vaporization. Functions approximately linear in x, the ortho mole fraction, are obtained when $L_{mix}-L_{eq}$, the difference in latent heats, and $E_{eq}-E_{mix}$, the difference in the internal energy, are divided by $x_{mix}-x_{eq}$, the corresponding difference in the ortho mole fraction. The subscript "eq" indicates the ortho-para mixture that is at equilibrium at 20.4° K, containing 0.21 percent of ortho- and 99.79 percent of parahydrogen. The subscript "mix" refers to any other mixture for which data were obtained. When the line for $\Delta E/\Delta x$ is horizontal, it indicates that ideal solution laws apply. The line has a clear indication of slope, as shown by the continuous lines in figure 28, indicating that ideal solution laws do not apply. In the graph for $\Delta E/\Delta x$, the points for the liquid include a contribution of about 7 percent related to change of composition due to fractionation. The lower dashed line shows the result when this correction is omitted. For the solid it was thought proper to omit the correction for this effect because departure from equilibrium due to slowness of diffusion in the solid would make it too uncertain. The upper dashed line shows the result for the solid when such a correction for fractionation is included.

The use of straight lines for $\Delta E/\Delta x$, the divided difference of the internal energy, has a theoretical justification apart from the fact that the scattering of individual values is so great as to obscure the exact shape of the curve for the liquid. If the internal energy of the liquid is a simple sum of independent energies of different molecular pairs, all of essentially equal probability of formation, then the energy has the form

$$E=x^2E_{oo}+2x(1-x)\ E_{op}+(1-x)^2\ E_{pp}. \quad (9.2)$$

In this case, the differences $E_{eq}-E_{mix}$ divided by the corresponding differences in x for the mixtures of different compositions will be linearly dependent on x. The slope of this line is $2\ E_{op}-E_{oo}-E_{pp}$ and the value of the ordinate at $x=-x_{eq}$ is $2\ (E_{pp}-E_{op})$. From the curves in figure 28, it will thus be found that $E_{pp}-E_{op}$ is 0.7 cal mole^{-1} and $E_{pp}-E_{oo}$ is 4.2 cal mole^{-1} for the liquid. For the solid the corresponding values are 0.6 cal mole^{-1} and 5.4 cal mole^{-1}, respectively. The relative size of $E_{pp}-E_{oo}$ as compared to $E_{pp}-E_{op}$ suggests that most of the deviation from ideal solution laws is due to special effects between o-H_2 molecules.

From the scattering of the points plotted, it appears that ordinates are uncertain to 0.2 or 0.3 cal mole^{-1} for the liquid and possibly to 1 cal mole^{-1} for the solid. The use of the straight line for $\Delta L/\Delta x$ in figure 29 is very nearly consistent with its use for $\Delta E/\Delta x$ and is allowed within the scattering of the data. Combining the results for the dependence upon composition with the results of Simon and Lange for normal hydrogen, the latent heat of vaporization of liquid hydrogen in calories per mole is approximately

$$217.0-0.27\ (T-16.6)^2+1.4x+2.9x^2 \quad (9.3)$$

for any mixture of o-H_2 and p-H_2, where x is the orthohydrogen mole fraction.

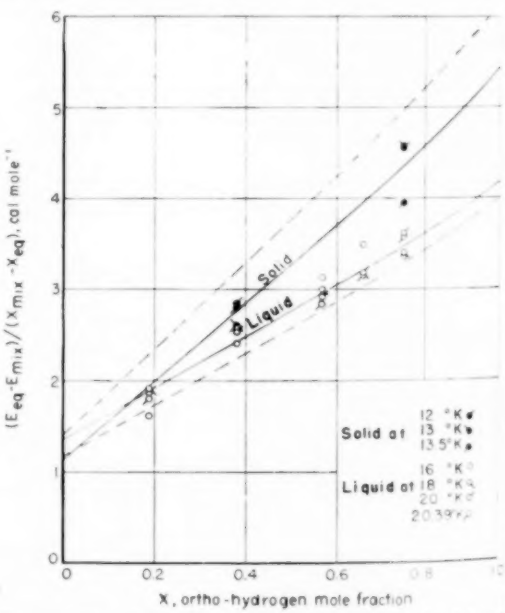

FIGURE 28. *Dependence of internal energy of solid and liquid* H_2 *upon the ortho-para composition.*

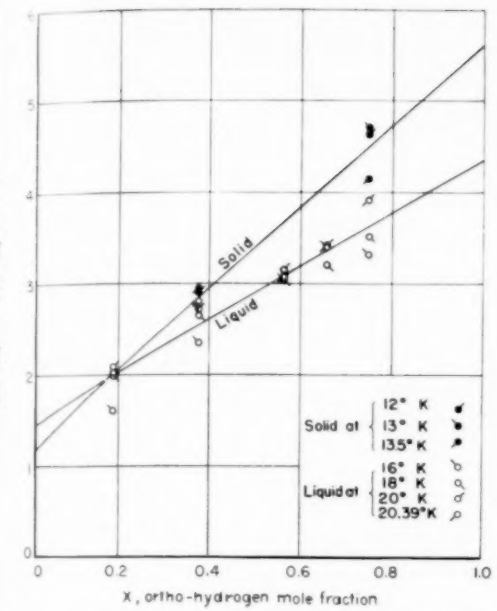

FIGURE 29. *Dependence of latent heats of vaporization and sublimation of hydrogen upon the ortho-para composition.*

The heats of fusion of para- and normal hydrogen are reported in table 38 as being equal within 0.03 cal mole^{-1}. On the basis of the two distinct straight lines for liquid and solid hydrogen in figure 29, it would be expected that the difference would be about 0.7 cal mole^{-1}. The reason for this discrepancy is not known, though it may suggest that the lines for the liquid and solid should be more nearly identical.

TABLE 38. *Latent heats of fusion*

Substance	Heat of fusion	T	P
	cal mole^{-1}	°*K*	*mm* Hg
Normal hydrogen	28.0	13.95[7]	54.0
Parahydrogen	28.0[3]	13.81[2]	52.8
Normal deuterium	47.0	18.72[3]	128.5
Hydrogen deuteride	38.1	16.60[4]	92.8

The manner in which the vapor pressures depend on composition and temperature has formed the basis for the treatment of latent heats of vaporization given in this section. Cohen and Urey [166] and Schäfer [164] have given theoretical discussions of the vapor pressures of ortho and para H_2 and D_2. Cohen and Urey did not expect deviations from the law of perfect solutions. Schäfer suggested that forces connected with rotation within the crystal lattice might account for vapor-pressure differences.

(c) Normal Deuterium

Clusius and Bartholomé [174] measured the heat of vaporization of normal deuterium, obtaining the value 302.3 cal mole^{-1} at 19.70° K.

(d) Mixtures of o-D_2 and p-D_2

The difference in latent heats of vaporization and the approximate difference in internal energies have been calculated from the vapor pressures of the normal and the 20.4° K equilibrium mixtures of ortho- and paradeuterium measured by Brickwedde, Scott, and Taylor [149]. PVT data for deuterium as determined by Schäfer were also used in the calculation. As there are data for only two compositions, giving only one difference of composition, it is not possible either to correct for fractionation or to test for deviation from Raoult's Law. It seems improbable that the law holds for deuterium, as it does not hold for hydrogen. The indicated differences in latent heats of vaporization are smaller than for hydrogen. Thus, $L_{norm}-L_{eq}=0.3$ cal mole^{-1} for the liquid and 1.0 cal mole^{-1} for the solid. The same values are obtained for the differences in internal energies, $E_{eq}-E_{norm}$. Cohen and Urey [166] on the basis of their theoretical calculations, concluded that differences in binding energy between corresponding forms should be half as great for D_2 as for H_2. Considering that the uncertainties in the data for D_2 are comparable with the magnitudes themselves, the data can not be said to conflict with the theoretical prediction.

(e) Hydrogen Deuteride

Brickwedde and Scott [146] measured the heat of vaporization of hydrogen deuteride, obtaining the value 257 cal mole^{-1} at 22.54° K.

3. Latent Heats of Fusion

The latent heats of fusion of hydrogen, parahydrogen, normal deuterium, and hydrogen deuteride were measured by Simon and Lange [171], Clusius and Hiller [172], Clusius and Bartholomé [174], and by Brickwedde and Scott [150], respec-

tively, and are listed in table 38 with corresponding vapor pressures and temperatures.

X. The Temperature-Entropy Diagram

1. Data

Data of several different types were used in determining the temperature-entropy diagram. For the vapor, and for the gas below a density of 500 Amagats, values of the various quantities were obtained by interpolation from tables 14, 22, and 23. The particular difficulties encountered in treating the liquid region will be evident from the

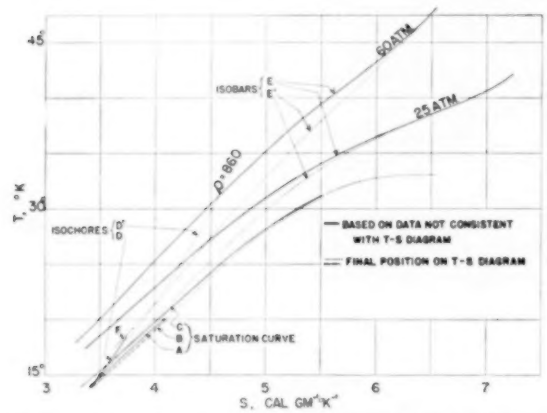

FIGURE 30. *Discrepancies in the thermal data for* H_2 *in the region of the liquid.*

following discussion. Discrepancies between the various data for the liquid are shown in figure 30.

Between the triple point and the boiling point, the entropy of liquid normal hydrogen at saturation pressure was obtained using calorimetric data for the solid and liquid and adding a theoretical value for the entropy of mixing. The result is shown as line B in figure 30. The entropy of the liquid was also calculated using the theoretical entropy of the ideal gas, correcting to the state of saturated vapor and subtracting the latent heat of vaporization. The latent heat of vaporization was determined in two ways—by direct calorimetric measurement and by using vapor pressures and other data with the Clapeyron equation. Line A is based on calorimetric latent heats and line C on latent heats from vapor pressures. At 20° K, line B indicates values 0.03 cal deg^{-1} g^{-1} greater than line A and 0.08 cal deg^{-1} g^{-1} greater than line C.

Lines of constant density could be obtained for the compressed liquid by integrating C_v/T, beginning at line B. Values of C_v from figure 26 were used. The results indicate that these constant density lines are approximately parallel at a given temperature for densities less than 500 Amagats. Data of table 14 indicate that there is a similar parallelism for higher densities near the critical temperature.

Values of entropy of the liquid for various pressures along the 17.34° K and 19.28° K isotherms were obtained by integration of the equation

$$(dS/dP)_T = -(dV/dT)_P. \qquad (10.1)$$

The values used for $(dV/dT)_P$ were based on smoothed values of volume for the liquid as given in table 32 for the temperatures 16.43° K, 18.24° K, and 20.33° K. The constant of integration was chosen to fit line B. From the results, a set of constant pressure lines, of which the segment F is typical, was obtained for various pressures. In addition, a point that should have been on the 860 Amagat density line was obtained by interpolation and a line D was drawn through it and through the 860 Amagat density point on line B as determined by eq 8.1. The line marked D' represents the final correlation.

An unsatisfactory set of values of entropy for the liquid along constant pressure lines was obtained by integrating the C_p data of Gutsche, figure 27. Curves E are the results for 25 and 60 atm, while the final correlation gave curves E'.

2. Final Correlation

In the final correlation, the saturation curve B was accepted and the isochores were considered parallel. The isochores at high density were given by integration of C_v/T, beginning on line B. The isochores at intermediate density were obtained by interpolation between values at high density and values below 500 Amagats. The interpolation was made along the 35° K isotherm from an entropy-density plot extending from $\rho = 860$ Amagats to $\rho = 340$ Amagats.

The extension of curve B to temperatures higher than were given by calorimetric data for the liquid was made from the lower parts of the interpolated isochores and the temperature-density relations for the liquid at saturation pressure given by eq 8.1.

The constant pressure lines were determined mainly from the vapor-pressure equation and the equation

$$(dS/dV)_T = (dP/dT)_V. \qquad (10.2)$$

At lower temperatures the lines were in fair agreement with Bartholome's PVT data, which served to locate them more closely.

The lines of constant enthalpy were determined from integrals of TdS under the constant pressure lines and were checked by integration along the isochores based on the equation

$$(dH/dT)_v = T(dS/dT)_V + V(dS/dV)_T. \quad (10.3)$$

The location of the curves within the dome is quite straightforward, as the fractionation of the ortho-para mixture is too small to affect these curves significantly.

The resulting temperature-entropy diagram for normal hydrogen is presented in composite form in figures 31, 32, and 33. The thermal units used are based on the calorie, the Kelvin degree, and the gram, with pressures in atmospheres and densities in Amagat units.

The diagram shows lines of constant enthalpy, pressure and density and, in the region of coexistance of liquid and vapor, lines of constant "quality." The painstaking construction of the curves pertaining to the liquid region, amounting to a correlation of the data for the liquid, has been made by Robert N. Schwartz, who has also drawn the remainder of the diagram on the basis of the tables of this paper.

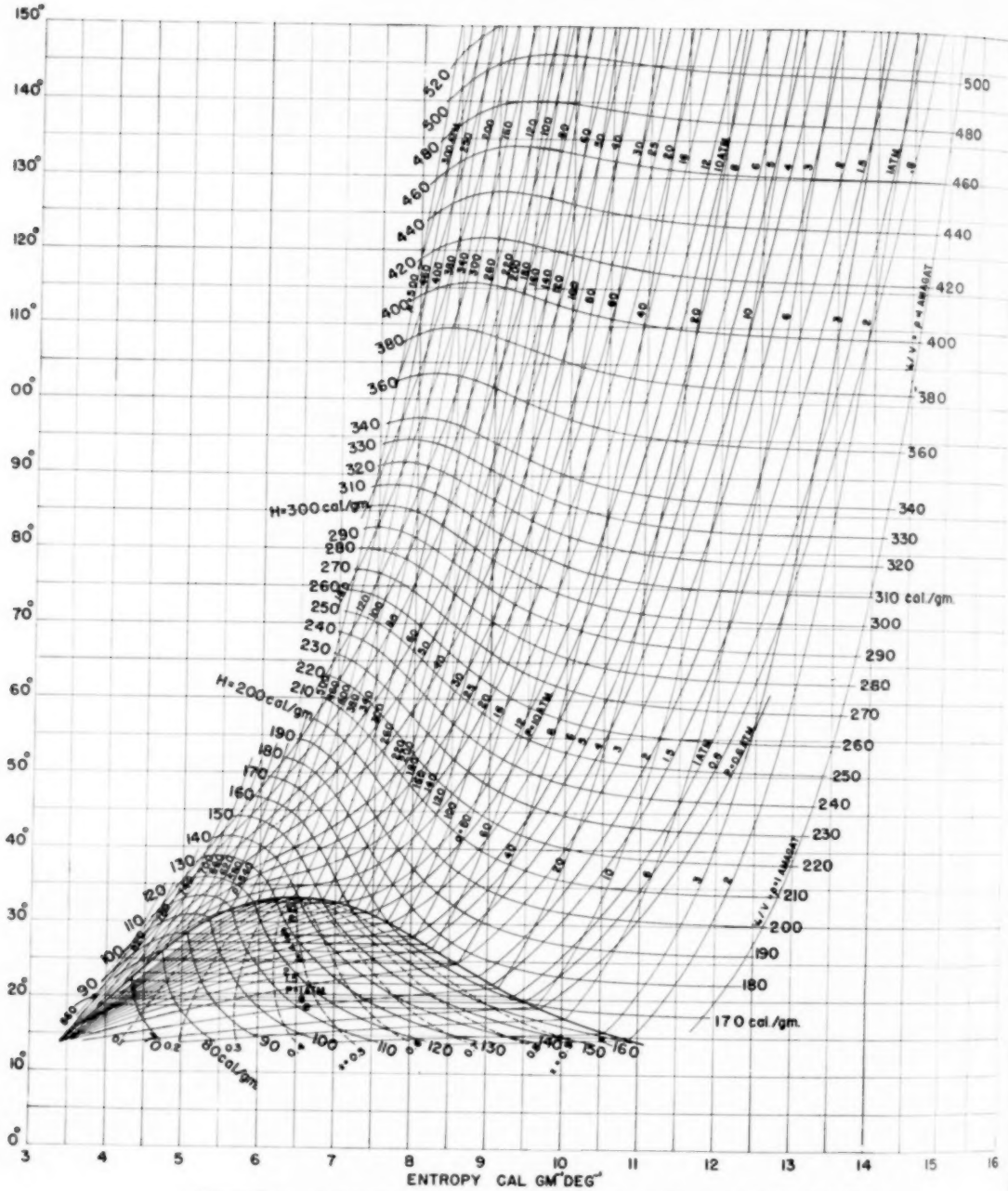

FIGURE 31. *Temperature-entropy diagram for* H_2 *in the region 0° to 150° K.*

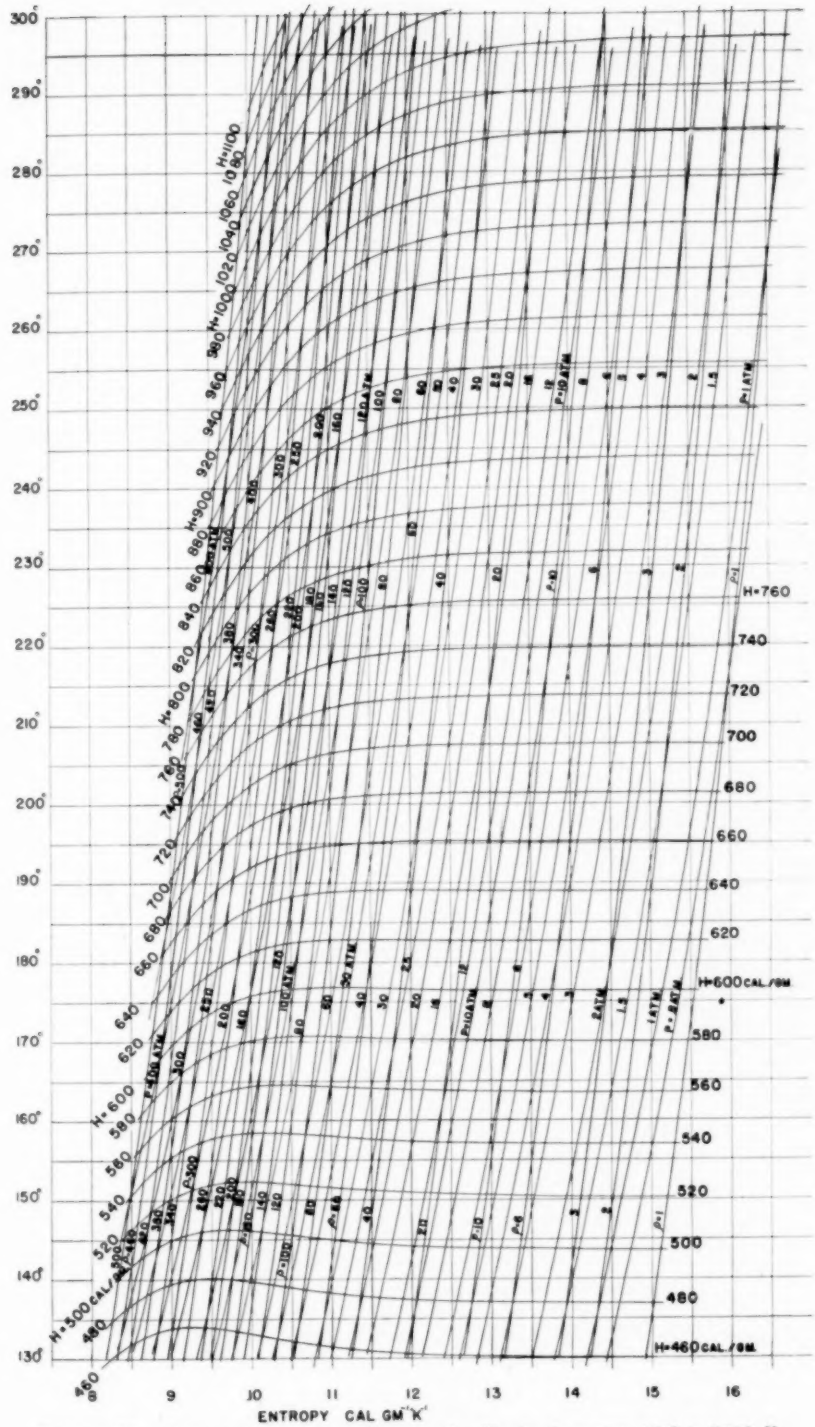

FIGURE 32. *Temperature-entropy diagram for* H_2 *in the region 130° to 300° K.*

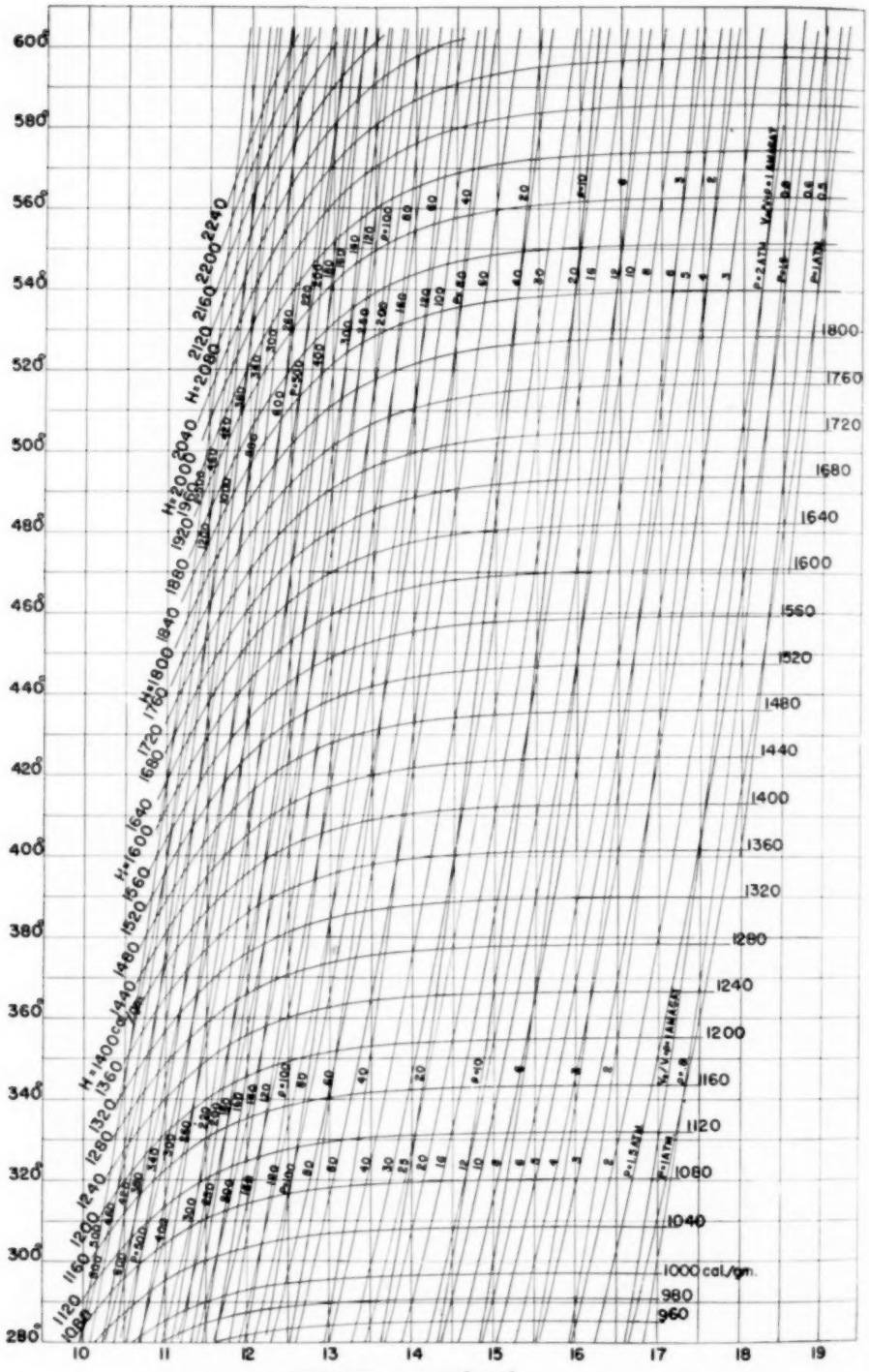

FIGURE 33. *Temperature-entropy diagram for* H_2 *in the region 280° to 600° K.*

XI. References

1. Thermodynamic Properties of the Hydrogens in the Ideal Gas State

[1] D. M. Dennison, Proc. Roy. Soc. (London) **115,** 483 (1927).
[2] F. Rasetti, Phys. Rev. **34,** 367 (1929).
[3] W. F. Giauque, J. Am. Chem. Soc. **52,** 4808 (1930).
[4] W. F. Giauque, J. Am. Chem. Soc. **52,** 4816 (1930).
[5] H. H. Hyman, Phys. Rev. **36,** 187 (1930).
[6] H. H. Hyman and C. R. Jeppesen, Nature **125,** 462 (1930).
[7] R. T. Birge and C. R. Jeppesen, Nature **125,** 463 (1930).
[8] R. Rydberg, Z. Physik **73,** 376 (1931).
[9] O. Klein, Z. Physik **76,** 226 (1932).
[10] J. L. Dunham, Phys. Rev. **41,** 721 (1932).
[11] R. W. Harkness and W. E. Deming, J. Am. Chem. Soc. **54,** 2850 (1932).
[12] C. R. Jeppesen, Phys. Rev. **44,** 165 (1933).
[13] H. C. Urey and D. Rittenberg, J. Chem. Phys. **1,** 137 (1933).
[14] G. N. Lewis and M. F. Ashley, Phys. Rev. **43,** 837 (1933).
[15] C. R. Jeppesen, Phys. Rev. **45,** 480 (1934).
[16] K. Mie, Z. Physik **91,** 475 (1934).
[17] C. O. Davis and H. L. Johnston, J. Am. Chem. Soc. **56,** 1045 (1934).
[18] H. L. Johnston and E. A. Long, J. Chem. Phys. **2,** 389 (1934).
[19] R. Wildt, Z. Astrophysik **9,** 176 (1934).
[20] H. Beutler, Z. physik. Chem. [B] **27,** 287 (1934).
[21] H. Beutler, Z. physik. Chem. [B] **29,** 315 (1935).
[22] G. K. Teal and G. E. MacWood, J. Chem. Phys. **3,** 760 (1935).
[23] Y. Fujioka and T. Wada, Sci. Papers Inst. Phys. Chem. Research (Komagome, Hongo, Tokyo) **27,** 210 (1935).
[24] C. R. Jeppesen, Phys. Rev. **49,** 797 (1936).
[25] I. Sandeman, Proc. Roy. Soc. Edinburgh **59,** 130 (1938–39).
[26] R. T. Birge, Rev. Modern Phys. **13,** 233 (1941).
[27] H. W. Woolley, J. Chem. Phys. **9,** 470 (1941).
[28] D. D. Wagman, J. E. Kilpatrick, W. J. Taylor, K. S. Pitzer, and F. D. Rossini, J. Research NBS **34,** 143 (1945) RP1634.
[29] G. N. Lewis and M. Randall, Thermodynamics and the free energy of chemical substances (McGraw-Hill Book Co., Inc., New York, N. Y., 1923).
[30] P. S. Epstein, Textbook on thermodynamics (John Wiley and Sons, Inc., New York, N. Y., 1937).
[31] F. H. Mac Dougall, Thermodynamics and chemistry (John Wiley and Sons, Inc., New York, N. Y., 1939).
[32] S. Glasstone, Textbook of physical chemistry (D. Van Nostrand Co., Inc., New York, N. Y., 1940).

2. Thermal Measurements on Gaseous Hydrogen

[33] O. Lummer and E. Pringsheim, Wied. Ann. **64,** 555 (1898).
[34] M. Pier, Z. Elektrochem. **16,** 897 (1910).
[35] N. Bjerrum, Z. Elektrochem. **18,** 101 (1912).
[36] A. Eucken, Sitzber. preuss. Akad. Wiss. **1912,** 141 (1912).
[37] K. Scheel and W. Heuse, Ann. Physik **40,** 473 (1913).
[38] I. Langmuir and G. M. J. Mackay, J. Am. Chem. Soc. **36,** 1708 (1914).
[39] I. Langmuir, J. Am. Chem. Soc. **37,** 417 (1915).
[40] J. M. Crofts, J. Chem. Soc. **107,** 290 (1915).
[41] M. C. Shields, Phys. Rev. **10,** 525 (1917).
[42] M. Trautz and K. Hebbel, Ann. Physik **74,** 285 (1924).
[43] J. H. Brinkworth, Proc. Roy. Soc. (London) **107,** 510 (1925).
[44] J. H. Partington and A. B. Howe, Proc. Roy. Soc. (London) **109,** 286 (1925).
[45] F. A. Giacomini, Phil. Mag. **50,** 146 (1925).
[46] R. E. Cornish and E. D. Eastman, J. Am. Chem. Soc. **50,** 627 (1928).
[47] F. R. Bichowsky and L. C. Copeland, J. Am. Chem. Soc. **50,** 1315 (1928).
[48] A. Eucken and K. Hiller, Z. physik. Chem. [B] **4,** 142 (1929).
[49] E. J. Workman, Phys. Rev. **37,** 1345 (1931).
[50] A. Eucken and O. Mücke, Z. physik. Chem. **18,** 167 (1932).
[51] K. Wohl and M. Magat, Z. physik. Chem. **19,** 117 (1932).
[52] A. Farkas, L. Farkas, and P. Harteck, Proc. Roy. Soc. [A] **144,** 481 (1934).
[53] W. T. David and A. S. Leah, Phil. Mag. **18,** 307 (1934).
[54] D. Rittenberg, W. Bleakney, H. C. Urey, J. Chem. Phys. **2,** 48 (1934).
[55] A. J. Gould, W. Bleakney, and H. S. Taylor, J. Chem. Phys. **2,** 362 (1934).
[56] R. W. Fenning and A. C. Whiffen, Phil. Trans. Roy. Soc. (London), **238,** 149 (1939).
[57] H. L. Johnston, I. I. Bezman, and C. B. Hood, J. Am. Chem. Soc. **68,** 2367 (1946).
[58] H. L. Johnston, C. A. Swanson, and H. E. Wirth, J. Am. Chem. Soc. **68,** 2373 (1946).

3. PVT Relations for Gaseous Hydrogens

[59] H. Kamerlingh Onnes and C. Braak, Commun. Phys. Lab. Univ. Leiden 97a (1906), 99a, 100a (1907).
[60] H. Kamerlingh Onnes and W. J. de Haas, Commun. Phys. Lab. Univ. Leiden **127c** (1912).
[61] P. Kohnstamm and K. W. Walstra, Koninkl. Akad. Wetenschappen Amsterdam, Proc. **17,** 203 (1914).
[62] H. Kamerlingh Onnes, C. A. Crommelin, and P. G. Cath, Commun. Phys. Lab. Univ. Leiden **151c** (1917).
[63] L. Holborn, Ann. Physik **63,** 674 (1920).
[64] J. Palacios Martinez and H. Kamerlingh Onnes, Commun. Phys. Lab. Univ. Leiden **164** (1923).
[65] H. Kamerlingh Onnes and F. M. Penning, Commun. Phys. Lab. Univ. Leiden **165b** (1923).
[66] C. A. Crommelin and J. C. Swallow, Commun. Phys. Lab. Univ. Leiden **172a** (1924).
[67] L. Holborn and J. Otto, Z. Physik **23,** 77 (1924).

[68] F. P. G. A. J. van Agt and H. Kamerlingh Onnes Commun. Phys. Lab. Univ. Leiden **176b** (1925).
[69] F. P. G. A. J. van Agt, Commun. Phys. Lab. Univ. Leiden **176c** (1925).
[70] L. Holburn and J. Otto, Z. Physik **33,** 1 (1925).
[71] L. Holburn and J. Otto, Z. Physik **38,** 359 (1926).
[72] G. P. Nijhoff and W. H. Keesom, Commun. Phys. Lab. Univ. Leiden **188d** (1927).
[73] E. P. Bartlett, J. Am. Chem. Soc. **49,** 687 (1927).
[74] E. P. Bartlett, H. L. Cupples, and T. H. Tremearne, J. Am. Chem. Soc. **50,** 1275 (1928).
[75] G. P. Nijhoff and W. H. Keesom, Commun. Phys. Lab. Univ. Leiden **188e** (1928).
[76] E. P. Bartlett, H. C. Hetherington, H. M. Kvalnes, and T. H. Tremearne, J. Am. Chem. Soc. **52,** 1363 (1930).
[77] A. van Itterbeek and W. H. Keesom, Commun. Phys. Lab. Univ. Leiden, **216c** (1931).
[78] A. van Itterbeek, Commun. Phys. Lab. Univ. Leiden, Supp. **70b** (1931).
[79] A. Michels, G. P. Nijhoff, and A. J. J. Gerver, Ann. Physik **12,** 562 (1932).
[80] W. E. Deming and L. E. Shupe, Phys. Rev. **40,** 848 (1932).
[81] A. Michels and A. J. J. Gerver, Ann. Physik **16,** 745 (1933).
[82] W. E. Deming and L. S. Deming, Phys. Rev. **45,** 109 (1934).
[83] J. B. M. Coppock, Trans. Faraday Soc. **31,** 913 (1935).
[84] G. E. Uhlenbeck and E. Beth, Physica **3,** 729 (1936).
[85] K. Schäfer, Z. physik. Chem. [B] **36,** 85 (1937).
[86] K. Schäfer, Z. physik. Chem. [B] **38,** 187 (1937).
[87] J. de Boer and A. Michels, Physica **5,** 945 (1938).
[88] R. Wiebe and V. L. Gaddy, J. Am. Chem. Soc. **60,** 2300 (1938).
[89] F. G. Keyes, Gas thermometer scale corrections based on an objective correlation of available data for hydrogen, helium, and nitrogen; from: Temperature, its measurement and control in science and industry, American Institute of Physics, (Reinhold Publishing Corporation, 1941).
[90] C. S. Cragoe, Slopes of the PV isotherms of some thermodynamic gases at pressures below two atmospheres; from: Temperature, its measurement and control in science and industry, American Institute of Physics (Reinhold Publishing Corporation, 1941); J. Research NBS **26,** 495 (1941) RP1393.
[91] A. Michels and M. Goudeket, Physica **8,** 347 (1941).
[92] A. Michels and M. Goudeket, Physica **8,** 353 (1941).
[93] A. Michels and M. Goudeket, Physica **8,** 387 (1941).

4. Viscosity of Gaseous Hydrogen

[94] M. Trautz and P. B. Baumann, Ann. Physik **2,** 733 (1929).
[95] M. Trautz and F. W. Stauf, Ann. Physik **2,** 737 (1929).
[96] M. Trautz and W. Ludewigs, Ann. Physik **3,** 409 (1929).
[97] M. Trautz and H. E. Binkele, Ann. Physik **5,** 561 (1930).
[98] M. Trautz and A. Melster, Ann. Physik **7,** 409 (1930).
[99] M. Trautz and R. Zink, Ann. Physik **7,** 427 (1930).
[100] M. Trautz and F. Kurz, Ann. Physik **9,** 981 (1931).
[101] M. Trautz and K. G. Sorg, Ann. Physik **10,** 81 (1931).
[102] M. Trautz and R. Heberling, Ann. Physik **20,** 118 (1934).
[103] B. P. Sutherland and O. Maass, Canadian J. Research **6,** 428 (1932).
[104] H. Adzumi, Bul. Chem. Soc. (Japan) **12,** 199 (1937).
[105] A. van Itterbeek and Miss A. Claes, Nature **142,** 793 (1938) and Physica **5,** 938 (1938).
[106] A. van Itterbeek and O. van Paemal, Physica **7,** 265 (1940).
[107] A. van Itterbeek and O. van Paemal, Physica **7,** 273 (1940).
[108] W. H. Keesom and P. H. Keesom, Physica **7,** 29 (1940).
[109] H. L. Johnston and K. E. McCloskey, J. Phys. Chem. **44,** 1038 (1940).
[110] R. Wobser and F. Müller, Kolloid-Beihefte **52,** 165 (1941).

5. Thermal Conductivity of Gaseous Hydrogen

[111] A. Schleiermacher, Wied. Ann. **36,** 346 (1889).
[112] A. Winkelmann, Wied. Ann. **44,** 177 and 429 (1891).
[113] P. A. Eckerlein, Ann. Physik **3,** 120 (1900).
[114] P. Gunther, Dissertation, Halle (1906).
[115] A. Eucken, Physik. Z. **12,** 1101 (1911).
[116] A. Eucken, Physik Z. **14,** 324 (1913).
[117] S. Weber, Ann. Physik **54,** 437 (1917).
[118] E. Schneider, Ann. Physik **79,** 177 (1926).
[119] E. Schneider, Ann. Physik **80,** 215 (1926).
[120] H. Gregory and C. T. Archer, Proc. Roy. Soc. [A] **110,** 91 (1926).
[121] K. F. Bonhoeffer and P. Harteck, Z. physik. Chem. [B] **4,** 113 (1929).
[122] P. Harteck and H. W. Schmidt, Z. physik. Chem. [B] **21,** 447 (1933).
[123] B. G. Dickens, Proc. Roy. Soc. (London) [A] **143,** 517 (1934).
[124] W. G. Kannuluik and L. H. Martin, Proc. Roy. Soc. (London) [A] **144,** 496 (1934).
[125] H. S. Gregory, Proc. Roy. Soc. (London) [A] **149,** 35 (1935).
[126] W. Northdurft, Ann. Physik **28,** 137 (1937).
[127] C. T. Archer, Proc. Roy. Soc. **165,** 474 (1938).
[128] H. Spencer-Gregory and E. H. Dock, Phil. Mag. **25,** 129 (1938).
[129] N. B. Vargaftik and I. D. Parfenov, J. Exptl. Theoret. Phys. (U. S. S. R.) **8,** 189 (1938).
[130] W. G. Kannuluik, Proc. Roy. Soc. (London) [A] **175,** 36 (1940).
[131] H. L. Johnston and E. R. Grilly, J. Chem. Phys. **14,** 233 (1946).

6. Viscosity and Thermal Conductivity of Gaseous Hydrogen at High Pressure

[132] D. Enskog, Kungl. Svenska Vetenskaps Akademiens Handl. **63,** No. 4 (1921).
[133] H. B. Phillips, J. Math. Phys. **1,** 42 (1922).

[134] J. H. Boyd, Jr., Phys. Rev. **35,** 1284 (1930).
[135] R. O. Gibson, Dissertation, Amsterdam (1933).
[136] E. W. Comings and R. S. Egly, Ind. Eng. Chem. **32,** 714 (1940).
[137] S. Chapman and T. G. Cowling, The mathematical theory of nonuniform gases, (Cambridge at the University Press, 1939).

7. Viscosity of Liquid Hydrogen

[138] J. E. Verschaffelt and C. Nicaise, Commun. Phys. Lab. Leiden **151g** (1917).
[139] W. H. Keesom and G. E. MacWood, Physica **5,** 745 (1938).
[140] H. E. Johns, Can. J. Research **17** [A] 221 (1939).

8. Vapor Pressures

[141] H. Kamerlingh Onnes and W. H. Keesom, Commun. Phys. Lab. Univ. Leiden, **137d** (1913).
[142] P. G. Cath and H. Kamerlingh Onnes, Commun. Phys. Lab. Univ. Leiden, **152a** (1917).
[143] J. Palacios Martinez and H. Kamerlingh Onnes, Commun. Phys. Lab. Univ. Leiden, **156b** (1922).
[144] F. Henning, Z. Physik **40,** 775 (1926).
[145] W. H. Keesom, A. Bijl, and Miss H. Van der Horst, Commun. Phys. Lab. Univ. Leiden, **217a** (1931).
[146] F. G. Brickwedde and R. B. Scott, The vapor pressures of mixtures of ortho and para hydrogen (Unpublished).
[147] E. Cremer and M. Polanyi, Z. physik. Chem. [B] **21,** 459 (1933).
[148] R. B. Scott, F. G. Brickwedde, H. C. Urey, and M. H. Wahl, J. Chem. Phys. **2,** 454 (1934).
[149] F. G. Brickwedde, R. B. Scott, and H. S. Taylor, J. Research NBS **15,** 463 (1935) RP841; J. Chem. Phys. **3,** 653 (1935).
[150] F. G. Brickwedde and R. B. Scott, Vapor pressures, specific heats, heats of transition and molecular volumes of liquid and solid hydrogen deuteride (Unpublished).
[151] R. D. O'Neal and M. Goldhaber, Phys. Rev. **58,** 574 (1940).
[152] W. F. Libby and C. A. Barter, J. Chem. Phys. **10,** 184 (1942).

9. Melting Curves

[153] H. Kamerlingh Onnes and W. van Gulik, Commun. Phys. Lab. Univ. Leiden **184a** (1926).
[154] W. van Gulik and W. H. Keesom, Commun. Phys. Lab. Univ. Leiden **192b** (1928).
[155] F. Simon, M. Ruhemann, and W. A. M. Edwards, Z. physik. Chem. [B] **6,** 331 (1929).
[156] W. H. Keesom and J. H. C. Lisman, Commun. Phys. Lab. Univ. Leiden **213e** (1931).
[157] W. H. Keesom and J. H. C. Lisman, Commun. Phys. Lab. Univ. Leiden **221a** (1932).

10. PVT Relations for Condensed Phases

[158] J. Dewar, Proc. Roy. Soc. [A] **73,** 251 (1904).
[159] H. Kamerlingh Onnes and C. A. Crommelin, Commun. Phys. Lab. Univ. Leiden **137a** (1913).
[160] H. Augustin, Ann. Physik **46,** 419 (1915).
[161] E. Mathias, C. A. Crommelin, and H. Kamerlingh Onnes, Commun. Phys. Lab. Univ. Leiden **154b** (1921).
[162] W. H. Keesom, J. de Smedt, and H. H. Mooy, K. Akad. Wetensch. Amsterdam, Proc. **33,** 8, 814 (1930); Commun. Phys. Lab. Univ. Leiden **209d** (1930).
[163] R. B. Scott and F. G. Brickwedde, J. Research NBS **19,** 237 (1937) RP1023.
[164] K. Schäfer, Naturwissenschaften **26,** 563 (1938).
[165] Helen D. Megaw, Phil. Mag. **28,** 129 (1939).
[166] K. Cohen and H. C. Urey, J. Chem. Phys. **7,** 157 (1939).

11. Thermal Properties of Condensed Hydrogen

[167] W. H. Keesom, Commun. Phys. Lab. Univ. Leiden **137***e* (1911).
[168] A. Eucken, Verh. deut. Phys. Ges. **18,** 18 (1916).
[169] A. Eucken, Verh. deut. Phys. Ges. **18,** 4 (1916).
[170] W. H. Keesom and H. Kamerlingh Onnes, Commun. Phys. Lab. Univ. Leiden **153***a* (1917).
[171] F. Simon and F. Lange, Z. Physik **15,** 312 (1923).
[172] K. Clusius and K. Hiller, Z. physik. Chem. [B] **4,** 158 (1929).
[173] K. Mendelssohn, M. Ruhemann, and F. Simon, Z. physik. Chem. [B] **15,** 121 (1931).
[174] K. Clusius and E. Bartholomé, Z. physik. Chem. [B] **30,** 237 (1935).
[175] A. Pitt and W. J. Jackson, Can. J. Research **12,** 686 (1935).
[176] E. Bartholomé and A. Eucken, Z. Elektrochem. **42,** 547 (1936).
[177] E. Bartholomé, Z. physik. Chem. [B] **33,** 387 (1936).
[178] H. Gutsche, Z. physik. Chem. [A] **184,** 45 (1939).

12. Unclassified

[179] G. Rutledge, Phys. Rev. **40,** 262 (1932).
[180] H. J. Hoge and F. G. Brickwedde, J. Research NBS **22,** 351 (1939) RP1188.
[181] Mathematical Tables Project, Tables of Lagrangian Interpolation Coefficients, (Columbia University Press, 1944).

WASHINGTON, August 7, 1947.

U. S. Department of Commerce
National Bureau of Standards

Research Paper RP1933
Volume 41, November 1948

Part of the Journal of Research of the National Bureau of Standards

Chemical Durability, Specular Gloss, and Transmittance of Optical Glasses

By Donald Hubbard and Gerald F. Rynders

The chemical durability of three types of optical glass (BSC 517, BaC 572, and F 620) and chemical Pyrex have been studied over an extended pH range by means of an interferometer procedure. The accompanying effect on the appearance (gloss retained) and on the transmittance of the specimens has also been determined. The results illustrate the confusion that might arise from choosing any of the above three properties as an indicator for the serviceability of optical glasses. Below pH 6, in the range of maximum durability for the optical glasses, differential solution of the alkali and heavy metal oxides brings about the formation of silica-rich, reflection-reducing films, which decrease specular gloss of the surface and improve the transmittance of the specimens.

I. Introduction

As early as 1892 it was observed that old, tarnished photographic lenses sometimes gave more satisfactory performance than new lenses of the same aperture [1].[1] Efforts to determine the reasons, for the purpose of improving the efficiency of optical systems, have resulted in the familiar modern lenses with reflection-reducing surfaces and increased transmittance [1 to 6]. Although the most effective nonreflecting surfaces are obtained by deposition of films of chosen index of refraction [2] and controlled thickness,[3] [5 to 8], less effective but useful films can be produced by leaching the silicate glasses with numerous aqueous solutions [3, 9, 10]. In the latter cases the rate of formation of these reflection-reducing films has been considered to be an indicator of the chemical durability of the glass [10, 11]. As the three properties of glass, durability, nonreflecting films, and increased transmittance, seem to be so intimately associated, they have been compared in the present investigation over an extended pH range for three types of optical glasses and chemical Pyrex.

[1] Figures in brackets indicate the literature references at the end of this paper.

[2] A film whose index of refraction is equal to the square root of the refractive index of the base glass.

[3] A layer whose thickness is approximately one-fourth the wavelength of light.

II. Materials and Procedure

The three optical glasses chosen for comparison with chemical Pyrex were a borosilicate crown (BSC 517), a barium crown (BaC 572), and a flint (F 620).[4] The compositions of these glasses are given in table 1.

TABLE 1. *Composition (weight percent) of the glasses tested*

Oxide	BSC 517 [1]	BaC 572 [1]	F 620 [1]	Chemical Pyrex [2]
SiO_2	66.4	49.7	45.6	81.0
B_2O_3	12.4	3.6		13.0
Na_2O	8.4	0.4	3.6	3.6
K_2O	11.8	7.7	5.2	0.2
BaO		30.8		
PbO			45.1	
ZnO	0.5	7.2		
As_2O_3	.5	0.2	0.5	.002
Sb_2O_3		.4		
R_2O_3				2.2

[1] Calculated from batch composition.
[2] Analysis by Francis W. Glaze.

The attack experiments were made by the interferometer method [12 to 15] because it offered a rapid and convenient means of studying the relative rates of solution of the glasses over a wide

[4] Terminology recommended by the American Ceramic Society committee on glass nomenclature and standard definitions.

pH range. Although the interferometer procedure is not highly accurate or precise, it is perhaps the only available method for measuring chemical durability that is equally fair to all types of glasses, regardless of their composition [16, 17]. Furthermore, as half of each specimen (Pulfrich slab) remains unexposed to the attacking solution, one is able to measure the desired three properties on a single specimen, namely, the chemical durability, the gloss retained, and the change in light transmittance. Of these three properties, the measurement of attack involves the greatest uncertainties; however, for the largest attacks encountered the interferometer procedure is considered to be sensitive to approximately one-quarter of a fringe.

Rectangular specimens (Pulfrich slabs 19 by 30 by 5mm, pitch polished on one face and optically flat to within one-half fringe) were partially immersed in the desired buffer solutions, the surfaces of which were covered with a thin layer of liquid petrolatum to prevent evaporation during the period of the test. Specimens of each glass were exposed for 6 hr at 80° ±0.2°C to Britton-Robinson universal buffer solutions [18] covering a pH range from 1.8 to 11.9. This range was extended to pH 0.65 by means of a sodium acetate-hydrochloric acid buffer. All exposures were made simultaneously.

The extent of the attack was determined by observing the displacement of the interference fringes when the exposed specimens were placed under a fused-silica flat. Observations were made with a Pulfrich viewing apparatus by using unfiltered helium light for illumination.

The change in appearance of the glasses caused by the various treatments was evaluated by observing the percentage of specular gloss retained by the exposed area for 45° incident beam compared with the unexposed portion of the specimen. The measurements were made by means of the Hunter Gloss Meter [19 to 21], by using an adapting shield for supporting the small specimens.

The transmittance of the treated and untreated areas was determined after the specimens had been reground on the unpolished surface with superfine emery to insure that this area was uniform and contributed no uncertainty to the measurements. Thus the change in transmittance resulting from attack is attributable to one surface.[5] To obtain information concerning the effect on appearance of the surface brought about by increased attack in the alkaline range, the three optical glasses were exposed to 5 percent of NaOH solution at 80°C for different periods of time, ranging from 15 min to 4 hr.

III. Data and Discussion

The data plotted in figure 1 from table 2 show the curves for attack, gloss retained, and change in transmittance obtained for a borosilicate optical glass, BSC 517, after 6 hr of exposure at 80°C over the range pH 0.65 to pH 11.9. This glass showed detectable attack in the acid range with an appreciable increase between pH 5 and pH 9, followed by a more pronounced increase in attack for increasing alkalinity beyond pH 9.

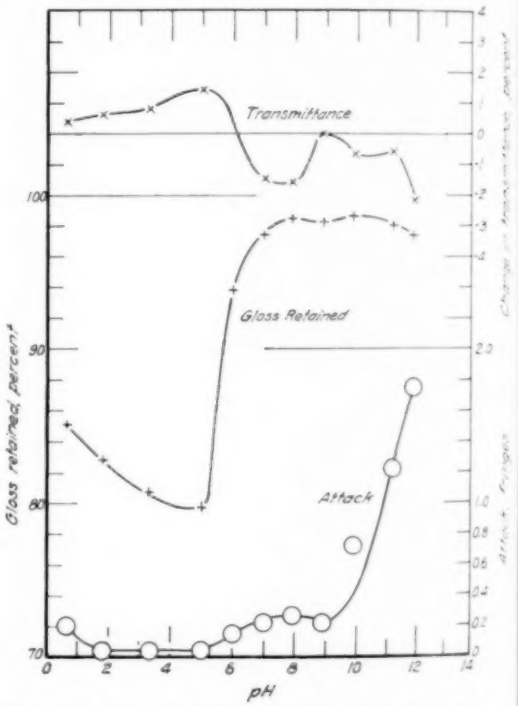

FIGURE 1. *Comparison of the attack-*pH *curve with the accompanying effect on specular gloss of the surface and the change in transmittance for* BSC *517 optical glass after 6-hr exposure at 80° C.*

[5] Transmittance measurements were made by Richard S. Hunter, formerly of the Photometry and Colorimetry Section of the National Bureau of Standards.

At no pH value does the chemical durability of this optical glass compare favorably with that for Pyrex, an acceptable laboratory glassware (fig. 2). It is interesting to note that Pyrex demonstrated little or no change in appearance (gloss retained) or transmittance for the entire pH range except for the high alkalinities above pH 11, where the attack became increasingly vigorous. In contrast to the behavior of Pyrex, optical glass BSC 517 showed a large decrease in gloss in the pH region of optimum durability of the glass, with only a slight change in specular gloss for the region of more pronounced attack. However, the transmittance of the specimens showed an appreciable improvement in the pH range of maximum durability and a decrease in the pH range of increasing attack. Essentially these same features are shown in a somewhat exaggerated and confused fashion by the data obtained on the other optical glasses, BaC 572 and F 620 (figs. 3 and 4).

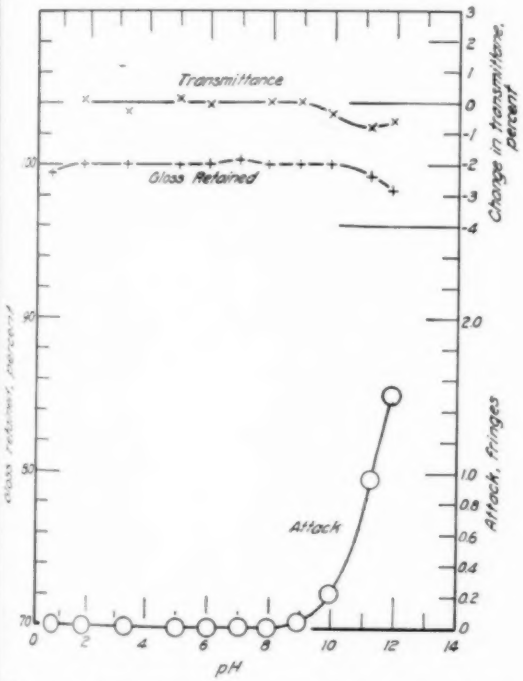

FIGURE 2. *Comparison of the attack-pH curve with the accompanying effect on specular gloss of the surface and the change in transmittance for chemical Pyrex glass after 6-hr exposure at 80° C.*

TABLE 2. *Values for chemical durability, gloss retained, and change in transmittance of three optical glasses and Pyrex after exposure for 6 hr at 80° C to buffers in the range pH 0.65 to pH 11.9*

Glass	pH	Attack	Gloss retained	Change in transmittance	Condition of exposed surfaces
		Fringes	*Percent*	*Percent*	
BSC 517	0.65	2⅛	85.1	+0.4	Good, green to purple.
	1.8	Detectable	82.8	+.6	Good, green.
	3.3	do	80.7	+.8	Good, purple.
	5.0	do	79.7	+1.4	Good, purple, dull.
	6.0	1/16+	93.8		Good, no color.
	7.0	¼−	97.4	−1.5	Do.
	7.9	¼+	98.5	−1.6	Do.
	8.9	¼−	98.2	0.0	Do.
	9.9	¾−	98.6	−.7	Do.
	11.2	1¼−	98.0	−.6	Do.
	11.9	1¾	97.4	−2.2	Do.
BaC 572	0.65	¾	89.2	Pitted	Pitted, dull.
			96.9		
	1.8	1/16	90.4	+1.0	Good, purple.
	3.3	Detectable	92.9	+1.3	Good, greenish purple.
	5.0	¼−	88.2	+1.1	Good, green.
	6.0	¾	86.6	−0.2	Good, purple.
	7.0	2¼+	94.1	−.3	Good, no color, dull.
	7.9	¾+	87.4	−.7	Do.
	8.9	½+	96.5	+0.2	Do.
	9.9	¾−	97.4	.0	Do.
	11.2	¾+	98.1	+.2	Do.
	11.9	1¼−	95.9	−1.0	Do.
MF 620	0.65	Not detectable.	99.3	+1.7	Good, no color.
	1.8	Detectable	88	+1.1	Good, dull.
	3.3	do	88.4	+0.5	Good, slightly dull.
	5.0	do	74.6	+2.2	Good, grey purple.
	6.0	1/16+	83.5	+2.2	Good, dull purple.
	7.0	½+	83.0	−0.5	Good, dull (slight).
	7.9	½+	80.1	−5.8	Good, dull.
	8.9	½−	91.8	−8.8	Good, no color.
	9.9	1/16+	96.7	−2.7	Do.
	11.2	½−, surface cut 1.	98.9		Do.
	11.9	1−	99.8	−4.6	Do.
Pyrex	0.65	Not detectable.	99.4		Good, no color.
	1.8	do	100	+0.1	Do.
	3.3	do	100	−.3	Do.
	5.0	do	100	+.1	Do.
	6.0	do	100	−.1	Do.
	7.0	do	100.3	Broke	Do.
	7.9	do	100	0.0	Do.
	8.9	Detectable	100	.0	Do.
	9.9	¼−	100	−.4	Do.
	11.2	1−	99.2	−.8	Do.
	11.9	1½	98.3	−.6	Do.

The gloss-pH curve for BSC 517 indicates that gloss might well be used under certain conditions as a sensitive indicator of the pH at which chemical changes take place between the glass and the buffer

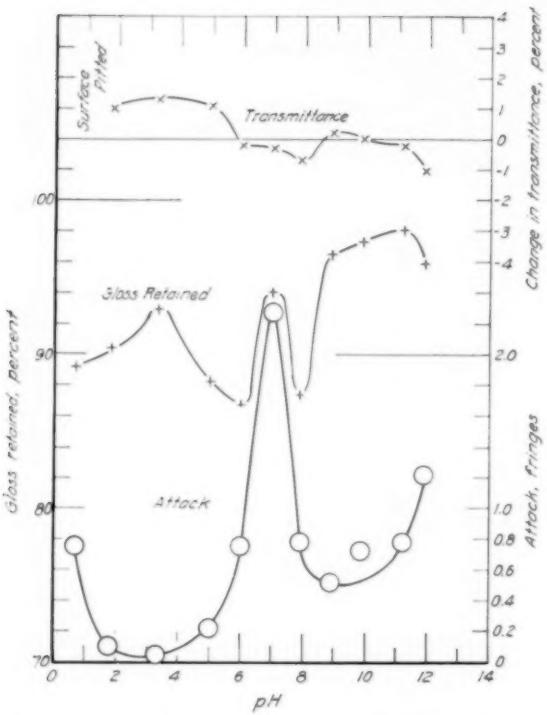

FIGURE 3. *Comparison of the attack-*pH *curve with the accompanying effect on specular gloss of the surface and the change in transmittance for* BaC *572 optical glass after 6-hr exposure at 80° C.*

solutions. For example, in figure 1, gloss is a more sensitive indicator of change in reaction near pH 5 than either the interferometric or transmittance curves. However, in the high-alkaline range beyond pH 9 the gloss gives no indication of the vigorous attack upon the glass that is demonstrated by the interferometer.

This fact is further emphasized by the data for attack and gloss retained for specimens of the three optical glasses after exposure to 5-percent NaOH solution at 80° C for various periods of time (table 3 and fig. 5). The attack, although vigorous, did not seriously affect the appearance of the polished surfaces except in the case of the F 620 after 3- and 4-hr exposures. The attack-time curve for all of the glasses appears to be linear.

All of these results can be partially rationalized. In general, the durability of the three optical glasses is best in the acid range below pH 5. In such solutions there is a preferential dissolving of

TABLE 3. *Values for chemical durability and gloss retained for three typical optical glasses after exposure to 5-percent NaOH at 80° C for various periods of time*

Glass	Time	Attack	Gloss retained	Condition of exposed surfaces
	hr	*Fringes*	*Percent*	
BSC 517	¼	¼	99.6	Good, no color.
	½	½	98.7	Do.
	1	1	98.5	Do.
	2	2	97.7	Do.
	3	3+	97.7	Do.
	4	4+	96.7	Do.
BaC 572	¼	¼+	100	Do.
	½	½+	99.5	Do.
	1	1 +	99.1	Do.
	2	2¼−	98.6	Do.
	3	3¼+	98.6	Do.
	4	4¼	98.6	Do.
F 620	¼	¼−	99.4	Do.
	½	¼+	98.5	Do.
	1	¾+	98.5	Do.
	2	1¾	98.1	Do.
	3	2½+	95.9	Do.
	4	3½	74.0	Fair, frosted.

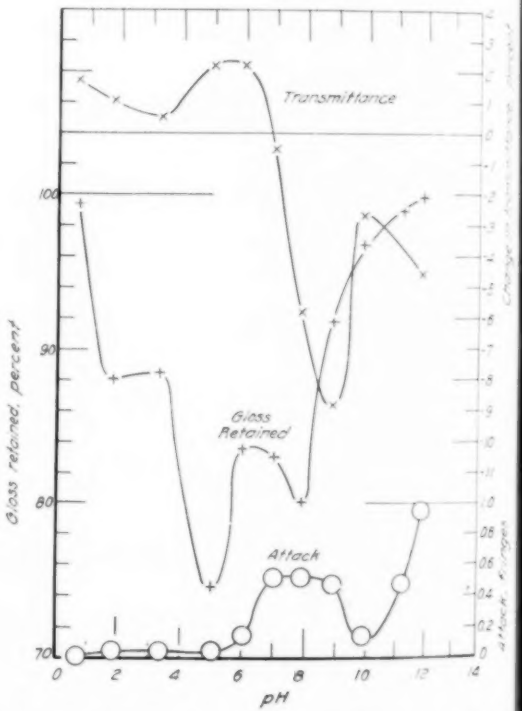

FIGURE 4. *Comparison of the attack-*pH *curve with the accompanying effect on the specular gloss of the surface and the change in transmittance for* F *620 optical glass after 6-hr exposure at 80° C.*

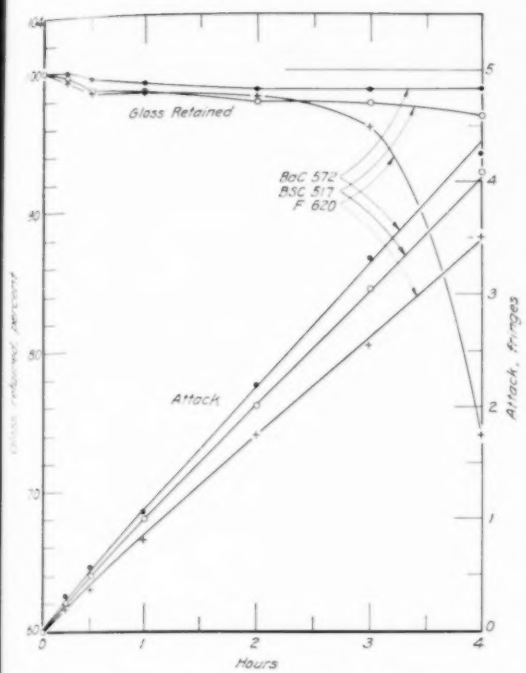

FIGURE 5.—*Comparison of the attack-time curves and the accompanying change in specular gloss of the surfaces for three typical optical glasses exposed to 5 percent of* NaOH *at 80° C.*

alkali and other metal ions, leaving behind a silica-rich surface layer of index of refraction considerably lower than the index of the base glass. These silica-rich layers are of uncontrolled thickness and furnish reflection-reducing films that lower the specular gloss of the surface and improve the transmittance. However, these films are not of the correct index of refraction, $i_{film} = \sqrt{i_{glass}}$, nor are they adjusted to the optimum thickness, $t_{film} = 1/4\ \lambda$, for the maximum improvement of transmittance or reduction of surface reflection [6, 7, 8]. In the alkaline range the silica layer is dissolved, thus preventing the formation of a reflection-reducing film with the attendant improvement in transmittance. Within this range where silica-rich layers are no longer formed, interference colors do not appear (last column of table 2). Obviously, the amount of stain developed by an exposed sample of glass cannot be used as a reliable measure of the amount of attack [22]. However, useful and interesting information can be obtained from these stains if the specimens have been exposed to a solution in which certain constituents of the glass [23 to 26] are preferentially dissolved.

The attack on these optical glasses by the buffer solutions for the range pH 5 to pH 8 is accompanied by a reduction in transmittance. The more pronounced attack in the alkaline solutions above pH 9 does not seriously affect the percentage of transmittance of glasses BSC 517 and BaC 572 until the highest pH is reached.

From this set of comparisons it is easy to understand how so much confusion might arise in choosing an adequate serviceability test for optical glasses. However, the data are interesting in that they show at a glance the best pH region for leaching to produce reflection-reducing surfaces and increased transmittance, with the accompanying improved performance of optical elements. The data on gloss retained and the general tarnished appearance of the surface after exposure in acid solutions could easily be used superficially and wrongly to condemn the optical glasses. It is evident that this test alone does not differentiate a desirable reflection-reducing film from a pitted, etched, or otherwise damaged surface. The transmittance data are necessary to establish this distinction.

IV. Conclusions

The specimens used in the interferometer procedure for determining the chemical durability of glass lend themselves readily to a quantitative evaluation of the change in appearance (gloss retained) and the transmittance of the glass brought about by controlled exposures to solutions. The results obtained present an over-all picture of some desirable as well as undesirable characteristics of the optical glasses studied. The data reemphasized the difficulty of using any one of the three properties, chemical durability, gloss retained, or change in transmittance after exposure, alone as an indicator of serviceability. In fact, in the absence of additional information, such as long-time atmospheric-exposure test or hygroscopicity of the glass, it is doubtful that these three properties either singly or combined are a reliable indicator of the ability of optical glasses to maintain clear polished surfaces in service.

V. References

[1] H. D. Taylor, The adjustment and testing of telescope objectives (T. Cook, York, Eng., 1896).

[2] F. Kollmorgen, Trans. Illum. Eng. Soc. **11,** 220 (1916).

[3] F. E. Wright, The manufacture of optical glass and of optical systems. U. S. Ordnance Dept. Document 2037, (Govt. Printing Office, Washington 25, D. C., 1921).

[4] J. Strong, J. Opt. Soc. Am. **26,** 73 (1936).

[5] C. H. Cartwright and A. F. Turner, Bul. Am. Phys. Soc. **13,** 10 (1938).

[6] K. B. Blodgett, Phys. Rev. **55,** 391 (1939).

[7] C. H. Cartwright, J. Opt. Soc. Am. **30,** 110 (1940).

[8] C. H. Cartwright and A. F. Turner, Decreasing the reflection of light from surfaces such as glass lenses. U. S. Patent 2,207,656.

[9] Frank L. Jones and Howard J. Homer, J. Opt. Soc. Am. **31,** 34 (1941).

[10] Frank L. Jones, J. Soc. Motion Picture Engrs. **37,** 256 (1941).

[11] Donald Hubbard and Edgar H. Hamilton, J. Research NBS **27,** 143 (1941) RP1409.

[12] Relative durability of optical glass, Tech. News Bul. NBS 221, p. 88 (1935).

[13] E. Berger, Glastech. Ber. **14,** 351 (1936).

[14] Donald Hubbard, Edgar H. Hamilton, and Alfred N Finn, J. Research NBS **22,** 339 (1939) RP1187.

[15] Donald Hubbard and Gerald F. Rynders, J. Research NBS **39,** 561 (1947) RP1848.

[16] G. W. Morey, The properties of glass (Reinhold Publishing Corp., New York, N. Y., 1938).

[17] C. J. Phillips, Glass: The miracle maker (Pitman Publishing Corp., New York, N. Y., 1941).

[18] H. T. S. Britton, Hydrogen ions, 2d ed., table 57(c) p. 225 (D. Van Nostrand & Co., Inc., New York, N. Y., 1932).

[19] Richard S. Hunter, Natl. Paint, Varnish Lacquer Assn. Circ. **456,** p. 69 (1934).

[20] Richard S. Hunter, Proc. Am. Soc. Testing Materials **36,** [2] 783 (1936).

[21] Richard S. Hunter, J. Research NBS **18,** 19 (1937) RP958.

[22] M. S. Tarnopol and A. E. Junge, Am. Ceram. Soc. **29,** 36 (1946).

[23] E. Berger, J. Soc. Glass Tech. **20,** 257 (1936).

[24] Frank L. Jones, J. Am. Ceram. Soc. **24,** 119 (1941).

[25] Gordon F. Brewster, Norbert J. Kreidl, and Tayler G. Pott, J. Soc. Glass Tech. **31,** 153 (1947).

[26] Frank L. Jones and T. J. Zak, U. S. Patent 2,369,741 (1945).

WASHINGTON, May 5, 1948.

U. S. Department of Commerce
National Bureau of Standards

Research Paper RP1934
Volume 41, November 1948

Part of the Journal of Research of the National Bureau of Standards

Bending Tests of Large Welded-Steel Box Girders at Different Temperatures

By Ambrose H. Stang and Bernard S. Jaffe

Tests were made to determine the effect of constraint caused by geometrical shape and by differences in temperature on the ductile behavior of welded structures. Four large box girders of identical design were fabricated from fully killed steel from the same heat. The box girders were tested as simply supported beams, one girder being tested at each of the following temperatures: −40°, 0°, 40°, and 80° F. The girders tested at −40° and 0° F broke with a square type of fracture. The other two girders could not be broken with the available equipment, although deflections at midspan of more than 16 inches were induced on a 22-foot span. The results of these tests are discussed and compared.

I. Introduction

The failure of several welded-steel ships during the early part of World War II indicated that problems needed to be solved to place the design of welded structures on a sound basis. One of these problems was the effect of constraint caused by geometrical shape and by differences in temperature on ductile behavior. This constraint is believed to result in multidirectional stresses that are "locked-up" in the structure and not caused directly by applied loads. To study this problem, the Structural Steel Research Committee of the Welding Research Council outlined the tests reported in this paper.

The box-girder type of specimen was chosen, because it simulates to a large extent the geometry or shape that was suspected of having caused trouble in ships and other welded structures. Four box girders of identical design and all from one heat at the steel mill were fabricated by the Ingalls Shipbuilding Corporation, Pascagoula, Miss., and tested as beams, simply supported, in the laboratory of the Engineering Mechanics Section, National Bureau of Standards. The steel was a plain low-carbon open-hearth steel (ASTM A–7) fully killed and had good notch-toughness properties at relatively low temperatures. The same sequence of welding was used on each of the girders. Great care was taken to eliminate defects of workmanship during the welding and any possible incipient cracks prior to testing.

One girder was tested at each of the temperatures −40°, 0°, 40°, and 80° F. The girders tested at −40° F and at 0° F broke with a square type of fracture. It was impossible to break the other two girders with the available equipment, although deflections at midspan of more than 16 in. were induced during the tests on a 22-ft span.

II. Box Girders

1. Design

The details of the box girders are shown in figure 1. Each girder consisted of a bottom plate, A, 1½ in. thick; of two side plates, B1 and B2, each 1½ in. thick; of a top plate, C, 2½ in. thick; and of nine diaphragms, D, 1½ in. thick. The bottom plate, A, was made up of four separate plates—A1, A2, A3, and A4—with three transverse welds. The diaphragms, D, had snipes, 2½ in. on a side, at each of the top corners, and smaller ones at the two bottom corners, as well as a central hole 6 in. in diameter. Backing-up bars, E and F, were used as indicated in figure 1.

The center of gravity of the cross section of the box girder was approximately 10 in. below the top of the girder. The moment of inertia of the section about the neutral surface was about 14,500 in.⁴

2. Fabrication

The sequence of assembling and welding of the parts of the girder was the same for each of the girders and was as follows:

Plates A1, A2, A3, A4, B1, B2, and D were assembled, fitted, and tack-welded securely by welding one pass on the diaphragm plates, D, to the A and B plates. The outside welds of the two longitudinal butt joints joining the A to the B plates were made; the center diaphragm was welded and welding of the other diaphragms progressed to the ends. The back-up bars, E, were installed on top of the A plates for the later transverse welds between the A1 and A2 plates and between the A3 and A4 plates. The inside welds of the two longitudinal butt joints between the A and B plates were completed, and the snipes at the bottom of the diaphragms were welded. The back-up bars, F, were installed for the longitudinal butt joints between the B and C plates, and the strain gages were installed on the inside of the girder. The C plate was fitted to the B plates, and the longitudinal butt joints between them were made. The transverse butt joints between the A1 and A2, the A3 and A4, and the A2 and A3 plates were made, in that order, to complete the fabrication. The tops of the diaphragms, D, were not welded to the bottom of the C plate but formed a smooth bearing surface for plate C.

If cracks in the weld metal were revealed at any time by magnafluxing, the metal around the crack was chipped out and rewelded before the subsequent welding pass was made.

The welding sequence, as described above, was designed to set up large shrinkage stresses and produce high values of locked-up stresses.

III. Coupons

Extra lengths of the steel plates, A, B1, and B2, were furnished with each girder. Chemical analysis of this material showed percentage contents as follows: Carbon, 0.22; manganese, 0.56; phosphorus, 0.015; and sulfur, 0.026.

From each of these lengths two tensile coupons, in the direction of rolling, were machined, six for each girder. The coupons were 12 in. long, 1⅛ in. in diameter in a reduced section 9 in. long, and were threaded at both ends to fit the adaptors of the pulling rods.

The tensile tests were made in a horizontal Amsler testing machine, 100-kip capacity, at the same temperature as that at which the corresponding box girder was tested. For those coupons tested at temperatures below 80° F, the temperature was maintained by carbon dioxide ice in an insulated box surrounding the specimen. For temperatures of −40° F and of 0° F, the temperature was measured by means of two copper-constantan thermocouples attached one to each end of the reduced section of the specimen. A mercury thermometer was used for measuring the temperature for tests at 40° and at 80° F.

The average results of the coupon tests are given in table 1.

TABLE 1. *Average results of tensile tests of coupons*

Coupon length parallel to direction of rolling. Each value is the average for the 6 coupons tested at the same temperature

Temperature	Young's modulus	Poisson's ratio (elastic)	Proportional limit (offset 3×10^{-3})	Yield strength	Tensile strength	Elongation in 4 in.	Reduction of area
°F	*Kips/in.²*		*Kips/in.²*	*Kips/in.²*	*Kips/in.²*	*Percent*	*Percent*
−40	29,390	0.273	28.3	[a] 33.9	68.7	39.9	56.1
0	30,010	.280	25.8	[a] 32.8	70.1	34.9	53.4
+40	30,180	.295	22.4	[b] 31.4	67.7	36.6	55.7
+80	28,580	.270	21.3	[b] 30.2	65.6	37.4	53.2

[a] Yield point by drop-of-beam method.
[b] Yield strength, 0.002-offset method.

The axial strains and the transverse strains were each determined by means of two SR–4 bonded resistance wire strain gages (A5 or A3) attached at midlength of the specimen. Young's modulus of elasticity and Poisson's ratio in the elastic range, and axial strain-stress and axial strain—Poisson's ratio data for plastic strains—were computed from these data. The remainder of the results given in table 1 were computed in the conventional manner.

The values in table 1 show that the proportional limit and yield-strength values decreased as the temperature increased. The other values did not appear to be influenced by the temperature.

Figure 2 shows the average values for the stress-strain and Poisson's ratio–axial-strain relations. The latter values did not appear to vary consistently with temperature. In the stress-strain diagram, the stresses at the knee of the curves decreased as the temperature increased, but on the later ascending portions of the curves, the temperature effects appear to be negligible.

IV. Tests of Box Girders

1. General

Each box girder was tested as a simple beam, supported on cylindrical bearings on a horizontal span of 22 ft, and loaded by two equal loads, 5 ft apart and each 8 ft 6 in. (102 in.) from the nearer support. Figure 3 shows the box girder in the testing machine for the test at 80° F.

For tests at temperatures lower than 80° F, the girder was enclosed in an insulated box and cooled with carbon dioxide ice. To obtain and maintain the low temperature, some of the ice was piled on top of the girder and some placed in the ends of the girder through the holes at the middle of the end diaphragms. Cooling was hastened and regulated by forced circulation through a closed circuit consisting of a blower, pipe to the girder, the girder and a return pipe to the blower as shown in figure 4. The temperatures were measured by means of six copper-constantan thermocouples near midspan. Three thermocouples were on top of plate C and three on the bottom of plate A3.

2. Strain Gages

The strains at various locations between the lines of load application were measured with SR-4 bonded-resistance wire-strain gages. The locations of the strain gages are shown in figure 5. Gages 22, 23, 54, and 55 on the bottom edges of the plates B were single gages, A1 or A3. The gages at other locations were rosette gages, AR–1 or AR–2. The nominal gage length was 13/16 in. for all gages.

For the girder tested at −40° F, the strains were measured with scanning switches and recorders shown in figure 4 to the left of the girder. Portable strain indicators were used during the other tests.

3. Deflections

The deflection of the girder at midspan was measured by the taut-wire mirror-scale method. Deflection readings were generally taken as soon as the load was attained and also at the same load, when the strain readings for that load had been completed.

4. Method of Test

The girders were loaded in a number of steps, gradually increasing the load each time but relaxing the load completely between increments of loading. Strains were measured at the various loads and at the zero loads after the load had been removed. For the girder tested at 40° F the load was held for a period at 1,200 kips, during which several sets of strain readings were taken, the last set of readings being started 2 hr and 40 min after the 1,200-kip load had been reached. A set of readings, when the portable strain indicators were being used, took from 15 to 20 min.

Loading was continued until either the girder was broken or until the middle of the girder was nearly in contact with the supporting girder.

5. Load-Bending Moment Relation

From the condition of the tests, the bending moment between the points of load application where the strain gages were located was equal to 51 P-kip-in. if the total load, P, is in kips.

V. Results and Discussion

1. Average Axial Strains

As was to be expected from the general agreement of the stress-strain curves for the coupons at different temperatures, the load-strain relations for the girders were not much affected by differences in temperature. Consequently, in this report it has seemed adequate to treat mainly the load-strain relations at a single temperature, namely 40° F. The variations for the girder tested at that temperature are similar to those for the other girders tested at other temperatures.

The average strains at a given load for the gages at equal distances from the top of the girder were averaged and have been plotted—for the girder tested at 40° F—in figures 6 to 17. In these figures, the inclined dotted line terminated by a horizontal bar represents the load-strain relation as computed by the ordinary beam theory for the location of the gages under consideration and using the average value for Young's modulus for the coupons, as given in table 1 for this girder. The load at the end of this line corresponds to the average proportional limit stress from table 1.

Tensile strains are plotted to the right. Compressive strains are plotted to the left and indicated as negative. The observed average strains due to the load are shown as open circles. The sets, remaining after the load was removed, are shown as solid circles.

807127—48——9

In general, it may be noted in these figures that the load-axial strain curves practically coincide with the theoretical lines for loads in the lower elastic range. The observed strains at the proportional limit values were generally larger than the computed values. The set values for the greater loads are generally a very large fraction of the corresponding strain-under-load values.

The load-strain curves for gages on the bottom of plate A, figures 12 to 15, are of especial interest. For the gages not on a weld, figures 12 and 13, the strain was much less in the plastic range for the gages that were opposite a diaphragm, figure 12, than for those not opposite a diaphragm, figure 13. These strains in the bottom of plate A not on a weld were, in the plastic range, much larger than for the gages that were on a weld, figures 14 and 15. This same phenomenon may be observed during the tensile test of a steel coupon, which has a transverse weld at midlength. For some grades of steel and of weld metal, the weld metal reduces in section very little, after the yielding of the plates commences, whereas there is a visible reduction in section of the adjacent plate material. The permanent sets for the gages on a weld were negative for loads up to more than 1,200 kips. The difference between the load-strain and the load-set curves, at a given load, is, however, very nearly equal at each of these four locations.

The load-axial strain data, obtained during these tests, throws some light on the question as to whether sections plane before loading remain plane after a load is applied. To answer this query, the average axial strains on plates B and C for all the girders have been plotted in figure 18, against the location of the gages on the girder. The solid line is for the 600-kip load (average for four girders). This line cuts the zero-strain line at the computed location of the neutral surface, and all the values are close to this one line. The dash lines have been drawn through the average values for the 1,200-kip load (average for three girders, since the girder tested at −40° F did not attain this load), and certainly no one line can be drawn through these values so that the strain values at different distances from the top of the girder are close to it. It seems that for these box girders, with diaphragms at various locations along their length, plane sections did not remain plane under loads in the plastic range.

It was suggested that this apparent warping of an initially vertical plane section was due to the timing under which the gage readings were taken and that if the load—while in the plastic range—were applied for some time before the reading of the gages was started, the sections would be found still plane. The procedure had been to start taking the strain readings about as soon as the load was reached. To study this effect during the testing of the girder at 40° F, several sets of readings at a load of 1,200 kips were taken, as has been stated. The average strain values from the readings, started as soon as the load was reached, are plotted in figure 19 against the location on the girder as open circles. As for figure 18, no one line would represent the data well. The strain values from the readings, started 2 hr and 40 min after the 1,200-kip load had been reached, are plotted as solid circles in figure 19. They show the commonly observed phenomenon of continued yielding in both tension and compression with a consequent still greater warping. It may be noted that the gages under consideration were not located in the plane of a diaphragm (see fig. 5).

2. Deflections at Midspan

The load-deflection curves for the girders are shown in figure 20. The temperature apparently had no significant influence on the deflection. The arrow heads indicate the load and deflection at the failure of the girders, which were tested at −40° and at 0° F. These failures were on the rising portion of the curve. The results indicate that the restraints induced by the welding of the ductile plates were of such magnitude as to result in rather brittle failure for temperatures as high as 0° F. The temperature of 40° F was evidently not low enough to induce failure.

The break in the load-deflection curve, figure 20, for the girder tested at 80° F, at a deflection of 11.56 in. and a load of 1,530 kips was due to the fact that during the test of this girder, the test was stopped at this deflection when the middle of the girder nearly came in contact with the supporting girder. During this first portion of the test, the supports for the girder were as shown in figure 3. Since fracture had not occurred, the box girder was taken out of the machine, the cylindrical supports were raised about 6 in. by the blocks shown in figure 21, and the

girder was again placed in the testing machine. The second portion of the test was made 7 days after the first portion of the test. On reloading, the load-deflection curve between loads of 1,530 and 1,650 kips was not a smooth continuation of the load-deflection curve obtained during the first portion of the test but was much steeper. After the load of 1,650 kips had been attained, the deflection increased with little increase in load until the curve became practically a continuation of that obtained during the first portion of the test. The moving of the girder and the time between the two portions of the test evidently contributed to bringing about some change in the load-deflection relation for this girder, which had already been subjected to plastic yielding.

3. Maximum Loads

Table 2 gives a summary of the maximum values obtained at the failure of the girders that broke during the tests at −40° and at 0°F, as well as the maximum values reached during the other two tests when failure did not occur.

The fractured surface of the girder tested at −40° F is shown in figure 22. The fracture was partly in the weld between the plates A1 and A2 and partly in plate A2. The fracture at midspan of the girder tested at 0° F is shown in figure 23. This fracture took place in plate A2 and not in any portion of a transverse weld.

Figure 21 shows the girder tested at 80° F with a deflection of more than 18 in.

TABLE 2. *Summary of flexural tests of box girders*

Temperature	Maximum load	Maximum moment [a]	Modulus of rupture [a]	Maximum deflection
°F	*Kips*	*Kip-in.*	*Kips/in.²*	*in.*
−40	[b] 1,165	59,400	63.1	2.45
0	[b] 1,476	75,300	79.9	8.83
+40	[c] 1,670	85,200	90.4	16.16
+80	[c] 1,685	85,900	91.2	18.06

[a] As computed from the load at failure or from the maximum load that was reached.
[b] Load at failure.
[c] Maximum load that was reached. No failure.

VI. Summary

Bending tests were made on large welded-steel box girders at temperatures of −40°, 0°, 40°, and 80° F. Tensile tests of the material at these temperatures showed that the steel was as ductile at the lowest as at the highest temperature. Due to the constraint induced in the girders by the welding, square types of fracture occurred in the girders tested at −40° and at 0° F but did not occur in the girders tested at 40° and at 80° F.

VII. Appendix

A fifth box girder, the material of which was a semikilled steel instead of the fully killed steel used in the other four girders, was also tested at room temperature, about 80° F. This box girder was the same size as the others and differed from the design shown in figure 1 only as follows:

The two diaphragms D were omitted; the bottom A plate was made of three plates with two transverse welds. Figure 24 shows the details of the bottom view of this girder of semikilled steel. It failed with a square type of fracture after being tested in a manner similar to that for the other four girders.

The load-deflection curve for the girder of semikilled steel is shown in figure 25 by open circles and solid line. The load-deflection curve for the girder of fully killed steel, which was tested at 0° F, is also shown in this figure, by solid circles and dash line. The results of the tests of these two girders are compared in table 3.

TABLE 3. *Results of flexural tests of two box girders*

Girder steel	Semikilled	Fully killed
Temperature of test, °F	80	0
Maximum load, kips	1,397	1,476
Maximum moment, in.-kips	71,200	75,300
Modulus of rupture, kips/in.²	75.6	79.9
Maximum deflection, in.	8.00	8.83
Energy to failure, kip-in.	8,350	10,060

These results show that the girder of fully killed steel tested at 0° F was superior in the load properties, as given in table 3, to the girder of semikilled steel, which was tested at 80° F.

WASHINGTON, April 9, 1948.

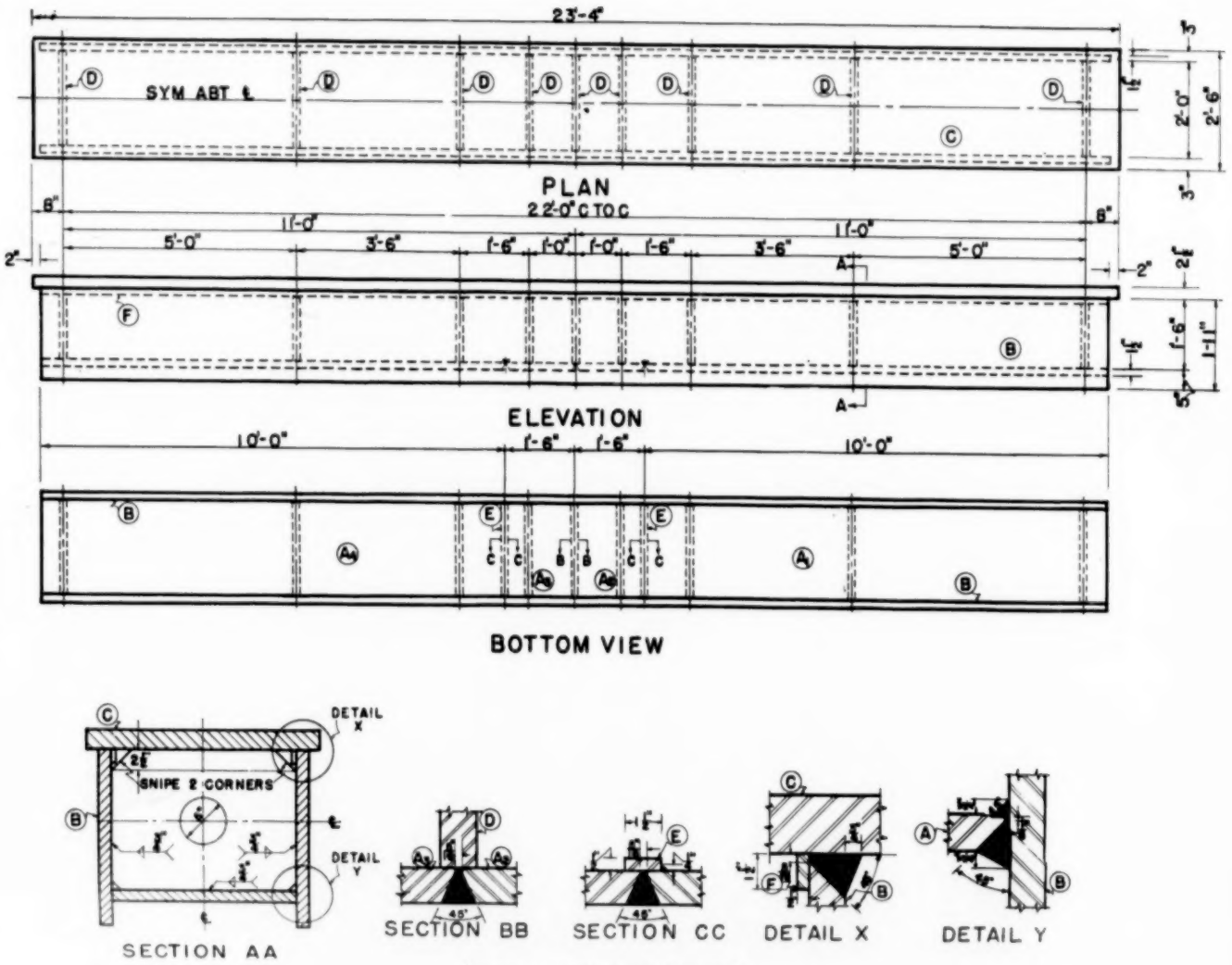

FIGURE 1. *Details of the box girders.*

SECTION AA SECTION BB SECTION CC DETAIL X DETAIL Y

FIGURE 1. *Details of the box girders.*

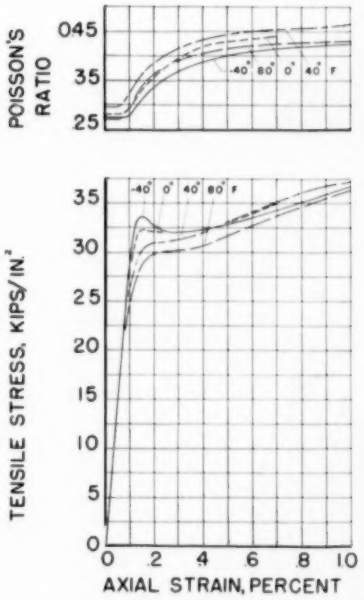

FIGURE 2. *Average results of tensile tests of coupons.*

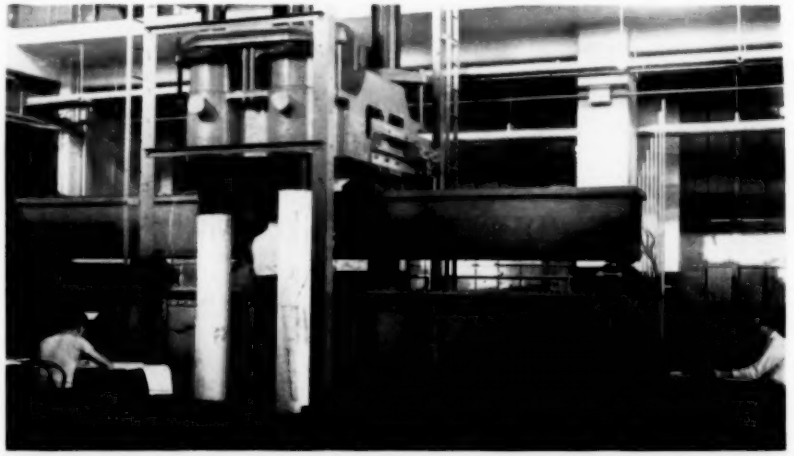

FIGURE 3. *Box girder in the testing machine, at 80° F, before test.*

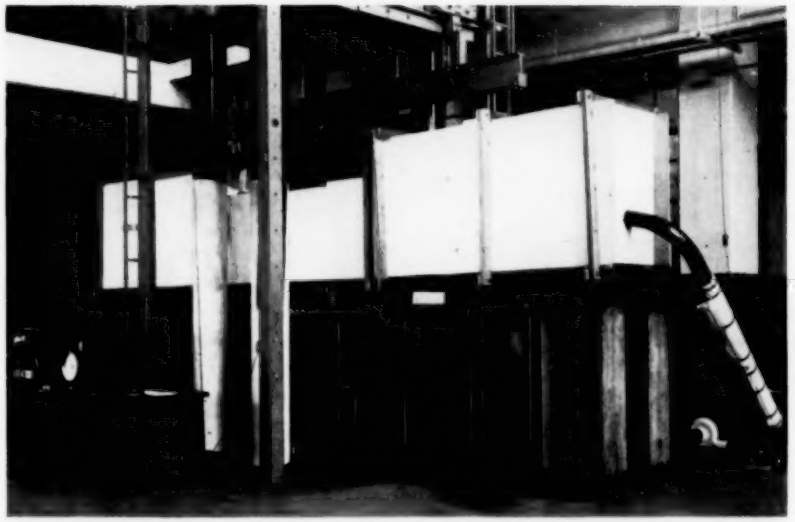

FIGURE 4. *Enclosure of the box girder for tests at temperatures below 80° F.*

Note the frost covered blower and pipes of the forced-circulation system.

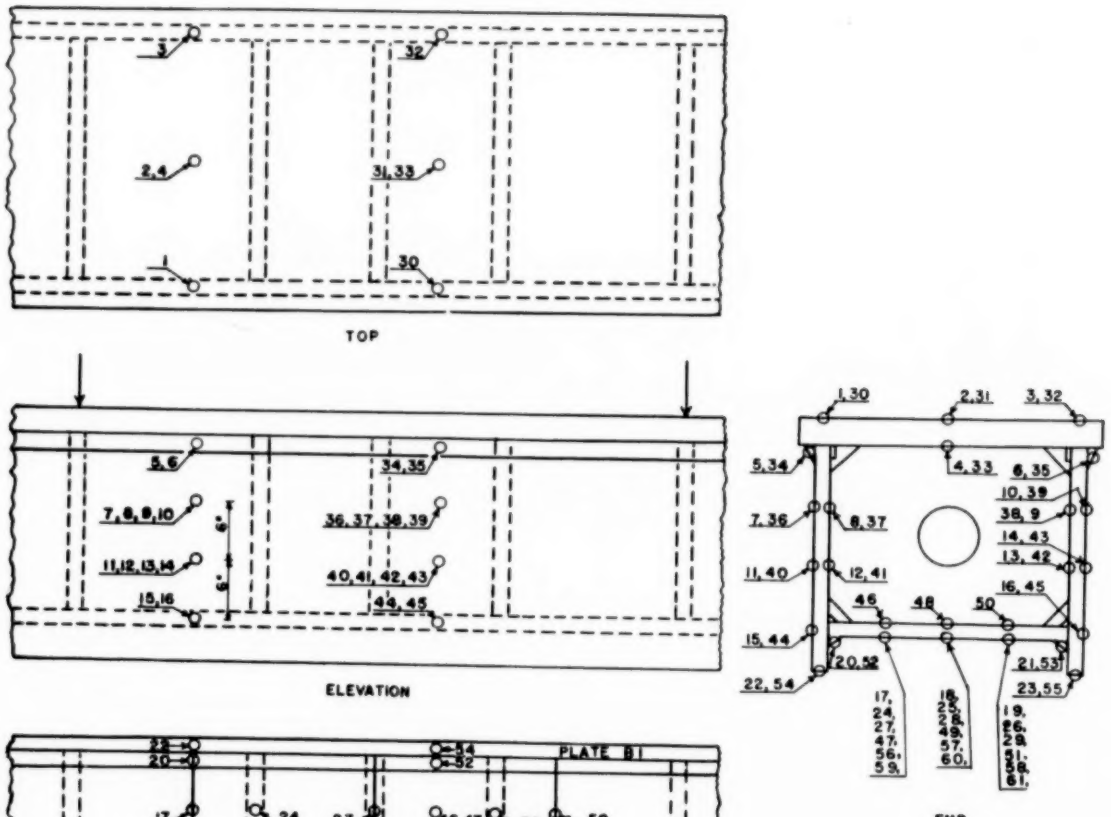

FIGURE 5. *Location of wire-strain gages.*

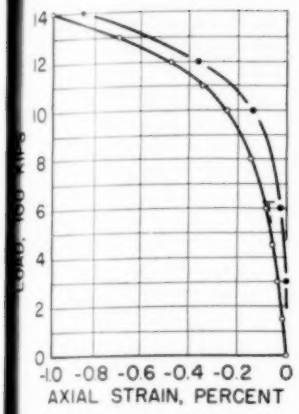

FIGURE 6. *Average axial strains in the top of plate C of the girder tested at 40° F (6 gages).*

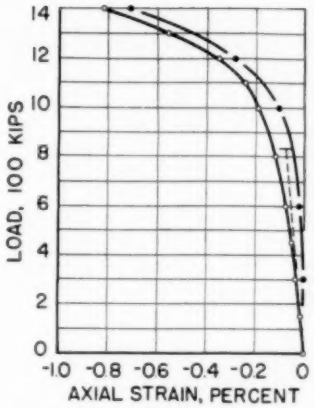

FIGURE 7. *Average axial strains in the bottom of plate C of the girder tested at 40° F (2 gages).*

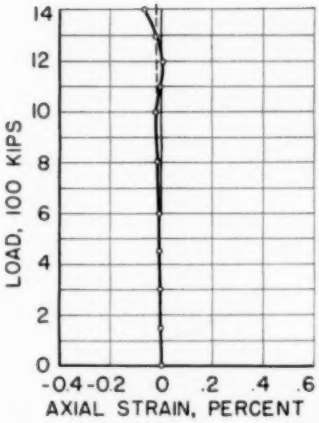

FIGURE 8. *Average axial strains in plates B at 9.25 in. from the top of the girder tested at 40° F (8 gages).*

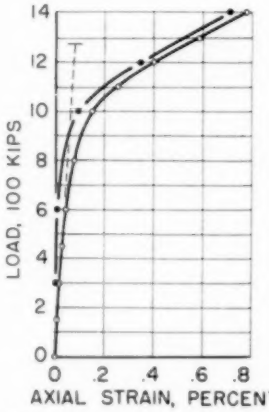

FIGURE 9. *Average axial strains in plates B at 15.25 in. from the top of the girder tested at 40° F (8 gages).*

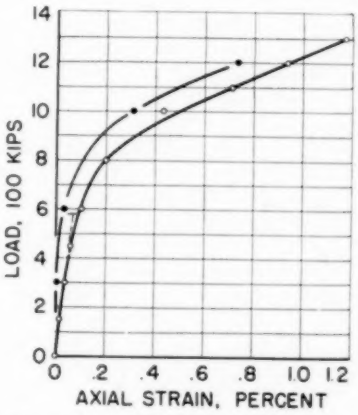

FIGURE 10. *Average axial strains in the top of plate A of the girder tested at 40° F (3 gages).*

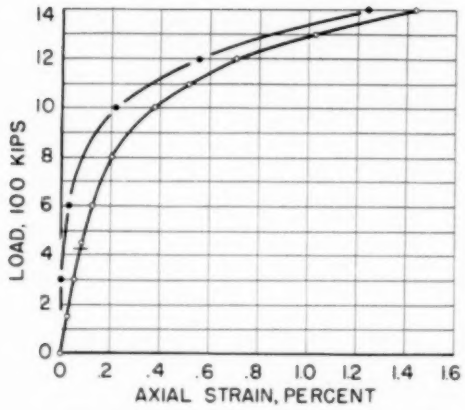

FIGURE 11. *Average axial strains in plates B opposite the midheight of plate A of the girder tested at 40° F (4 gages).*

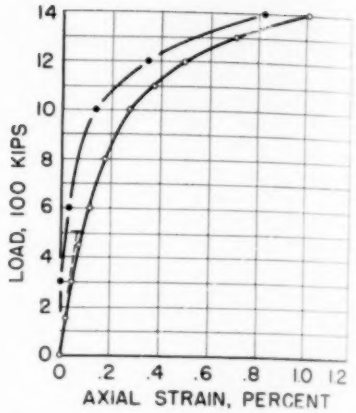

FIGURE 12. *Average axial strains in the bottom of plate A,—not on a weld, opposite a diaphragm—of the girder tested at 40° F (6 gages).*

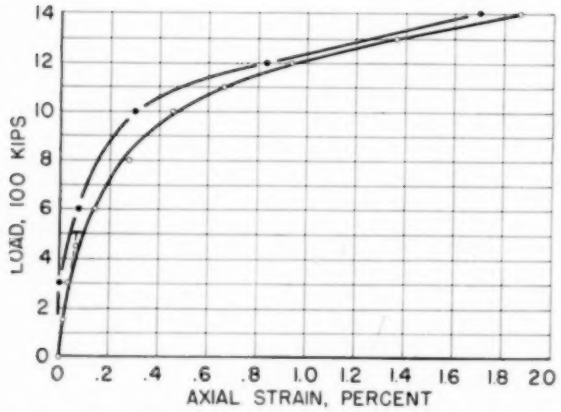

FIGURE 13. *Average axial strains in the bottom of plate A,—not on a weld, not opposite a diaphragm—of the girder tested at 40° F (3 gages).*

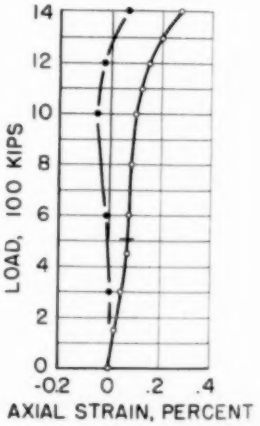

FIGURE 14. *Average axial strains in the bottom of plate A,—on a weld, opposite a diaphragm—of the girder tested at 40° F (3 gages).*

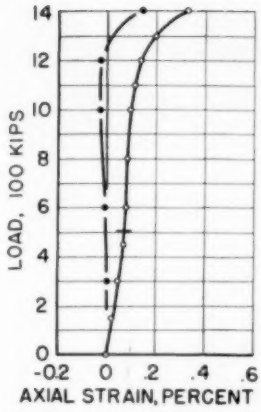

FIGURE 15. *Average axial strains in the bottom of plate A,—on a weld, not opposite a diaphragm—of the girder tested at 40° F (6 gages).*

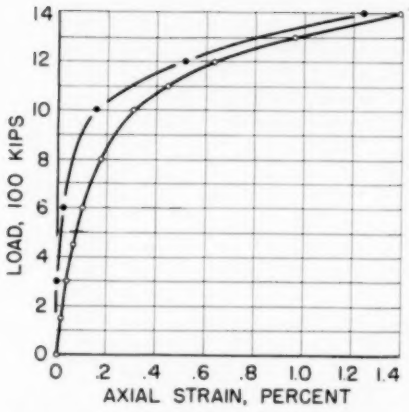

FIGURE 16. *Average axial strains in the welds between plates A and B of the girder tested at 40° F (4 gages).*

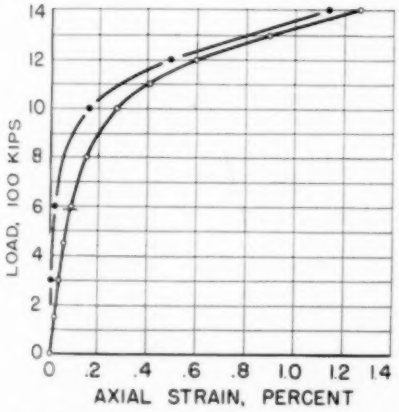

FIGURE 17. *Average axial strains in the bottom edge of the plates B of the girder tested at 40° F (4 gages).*

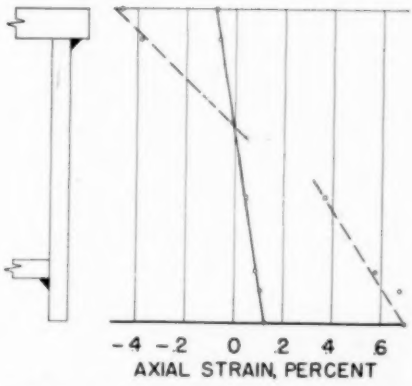

FIGURE 18. *Average axial strains versus gage location, on plates B and C for loads of 600 kips (solid line) and of 1,200 kips (dash line).*

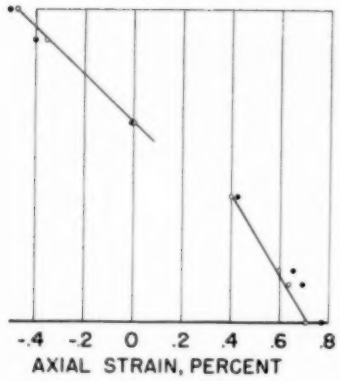

FIGURE 19. *Average axial strains versus gage location for a load of 1,200 kips on the girder tested at 40° F.*

Open circles are for readings started as soon as the load was reached; solid circles for readings started 2 hr 40 min after the load was reached.

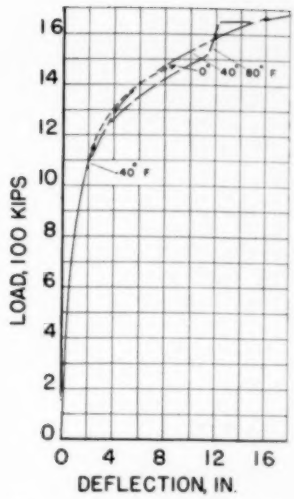

FIGURE 20. *Deflection at midspan for the girders.*

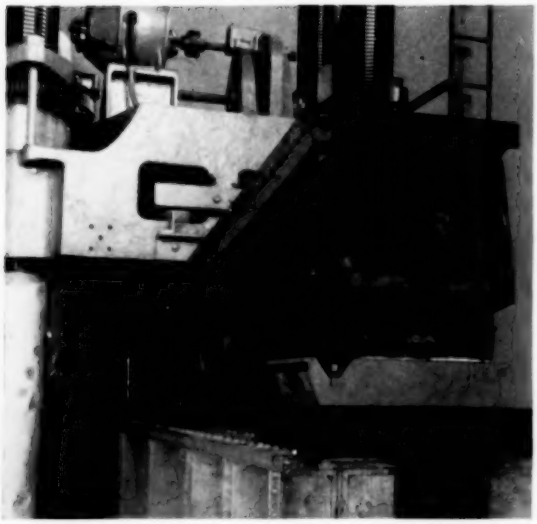

FIGURE 21. *Girder tested at 80° F when the deflection was 18.06 in.*

FIGURE 22. *Fractured surface of the girder tested at —40° F.*

FIGURE 23. *Fracture at midspan of the girder tested at 0° F.*

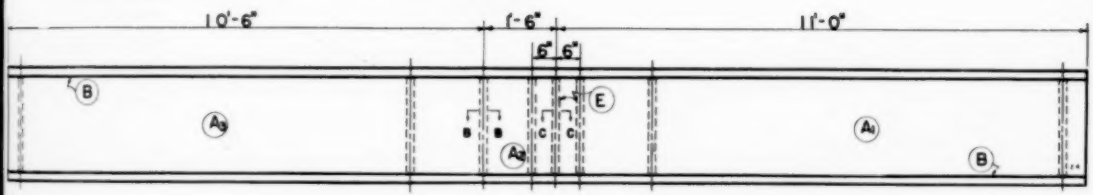

FIGURE 24. *Bottom view of the girder of semiskilled steel.*

Other details are shown in figure 1.

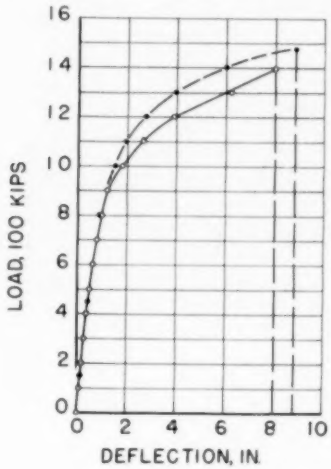

FIGURE 25. *Load—deflection curves for two box girders.*

Solid line, open circles, a girder of semikilled steel tested at 80° F. Dash line, solid circles, a girder of fully killed steel tested at 0° F.

U. S. Department of Commerce
National Bureau of Standards

Research Paper RP1935
Volume 41, November 1948

Part of the Journal of Research of the National Bureau of Standards

Standards for Low Values of Direct Capacitance

By Charles Moon and C. Matilda Sparks

In the measurement of small capacitances, such as the interelectrode capacitance of vacuum tubes, standards are needed for checking the calibration of the measuring equipment. The design, construction, and measurement of a group of small primary and secondary standards of capacitance for this purpose are described, the values of which range from 0.001 to 5.0 micromicrofarads. Capacitators of 0.1 $\mu\mu$f and above are of the Kelvin guard-ring type; those of 0.1 $\mu\mu$f and smaller are of a new "guard-well" type, which permits the construction of primary standards for values as low as desired.

I. Introduction

For several years there has been a demand from industrial and governmental laboratories for testing and certifying small direct-capacitance standards for use in checking the calibration of bridges, or test sets, which in turn are used to measure the interelectrode capacitance of electron tubes. The direct capacitance (coefficient of capacitance) is the ratio of the charge on the guarded electrode to the potential of the high-voltage plate, when the shield is at the same potential as the guarded electrode. The values of the standards required range from 0.001 to 100 $\mu\mu$f. The work described in this paper was undertaken to supply the need for capacitance standards of 5 $\mu\mu$f and below, as larger standards can be readily measured by established methods.

The capacitors described are of the three-terminal type, consisting of a guarded electrode, a high-voltage plate, and a shield. A number of small primary standards have been built, the values of which can be computed from their linear dimensions. Some of these are of the classical Kelvin guard-ring type, whereas others are of a new design.

The values of these small capacitance standards have been computed and measured by subdividing or stepping down from larger standards. The values of the larger capacitance standards were obtained by a well-established method in terms of resistance and time.

A comparison of the results obtained by direct computation and by subdivision is given.

II. Conventional Kelvin Guard-Ring Standards of Capacitance

The conventional Kelvin guard-ring construction was chosen for standards in the range of 0.1 to 5.0 $\mu\mu$f.

The design of the guard-ring capacitators constructed for this work is shown by the sectional drawing in figure 1. This design makes possible very precise construction. The guarded electrode, G, sometimes called the "island," is held rigidly and accurately centered in the guard ring, GR, by means of a Pyrex-glass disk, D. The glass disk is held in the guard ring by a spring clamping ring, B, shown in detail in figure 1, which is tight-

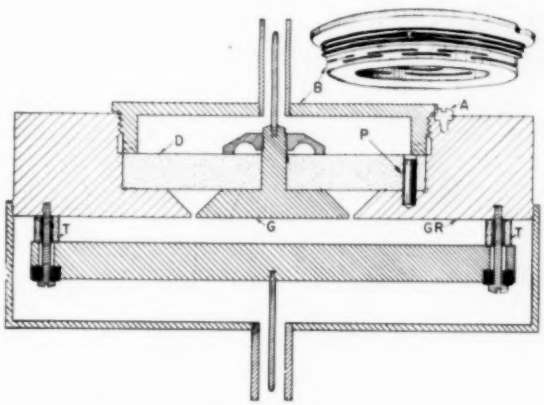

FIGURE 1. *Kelvin guard-ring capacitor.*

D, Pyrex glass disk; *P*, locating pin; *T*, spacers; *G*, guarded electrode or island; *GR*, guard-ring; *A*, locking screw; *B*, spring clamping ring.

ened down to exert firm pressure on the glass disk. The head of a locking screw, A, engages a notch in the edge of the clamping ring so that the unit can be taken apart and reassembled with the same force on the glass disk. After a preliminary assembly, the common surface of the guard ring and the island is ground and lapped optically flat. The construction is such that the island with the Pyrex disk can be removed for cleaning and for correcting constructional imperfections, such as the removal of slight burs. It can then be reassembled with the surface of the island and guard ring in practically the same plane.

The island and guard ring are of the same material (brass or dural); the insulation is Pyrex glass. The island and glass disk, D, are fitted together with a ground joint and afterward machined together so that they are exactly concentric. The

TABLE 1. *Dimensions and computed capacitance of Kelvin guard-ring capacitors*

Capacitor	Nominal value	Computed capacitance	Diameter Island	Diameter hole	Width gap	Length spacers
	$\mu\mu f$	*abs* $\mu\mu f$	*cm*	*cm*	*cm*	*cm*
3	0.1	0.10134	1.0034	1.0058	0.0012	0.6929
1	1.0	1.0019	2.3945	2.3997	.0026	.3991
2	1.0	1.0014	2.3900	2.4119	.0110	.4006
5	5.0	5.0013	5.9911	6.0012	.0050	.5003

recess in the guard ring for the glass disk is machined so that when heated to 15 or 20 deg C above room temperature, it will just slip onto the glass disk. Then starting at about 40° C, the glass is lapped in place with very fine emery and the lapping continued until a temperature of 4 or 5 deg above that of the room is reached. After washing away the abrasive, the glass disk fits in the brass ring at room temperature with practically no side shake. A hole is drilled in the edge of the glass and in the guard ring for a small dowel or locating pin, P, which is inserted after the assembly is made by a wringing motion. The high-voltage electrode is held at a fixed distance from the guard ring and island by three insulated screws that pass through three equal-length spacers of Pyrex-glass tubing, T, the ends of which are plane and parallel.

Four capacitors of this type have been constructed. The principal dimensions and computed capacitances are given in table 1.

III. Sources of Error in Guard-Ring Capacitors

The factors that must be considered in guard-ring capacitors are 1. Errors in the mechanical dimensions; 2. coplanarity of the guarded electrode and the guard-ring; 3. eccentricity of the guarded electrode with respect to the guard-ring; 4. flatness of the electrodes; 5. parallelism of guarded electrode and the high-voltage electrode; 6. effect of the width of the gap between the guarded electrode and the guard-ring; 7. sufficient width of guard-ring to avoid fringing.

The construction of the various parts of the guard-ring standards is such that accurate measurements of the parts can be readily made. The diameters of the guarded and guard electrodes were measured by a universal measuring microscope reading to 1 μ. The other dimensions needed were determined by comparison with Johansson gages by using a micrometer comparator that was sensitive to 0.1μ. Based on the dimensional measurements, experience with the guard-ring type capacitors of 1.0 $\mu\mu$f and larger indicates that an accuracy in the computed capacitance of better than 0.1 percent can be attained. This includes errors of measurement and the possibility of the inclusion of some foreign material between the parts in making the assembly.

Possibilities of error due to factors 2 to 5 listed above, are largely eliminated by the precision of the construction, and in no case has a correction been made for any of them. True coplanarity of island and guard-ring is the most difficult of the five to detect. An optical flat will show any tilting of the island with respect to the guard-ring but not necessarily an axial displacement with no tilting. The effect of displacing the guarded electrode in regard to the surface of the guard-ring is shown in figure 2. The change in capacitance for small displacements is approximately linear and from 1½ to 2 times as large as would be found by treating the displacement as if it were merely an increase in the distance between the plates.

For the 1-$\mu\mu$f capacitor, the change in capacitance is 2.8 percent for a displacement of 60 μ. Hence for 1-μ displacement, the error would be 0.05 percent. One-micron displacement on the 5-$\mu\mu$f unit would cause a change in capacitance

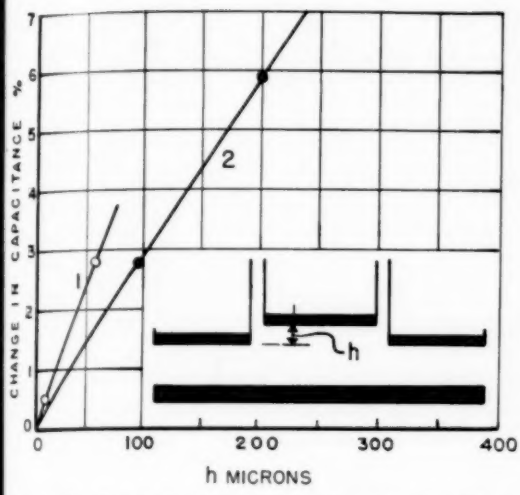

FIGURE 2. *Graph showing measured change in capacitance of guard-ring capacitors when the guarded electrode is not coplanar with the guard-ring.*

Curve 1 is for capacitor 2 in table 1. Curve 2 is for capacitor 5 in table 1.

of 0.03 percent. The difference in the level of the island and guard-ring of a capacitor that was taken apart and reassembled a large number of times was measured with an optical comparator. The displacement was found to be about 1 fringe, or ½ μ. The insignificance of the difference in level was verified by relapping the surface. Only a few strokes were required to bring the two surfaces to the same level. No measurable difference in capacitance was caused by the relapping.

The capacitance in electrostatic units of the Kelvin guard-ring capacitors in vacuum has ordinarily been computed by the simple formula.

$$C=K\left(\frac{\overline{a}^2}{4d}\right). \tag{1}$$

The computations have also been made by using the following unpublished formula by Chester Snow, which has an extra correction for the width of the gap:

$$C=K\left[\frac{\overline{a}^2}{4d}-\frac{\pi\overline{a}}{2}\left(\frac{a_2-a_1}{2\pi d}\right)^2\coth\left(\frac{\pi\overline{a}}{d}\right)\right], \tag{2}$$

where

C=capacitance in cgs electrostatic units
a_1=radius of the guarded electrode or island
a_2=radius of the hole in the guard ring
$\overline{a}=(a_1+a_2)/2$
d=separation of electrodes
K=dielectric constant of air.

The correction for the width of the gap computed from eq 2, for the widest gap used, was only 1 part in 100,000.

If the capacitance of a capacitor in electromagnetic units is taken as $1/(2.99776\times10^{10})^2$ times capacitance in electrostatic units, and the dielectric constant of air as 1.000567 [1],[1] the simple formula (1), expressed in micromicrofarads, reduces to

$$C=\frac{\overline{a}^2}{3.59259d}. \tag{3}$$

This formula has been used in computing the values in table 1.

The width of the guard ring must either be wide enough to eliminate any measurable fringing, or some corrective device must be added, such as the system of guard hoops used by Brooks, Defandorf, and Silsbee [2] in the absolute electrometer, or a resistive shield of the type employed by Slonczewski [3]. Some experimental tests with these devices were made on 1.0-$\mu\mu$f capacitor 2, which was fitted with spacers 4.040 cm long, whereby its nominal value was changed to 0.1 $\mu\mu$f. This spacing was so large that some voltage-dividing device was necessary. It was accordingly fitted in succession with a system of guard hoops and a resistive shield. The guard-hoop system was made up of nine hoops spaced about 4 mm apart connected together by 1,000-ohm resistors between the hoops and also between the end hoops and the capacitor electrodes. The capacitor with guard hoops is shown in figure 3. The resistive shield was a helix of 40 turns of advance wire, resistance 8,000 ohms, wound inside a paper tube. Difficulty was encountered in getting the two ends of the helix to terminate exactly in the plane of the electrodes. Some interesting results of connecting these devices to a capacitor in different ways were obtained and are given in table 2. From these results it is evident that when a corrective device, such as a resistive shield or voltage-divider hoops, is used in a capacitor that has a large plate separation, the construction must be precise, because it then plays an important part in the capacitance. The lines

[1] Figures in brackets indicate the literature references at the end of this paper.

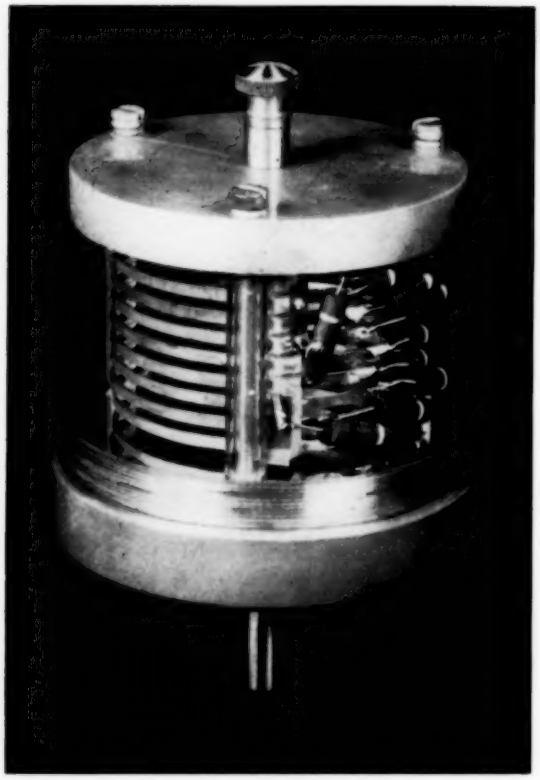

FIGURE 3. *Capacitor 2 fitted with guard-hoop system.*

of electrical force are ordinarily pictured as streaming in parallel lines normal to the two electrodes, and the hoop system as being simply a device for preventing the bulging of the lines at the edge of the plates. Experiments indicate that when the separation between the plates is very large the high-voltage plate plays a very small part in the capacitance. A shift in an axial direction of the hoop system of 0.5 mm caused a larger change in capacitance than a hole of a diameter equal to that of the island cut through the center of the high-voltage plate. Similar conclusions were reached in the experimental study of the absolute electrometer [2]. As new designs for absolute capacitors in the range of 0.1 $\mu\mu$f and below have been developed, no attempt has been made to construct precision capacitors either with guard hoops or resistive shields. The values given in table 2 are not to be taken as indicating the accuracy that could be had by more careful construction because neither of the devices was precision made. The results given in table 2, with the voltage-dividing system connected to one electrode only, indicate a method of testing, whether or not such a device is needed. If no change of capacitance is observed, whatever the manner of connecting the system, no corrective device is needed. To make this test, it is not necessary to construct an elaborate device, as a single metal ring, as shown in the inset of figure 4, will suffice. The results, which are self-explanatory, are shown in figure 4.

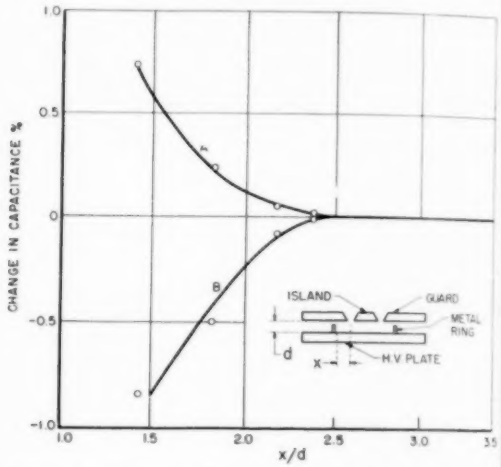

FIGURE 4. *Curves showing the change in capacitance caused by fringing when a metal ring was in contact with either the guard-ring, curve B, or the high-voltage plate, curve A, of a guard-ring capacitor 1 of table 1.*

Four rings of different diameters were used, d was constant.

TABLE 2. *Results of tests under various conditions, with two voltage-dividing devices used to overcome fringing in a guard-ring capacitor*

Computed capacitance (assuming no fringing): 0.099 $\mu\mu$f
Measured capacitance (without voltage dividing device): 0.095 $\mu\mu$f

Manner of connecting voltage dividing device, if any	Capacitance in micro-microfarads with—	
	Resistive shield	Guard hoops
Properly connected to both plates	0.098	0.10
To guard ring only	.044	.04
To high-voltage plate only	.180	.18
Floating (insulated from both plates)	.096	.09

IV. New Designs of Primary Capacitors of Very Low Value

Below 0.1 $\mu\mu$f, the classical guard-ring capacitor is not so suitable, because either the diameter of

the island must be very small or the separation of the electrodes must be large.

For capacitance standards of 0.1 $\mu\mu$f and smaller, two new capacitors, in which the guarded electrode is at the bottom of a recess, or well, in the guard electrode, have been developed.[2] These are referred to in the paper as the "guard-well" type. This design permits the making of primary standards as small as desired in capacitance and at the same time keeping the linear dimensions large enough to be constructed and measured accurately.

Two forms of guard-well capacitors have been constructed. One form is shown in figure 5 and is referred to in this paper as the "rectangular type." The other form, referred to as the "circular type," is shown in figure 6 (a fixed capacitance unit) and figure 7 (a continuously variable capacitance unit).

As shown schematically in figure 5, the rectangular-type capacitor consists of a rectangular guarded electrode or island, F, which is at the bottom of a slot of depth d and a high-voltage electrode, E, which is spaced a short distance, c, above the top of the slot. One standard was built to verify the formula developed by Chester Snow for a guard-well capacitor of the rectangular type. The construction and measurement of the dimensions of this capacitor are more difficult than for the circular ones shown in figure 6, for which he later developed a precise formula. The mounting of the guarded electrode in the circular capacitor is identical with that of the guard-ring capacitor shown in figure 1. Actually, by the addition of an annular ring, H, of thickness, d, with plane parallel sides and a hole having a diameter slightly larger than the diameter of the island, the standard guard-ring capacitor shown in figure 1 can be converted to the new design shown in figure 6.

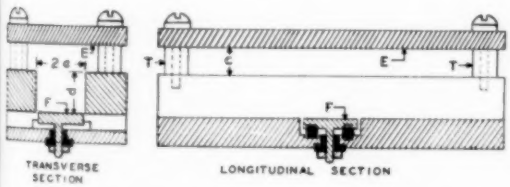

FIGURE 5. *Rectangular type of guard-well capacitor.*

F, guarded electrode.

[2] The fundamental idea for this design was contributed by F. B. Silsbee, Chief, Division of Electricity and Optics. Formulas for computing the capacitance of these new designs have been derived by Chester Snow and will be published in the near future.

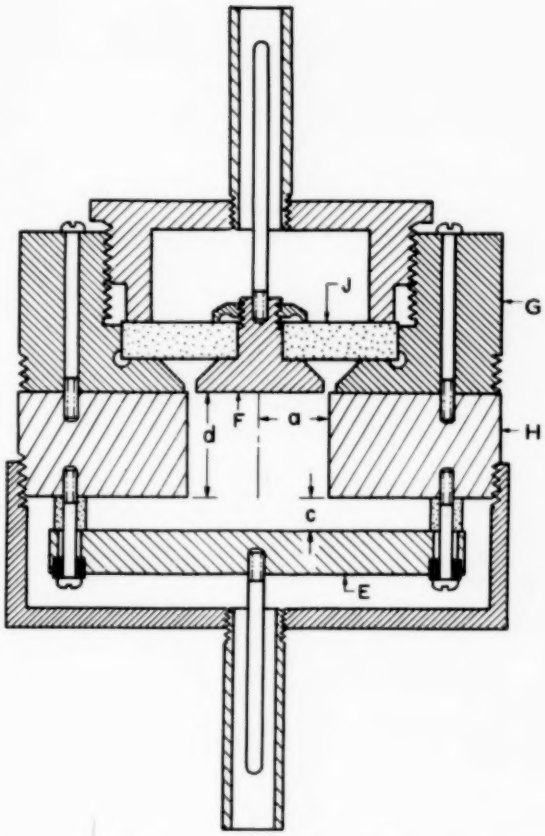

FIGURE 6. *New type of primary capacitor.*

This capacitor consists essentially of the parts of the guard-ring capacitor shown in figure 1 with the addition of the annular ring, *H*.

The dimensions of a circular capacitor, fitted with three annular rings, H, and giving nominal values of capacitance of 0.1, 0.01, and 0.001 $\mu\mu$f are given in table 3, along with the computed and measured values.

The depth, d, of each of the three rings was adjusted by trial until the measured capacitances were those given in the table. The measured values of capacitance of these three small units were obtained by subdividing a value of 1 $\mu\mu$f, which had been previously established. (The method of subdivision will be described later.)

After the units had been adjusted experimentally to have the measured values given in the table, under the heading of measured capacitance, their dimensions were used to compute their capacitances by the formula derived by Dr. Snow. A

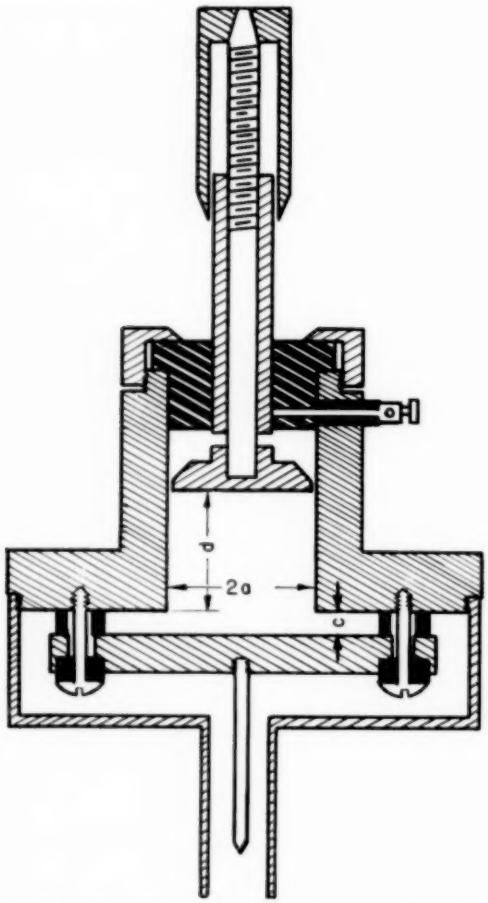

FIGURE 7. *Continuously variable capacitor of the guard-well type.*

The capacitor has a range from 0.1 to 0.001 $\mu\mu$f.

comparison of the measured and computed values of capacitance is a good indication of the accuracy obtained in subdividing 1 $\mu\mu$f. (See table 3).

TABLE 3. *Dimensions of new circular type of primary standards of direct capacitance*

Nominal capacitance	Dimensions			Capacitance	
	a	c	d	Computed	Measured
$\mu\mu f$	*cm*	*cm*	*cm*	$\mu\mu f$	$\mu\mu f$
0.1	1.680	.2098	1.733_1	0.09976	0.1000
.01	1.680	.2098	3.334_2	.009947	.00997
.001	1.680	.2098	4.928_2	.001016	.00101
.....	1.680	.2098	0	3.745	.....

• When $d=0$, the capacitor becomes a conventional Kelvin guard-ring type.

A variable model of the circular capacitor has been made, in which the low-voltage electrode is mounted on a micrometer screw, making the depth d and therefore the capacitance, continuously variable. The range is from 0.1 to 0.001 $\mu\mu$f (see fig. 7).

The computed variations of capacitance with dimensions of a capacitor of this form is illustrated by the curve in figure 8, from which it will be seen that a capacitance as small as desired can readily be obtained.

The formulas for computing the capacitance of both the linear and circular capacitors have been derived on the assumption that the gap between the island and the annular ring is infinitely small, that the edges of the hole in the annular guard ring are not rounded, and that the guard ring and high-voltage plate extend to infinity. Measurements on an experimental model show that the gap between the island and the annular ring can be as large as several thousandths of an inch, which was anticipated because the electric field is very weak in that vicinity, also that the high-voltage plate need extend over the edge of the annular ring, or the edges of the bars in the rectangular model, for a distance of only three or four times the length of the spacers used to separate the high-voltage plate from the ring or bars.

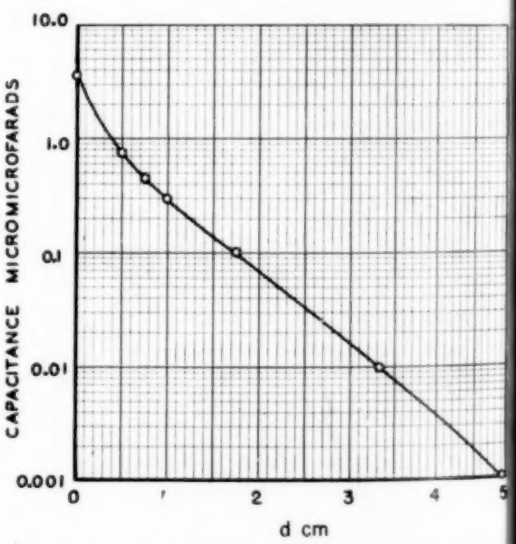

FIGURE 8. *Graph showing change in capacitance with depth d of the annular ring, H, plotted from data in table 3 and other computed values.*

A further increase in the size of the high-voltage plate has no measureable effect and is undesirable because it increases the capacitance to ground of the high-voltage electrode. The edges of the hole in the guard ring of the circular type and the edges of the bars in the rectangular type were rounded to a radius estimated to be 0.02 mm without any measurable effect on the capacitance. As this is more than is required to remove incidental burs, the rounding was carried no further.

Snow's formulas for computing the capacitance of the new designs are:

For the rectangular type, the coefficient of capacitance C' (per unit length of slot), is given by

$$\pi C' = \frac{1}{\gamma} \sum_{s=1}^{\infty} \frac{(1+\epsilon_s') \sinh \gamma\alpha_s'}{\alpha_s'^2 \sinh (\beta+\gamma)\alpha_s'},$$

where $\cos \alpha_s' = 0$.

The coefficient C for the circular type is given by

$$\frac{C}{a} = \frac{1}{\gamma} \sum_{s=1}^{\infty} \frac{(1+\epsilon_s) \sinh \gamma\alpha_s}{\alpha_s^2 \sinh (\beta+\gamma)\alpha_s},$$

where α_s is the s^{th} positive root of the Bessel function $J_0(\alpha) = 0$; a is the radius of the cylindrical hole (or the half-width of the slot); C and d have dimensions indicated in figures 5 and 6; $\gamma = c/a$ and $\beta = d/a$; ϵ_s (and ϵ_s') $= 0$ except ϵ_1 (or ϵ_1').

$$\epsilon_1 = \frac{2}{\pi} \left(\frac{\gamma\alpha_1}{\pi}\right)^2 \left[\sum_{k=1}^{n} P_k + R_{n+1}\right],$$

where

$$P_1 = \frac{S\left(\frac{\gamma\alpha_1}{\pi}\right) - \left(\frac{\gamma\alpha_1}{\pi}\right)^2 T\left(\frac{\gamma\alpha_1}{\pi}\right)}{\alpha_1(\coth \gamma\alpha_1 + \coth \beta\alpha_1)},$$

and for $k > 1$,

$$P_k = \frac{1}{\alpha_k (\coth \gamma\alpha_k + \coth \beta\alpha_k)} \left\{S\left(\frac{\gamma\alpha_k}{\pi}\right) - \frac{\alpha_1^2}{\alpha_k^2 - \alpha_1^2}\left[S\left(\frac{\gamma\alpha_1}{\pi}\right) - S\left(\frac{\gamma\alpha_k}{\pi}\right)\right]\right\},$$

where α_k is the k^{th} positive root of the Bessel function $J_0(\alpha) = 0$.

$$S(u) = \sum_{n=1}^{\infty} \frac{1}{n(n^2+u^2)},$$

and

$$T(u) = \sum_{n=1}^{\infty} \frac{1}{n(n^2+u^2)^2}.$$

For values of u less than 1, $S(u)$ can be evaluated by

$$S(u) = 1.20206 - 1.03693u^2 + 1.00835u^4 - 1.00201u^6 + 1.00049u^8 - u^{10} \sum_{n=1}^{\infty} \frac{1}{n^{11}(n^2+u^2)},$$

and $T(u)$ by

$$T(u) = 1.03693 - 2.01670u^2 + 3.00602u^4 - 4u^6 \sum_{n=1}^{\infty} \frac{1}{n^7(n^2+u^2)^2} - 3u^8 \sum_{n=1}^{\infty} \frac{1}{n^9(n^2+u^2)^2}.$$

The remainder, R_{n+1}, is computed by

$$R_{n+1} \equiv \sum_{k=n+1}^{\infty} P_k \approx \frac{1}{4\pi(1+\coth \gamma\alpha_{n+1})} \left\{\frac{0.1544 + \log\ (1+x_n^2)}{x_n^2} + 2 \log \left(\frac{1+x_n^2}{x_n^2}\right)\right\},$$

where $x_n = \gamma\left(\frac{\alpha_n}{\pi} + \frac{1}{2}\right)$. (Computations were made with $n = 4$).

In the case of ϵ_1', the formula is the same except that the n^{th} root α_n of $J_0(\alpha) = 0$ is replaced by

$$\alpha_n' = (2n-1)\frac{\pi}{2},$$

the n^{th} root of $\cos \alpha = 0$.

V. Auxiliary Tools

Several auxiliary tools were found convenient for use in measuring the small capacitors. Two of these will be described. One was a low-range continuously variable capacitor by which small differences between units could be taken up. The other was a "decade" capacitor consisting of small sections by which an accurate step-up from 0.1 to 1 $\mu\mu$f could be achieved.

The design of this variable low-range capacitor is an adaptation of that described by G. Zickner [4]. This capacitor, figure 9, consists of two active electrodes shielded by a third electrode and separated by a fixed plate or septum connected to the shield and in which a semicircular opening is cut. The capacitance is varied by a rotatable plate also connected to the shield that covers part or all of the opening in the septum. The advantage of this type of unit is that the minimum direct capacitance is exactly zero, the scale is linear, and the full-scale value can be made as

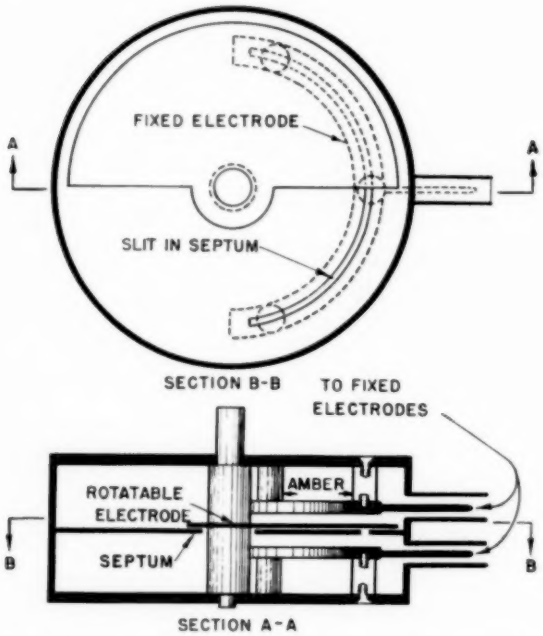

FIGURE 9. *Continuously variable low-range capacitor (schematic).*

small as desired by using a narrow annular slit in the septum in place of the semicircular opening used by Zickner. The capacitance range depends upon the width of the slit and the spacing of the fixed electrodes. The construction of the Zickner-type capacitor started with the chassis and worm gearing of a variable capacitor. The group of stator plates was replaced by two ¼-in.-thick full circular brass plates, which served as supports for the fixed electrodes, between which a thin brass plate, which fuctioned as a septum, was interposed. In this plate a 4-mm annular slit was cut with the axis of the rotor as its center. The slit extended over an arc of about 150°. In place of the semicircular plates used by Zickner, the fixed electrodes were, in this case, semi-annular rings of brass about 1.5 cm wide. A single semicircular plate on the rotating shaft, which slid in close contact with the septum, served to vary the area of the opening and hence the capacitance.

The 4-mm slit in the septum resulted in a variable capacitor having a range from 0 to 0.3 $\mu\mu$f. One division on the scale is equivalent to 0.000170 $\mu\mu$f.

In addition, a second unit was built in the same chassis having dimensions whereby a range of capacitance from 0 to 5.8 $\mu\mu$f was obtained. The change in capacitance per division of the large range is 0.00292 $\mu\mu$f.

A capacitance of 0.1 $\mu\mu$f was the smallest value for which it seemed desirable to make a standard of the guard-ring type and about as large as practical for the guard-well type. An accurate independent means of stepping up from 0.1 to 1 $\mu\mu$f seemed desirable. For this purpose a decade capacitor was designed that is thought to be free from any "switching" errors. It consists of five units: two of 0.1 $\mu\mu$f, two of 0.2 $\mu\mu$f, and one of 0.4 $\mu\mu$f. These are symmetrically arranged around and connected to central coaxial terminals, as shown in figure 10.

Each unit of the decade, as shown by the cut-away part, consists of a pair of plates insulated

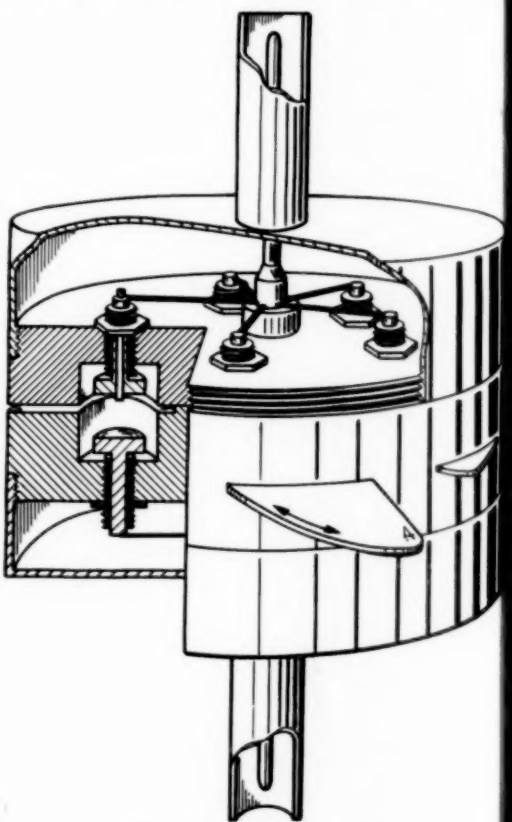

FIGURE 10. *Decade capacitor.*
Vernier screw shown in upper electrode.

from the housing and a pivoted shutter that is connected to the housing. When closed, this shutter completely isolates one terminal from the other so that the capacitance of the unit is strictly zero. The groove for the shutter is shown in the cutaway part, but the shutter is omitted. On the right are shown two shutters, the one for the 0.1 $\mu\mu$f unit closed, and the other for the 0.4 $\mu\mu$f unit open. A rough adjustment of the capacitance of a unit of this type can be readily made by adjusting the distance between the plates and then a very close adjustment by means of the vernier screw in the center of one of the electrodes, a detail of which is shown in the upper electrode. The units were thus adjusted to be equal or exact multiples of each other within the limits of sensitivity of the bridge used for measuring their capacitance and have held this adjustment for over a year.

VI. Bridges

It is not within the scope of this paper to discuss the methods of measuring direct capacitance. Since all of the bridges used have either been adequately described elsewhere or are commercially available equipment, the discussion will be largely confined to factors that affect the accuracy of measurement and methods of using the bridges in the measurement of the various capacitors.

For intercomparing the standards of 5 $\mu\mu$f and lower, the instrument found most useful was a Western Electric Direct Capacitance Test Set Model D–160936. This set, shown schematically in figure 11, consists of an alternating-current bridge built into a cabinet complete with an oscillator and tuned detector working at a fixed frequency of 465 kc/sec. The ratio arms AD and DC are of the inductive type, very closely coupled. Special conductance and capacitance units are provided that are direct reading for capacitances from 0.00005 to 110 $\mu\mu$f and for conductances from 0 to 10 μmho.

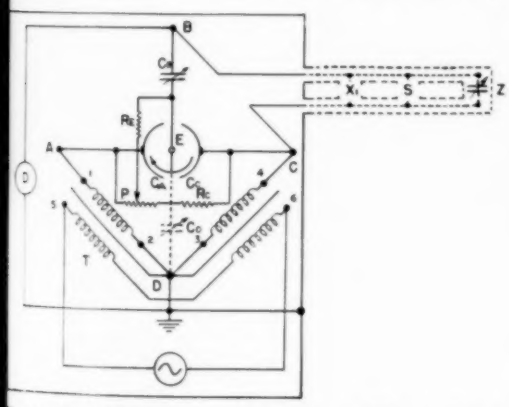

FIGURE 11. *Schematic sketch of Western Electric Direct Capacitance Test Set Model D–160936 showing method of connecting capacitors in parallel.*

The residual admittances fall either across the detector corners of the bridge, so that they do not enter into the balance equation, or across the ratio arm CD. If the coupling between the ratio arms were 100 percent, no error would be caused by the burden on one arm. Since 100-percent coupling cannot be quite obtained, a slight error is caused by the unequal loading of the ratio arms. In all measurements, the residual admittances across the CD arm were either small or were kept practically constant during a given measurement so that no appreciable error was introduced from this source.

When two or more capacitors were connected in parallel, coaxial leads were used to connect the units to both terminals of the test set. The test set was not designed to be a precision instrument, but it has the stability and sensitivity necessary for the measurement of very small capacitors. In this work the test set was used merely as a balance to determine the equality of two capacitances by a substitution method. For this purpose it was well suited. The only alteration made in the test set was in the detector tuning unit, which was changed so that it could be tuned with a larger than normal capacitance to ground at the B terminal.

The small primary capacitance standards were measured by subdividing a 1,000-$\mu\mu$f variable standard capacitor in a Schering bridge.

The method is old and in general use for calibrating variable capacitors by stepping up, subdividing, etc. An unknown three-terminal capacitor, x, was compared with a calibrated variable standard having a range of capacitance of 1,000 $\mu\mu$f between 100 and 1,100 scale divisions. This difference in capacitance of approximately 1,000 $\mu\mu$f was accurately known, having been predetermined in the well-known Maxwell commutator bridge [7] in terms of resistance and time with an accuracy of about 0.01 percent.

The standard and the unknown, which was a three-terminal variable with a full-scale range of

TABLE 4. *Value of 0.1 micromicrofarad unit of decade capacitor in terms of various small primary capacitance standards and from Maxwell commutator bridge data*

Capacitor	Small primary standard (guard-ring type)	Computed capacitance	Derived value of 0.1 $\mu\mu$f of decade capacitor				
			Observer				Deviation from mean
			1	2	3	Average (3 observers)	
	$\mu\mu$f	abs $\mu\mu$f	abs $\mu\mu$f	abs $\mu\mu$f	abs $\mu\mu$f	abs $\mu\mu$f	Percent
5	5.0	5.0013	0.10014	0.10008	0.10017	0.10013	−0.01
1	1.0	1.0019	.10011	.10005	.10007	.10008	−.06
2	1.0	1.0014	.10011	.10014	.10014	.10013	−.01
3	.1	.10134	.10018	.10020	.10025	.10021	+.07
	New Type						
4	.1 circular	.09974	.10005	.10005	.10006	.10005	−.09
6	.025 rectangular	.02494	.10030	.10019	.10022	.10024	+.10
Mean			0.10015	0.10012	0.10015	0.10014	±0.05
By stepping down from Maxwell commutator bridge data			0.10016		0.10009	0.10013	

100 $\mu\mu$f, were connected in parallel in the measuring arm of the bridge.

The change-of-standard method was employed for determining the unknown direct capacitance in the following manner: Starting with the standard set on the 100 scale point and with the unknown capacitor connected, the bridge is balanced holding the standard and unknown fixed. The unknown is then disconnected and the bridge rebalanced by increasing the standard. Leaving the standard fixed at this new position, the above procedure was repeated so that the value of the unknown was transferred to the standard in 10 additive steps, at the end of which addition the standard scale reading was very nearly 1,100.

Normally the value of the standard will not be exactly 10 times the unknown. Since in our case both were calibrated variable capacitors, the difference could be read on either instrument. The difference, Δ, was usually so small that a precise calibration of the scale used to read the difference was not important.

If y=capacitance difference on the standard between scale points 100 and 1,100; x=capacitance of unknown; $y-10x=\Delta$; then $x=Y-\Delta/10$. The above procedure was repeated to subdivide the 100-$\mu\mu$f variable standard and finally a 10-$\mu\mu$f variable standard both of which were of the three-terminal type.

In subdividing the 10-$\mu\mu$f variable, the 1-$\mu\mu$f and the 5-$\mu\mu$f primary standards were used as unknowns, and their capacitances were thus obtained in terms of a capacitance difference of 1,000 $\mu\mu$f measured on a variable capacitor in the Maxwell commutator bridge.

For measuring secondary units of 5 $\mu\mu$f and larger, a calibrated variable capacitor can be used as a satisfactory reference standard. The calibration of a secondary capacitor by using the Schering bridge has been made both by stepping up from the 5-$\mu\mu$f guard-ring capacitor and also by stepping down from a 1,000-$\mu\mu$f variable capacitor, which had been measured in a Maxwell commutator bridge. The agreement between the values by the two methods was well within 0.1 percent.

The results given in table 4 indicate that a capacitance of 0.1 $\mu\mu$f can be realized, with an accuracy of about 0.1 percent, either from absolute standards or by methods of subdividing large units. Standards 3 and 6 are considered to be the least reliable of the group. Omitting the values obtained from standards 3 and 6, the mean value of the 0.1-$\mu\mu$f fixed standard is lowered by 0.04 percent, or to 0.10010 $\mu\mu$f, which is believed to be its most probable value.

VII. Summary and Conclusions

A number of primary standards of capacitance have been built, the construction being such that their capacitance should remain permanent over long periods. A number of auxiliary tools have been made to use in intercomparing the primary

standards and in comparing primary standards with unknown secondary standards.

The methods of measuring the primary standards are described, including the transfer of a capacitance difference on a large variable capacitor measured in the Maxwell commutator bridge to the Schering bridge where this capacitance difference is subdivided and compared with some of the newly designed low-capacitance standards.

The capacitance values of the primary standards have been computed from their dimensions.

Results of measurements by the various test methods and a comparison with the computed values of the standards is given.

From measurements and intercomparisons on a number of small capacitance units, it seems that an accuracy of about 0.1 percent can be obtained in the calibration of capacitors from 5 $\mu\mu$f to perhaps as low as 0.1 $\mu\mu$f. For 0.01 $\mu\mu$f, the accuracy is probably ± 0.5 percent, and for 0.001 $\mu\mu$f about ± 2 percent.

The computed capacitance of the smaller primary standards agrees within about 0.1 percent with the values obtained by a method of subdivision from larger units, the values of which were determined by bridge methods in terms of resistance and time.

The Bureau is now equipped with a set of reference standards of capacitance in the range from 0.001 to 100 $\mu\mu$f. Test methods have been developed so that secondary standards of equivalent range can be tested and certified with the precision needed to determine the interelectrode capacitance of electron tubes.

The authors express their appreciation to R. L. Driscoll for making some of the computations; to Thelma Hollis for many of the electrical measurements; to A. H. Scott for the Schering bridge measurements; and L. P. Slivka for his painstaking work in the construction of several of the capacitors.

VIII. References

[1] L. G. Grant and D. L. Woernley, Phys. Rev. [2], **69,** 101 (Jan.-June 1946).

[2] H. B. Brooks, F. M. Defandorf, and F. B. Silsbee, J. Research NBS **20,** 253 (1938) RP1078.

[3] T. Slonczewski, Rev. Sci. Instr. **18,** 848 (Nov. 1947).

[4] G. Zickner, Elek. Nachr-Tech. **7,** 443 (1930); B. Hague, AC Bridge methods, 4th ed., p. 344 (Pitman Publishing Corp., New York, N. Y., 1938).

[5] U. S. Patent 2309490 (Jan. 26, 1943); U. S. Patent 2326274 (Aug. 10, 1943).

[6] ASTM Standards, part III-B Supplement, p. 109 (1947).

[7] H. L. Curtis and C. Moon, BS Sci. Pap. **22,** 487 (1927) S564; J. C. Maxwell, Electricity and magnetism **1,** ed. 2, Art 771 (The Clarendon Press, Oxford, London, 1892).

WASHINGTON, June 2, 1948.

U. S. Department of Commerce
National Bureau of Standards

Research Paper RP1936
Volume 41, November 1948

Part of the Journal of Research of the National Bureau of Standards

Experimental Verification of Theory of Landing Impact

By Walter Ramberg and Albert E. McPherson

Drop tests of an idealized wing and alighting gear were made to provide an experimental check on methods for computing the transient bending stresses in the wing produced by a symmetrical vertical landing impact. The model was dropped in a nearly strain-free condition to make contact at a point below the center of gravity. The forces in the alighting gear, acceleration at the "fuselage", and bending strains in the wing were recorded as a function of time.

According to the statistical theory of Biot and Bisplinghoff, the computed maximum bending stresses, using the first three flexural modes, were found to be 43 to 137 percent greater than the measured values. Using the actual forcing function reduced the difference to less than 20 percent.

I. Introduction

The tests described in this paper [1] were made for the Bureau of Aeronautics, United States Navy Department, to provide an experimental verification of analytical methods for determining the transient oscillations in the structure of an airplane during landing impact.

The practical importance of this problem for the safe operation of large airplanes has been stressed by Biot and Bisplinghoff [1] [2], Keller [2], and Yorgiadis [3].

The analysis of the transients during landing impact is complicated by the fact that these transients involve many natural modes of vibration of the airplane, and response in each mode depends on the force-time curve at the point of contact. The force-time curve will vary from one landing to the next of a given airplane. In view of these complications, Biot and Bisplinghoff proposed an ingenious statistical approach to the landing problem. In this approach the vibration of the structure in a given mode is reduced to that of an equivalent linear oscillator, and the maximum amplitude in that mode is estimated from an envelope of "dynamic response factors", which bounds the response to impact force-time curves of any shape that may be expected in the landing. An upper limit to the resultant amplitude is obtained by adding up the maximum amplitudes in the various modes.

Application of Biot and Bisplinghoff's statistical approach involves the following assumptions, which may affect the accuracy of the result:

1. The maximum amplitude in the various modes is added up without regard to phase differences. This will lead to a resultant that may be considerably larger than the resultant when phase differences are taken into account.

2. The most severe impact force-time curve during the landing approaches in effect one of the impact force-time curves that were used by Biot and Bisplinghoff to derive their envelope of "dynamic response factors". Further measurements of landing impacts in service and of impact force-time curves in drop tests of landing gear may lead to modifications of the envelope of dynamic response factor. The envelope should be raised if service showed more severe impact force-time curves than those assumed by Biot and Bisplinghoff. It could be lowered if they were found to be consistently less severe.

3. It is sufficient to confine the analysis to the first few modes of vibration. Inclusion of modes of higher order than about the fifth is impracticable, because they are either unknown or too difficult to determine. This may lead to an exces-

[1] This paper was presented before the Sixth International Congress for Applied Mechanics in Paris on Sept. 27, 1946.

[2] Figures in brackets indicate the literature references at the end of this paper.

sively low value of the resultant if the higher modes contribute a significant proportion to the resultant.

4. The force-time curve at the landing gear is independent of the flexibility of the airplane structure. Actually there may be ar appreciable coupling between the elastic deflection of the structure and the action of the landing gear.

5. The effect of damping is negligible. Damping may introduce coupling between the various modes of vibration of the airplane, thereby making it impossible to analyze the vibration in any given mode apart from that in all other modes.

6. Nonlinear effects are negligible. Nonlinear effects caused by buckling of the sheet, slipping of rivets, exceeding of the proportional limit of the materials in portions of the structure may introduce coupling between various modes.

II. Description of Model

1. Wing

The wing was designed to have a mass and flexural-rigidity distribution approximating that of a $\frac{1}{10}$-scale model of a large military airplane. The assembled model is shown in figure 1. The wing was a tapered box beam of rectangular section. It was constructed of aluminum alloy sheet and angles fastened with $\frac{1}{8}$-in. rivets. The nominal cross-sectional dimensions at several stations along the wing are shown in figure 2.

The flexural rigidity, EI, at various stations along the completed wing was computed from measurements of extreme fiber strains when the wing was subjected to a known bending moment. The results are given in figure 3.

The mass distribution of the wing was measured by a volumetric method. This involved stripping the wing of the engine weights and measuring the change in weight as the wing was lowered into a large container of water. The measured values of mass per inch are shown in figure 4, a. Figure 4, b shows the magnitude and location of concentrated masses corresponding to the engines and fuselage.

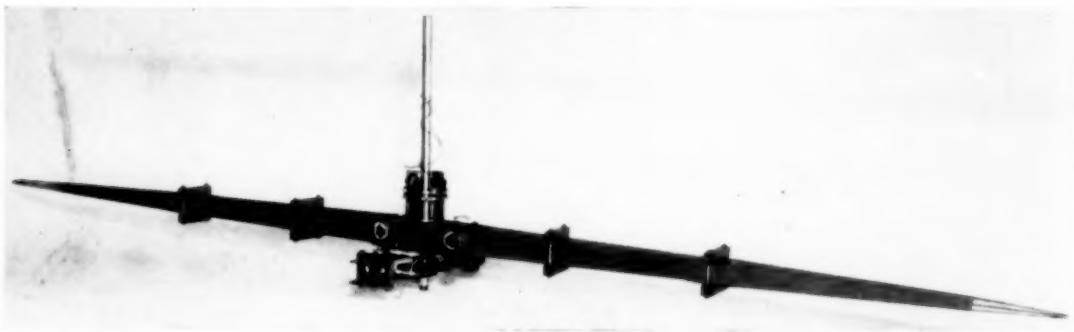

FIGURE 1. *Idealized model.*

An experimental verification of Biot and Bisplinghoff's analysis was decided upon in order to determine the adequacy of the assumptions and to indicate the minimum number of modes of vibration that must be included to estimate maximum bending moments and accelerations at various stations along the wing.

The experimental verification was started with the tests described in this paper. These tests are concerned with the simplest case, namely that of measuring the flexural transients in a symmetrically tapered model wing when the model is subjected to a vertical impact force directly below the center of gravity. Four engine masses were mounted symmetrically on the wing so as to subject it to bending without torsion during the landing impact.

2. Alighting Gear

(a) Damper

Adjustment of the damping force over a wide range was made possible with a fluid damper built into the center of the model. The damper, figures 5 and 6, consisted essentially of a piston forcing fluid out of 8 adjustable ports in a cylinder. The ports were located in the side of the cylinder

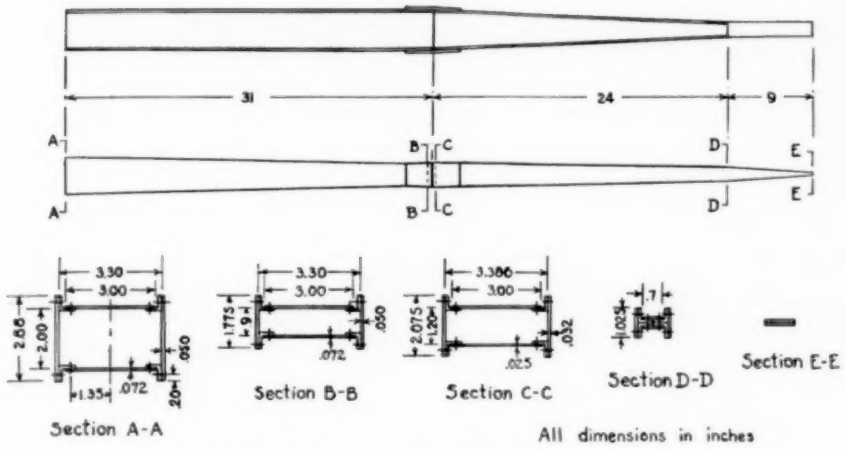

FIGURE 2. *Nominal cross-sectional dimensions of model wing.*

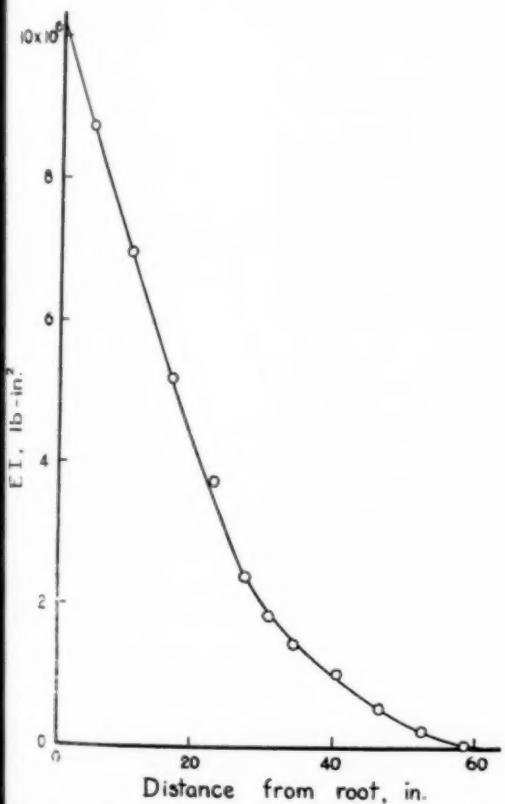

FIGURE 3. *Flexural rigidity distribution for model wing.*

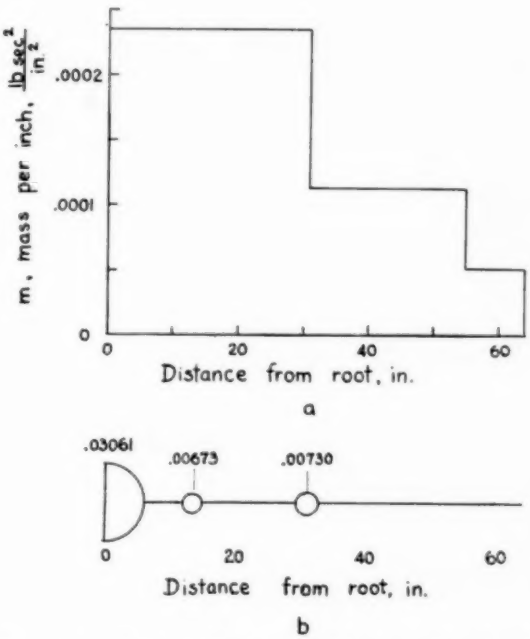

FIGURE 4. *Mass distribution for model wing; a, distributed mass; b, concentrated mass, lb sec²/in².*

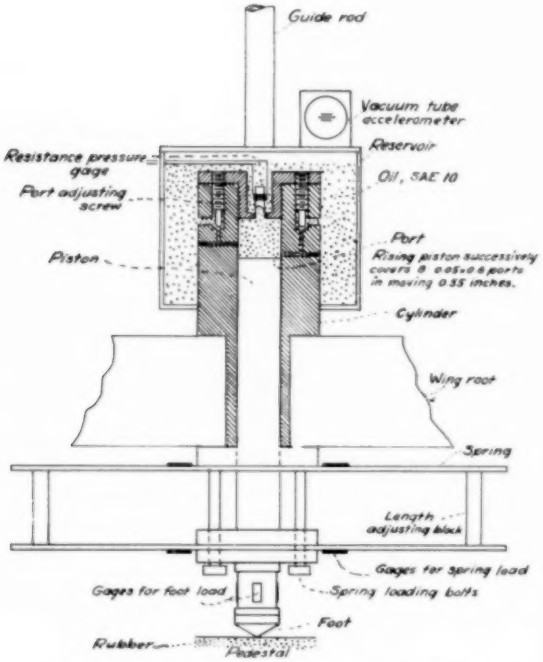

FIGURE 5. *Schematic diagram of alighting gear.*

wall at 0.07-in. intervals along the path of travel of the piston. As the piston traveled up the cylinder, it successively closed off the ports. The shape of the curve of damping force versus piston displacement could be changed by adjusting the initial opening of the various ports.

(b) Spring

The cushioning action of the air pressure in an oleo strut was approximated in the model by a pair of double cantilever springs shown near the bottom of figure 5. The springs were designed to have a wide range of adjustment of stiffness. The stiffness was changed by moving the length-adjusting block either closer or farther from the vertical centerline of the model. The springs were attached between the landing foot and the root of the model. The initial load applied by the spring between root and wing could be adjusted with the spring-loading bolts shown in figure 5.

(c) Landing Foot

The landing foot of the model is shown at the bottom of figures 5 and 6. It had a conical impact surface, which was intended to give a nonlinear force-displacement relation as the foot compressed the rubber-surfaced landing pedestal. A nonlinear force-displacement relation was desired to simulate the nonlinear characteristics of the tire in an actual airplane. The shape of the force-displacement curve was varied by changing the thickness of the rubber and by using natural rubber, Neoprene, and combinations of the two.

III. Tests

1. Release Gear

The release gear shown in figure 7 was developed to drop the model in the nearly "strain-free condition" that should hold during free fall. This prevents the setting up of vibrations excited by the sudden removal of the dead-weight forces upon release of the model. It has been found that such vibrations may interfere seriously with the interpretation of the strains and accelerations recorded during drop tests of full-size airplanes.

The release gear supports the model at several stations along the wing with forces that are adjusted to be nearly in balance with the local dead-weight forces. Upon release, the supports are removed at an acceleration greater than gravity, thus leaving the model free to fall in its nearly strain-free condition.

The support is applied to the model by eight pointed screws, *B*, at the ends of six arms. As figure 7. The screws, *B*, were carefully adjusted until strain gages attached to the model near the root and near the first engine indicated the model was in a "strain-free condition". Strain reading

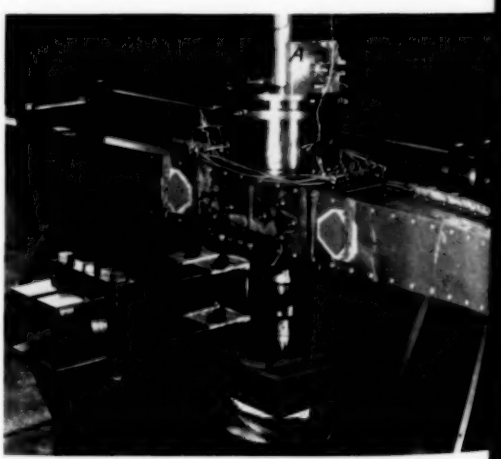

FIGURE 6. *Center section of idealized model.*

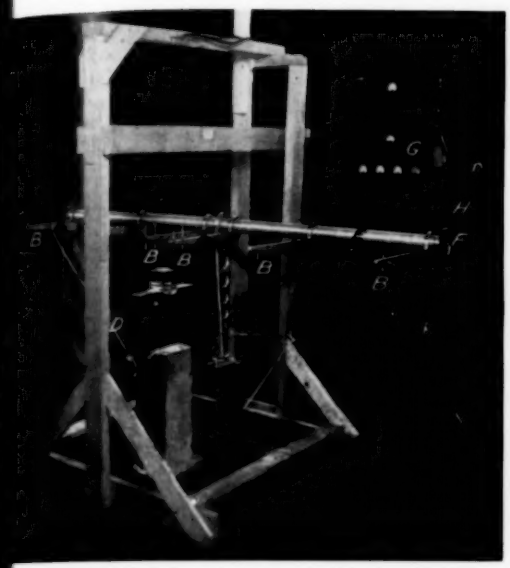

FIGURE 7. *Release gear.*

orresponding to the "strain-free" condition were etermined as the average of readings for the $+g$ nd the $-g$ condition. The $+g$ condition was btained by holding the model above the center f gravity with the landing foot vertical below the enter of gravity; the $-g$ condition was obtained y turning the model through 180° about the ing axis to place the landing foot vertically bove the center of gravity.

The model was released by cutting an 0.04-in. teel wire attached to lever C, which held the elease gear in the supporting position. The upports were swung away from under the model t an acceleration greater than g by heavy rubber nds, D, which rotated the main support rod, , about ball bearings at the ends. A friction tch at F on rod E prevented the arms, A, from inging back into the model.

2. Instrumentation

The instrumentation of the model included ick-ups for measuring bending moment near the uselage and near the first outboard engine, accel- ation at the fuselage, force transmitted through e springs, and force transmitted through the amper.

All quantities except acceleration were measured ith pick-ups by using strain-sensitive wire. The gnal of these pick-ups was amplified with the four-channel equipment shown at G in figure 7. It was then recorded in the six-channel recorder, H. The amplifying equipment included in each channel a 1,000 c/s carrier-current Wheatstone bridge and a band-pass filter to give nearly flat response up to 100 c/s; at 200 c/s the response was down about 20 percent. The recorder was equipped with galvanometers having a natural frequency of 430 c/s and a response that was flat up to 100 c/s.; the response rose about 20 percent at 200 c/s; it dropped off rapidly above 300 c/s.

Acceleration was measured with a vacuum-tube acceleration pick-up developed at the National Bureau of Standards. The pick-up contains two separate flexibly mounted plates on opposite sides of a fixed cathode. The plates are deflected elastically by the accelerations, thereby increasing the current between one plate and the cathode and decreasing it between the other plate and the cathode. The total change in current is recorded through a Wheatstone bridge. The pick-up has a fundamental frequency of about 800 c/s. The output was fed through a low-pass filter into the recorder, H, giving a flat response up to 200 c/s.

The bending moments at various stations on the wings were measured by attaching pairs of wire-strain gages to the top and bottom of the wing and connecting them in opposition in a Wheatstone bridge circuit so that the output was proportional to the extreme fiber-bending strain. In addition, gages in corresponding positions on the right and left halves of the wing were connected in series to average their output electrically. The over-all circuit from gages through Wheatstone bridge, amplifier, and oscillograph was calibrated statically before each set of drop tests by applying known bending moments to the wing and recording the output.

The acceleration at the fuselage was measured with the vacuum-tube acceleration pick-up, A, figure 6. The pick-up and circuit were calibrated with an acceleration of 2 g applied before each set of drop tests by reversing the accelerometer in the earth's gravitational field and recording the output.

The force transmitted through the spring was measured by attaching wire-strain gages, B, figure 6, to each of the eight leaves of the spring and connecting them into a Wheatstone bridge circuit in such a way that their output was proportional

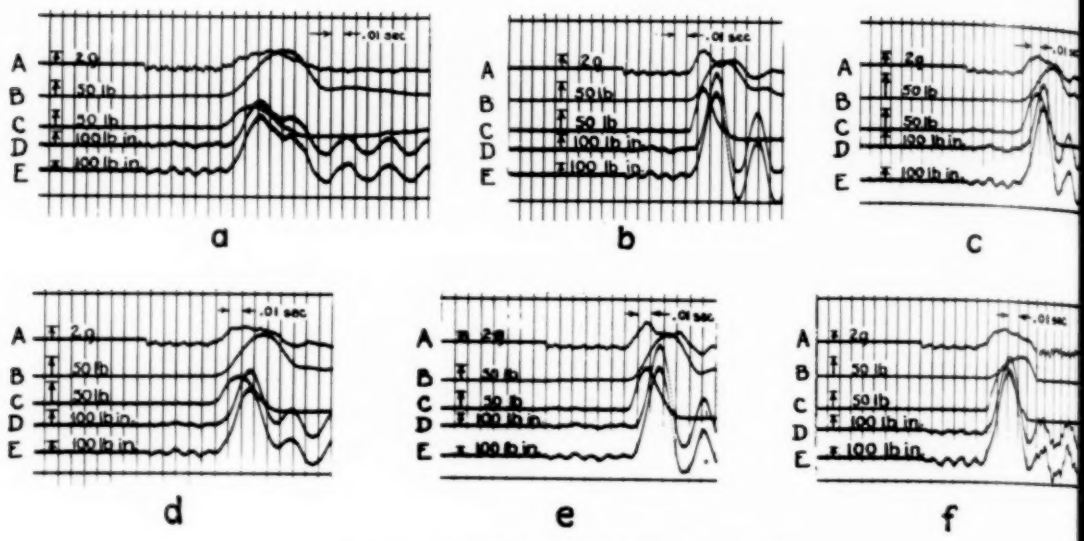

FIGURE 8. *Drop tests from a height of about 0.7 in.*

Pressure relief ports open ¼ turn in tests a to e. In test f, ports 1 to 5 open one-fourth turn, and ports 6 to 8 closed. *A*, fuselage acceleration; *B*, spring; *C*, damper; *D*, outboard bending; *E*, root bending.

Test	Initial spring loading	Number of rubber pads under landing foot	
		Natural	Neoprene
	lb.		
a	0	5	0
b	0	0	2
c	0	2	2
d	0	2	4
e	0	1	4
f	43	2	4

to the total force transmitted by the spring. A static calibration was obtained before each set of tests by applying known forces and recording the output.

The force transmitted through the damper was measured by a small pressure gage at the top of the cylinder chamber, figure 5. This pressure gage consisted of an aluminum alloy tube ½-in. long, ⅜ in. in diameter, and of 0.0035-in. wall thickness. The tube had one end closed and the other end open to the fluid in the cylinder. On the outside of the tube 0.001-in. constantan wire was wound and cemented into place taking care to insulate the wire from the tube and to bring out firmly anchored lead wires. A static calibration of the gage showed it to have a linear change in resistance with pressure up to pressures of 300 lb/in.^{2}, corresponding to forces of 500 lb transmitted through the damper.

IV. Results

The records showing the results of the drop tests from a height of about 0.7 in. are shown in figure 8. Six drops were made in which the landing conditions were varied by changing the softness of the rubber on which the model was dropped, the initial spring loading, and the opening of the pressure relief ports in the damper. The initial spring loading of 43 lb, for impact, (figure 8, *f*) corresponds to supporting the whole weight of the model on the springs.

The shortest impact, lasting about 0.050 sec. is shown in figure 8, f, and the longest impact, last-

ing about 0.086 sec, is shown in figure 8, a. The ratio of impact time to the period of the model in its fundamental bending mode approximately covers the range of this ratio for large airplanes.

The maximum observed bending moments in the wing at stations 1.5 in. and 14.5 in. from the root are given in table 1. In addition, table 1 gives the maximum observed accelerations at the root, the duration of the impact, and the maximum impact force. The maximum impact force was obtained as the maximum value of the sum of the forces transmitted through the springs and the damper.

TABLE 1. *Maximum values of the applied impact force (sum of spring and damper forces), bending moments at 1.5-in. and 14.5-in. stations, and accelerations at root*

Record	Maximum impact force per half wing	Bending moment $M_{b,1.5}$	Bending moment $M_{b,14.5}$	Maximum acceleration at root		Impact duration
	lb	*lb-in.*	*lb-in.*	*in/sec²*	*g*	*sec*
a	95	750	370	1,580	4.1	0.086
b	105	1,130	650	1,930	5.0	.076
c	100	1,060	550	1,580	4.1	.062
d	92	970	540	1,510	3.9	.060
e	120	1,370	820	2,220	5.8	.052
f	113	1,170	600	1,620	4.2	.050

V. Analysis

1. Normal Modes of Vibration

The normal modes of vibration of the model wing in bending were computed by considering the mass to be concentrated at the root and at nine stations along each half-wing. The distributed mass of the portion of the wing between adjacent stations was distributed to those stations in inverse proportion to the distance from each station to the center of gravity of the portion of wing being considered. The values are given in table 2. Influence coefficients were then computed between the mass points by treating each half-wing as a simple beam clamped at the root. The first three flexural modes of the wing in free-free vibration were computed from these influence coefficients and from the given mass distribution using a dynamic matrix and iteration procedure as explained by Duncan and Collar [4]; the deflection at the root of the wing was obtained from the condition that the center of gravity of the wing must remain at rest for free-free vibration. In the case of the second and third mode, the iteration procedure had to be modified to prevent convergence to the fundamental mode. This was accomplished by removing any proportion of lower modes present with the help of the orthogonality relations as outlined for propeller blades in [5].

The deflections in each mode r were normalized by dividing the deflection, $y_i^{(r)}$, at a given station, i, by that at the tip station. The values are given in table 2.

The normalized deflection, $\eta_i^{(r)}$, were substituted in the following formula to obtain the generalized mass, M_r, of the equivalent linear oscillator in mode r (see [1]):

$$M_r = \sum_{i=0}^{9} m_i [\eta_i^{(r)}]^2, \tag{1}$$

where m_i is the mass at station i. The values are given in table 3, together with the frequencies and periods in each mode.

TABLE 2. *Distribution of mass and flexibility along half-wing ande shap of natural modes*

Station No.	Station, inches from root	Mass	Flexibility, $1/EI$	Normalized deflection in mode, η_0	Normalized deflection in mode, η_1	Normalized deflection in mode, η_2	Normalized deflection in mode, η_3
		lb-sec²/in.	10^{-6}/*lb-in.*³				
0	0	0.03142	0.095	1	−0.08006	0.03631	−0.01834
1	6.5	.00161	.116	1	−.07069	.02350	−.00408
2	13.5	.00850	.162	1	−.03855	−.01493	.03395
3	21.5	.00205	.250	1	.02970	−.07756	.07531
4	31.0	.00899	.541	1	.16044	−.13320	.05838
5	41.0	.00106	.975	1	.35362	−.07605	−.13514
6	49.0	.000728	2.60	1	.52797	.03033	−.28579
7	53.5	.000510	5.15	1	.64232	.18102	−.29425
8	59.0	.000295	27.5	1	.80679	.48114	.00996
9	64.0	.000129	200	1	1.00000	1.00000	1.00000

TABLE 3. *Natural period, generalized mass, and bending moment for each natural mode*

Mode, r	ω_r	Period, T_r	Generalized mass, M_r	Bending moment at 1.5 in. for unit tip deflection, $\frac{(M_{b,1.5})_r}{y_{tip}}$	Bending moment at 14.5 in. for unit tip deflection, $\frac{(M_{b,14.5})_r}{y_{tip}}$
	rad/sec	*sec*	*lb sec²/in.*	*lb-in.*	*lb-in.*
0	0		0.055292	0	0
1	199.48	0.0315	.001322	4,421	3,071
2	544.60	.01153	.000437	−6,213	−1,763
3	1,025.06	.00613	.000315	7,238	−598

Table 3 shows also the bending moments per unit-tip deflection in each mode at the two stations, 1.5 and 14.5 in. from the root, at which measurements were made. The bending moments were computed by considering the wing to be loaded at stations $i=1, 2, \ldots, 9$ by transverse forces $\omega_r^2 m_i \eta_i^{(r)}$ where ω_r is the frequency in the rth mode.

2. Dynamic Response According to Theory of Biot and Bisplinghoff

The dynamic response of the model wing was computed by using Biot and Bisplinghoff's theory [1] for each of the 6 impacts shown in figure 9. These were obtained from the records of figure 8 by adding the spring and damper forces shown as B and C and dividing by 2.

(a) Bending Moment

The maximum bending moments $M_{b,1.5}$ and $M_{b,14.5}$ at stations 1.5 in. and 14.5 in. from the root were computed by adding up the maximum bending moments $(M_{b,1.5})_r$ and $(M_{b,14.5})_r$ for the first 3 modes $r=1, 2, 3$. Two sets of values were computed, the first an upper limit corresponding to the envelope of dynamic response factors γ_r given in figure 13 of [1], and the second a closer approximation corresponding to the response factor for that impact in figure 12 of [1] that came closest to the actual impacts shown in figure 9.

The bending moments in each mode r were obtained by multiplying the bending moments per unit tip deflection in table 3 by the tip deflection $\gamma_r Q_r / M_r \omega_r^2$, where Q_r is the generalized force in mode r. The generalized force was computed as the product of the maximum observed impact force and the normalized deflection at the root in mode r.

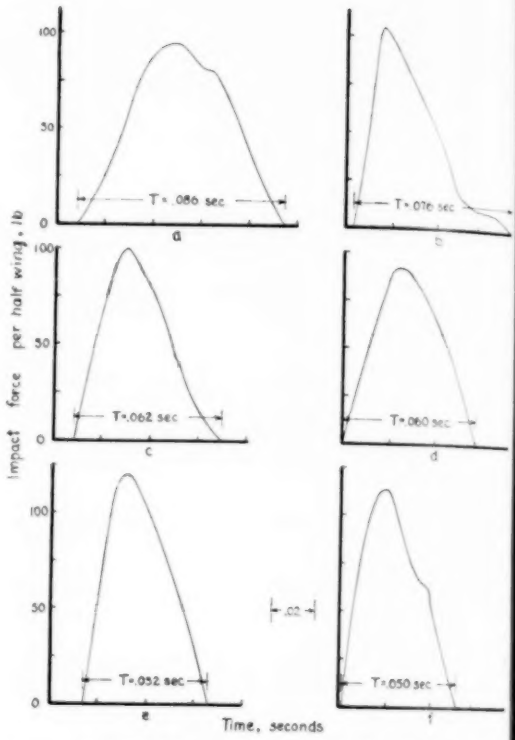

FIGURE 9. *Total impact force per half wing for tests in figure 8.*

TABLE 4. *Bending moments according to theory of Biot and Bisplinghoff, lb-in.*

Bending moments	Drop					
	a	b	c	d	e	f
$(M_{b,1.5})$ 1 envelope	−1,170	−1,321	−1,278	−1,182	−1,350	−1,[illegible]
$(M_{b,1.5})$ 2 envelope	−231	−270	−275	−256	−349	−[illegible]
$(M_{b,1.5})$ 3 envelope	−38	−42	−46	−43	−63	−[illegible]
$(M_{b,1.5})$ 1 best fit	−735	−1,173	−673	−650	−909	−[illegible]
$(M_{b,1.5})$ 2 best fit	−182	−203	−183	−175	−242	−[illegible]
$(M_{b,1.5})$ 3 best fit	−38	−42	−40	−37	−49	−[illegible]
$(M_{b,14.5})$ 1 envelope	−813	−918	−888	−821	−1,077	−1,[illegible]
$(M_{b,14.5})$ 2 envelope	−66	−77	−78	−73	−99	−[illegible]
$(M_{b,14.5})$ 3 envelope	3	3	4	4	5	[illegible]
$(M_{b,14.5})$ 1 best fit	−511	−815	−467	−451	−673	−[illegible]
$(M_{b,14.5})$ 2 best fit	−52	−58	−52	−50	−69	−[illegible]
$(M_{b,14.5})$ 3 best fit	3	3	3	3	4	[illegible]
$(M_{b,1.5})$ envelope	−1,439	−1,633	−1,589	−1,481	−1,[illegible]	−1,[illegible]
$(M_{b,14.5})$ envelope	−876	−992	−962	−900	−1,171	−1,[illegible]
$(M_{b,1.5})$ best fit	−955	−1,418	−896	−862	−1,[illegible]	−1,[illegible]
$(M_{b,14.5})$ best fit	−560	−870	−516	−498	−738	−[illegible]

The results of the computations are given in table 4. Examination of this table shows that the third flexural mode contributes less than 4 percent to the bending moment at the two stations. In view of this rapid convergence, it would have been sufficient in this particular case to confine the analysis to the first two flexural modes.

Comparison of the maximum bending moments computed, table 4, with those observed experimentally, table 1, shows that the computed values using the best fit impact curve are from 15 percent less to 51 percent more than those observed, and using the envelope impact curve are from 43 to 137 percent more than those observed.

(b) Acceleration at Root of Wing

A dynamic response factor α for acceleration, analogous to the dynamic response factor γ for deflections as given in figure 13 of [1], was determined as follows:

From equations (I–8) and (I–10) of [1],

$$\ddot{y}_{tip}^{(r)}(t)=\frac{Q_{r(t)}}{M_r}-\frac{\omega_r}{M_r}\int_0^t Q_r(\tau)\sin\omega_r(t-\tau)d\tau, \quad (2)$$

where

$\ddot{y}_{tip}^{(r)}(t)$ = acceleration in mode r at tip
$Q_r(t)$ = generalized force in mode r as a function of time
τ = variable of integration
t = time.

If we denote by Q_r the maximum value of $Q_r(t)$ and let $p_r(t)$ be a unit impact force defined by

$$p_r(t)=\frac{1}{Q_r}Q_r(t), \quad (3)$$

we obtain the dynamic response factor $\alpha^{(r)}(t)$ for acceleration as

$$\alpha^{(r)}(t)=\frac{\ddot{y}_{tip}^{(r)}}{Q_r/M_r}(t)=p_r(t)-\omega_r\int_0^t p_r(\tau)\sin\omega_r(t-\tau)d\tau. \quad (4)$$

The dynamic response factor $\alpha^{(r)}(t)$ can be considered as the ratio of the actual acceleration $\ddot{y}_{tip}^{(r)}(t)$ at the tip to the steady acceleration resulting from applying the peak generalized force Q_r to the generalized mass M_r.

The value of $\alpha^{(r)}(t)$ was evaluated for impacts of triangular shape and sinusoidal shape by using the analyses presented in eq 16 to 19 of [6]. The peak values α of $\alpha^{(r)}(t)$ are plotted in figure 10 as a function of the ratio of impact pulse period T to mode period $T_r=2\pi/\omega_r$. The dynamic response factor α for acceleration decreases rapidly as the ratio T/T_r is increased above 0.8. For T/T_r greater than 7, α is less than 0.20. As T/T_r approaches zero, α approaches 1.

The maximum acceleration $\ddot{y}_0$ at the root of the wing was computed by adding up the maximum accelerations $\ddot{y}_0^{(r)}$ for the first four modes $r=0$, 1, 2, 3, where $r=0$ corresponds to motion as a rigid body. Two sets of values were computed, as in the case of the bending moments, the first corresponding to the envelope of dynamic response factors α in figure 10 and the second corresponding to that one of the two shapes of the curve of impact force versus time, assumed for figure 10, that comes closest to the actual impact shown in figure 9.

The accelerations $\ddot{y}_0^{(r)}$ in each mode were obtained from

$$\ddot{y}_0^{(r)}=\frac{\alpha Q_r\eta_0^{(r)}}{M_r}, \quad (5)$$

where $\eta_0^{(r)}$ is the normalized deflection at the root. For the rigid body mode $r=0$,

$$\ddot{y}_0^{(0)}=Q_0/M_0, \quad (5a)$$

where Q_0 is one-half of the maximum impact force applied, and M_0 is one-half of the mass of the wing.

The results of the computation are given in table 5. Examination of table 5 shows that the second and third flexural modes contribute less than 4 percent to the acceleration at the root. It would have been sufficient in this case to con-

TABLE 5. *Acceleration at root of wing according to theory of Biot and Bisplinghoff in./sec²*

Acceleration	Drop					
	a	b	c	d	e	f
$\ddot{y}_0^{(0)}$	1,720	1,900	1,810	1,665	2,172	2,046
$\ddot{y}_0^{(1)}$ (envelope)	244	257	279	259	367	357
$\ddot{y}_0^{(2)}$ (envelope)	52	63	74	69	105	102
$\ddot{y}_0^{(3)}$ (envelope)	9	12	14	14	21	20
$\ddot{y}_0^{(1)}$ (best fit)	180	132	78	80	201	217
$\ddot{y}_0^{(2)}$ (best fit)	29	43	48	62	56	41
$\ddot{y}_0^{(3)}$ (best fit)	3	6	4	4	11	6
$\ddot{y}_0$ (envelope)	1,995	2,232	2,177	2,007	2,665	2,525
$\ddot{y}_0$ (best fit)	1,932	2,081	1,940	1,811	2,440	2,310

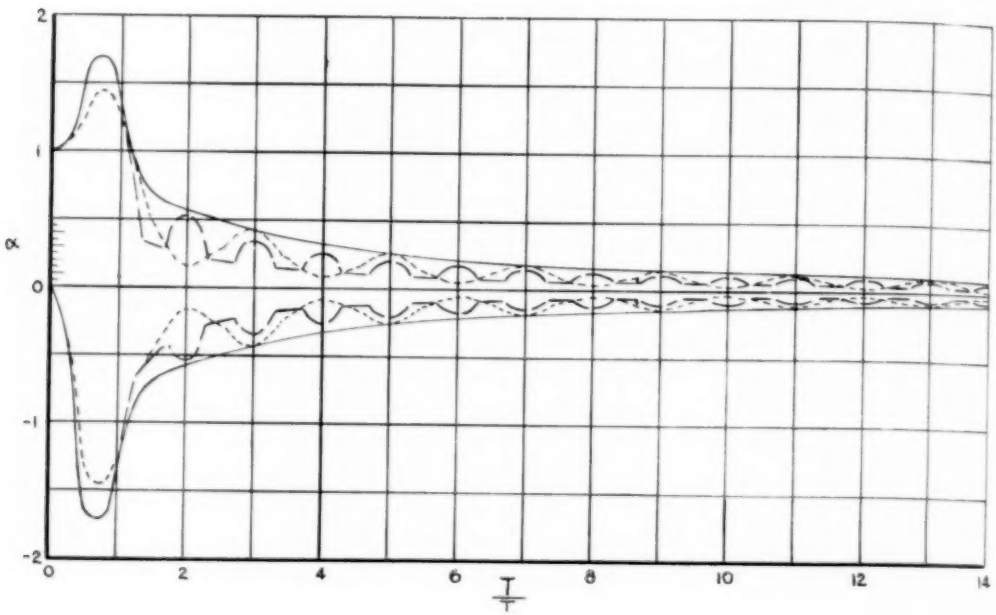

FIGURE 10. *Dynamic response factor for acceleration.*
– – – Triangular pulse; _ _ _, sinusoidal pulse; _____, envelope.

fine the analysis to the rigid body motion and the fundamental flexural mode.

Comparison of the maximum computed accelerations at the root, table 5, with those observed experimentally, table 1, shows that the computed values using the envelope curve are from 16 to 56 percent more than those observed and, using the best fit curve, are from 8 to 43 percent more than those observed.

3. More Exact Analysis, Including Effect of Phase Differences

A basic assumption in the theory of [1] is that the maximum response of the wing in each mode may be added without regard for phase. The resulting error was computed by making a more exact analysis for the impact-time relation shown in figure 9, d.

The tip deflection in mode $r(r=1, 2, 3)$ was computed from eq (1—10) of [1]

$$y_{\text{tip}}^{(r)}=\frac{1}{M_r\omega_r}\int_0^t Q_r(\tau)\,\sin\,\omega_r(t-\tau)d\tau, \qquad (6)$$

where $Q_r(t)$ is the generalized force in mode r computed by multiplying the impact force-time relation figure 9, d by the normalized deflection at the root, $\eta_0^{(r)}$. The integrations were carried out numerically. The resulting tip deflections in each of the first three flexural modes are shown in figure 11, a.

The bending moments $M_{b,\,1.5}$ at 1.5 in. from the root were computed by multiplying the tip deflections in each mode by the corresponding factor in table 3. The resulting bending moment in each of the first three modes and their sum, as well as the observed bending moment, are shown in figure 11, b. Figure 11, c shows corresponding values at 14.5 in. from the root.

The acceleration at the root in the rigid body mode $r=0$ was computed from eq 5a after replacing Q_0 by $Q_0(t)$. The acceleration in the flexural modes $r=1, 2, 3$ was obtained from

$$\ddot{y}_0^{(r)}=\ddot{y}_{\text{tip}}^{(r)}\eta_0^{(r)}=\left[\frac{Q_r(t)}{M_r}-\omega_r^2 y_{\text{tip}}^{(r)}\right]\eta_0^{(r)}. \qquad (7)$$

where $y_{\text{tip}}^{(r)}$ is the tip deflection given in figure 11, a. The results of the computation are given in figure 11, d, together with the observed acceleration at the root.

Examination of figures 11, b to 11, d shows that the observed maximum bending moment

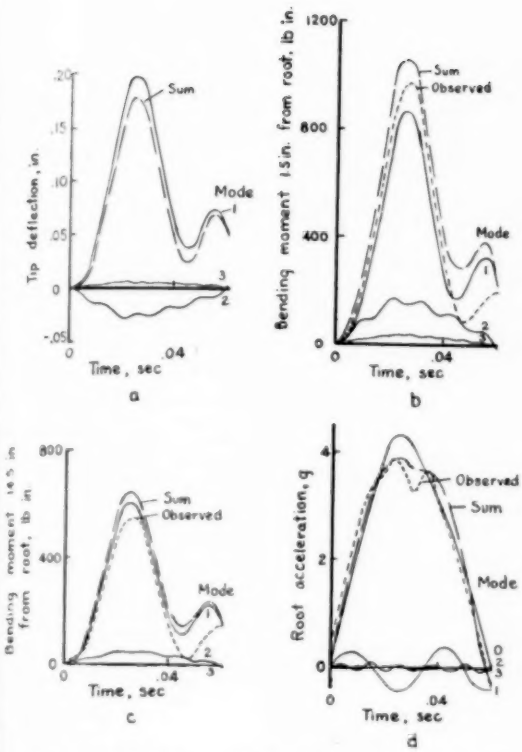

FIGURE 11. *Detailed analysis for the impact force-time relation in figure 9,d.*

and accelerations differed less than 20 percent from the computed values, when the phase differences were taken into account and when the actual impact force-time curve was used.

Comparison of the response in the individual modes in figure 11 shows that the error caused by neglecting phase differences was negligible (less than 1%) in the case of bending moments. In the case of acceleration at the root, the error was about 23 percent.

The good agreement observed for bending moment is primarily the result of the following two factors.

In aircraft structures (or models simulating aircraft), the periods of natural vibration T_r are as short or shorter than the duration of the impact T. In such a case, a maximum bending moment and deflection response in all the modes occurs in phase at a time a little later than the maximum applied impact force. The response in the different modes drops off rapidly as the number of the mode increases. Hence the contribution of the higher modes becomes negligible.

The phase difference can be important in the case of acceleration, as the acceleration in the first flexural mode may be, and in this example was, opposed in phase to that of the rigid body motion at the peak. Neglect of phase in the case of acceleration near the tip of the wing would probably lead to results so inaccurate as to be useless.

VI. Summary

An experimental verification of Biot and Bisplinghoff's analysis of landing impact is presented. An airplane model was built having a distribution of mass and of flexural rigidity along the wing approximately proportional to that for a four-engine military airplane. The four engine masses were mounted symmetrically on the wing so as to excite flexural vibrations without torsion when the model was dropped vertically to receive a landing impact below the center of gravity. The model contained an alighting gear with means for adjusting the time history of the impact force acting on the wings. Measurements were made of impact force, bending moments at two stations, and root acceleration for six landing conditions.

The observed maximum bending moments were compared with those computed by Biot and Bisplinghoff's method. The computed bending moment, using a response factor given by an envelope curve due to Biot and Bisplinghoff, was 43 to 137 percent larger than the observed bending moment. Use of an approximation to the actual impact-time relation gave bending moments from 15 percent less to 51 percent greater than the observed bending moments.

A more exact analysis, taking account of phase differences was made for one of the actual impact force-time curves. This gave maximum bending moments that differed less than 20 percent from the observed bending moments. Comparison of the computed response in the individual modes showed that the neglect of phase differences between the different modes, in accordance with Biot and Bisplinghoff's analysis, would have caused an error in maximum bending moment of less than 1 percent.

The observed maximum accelerations at the wing root were compared with those computed from an extension of Biot and Bisplinghoff's anal-

ysis, which involved the computation of response factor curves for acceleration. The computed acceleration, using a response factor given by the envelope to these curves, was 16 to 56 percent greater than the measured acceleration. Use of the most closely fitting impact curve reduced this error to 8 to 43 percent. It should be noted in this connection that larger differences may be expected at the wing tips, since these are more affected by flexural vibrations.

The more exact analysis for one of the impacts showed that the neglect of phase differences caused an error in computed maximum accelerations at the root of about 23 percent. This error would probably be much greater for acceleration at the wing tip.

The authors thank their colleagues Samuel Levy, for the analysis reported in this paper, and Eileen D. Segal, for the numerical computations of dynamic response.

VII. References

[1] M. A. Biot and R. L. Bisplinghoff, Dynamic loads on airplane structures during landing, NACA Wartime Report W-92 (Oct. 1944).

[2] E. G. Keller, J. App. Mech. **11,** No. 4, A-219 to A-228 (1944).

[3] Alexander J. Yorgiadis, J. Inst. Aero. Sci. **12,** No. 4, 421 (1944).

[4] W. J. Duncan and A. R. Collar, Phil. Mag. Ser. **7,** [17], No. 115, 866 (1934).

[5] Walter Ramberg and Samuel Levy, NBS J. Research **21,** 639 (1938) RP 1148.

[6] J. M. Frankland, Effects of impact on simple elastic structures, David W. Taylor Model Basin, Report 481 (1942).

Washington, July 9, 1948.

U. S. Department of Commerce
National Bureau of Standards

Research Paper RP1937
Volume 41, November 1948

Part of the Journal of Research of the National Bureau of Standards

Copolymerization [1]

By Robert Simha and Leo A. Wall

A critical discussion of the mechanism of formation of copolymers by addition polymerization is presented. It deals mainly with the following three fundamental aspects: First, the quantitative treatment of the reaction starting with a scheme consisting of initiation, growth, and termination mechanisms. Expressions for the instantaneous and total copolymer composition and for the over-all rate of reaction as function of monomer composition and of conversion are derived in terms of quantities characteristic of the reaction. Graphical and numerical methods for the determination of these parameters from experimental data are given in detail. The statistical distribution of molecular weights and compositions in the product is considered in relation to the constants of the reaction and to the analogous case of simple polymers.

Second, methods for the analysis of copolymer compositions are discussed and experimental results are summarized. Reactivity ratios describing the behavior in growth of a given radical toward a pair of monomers are tabulated for a series of systems.

Third, these results are interpreted on the basis of resonance and of electrostatic and steric effects as encountered in the study of certain organic reactions.

In addition, degradation of copolymers is briefly considered in the light of the possible types of sequences in the chain. A numerical relation between yield and copolymer composition is derived.

The problems remaining are principally the following: Experimental methods of copolymer analysis, determination of over-all rates of reaction and of individual rate constants, and a more fundamental correlation between structure of monomers and behavior in copolymerization. Also, systematic data on the thermodynamic and rate properties of copolymer solutions should be of great interest, and studies of the bulk properties and their relation to copolymer structure represent a field where research has only recently been initiated.

I. Introduction

Following the extensive experimental and theoretical attack on the general problem of chain polymerization reactions, recent years have brought a series of fundamental investigations regarding copolymerization reactions. A framework for the analysis of over-all monomer consumption and resulting change in average polymer composition has been created [1, 18, 26, 31] [2] and tested experimentally [5, 18]. Equations for the size and composition distributions have also been developed [26, 28]. However, no systematic experimental results on such distributions are available at present. Finally, interpretations of the differences in relative reactivities have been made on the basis of the electronic structure of the individual monomers [15, 24]. It is the purpose of this article to review the main points of these theoretical and experimental investigations. In respect to the former, stress will be laid on those aspects which also have been examined experimentally.

[1] This article is scheduled to appear as a chapter in a forthcoming American Chemical Society Monograph, published by the Reinhold Publishing Co., New York, N. Y.

[2] Figures in brackets indicate the literature references at the end of this paper.

II. List of Important Symbols

A, B = respective numbers of monomer molecules of copolymerizing species. Also used to indicate species.

A_0, B_0 = initial values of A and B.

z = ratio A/B.

z_0 = initial value of z.

C = catalyst concentration.

$n_{rs}(A)$ = number of radical chains with an active A-end containing r A-units and s B-units.

$n_{rs}(B)$ = number of radical chains with an active B-end, containing r A-units and s B-units.

A^* = total number, $\sum_{r,s} n_{rs}(A)$ of radical chains with an active A-end.

B^* = total number, $\sum_{r,s} n_{rs}(B)$ of radical chains with an active B-end.

N_{rs} = number of stable polymer chains contain r A-units and s B-units.

I_A = first order rate constant for initiation of monomer species A.

I_B = first order rate constant for initiation of monomer species B.

I = rate constant for production of radicals from catalyst.

$k_{sA}(A)$ = rate constant for propagation by addition of A-monomer to a radical with an active A-end.

$k_{sB}(A)$ = rate constant for propagation by addition of B-monomer to a radical with an active A-end.

$k_{sA}(B)$ = rate constant for propagation by addition of A-monomer to a radical with an active B-end.

$k_{sB}(B)$ = rate constant for propagation by addition of B-monomer to a radical with an active B-end.

$k_{sA}(r,s,A)$ = rate constant for propagation defined in the same manner as $k_{sA}(A)$ above, but dependent on composition r,s of growing radical.

$k_t(A, A)$ = rate constant for mutual termination of two radicals with active A-ends.

$k_t(A, B)$ = rate constant for mutual termination of two radicals with active A- and B-ends, respectively.

$k_t(B, B)$ = rate constant for mutual termination of two radicals with active B-ends.

σ = reactivity ratio $k_{sA}(A)/k_{sB}(A)$

μ = reactivity ratio $k_{sB}(B)/k_{sA}(B)$

$V_A + V_B$ = over-all rate of copolymerization per unit number of radicals.

w_p = total weight of polymer at a given instant.

w_0 = initial weight of monomer.

l = degree of polymerization of radical or stable polymer.

y = composition deviation of individual chain from the mean.

$w(l, y)$ = distribution function of composition and chain length expressed as weight fraction in terms of above quantities l and y.

λ = number of average degree of polymerization of radical chains.

$P_i(A)$ = probability of occurence of i A-units in succession in a copolymer chain.

$P_i(B)$ = probability of occurence of i B-units in succession in a copolymer chain.

$\omega(A)$ = probability of formation of an A-A linkage by propagation.

$\omega(B)$ = probability of formation of B-B linkage by propagation.

III. Quantitative Treatment

1. General Remarks on Chain Polymerization Reactions

It is well established today that initiation, growth, and termination are the principal, although not necessarily the only mechanisms that determine the kinetics of chain polymerization reactions. The rates of these individual steps vary widely. The growth reaction is the fastest. The initiation, which produces, by one means or another, out of a stable monomer an activated radical is by far the slowest step, whenever long chains are formed. Otherwise, the supply of active monomer would be too large compared with the demand of the growth reaction for stable monomer.

The crucial step then, to begin with, is the production of a certain number of radicals able to grow before they are terminated. Their total concentration is determined by the initiation and termination only, since the growth merely changes their molecular weight. If they are terminated much faster than they are produced, an equilibrium is established. The exact condition for this to be true requires the mean life time of the active radicals to be small in comparison with that of stable monomer. This defines a quasistationary state and allows the expression of the "steady state" concentration of free radicals by means of an "equilibrium" constant given by the ratio

$$\text{Equilibrium constant} = \frac{\text{rate of production of free radicals}}{\text{rate of destruction of free radicals}}$$

This additional, and in most cases of interest, valid assumption simplifies considerably the quantitative treatment. It is then possible to develop completely the kinetics of the polymerization reaction and the resulting molecular size distribution [12] on the basis of a postulated reaction mechanism.

It will be shown here how to carry this program through when two or more competing monomer species are present. Additional problems then arise. One of the most important questions is concerned with the change in average polymer composition with changing composition of monomer residue. The mean composition depends on the relative rate with which the different

species enter the growing chain and hence, upon the relative growth rates, if we exclude the insignificant number of dimers, trimers, and other very short chains. In addition to the inhomogeneity in respect to chain length necessarily occuring in polymerizing systems, there will now exist also fluctuations of the composition from chain to chain. These fluctuations depend upon those in the long chain radicals. All three steps are essential for the determination of the distribution curves.

2. Basic Reaction Scheme and Equations

After these general remarks, we turn to the treatment of the copolymerization of a binary system, assuming the simplest possible reaction scheme, as indicated above. No kinetic studies exist at present that would necessitate the consideration of additional elementary acts, as is the case for one-component systems. In view of what was said previously this would not effect the calculation of average polymer compositions. In what follows, let $n_{rs}(A)$ be the number of growing radical chains, each of which contains altogether r units of component A and s units of component B, while having an activated end consisting of an A-type monomer. $n_{rs}(B)$ is then correspondingly defined. N_{rs} represents the number of stabilized chains of specified composition. C is a catalyst molecule and R a radical produced by its decomposition. The following scheme may then be considered.

Initiation:

$$A \xrightarrow{I_A} n_{10}(A)\,;\quad B \xrightarrow{I_B} n_{01}(B)$$
$$C \xrightarrow{I} 2R$$

Growth:

$$\left.\begin{aligned} n_{rs}(A) + A &\xrightarrow{k_{gA}(A)} n_{r+1,s}(A) \\ n_{rs}(A) + B &\xrightarrow{k_{gB}(A)} n_{r,s+1}(B) \\ n_{rs}(B) + A &\xrightarrow{k_{gA}(B)} n_{r+1,s}(A) \\ n_{rs}(B) + B &\xrightarrow{k_{gB}(B)} n_{r,s+1}(B) \end{aligned}\right\} \quad (1)$$

Termination:

$$\left.\begin{aligned} n_{rs}(A) + n_{ik}(A) &\xrightarrow{k_t(A,A)} N_{r+i,s+k} \text{ or } N_{rs}+N_{ik} \\ n_{rs}(A) + n_{ik}(B) &\xrightarrow{k_t(A,B)} N_{r+i,s+k} \text{ or } N_{rs}+N_{ik} \\ n_{rs}(B) + n_{ik}(B) &\xrightarrow{k_t(B,B)} N_{r+i,s+k} \text{ or } N_{rs}+N_{ik} \end{aligned}\right\}$$

In writing the initiation equation we have considered two types of activation. In the catalyzed activation the elementary act consists in a decomposition of the catalyst C. In the equations for growth and termination, we have differentiated between A-A, A-B, B-A, and B-B addition of monomer to radical and radical to radical, respectively. The rates of consumption of monomer are given according to eq 1 by

$$-\frac{1}{A}\frac{dA}{dt} = I_A + k_{gA}(A)\sum_{r,s} n_{rs}(A) + k_{gA}(B)\sum_{r,s} n_{rs}(B)$$
$$-\frac{1}{B}\frac{dB}{dt} = I_B + k_{gB}(A)\sum_{r,s} n_{rs}(A) + k_{gB}(B)\sum_{r,s} n_{rs}(B). \quad (2)$$

The terms I_A and I_B are omitted for a catalyzed polymerization. Otherwise, they are small and can be neglected in comparison with the growth terms in eq 2. The summations are carried out over all values of r and s. The concentrations of free radicals $\Sigma n_{rs}(A)$ and $\Sigma n_{rs}(B)$ in a steady state obey the following relations if the initiation term is omitted:

$$\frac{d\sum n_{rs}(A)}{dt} = k_{gA}(B)A\sum n_{rs}(B) - k_{gB}(A)B\sum n_{rs}(A) - k_t(A,A)\sum n_{rs}(A)\sum n_{ik}(A) - k_t(AB)\sum n_{rs}(A)\sum n_{ik}(B) = 0. \quad (3)$$

An analogous equation results for $\Sigma n_{rs}(B)$. Equation 3 expresses the fact that A-type radicals are produced by addition of A-type monomer to B-type radicals, and they are destroyed by adding B-type monomer and by termination with an A- or B-type radical. The terms contributed by the chain-breaking reaction are small compared with the growth terms in eq 3, if long chains are to be formed. Hence, they may be neglected, and we obtain the simple relation:

$$\sum n_{rs}(A) = \frac{k_{gA}(B)A}{k_{gB}(A)B}\sum n_{rs}(B). \quad (3a)$$

It expresses the fact that free radicals with an active end A are produced as rapidly by addition of monomer A to free radicals with an active end B as they are destroyed by addition of monomer B to free radicals with an active end A.

3. Compositional Relationships: Average Composition, Relation to Conversion

Insertion of eq 3a into eq 3 leads to the following

relation for the change in composition of monomer residue:

$$\frac{dA}{dB}=\frac{A\,k_{gA}(B)\,k_{gA}(A)A+k_{gB}(A)B}{B\,k_{gB}(A)\,k_{gA}(B)A+k_{gB}(B)B}. \quad (4)$$

It has been assumed in eq 1 that the rate constants are essentially independent of chain length, an assumption commonly made in chain polymerization reactions and shown to be true in polycondensation reactions [11].[3] Furthermore, they are independent of chain composition r,s in eq 1. Herington and Robertson [12] have established equations that allow in principle a deduction of such a dependence from molecular-weight distributions. Analogous relations for copolymerizing systems have been developed by Simha and Branson [26]. However, the equations are too complex and experimental results nonexistent to merit further discussion here. It may be noted only that eq 4 is unaffected by any such assumption. If the growth rates depend upon the composition, then the constants $k_{gL}(M)$ in eq 4 represent mean values averaged over the radicals $n_{rs}(M)$ with the particular end M, that is, for instance:

$$k_{gA}(A)=\frac{\sum k_{gA}(r,s,A)n_{rs}(A)}{\sum n_{rs}(A)}$$

$$k_{gA}(B)=\frac{\sum k_{gA}(r,s,B)n_{rs}(B)}{\sum n_{rs}(B)}.$$

Equation 4 gives the relative rates of consumption of the two monomer species A and B under the approximations stated previously. It also represents the instantaneous average composition of copolymer formed at an instant in which the monomer residue consisted of A moles of species one and B moles of species two. This composition can not depend on the absolute magnitude of the growth rates k_g but only upon the relative rates of addition of each monomer species. Hence, the following parameters are defined [18:]

$$\begin{bmatrix}A+A\\A+B\end{bmatrix}=\sigma=\frac{k_{gA}(A)}{k_{gB}(A)},\quad \begin{bmatrix}B+B\\B+A\end{bmatrix}=\mu=\frac{k_{gB}(B)}{k_{gA}(B)}. \quad (5)$$

The symbols in the brackets indicate the modes of addition to which the constants σ and μ refer.[4]

Both parameters express the growth rate by means of addition of monomer of the same kind to an activated end relative to the addition of monomer of the other kind. Defining furthermore the mole ratio A/B as z, eq 4 is transformed into

$$\frac{dA}{dB}=z\frac{(\sigma z+1)}{(z+\mu)} \text{ or } \frac{dA}{dA+dB}=\left[1+\frac{1}{z}\frac{(z+\mu)}{(\sigma z+1)}\right]^{-1}. \quad (4a)$$

Figures 1, 2, and 3 show plots of eq 4a as a function of the mole fraction $A/A+B$ in the monomer residue for a set of various values of the parameters σ and μ. The straight line corresponds to a situation in which monomer composition and instantaneous polymer composition are

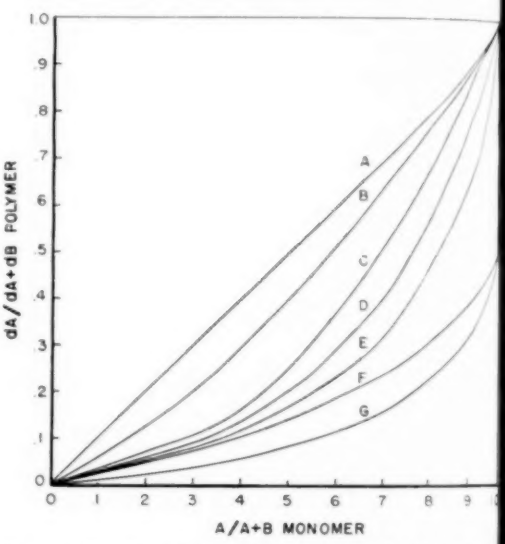

FIGURE 1. *Plot of instantaneous mole fraction of component A in polymer as function of mole fraction of A in monomer mixture.*

A, $\mu=1$, $\sigma=1$; B, $\mu=2$, $\sigma=1$; C, $\mu=5$, $\sigma=1$; D, $\mu=5$, $\sigma=\frac{1}{2}$; E, $\mu=5$, $\sigma=\frac{1}{5}$; F, $\mu=5$, $\sigma=0$; G, $\mu=10$, $\sigma=0$.

always equal. That is, σ and μ must both equal unity. In some instances, (figs. 2 and 3) it will be noted that the curves intersect the diagonal, indicating that for a particular monomer charge the above-mentioned equality between the two compositions holds true. The meaning of this special case is discussed below. It is easy to visualize the limiting trends of these curves. For instance, large μ and small σ, that is, preferential B-B and A-B addition must have the effect of

[3] H. W. Melville (lecture presented at the National Bureau of Standards on April 11, 1947) finds that growth and termination rates decrease but slightly with increasing chain length in the polymerization of vinyl acetate in the liquid phase.

[4] Various other symbols have been used for the ratios denoted here by σ and μ, namely, $1/\alpha, \beta$ [1], σ, ρ [3], α, β[28], r_1, r_2 (T. Alfrey, F. R. Mayo F., T. Walt, J. Polymer Sci. 1, 581 (1946).

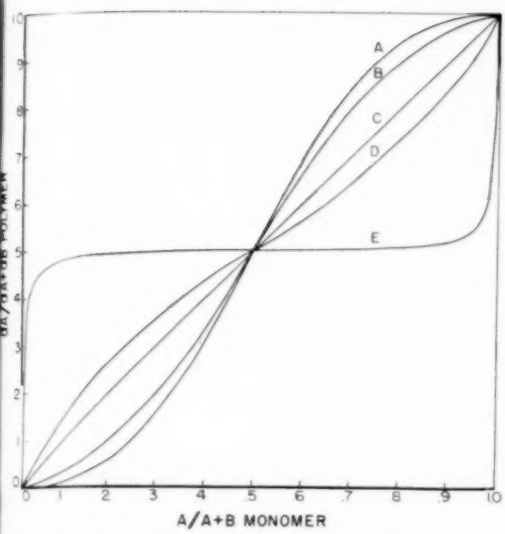

FIGURE 2. *Plot of instantaneous mole fraction of component A in polymer as function of mole fraction of A in monomer mixture.*

A, $\mu=\sigma=100$; B, $\mu=\sigma=5$; C, $\mu=\sigma=1$; D, $\mu=\sigma=0.5$; E, $\mu=\sigma=0.01$.

producing a copolymer deficient in A up to relatively high percentages of A in the monomer. The corresponding plots in figure 1 must therefore be of the type of F or G. If both σ and μ are very small, the copolymer will be predominantly of the alternating type and $dA/dA+dB$ will be close to 0.5 over a wide range of monomer composition, as shown in curve E of figure 2. Finally, if both σ and μ are very large no copolymer is formed, except in a very narrow range around $A/A+B=0.5$, where there occurs a transition from pure polymer B to pure polymer A. Curve A in figure 2 illustrates the approach to this situation. In principle, it is possible to determine from graphs of this type the values of the constants σ and μ, if the limiting slopes when A and B, respectively, approach zero are known. Substitution of $A/A+B=z/z+1$ into eq 4a leads to the result

$$\lim d\left[\frac{dA}{dA+dB}\right]\Big/d\left[\frac{A}{A+B}\right]=\begin{cases}\frac{1}{\mu}; \text{ when } \frac{A}{A+B}\to 0,\\ \frac{1}{\sigma}; \text{ when } \frac{A}{A+B}\to 1\end{cases} \tag{4b}$$

Integration of eq 4a gives the number of moles of monomer B left at any instant of the reaction as function of the composition z of the residue, namely,

$$\ln\frac{B_0}{B}=\frac{\mu}{\mu-1}\ln\frac{z}{z_0}+\frac{1-\sigma\mu}{(1-\sigma)(1-\mu)}\ln\frac{(\sigma-1)\,z-(\mu-1)}{(\sigma-1)\,z_0-(\mu-1)} \tag{6}$$

where B_0 and z_0 are the initial values of B and z. This equation forms at present the basis for the determination of the parameters σ and μ from an analysis of the copolymer composition. Applications will be discussed in the next section. First, however, we shall consider some general properties of the function represented by eq 6. Figure 4 shows a series of plots of log B_0/B versus log z/z_0 for fixed values of $z_0=0.4$ and $\mu=5$. If the rates of addition are independent of the nature of the active ends, $\sigma=1/\mu$, and a straight line is obtained. If active ends A increasingly favor the addition of monomer B, and ends B also favor the addition of B-type monomer ($\mu=5$), the lines are still practically straight. The slopes become smaller due to the slower disappearance of monomer A, although the variations are small and hence determinations of μ from such plots inaccurate.

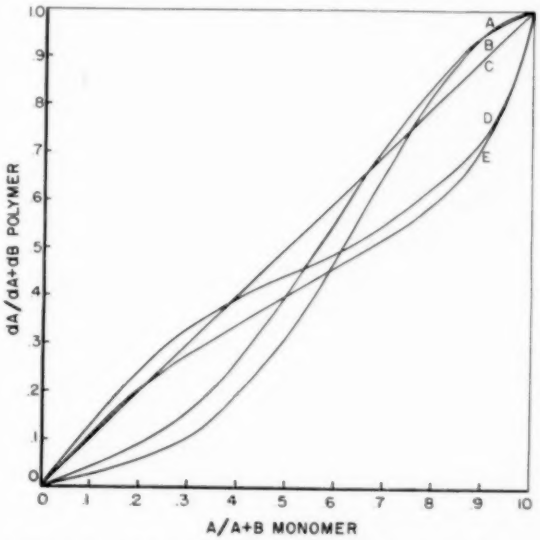

FIGURE 3. *Plot of instantaneous mole fraction of component A in polymer as function of mole fraction of A in monomer mixture.*

A, $\mu=10$, $\sigma=4$; B, $\mu=5$, $\sigma=3$; C, $\mu=1$, $\sigma=1$; D, $\mu=0.5$, $\sigma=0.2$; E, $\mu=0.8$, $\sigma=0.2$.

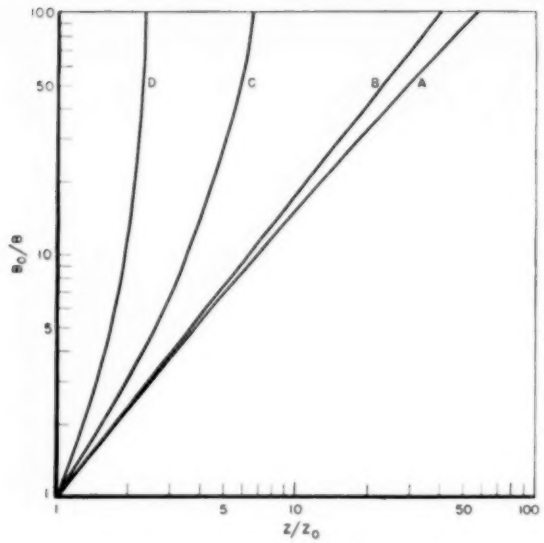

FIGURE 4. *Plots of log B_0/B vs log z/z_0.*
$z_0=0.4$; $\sigma=5$. A, $\sigma=0$; B, $\sigma=1/\mu$; C, $\sigma=2$; D, $\sigma=5$.

The final polymer formed consists, in these examples, entirely of species A, $z=\infty$, for $B=0$. When $\mu>1$ and $\sigma>1$, A-A and B-B linkages are more probable than cross-overs. The corresponding curves exhibit an upward curvature and possess a vertical asymptote shifting to the left as σ increases. In other words, the final polymer formed is a copolymer of fixed composition. Under such conditions the ratios between the rates balance the concentration ratios in the monomer residue in such a way that the polymer composition equals the composition of the monomer mixture or

$$\frac{dA}{dB}=\frac{A}{B}.$$

Relation 4a then gives for the critical composition z_c

$$z_c=\frac{\mu-1}{\sigma-1}. \tag{7}$$

Thus σ and μ must both be either smaller or larger than unity.

The fact that there exists a mixture of definite composition that copolymerizes without changing its composition, suggests an analogy with the familiar azeotropic mixtures often encountered in distillation processes [31]. One can construct curves analogous to distillation curves by considering the sum of the rates of consumption of

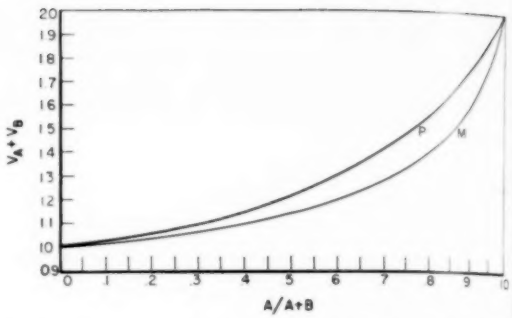

FIGURE 5. *Plot of over-all rate for unit concentration of radical V_A+V_B on an arbitrary scale vs mole fraction of A in monomer (M) and in polymer (P).*
$k_{gA}(A)=2k_{gB}(B)$; $\mu=1.5$; $\sigma=0.5$.

each monomer species as a function of the composition. Specifically, one may plot the over-all rate of polymerization V_A+V_B for unit concentration of free radicals [31]:

$$V_A+V_B=-\frac{1}{A+B}\frac{d}{dt}(A+B)\frac{1}{\sum n_{rs}(A)+\sum n_{rs}(B)}$$

By combining eq 2 and 3a the following result is obtained:

$$V_A+V_B=\frac{z(\sigma z+1)+z+\mu}{z+1}\cdot\frac{1}{\dfrac{\sigma z}{k_{gA}(A)}+\dfrac{\mu}{k_{gB}(B)}}.$$

Figures 5 and 6 show such plots, assuming A-A addition to be twice as fast as B-B growth. The curves for the polymer (P) are constructed from eq

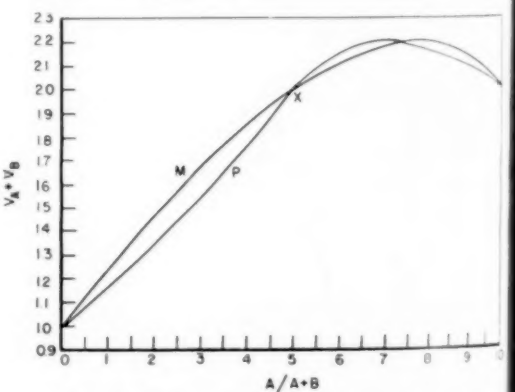

FIGURE 6. *Plot of V_A+V_B on an arbitrary scale vs mole fraction of A in monomer (M) and in polymer (P), showing "azeotropic" composition X.*
$k_{gA}(A)=2k_{gB}(B)$; $\mu=\sigma=0.5$.

a. The curves for the monomer (M) represent V_A+V_B as a function of $A/A+B=z/z+1$, according to the expression above. The abcissas of conjugate points on the two lines P and M indicate the composition of the copolymer and the composition of the corresponding monomer residue, respectively. Figure 6 depicts an "azeotrope." It will be noted that here the composition X does not correspond to an extremum in the curves, which represents a necessary thermodynamic condition for azeotropic boiling mixtures. Clearly the second intersection in figure 6 does not indicate a common composition for polymer and monomer. The discussion of these curves follows otherwise familiar lines. If μ and σ are both smaller than unity, that is, if cross-combinations are preferred, one derives from eq 6 that z never reaches the critical value z_c but approaches zero or infinity, depending on whether z_0 is respectively smaller or greater than z_c. If both reactivity ratios exceed unity, then the azeotropic composition is gradually approached.

It is of interest to follow the changes in composition taking place in the course of the copolymerization. Figure 7 depicts the relation between the instantaneous and total copolymer composition and the percentage conversion. Such curves are computed in the following manner. The extent of reaction, that is, the ratio between

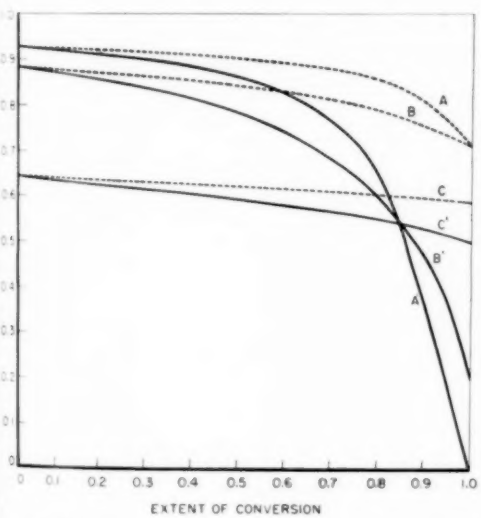

FIGURE 7. *Instantaneous (full lines) and total composition (dashed lines) as function of the extent of conversion.*
A, A', $\mu=5, \sigma=1/\mu, z_0=0.4$; B, B', $\mu=5, \sigma=2, z_0=0.4$; C, C', $\mu=5, \sigma=\mu, z_0=0.7$.

the weight of polymer at a given instant and the initial weight of the monomer mixture is given by the equation:

$$\frac{w_p}{w_0}=\frac{\left(1-\frac{B}{B_0}\frac{z}{z_0}\right)M_1 z_0+\left(1-\frac{B}{B_0}\right)M_2}{M_1 z_0+M_2} \qquad (8)$$

B/B_0 and z/z_0 have the same meaning as in eq 6. M_1 and M_2 are the molecular weights of the two monomers. With the aid of eq 6, B/B_0 can be eliminated and w_p/w_0 obtained as function of z/z_0. The instantaneous copolymer composition is directly given by eq 4a. The total composition resulting up to a given instant equals:

$$\int_0^{w_p}\frac{dB}{dA+dB}\,dw_p=\frac{1-\frac{B}{B_0}}{(z_0+1)-\frac{B}{B_0}(z+1)}, \qquad (9)$$

and is again obtained with the aid of eq 6. As is obvious, the difference between instantaneous and total values increases with time and is more pronounced for systems with widely different reactivity ratios. In case an azeotrope exists, and the initial composition has been suitably chosen, the changes are slight as shown in curves C and C'. On the whole, the total copolymer composition does not change very much over a wide range of conversion. These variations can be eliminated by compensatory addition of the more active species during the course of the polymerization.

4. Over-all rate of reaction

It is evident that the calculation of the average copolymer composition does not require a knowledge of the total concentration of free radicals but merely the ratio of A- and B-type radicals. For the over-all reaction rate, however, this information is required and obtained in the following manner. In a steady state and for the simplest case of a catalyzed reaction, we can write

$$\frac{d}{dt}(A^*+B^*)=IC-k_t(A,A)A^{*2}-2k_t(A,B)A^*B^*-k_t(B,B)B^{*2}=0, \qquad (3b)$$

where

$$A^*=\sum n_{rs}(A) \qquad B^*=\sum n_{rs}(B)$$

Combination of eq 3a, 3b, and 2 then leads to the

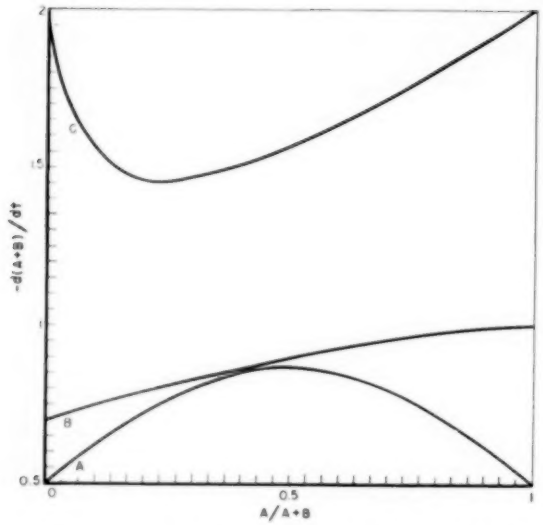

FIGURE 8. *Plots of copolymerization rate on an arbitrary scale vs composition of monomer mixture according to eq 2a.*

A, $\beta=\gamma=1$, $\mu=\sigma=0.5$, scale multiplied by 4; B, $\beta=\gamma=2$, $\mu=\sigma=1$; C, $\beta=1$, $\gamma=1.6$, $\mu=0.5$, $\sigma=2$.

following expression for the over-all rate of copolymerization [26]:

$$-\frac{d}{dt}(A+B)=\alpha\frac{\sigma A^2+2AB+\mu B^2}{(A^2+\beta AB+\gamma B^2)^{\frac{1}{2}}}, \tag{2a}$$

where:

$$\alpha=\left[\frac{IC}{k_t(A,A)}\right]^{\frac{1}{2}}k_{gB}(A);\beta=\frac{2\mu}{\sigma}\frac{k_{gA}(A)}{k_{gB}(B)}\frac{k_t(A,B)}{k_t(A,A)};$$

$$\gamma=\frac{\mu^2}{\sigma^2}\left[\frac{k_{gA}(A)}{k_{gB}(B)}\right]^2\frac{k_t(B,B)}{k_t(A,A)}=\left(\frac{\beta}{2}\right)^2\frac{k_t(A,A)k_t(B,B)}{k_t(A,B)^2}.$$

It should be noted again that in this derivation the initiation is described by a single constant I. This restricts the generality of this equation. For it is possible that the rate of production of the initial radicals varies with the composition of the mixture. In the most general case of the reaction scheme described, nine constants altogether would be needed to describe the process completely. As is to be expected under the assumptions made, the rate is proportional to the square root of the catalyst concentration, a familiar result in polymerization kinetics. Equation 2a contains besides σ and μ, three constants. A knowledge of these allows a determination of the product

$$k_t(A,A)k_t(B,B)/k_t(A,B).$$

No use has as yet been made of these relations. Rate studies on the system styrene-methyl methacrylate have been presented by Norrish and Brookman [21]. However, they have been interpreted on the basis of an equation that assumes the concentrations A^* and B^* to be independent of the monomer ratio z. Plots of the rate (eq 2a) as function of the monomer composition A are shown in figure 8 for a few extreme cases.

5. Composition, Size, and Intramolecular Sequence Distributions

For the considerations hitherto presented, it is necessary only to know the total concentrations of radicals $\Sigma n_{rs}(A)$ and $\Sigma n_{rs}(B)$, regardless of size and composition. In order to obtain the distribution of polymer sizes and compositions, we must consider the mode of production of individual radical chains of specified chain length and composition. From the postulated mechanism (eq 1) we find for the rate of production of these radicals

$$\begin{aligned}\frac{dn_{rs}(A)}{dt}=&k_{gA}(A)A n_{r-1,s}(A)+k_{gA}(B)A n_{r-1,s}(B)-\\&k_{gA}(A)A n_{rs}(A)-k_{gB}(A)B n_{rs}(A)-\\&k_t(A,A)n_{rs}(A)\Sigma n_{ik}(A)-\\&k_t(A,B)n_{rs}(A)\Sigma n_{ik}(B)\end{aligned} \tag{3c}$$

$$\begin{aligned}\frac{dn_{rs}(B)}{dt}=&k_{gB}(B)B n_{r,s-1}(B)+k_{gB}(A)B n_{r,s-1}(A)-\\&k_{gB}(B)B n_{rs}(B)-k_{gA}(B)A n_{rs}(B)-\\&k_t(B,B)n_{rs}(B)\Sigma n_{ik}(B)-\\&k_t(A,B)n_{rs}(B)\Sigma n_{ik}(A).\end{aligned}$$

Equation 3c may be compared with the corresponding eq 3 for the total concentrations of A- and B-radicals and interpreted in the same manner. The positive terms refer to the growth of smaller chains to the desired size by monomer addition, and the negative ones measure the rate of disappearance of the radicals in question by either further growth or termination. Equation 3c holds for r and s both larger than unity. The rate of production of species n_{10} (A) and n_{01} (B) is governed by the rate of initiation such that in the first set of eq 3c the positive terms are replaced by $I_A A$ and in the second one by $I_B B$ or corresponding expressions involving the catalyst concentration. In a steady state the left-hand side

of eq 3c vanish. The following quantities may be defined:

$$\omega(A)=\frac{k_{gA}(A)A}{k_{gA}(A)A+k_{gB}(A)B+k_t(A,A)\Sigma n_{tk}(A)+k_t(A,B)\Sigma n_{tk}(B)}$$

$$\omega(B)=\frac{k_{gB}(B)B}{k_{gB}(B)B+k_{gA}(B)A+k_t(B,B)\Sigma n_{tk}(B)+k_t(A,B)\Sigma n_{tk}(A)}$$

$$x=\frac{k_{gB}(A)k_{gA}(B)}{k_{gA}(A)k_{gB}(B)}=\frac{1}{\sigma\mu}.$$

It will be noted that $\omega(A)$ represents the probability of formation of an A-A linkage by propagation, $\omega(B)$ that of a B-B bond. x measures the probability of occurrence of B–A and A–B linkages relative to that of A–A and B–B bonds. The solution of eq 3c has been shown by Simha and Branson [26] to be

$$n_{rs}(A)=\left[\frac{I_A}{k_{gA}(A)}\sum_{j\geq 1}\binom{r-1}{j}\binom{s-1}{j-1}x^j+\frac{I_B}{k_{gB}(A)}\sum_{j\geq 1}\binom{r-1}{j-1}\binom{s-1}{j-1}x^j\right]\omega(A)^r\omega(B)^s$$

$$n_{rs}(B)=\left[\frac{I_A}{k_{gA}(B)}\sum_{j\geq 1}\binom{r-1}{j-1}\binom{s-1}{j-1}x^j+\frac{I_B}{k_{gB}(B)}\sum_{j\geq 1}\binom{r-1}{j-1}\binom{s-1}{j}x^j\right]\omega(A)^r\omega(B)^s. \quad (3d)$$

Equation 3d may be interpreted in the following manner [26]: The terms multiplied by I_A give the total number of possibilities of producing a chain of specified composition by initiation through an A-radical. For each combinatory factor in the sum is a measure of the number of ways in which one possible internal arrangement characterized by a fixed number of A–A, B–B, A–B and B–A configurations may be realized by permutations. The exponential factors indicate the probability of occurrence of these configurations. The summation is then carried out over all possible internal arrangements compatible with the condition of having r A-units and s B-units. It is taken between the extremes of having one long sequence of A-units followed by one sequence of B-units, ($j=1$), and the opposite extreme of a checker board arrangement of these two monomers. The I_B terms then stand for chains initiated by a B-radical. The meaning of the last equation may be seen also by specializing to the case $\sigma\mu=1$, in which propagation is independent of the nature of the growing end. Equation 3d then reduces to [10]

$$n_{rs}=n_{rs}(A)+n_{rs}(B)=\left[\frac{I_A}{k_{gA}(A)}\binom{r+s-1}{s}+\frac{I_B}{k_{gB}(B)}\binom{r+s-1}{r}\right]\omega(A)^r\omega(B)^s. \quad (3e)$$

Clearly the first term enumerates all ways of obtaining the polymer n_{rs} from a nucleus n_{10}; the second term from a nucleus n_{01}.

From the known radical distribution, eq 3d, we obtain the distribution of stable polymer by means of the relations:

Combination:

$$\frac{dNrs}{dt}=k_t(A,A)\sum_{t,k}n_{r-t,\,s-k}(A)n_{tk}(A)+2k_t(A,B)\sum_{t,k}n_{r-t,\,s-k}(A)n_{tk}(B)+k_t(B,B)\sum_{t,k}n_{r-t,\,s-k}(B)n_{tk}(B).$$

Disproportionation:

$$\frac{dNrs}{dt}=n_{rs}(A)[k_t(A,A)\sum n_{tk}(A)+k_t(A,B)\sum n_{tk}(B)]+n_{rs}(B)[k_t(B,B)\sum n_{tk}(B)+k_t(A,B)\sum n_{tk}(A)] \quad (10)$$

Equation 10 determines the instantaneous distribution of sizes and compositions in a copolymer formed from a monomer mixture of a given composition $A/A+B$, which, in turn, determines the values of $\omega(A)$ and $\omega(B)$. If the rate of the reaction has been measured, integration then yields the total distribution obtained up to a given instant or degree of conversion.

For the practically important case of long chains eq 3d has been simplified by Stockmayer [28] in a manner analogous to that for simple polymers [12]. It will be noted that for the latter case ($s=0$), eq 3e reduces to

$$n_r=\frac{I}{k_g}\omega^r=\frac{I}{k_g}\left(\frac{A}{A+\frac{k_t}{k_g}\Sigma n_t}\right)^r,$$

the result obtained by Herington and Robertson [12] for the distribution of radical lengths. Its physical significance is obvious. Since ω deviates from unity only slightly because of the small concentration of radicals present, ω^r can, in a good approximation, be replaced for large r by $e^{-(1-\omega)r}$.

The final result is best expressed in terms of the number average chain length λ of radicals, which equals the ratio between the rate of reaction and the rate of production (or destruction) of radicals. Inserting this value and noting that the total concentration of radicals is obtained from an equation analogous to eq 3b, one finds for the fraction of radicals of specified size [12]:

$$\frac{n_r}{\Sigma n_i} = \frac{1}{\lambda} e^{-\frac{r}{\lambda}}.$$

To obtain the corresponding expressions for copolymers we denote the total chain length $r+s$ by l. Deviations in the composition of a chain from the average value as given by eq 4a will be measured by the quantity

$$y = \frac{r}{r+s} - \frac{dA}{dA+dB} = \frac{r}{l} - p_0. \qquad (11)$$

As we are concerned with large values of l, the sums in eq 3d may be approximated by integrals and the individual terms expressed by means of Stirling's formula. Considering that the deviation from the average composition will not be very large in long chains, one can furthermore expand the relevant expressions in terms of y. The final result may be expressed as a function of l and y [28]

$$w(l,y)dldy = \exp\left(-\frac{l}{\lambda}\right)\frac{l}{\lambda^2}dl \cdot \left[\frac{l}{2\pi p_0(1-p_0)\kappa}\right]^{\frac{1}{2}} \exp\left(-\frac{ly^2}{2p_0(1-p_0)\kappa}\right)dy, \qquad (12)$$

which gives the weight fraction of radicals with polymerization degrees between l and $l+dl$ and composition deviations between y and $y+dy$, irrespective of whether they terminate in A- or B-units. κ is defined by the relation

$$\kappa = [1-4p_0(1-p_0)(1-\sigma\mu)]^{\frac{1}{2}} = \frac{\sigma_A^2 + 2\sigma\mu_A AB + \mu_B B^2}{\sigma_A^2 + 2AB + \mu_B B^2}. \qquad (13)$$

It is a measure of the spread of the composition distribution. λ is again the number average degree of polymerization of radicals

$$\lambda = -\frac{d}{dt}(A+B)\cdot[k_t(A,A)A^{*2} + 2k_t(A,B)A^*B^* + k_t(B,B)B^{*2}]^{-1}, \qquad (14)$$

employing the notation of eq 3b and noting that the factor in the bracket represents the total rate of destruction of radicals which equals the rate of production in the steady state. The first factor the over-all rate of the reaction can be expressed as in eq 2a or by corresponding expressions for other reaction mechanisms. It is assumed in eq 12 that monomers A and B have equal molecular weights.

The instantaneous size distribution of the stable polymer follows from eq 10. If termination occurs by disproportionation, the weight fraction of copolymer in the specified range of l and y is directly given by eq 12. If a fraction ρ of the radical chains is terminated by combination, the weight fraction is obtained by multiplying eq 12 by a factor

$$1-\rho+\frac{\rho l}{2\lambda}.$$

Thus in the approximations used to simplify eq 3 and granted the validity of the reaction scheme and of eq 4, the distribution function consists of two factors. One characterizes the distribution of molecular weights and the other the distribution of molecular composition for a fixed molecular weight. The specific nature of the termination process affects the former factor, but not the composition distribution.

Finally, one derives from eq 12 the chain-length distribution irrespective of composition by integration over all compositions,

$$w(l)dl = \int_0^\infty w(l,y)dy\cdot dl = e^{-\frac{l}{\lambda}}\frac{l}{\lambda^2}dl. \qquad (12a)$$

Equation 12a has the same form as the result obtained for the instantaneous distribution in polymers produced by disproportionation [12]. The distribution of composition fluctuations is

$$w(y)dy = \int_0^\infty w(l,y)dl\cdot dy = \frac{3d\eta}{4(1+\eta^2)^{5/2}}$$

with

$$\eta = \left(\frac{\lambda}{2p_0(1-p_0)\kappa}\right)^{1/2} y. \qquad (12b)$$

Plots of the expression (eq 12) as function of the reduced variables l/λ and η are shown in figures 9 and 10, respectively, as presented by Stockmayer [28]. It will be noted that large values of η, i.e., large deviations from the average composition occur primarily in shorter chains, the longer chains

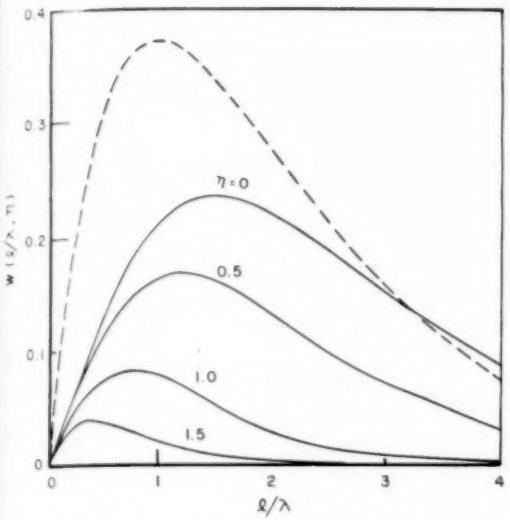

FIGURE 9. *Full lines: Chain length distribution, eq 12, (weight fractions), as function of reduced chain length l/λ for fixed values of the reduced composition deviation η.*
Dotted line: Chain length distribution, eq 12a, irrespective of chain composition.

having mainly the average composition. Finally, the composition distribution (eq 12b) is shown in figure 11 for different values of the parameter κ. With increasing value of κ, that is, increasing values of σ μ for a fixed p_0, the fluctuations in composition become larger. This is understandable, since in this instance self addition of A- and B-units becomes increasingly preferred. However, it will be seen that the deviations from the mean value $y=0$ are not large. Actually it can be derived from eq 12b that 88 percent by weight of the copolymer is found in the range $|y|<[2p_0(1-p_0)\kappa/\lambda]^{1/2}$, which is small for large values of λ. It should be noted again that application of these results to a complete copolymer product requires a knowledge of the complete reaction mechanism which determines the variation of the parameters λ and κ with average composition and conversion. No quantitative data seem to be available. Fractionation of various copolymer systems has actually indicated the existence of a dispersion in respect to composition [13, 17, 27].

The discussion of eq 3d has shown what is obvious, that even for a fixed composition in a given chain, there are a variety of possible internal arrangements of the species A and B in the chain corresponding to sequences of identical

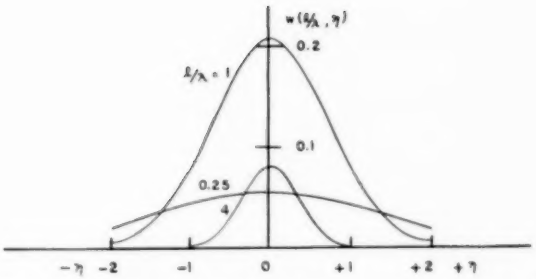

FIGURE 10. *Composition distribution, eq 12, as function of the reduced composition deviation η for fixed values of the reduced chain length l/λ.*

units of varying lengths. The frequency of occurrence of such sequences can be calculated and is of interest in connection with questions of structure [1,25,31] in copolymers. For sufficiently long chains the probabilities $P_i(A)$ and $P_i(B)$ of sequences of i A- or B-units produced by propagation are given by

$$\left.\begin{aligned} P_i(A) &= [1-\omega(B)][\omega(A)]^{i-1}[1-\omega(A)] \\ P_i(B) &= [1-\omega(A)][\omega(B)]^{i-1}[1-\omega(B)] \end{aligned}\right\} \quad i \geqq 1 \qquad (15)$$
$$P_0(A) = \omega(B);\ P_0(B) = \omega(A)$$

The ω's have the same meaning as in eq 3d, namely, that of propagation probabilities A-A and B-B. The validity of eq 15 is then immediately evident. Here the P_i's are normalized so as to represent fractions of the total number of A- or B-sequences, respectively. If based on the average concentration of A, $P_i(A)$ is multiplied by $dB/dA+dB$.

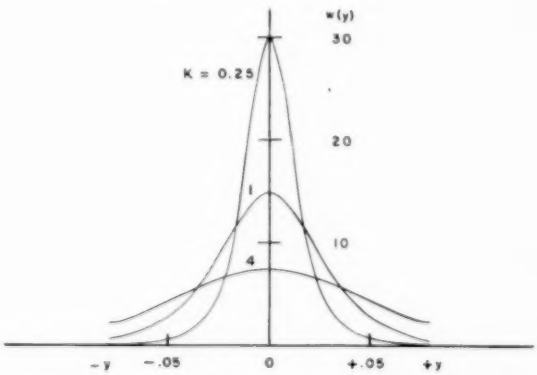

FIGURE 11. *Composition distribution, eq 12b, as function of the composition deviation y from the mean for fixed values of κ, eq 13, and assuming $\frac{\lambda}{2p_0(1-p_0)}=400$.*

If termination is effected by combination, the distribution (eq 15) of sequences in the radical chains is not strictly identical with that in the stable copolymer. Neglecting the effect of termination altogether, we simplify the equation for $\omega(A)$ and $\omega(B)$ to:

$$\omega(A)=\frac{\sigma A}{\sigma A+B};\ \omega(B)=\frac{\mu B}{A+\mu B} \qquad (16)$$

If the polymer in question has been obtained for instance, by copolymerizing mono and divinyl units, eq 15 gives the distribution of chain lengths between cross links and a number average chain

$$\frac{1}{1-\omega(A)}=1+\sigma\frac{A}{B},$$

length for a copolymer prepared from a monomer mixture containing B moles of cross-linking agent.

IV. Experimental Studies

1. Determination of Reactivity Ratios

The first thorough experimental investigation of copolymerization reactions has been made by Lewis, Mayo, and Hulse [15, 18], in which the parameters σ and μ were found for several pairs of monomers. As eq 6 cannot be solved readily for σ and μ, the following procedure was adopted: Equation 6 can be transformed into

$$\mu=\frac{\log\frac{B_0}{B}-\frac{1}{p}\log\frac{1-pz}{1-pz_0}}{\log\frac{z_0}{z}+\log\frac{B_0}{B}+\log\frac{1-pz}{1-pz_0}}, \qquad (6a)$$

where

$$p=(1-\sigma)/(1-\mu).$$

One experimental run gives a set of z,z_0 and B,B_0 values. Arbitrary values of p are then chosen, and the corresponding μ is computed using eq 6a. The value for σ is obtained from the expression for p. A plot of σ versus μ gives practically a straight line. A second run is utilized to get another σ-μ line. The intersection of two or more such curves then gives the unique values for σ and μ, satisfying theoretically all runs. In practice the intersection of three lines form a triangle, the area of which is a measure of the experimental errors. On this basis [18] table 1 and figure 12 represent, as an example, the best data obtained by Mayo and Lewis on the copolymerization of

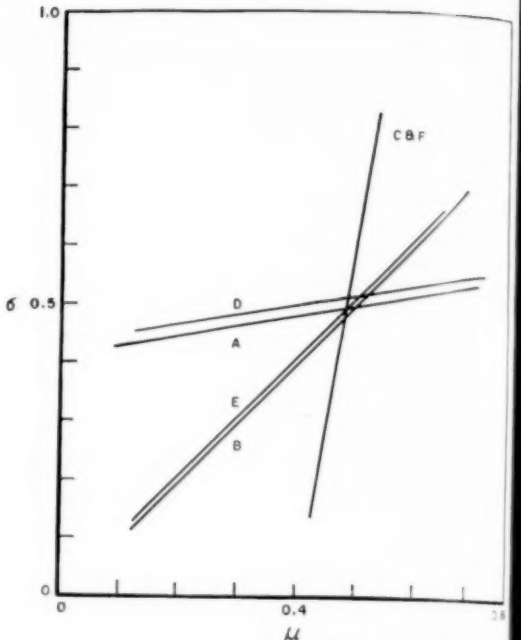

FIGURE 12. *Determination of μ and σ values from data in table 1.*

styrene and methyl methacrylate. The difficulties involved in the analysis of a partially polymerized system have been emphasized [14]. Separation of monomers from the polymer has been in most cases open to improvement. The usual techniques have been the precipitation of the polymer by suitable combinations of solvents and vacuum distillation. In general these methods do not adequately separate the polymers, as shown by the fact that the results obtained by the above workers [18] differed considerably, depending on the procedure used for the isolation of the polymer. The technique finally developed utilizes the relatively high vapor pressure of frozen benzene at temperatures near 0° C. This method, known as the frozen benzene technique, involves several precipitations, after which the polymer is dissolved in benzene and then the solution quickly frozen. Subsequently the benzene is sublimed off under vacuum. The polymer is then in the form of a very fine powder, which is easily handled. By using such means for the isolation of polymer, results [15] were produced that are very accurate for work of this nature.

Almost all of the monomer pairs so far studied

TABLE 1. *Styrene-methyl methacrylate copolymerization*

Experiment	Concentration of unreacted monomer				Reaction time	Polymer			σ	μ
	Original		Final							
	A_0	B_0	A	B						
					hr	*wt %*	*Carbon %*	*Carbon %*		
A	0.7980	0.2020	0.7435	0.1813	5	7.57	83.66	{83.77 83.94	0.48 to 0.50	0.48 to 0.50
B	.5010	.4990	.4571	.4556	5	8.74	76.52	76.61		
C	.2021	.7979	.1828	.7468	2.68	7.05	69.13	69.11		
D	.8064	.1936	.7450	.1796	89	7.53	83.98	84.00		
E	.5020	.4980	.4552	.4520	89	9.28	76.70	76.53	0.48 to 0.52	0.48 to 0.52
F	.1980	.8020	.1623	.7058	68.5	17.23	68.90	69.07		

have been those in which one monomer contained a different and easily analyzed element or group. In view of the availability and the high development of spectrometric and other physical methods of analysis [9, 16, 19], there is room for techniques using these methods for the study of copolymerization. Instead of analyzing the polymer, it should be possible to determine directly the composition of the monomer residue. One could place a sample of a polymerizing mixture in a high vacuum system and remove monomers from polymer by pumping off volatiles into a large residual volume or condensing in a liquid air trap. Then the volatiles could be analyzed by either mass, infrared, or ultraviolet spectrometry, depending on the nature of the system. An analysis of a relatively large bulk of residual monomers should be less subject to errors due to small amounts of monomers trapped in the polymer than an analysis of the polymer itself at low conversion. Such procedures should be particularly useful in copolymerization studies of isomers or compounds having small differences in their elemental analyses.

2. Summary of Reactivity Ratios

Table 2 summarizes the published results on monomer reactivities found by copolymerizing various pairs of monomers.[5] It is seen, for instance, that in the reaction of styrene and methyl methacrylate, the addition of styrene monomer to styrene radical occurs half as fast as the addition of methyl methacrylate monomer to styrene radical. Also methyl methacrylate monomer adds half as fast to a methyl methacrylate radical as does styrene monomer. Furthermore, styrene monomer adds to styrene radical twice as fast as vinylidene chloride monomer to styrene radical. On the other hand, vinylidene chloride monomer adds to vinylidene chloride radical approximately one seventh as fast as styrene monomer. The estimated degrees of precision are indicated whenever given by the authors. In the case of references [3, 5, 7, 38, 39], the reactivity ratios were obtained from plots according to eq 4a by fitting the "best" curve. As an example, the system styrene-dichlorostyrene investigated by Alfrey, Merz, and Mark [5] is shown in figure 13.

A special case investigated is that wherein one of the monomers does not polymerize with itself

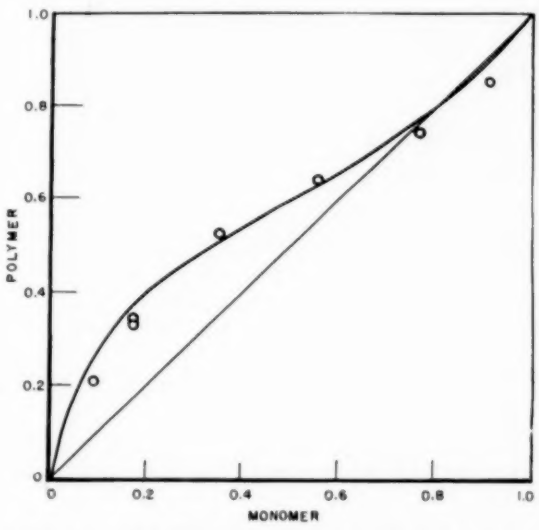

FIGURE 13. *Plot of instantaneous concentration of dichlorostyrene in polymer vs concentration of dichlorostyrene in monomer according to eq 4a and data in* [5].

[5] We are indebted to K. R. Henery-Logan and R. V. V. Nicholls for placing their results at our disposal prior to publication. The work was sponsored by the Office of Rubber Reserve.

807127—48——12

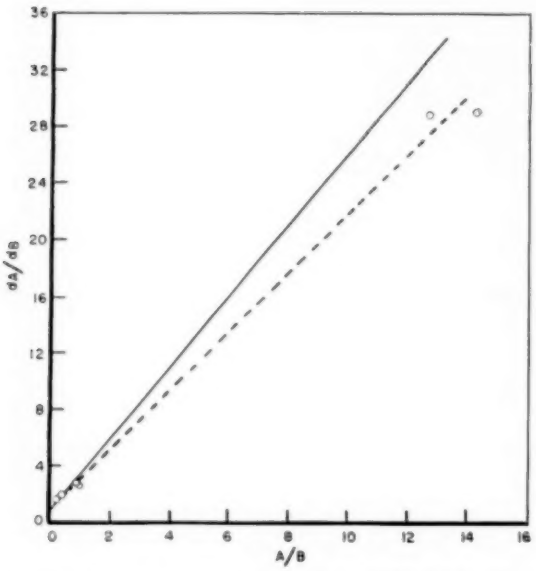

FIGURE 14. *Plot of instantaneous mole ratio in polymer vs mole ratio in monomer for system styrene-diethyl chloromaleate according to data in* [5].

but readily enters into copolymerization. Maleic anhydride [29] and its derivatives form a class of compounds exhibiting such a selectivity. Setting $\mu=0$ in the first eq 4a results in a linear relation. An experimental test on the system styrene-diethyl chloromaleate is shown in figure 14. The full line $\sigma=2.5$ is taken as the "best" value from a consideration of the data when plotted on a mole fraction basis.

The foregoing results substantiate rather well the assumptions under which the composition eq 4 has been derived, at least for the relatively low degrees of conversion at which it may be expected to hold. In attempts to consider the effect of composition on the addition rates [6] equations have been derived [20] for the case that the rates depend not only on the nature of the radical ends, but also on the preceding unit in the chain. The effects are small, and their detection would require considerable experimental accuracy.

Extensions of eq 4 to three-component systems and generalization to n-components [34] have been presented. Analysis of one four-component and seven three-component systems formed from styrene, methyl methacrylate, acrylonitrile, and vinylidene chloride indicates agreement with theory within experimental error. It is assumed in this comparison that the reactivity ratios of a pair A-B are independent of the medium and equal to the ratios obtained in the copolymerization of A and B alone.

Most of the published and analyzed results refer to bulk systems. In order to make valid comparisons for the monomer pairs studied, we shall confine the further discussion to the data in table 2. Some investigations in emulsion systems have been undertaken. For instance, the pairs given under footnote 5 and also the styrene-acrylonitrile combination [15] have been analyzed both in bulk and in emulsion. In the main no significant differences between the $\sigma-\mu$ values under the two different conditions are found.

[6] See also the discussion on page 524.

TABLE 2. *Reactivity ratios σ and μ for various monomer pairs*

Monomer A	σ	Monomer B	μ	Conditions	Reference
Styrene	0.520±.026	Methyl methacrylate	0.460±0.026	60° C, 0.1 mole % benzoyl peroxide, bulk	[42]
Do	.75	Methyl acrylate	.20	70° C, 0.4 mole % benzoyl peroxide, 40% monomer in toluene.	[5]
Do	.75 ±.07	do	.18 ± .02	60° C, 0.1 mole % benzoyl peroxide, bulk	[42]
Do	.30 ±.10	Methacrylonitrile	.16 ± .06	do	[43]
Do	.29 ±.04	Methyl vinyl ketone	.35 ± .02	do	[43]
Do	.41 ±.08	Acrylonitrile	.04	do	[15]
Do	31	Allyl chloride	.032	70° C, 0.5 mole % benzoyl peroxide, bulk	[3]
Do	0.54 ±.01	p-Chloroethyl acrylate	.10 ± .01	60° C, 0.1 mole % benzoyl peroxide, bulk	[43]
Do	1.85 ±.05	Vinylidene chloride	.085± .010	do	[40]
Do	2.00 ±.10	do	.14 ± .05	do	[15]
Do	55 ±.10	Vinyl acetate	.01 ± .01	do	[44]
Do	17 ±3	Vinyl chloride	.02	do	[40]
Do	90 ±20	Vinyl ethyl ether	0	do	[43]
Do	0.35 ±.025	Vinylthiophene	3.10 ± .45	60° C, 0.5 mole % benzoyl peroxide, bulk	[44]
Do	.55 ±.025	α-Vinylpyridene	1.135± .08	do	[44]
Do	.23 ±.07	Butadiene	1.48 ± .08	50° C, 0.1 mole % benzoyl peroxide, bulk	Footnote 7
Do	.78 ±.01	do	1.39 ± .03	60° C, 0.1 mole % benzoyl peroxide, bulk	[45]
Do	1.38 ±.54	Isoprene	2.05 ± .45	50° C, 0.1 mole % benzoyl peroxide, bulk	Footnote 7
Do	0.0	Chloroprene	6.30 ± .10	do	Do.

TABLE 2. *Reactivity ratios σ and μ for various monomer pairs*—Continued

Monomer A	σ	Monomer B	μ	Conditions	Reference
Styrene	.043±.09	Maleic anhydride	0	80° C, benzoyl peroxide, benzene solvent	[4]
Do	2.5	Diethyl chloromaleate	0	70° C, 0.4 mole % benzoyl peroxide, bulk	[3]
Do	0.13 ±.01	Monoethyl maleate	.035± .01	60° C, 0.2 mole % benzoyl peroxide, bulk	[41]
Do	8.5 ±.20	Dimethyl maleate	.03 ± .01	do	[41]
Do	5.0	Diethyl maleate	0	70° C, 0.4 mole % benzoyl peroxide, bulk	[5]
Do	6.52 ±.50	do	.005± .01	60° C, 0.1 mole % benzoyl peroxide, bulk	[42]
Do	0.19 ±.01	Maleonitrile	0	60° C, 0.2 mole % benzoyl peroxide, bulk	[41]
Do	.18 ±.10	Monoethyl fumarate	0.25 ±0.10	do	[41]
Do	.21 ±.02	Dimethyl fumarate	.25 ± .015	do	[41]
Do	.30 ±.02	Diethyl fumarate	.070± .007	60° C, 0.1 mole % benozoyl peroxide, bulk	[42]
Do	.19 ±.03	Fumaronitrile	0	60° C, 0.2 mole % benzoyl peroxide, bulk	[41]
Do	16 ±2	Trichloroethylene	.01 ± .01	60° C, 0.1 mole % benzoyl peroxide, bulk	[40]
Do	185 ±20	Tetrachloroethylene	0	do	[40]
Do	37 ±3	trans-Dichloroethylene	0	60° C, 0.2 mole % benzoyl peroxide, bulk	[41]
Do	210 ±15	cis-Dichloroethylene	0	do	[41]
Do	10	trans-Dichloroethylene	0	68° C, 0.1 weight % benzoyl peroxide, bulk	[39]
Do	50–100	cis-Dichloroethylene	0	do	[39]
Do	1.16 ±.09	p-Methoxystyrene	0.82 ± .07	60° C, 0.1 mole % benzoyl peroxide, bulk	[35]
Do	1.015± .06	p-Dimethylamino-styrene	.84 ± .05	do	[35]
Do	0.74 ±.03	p-Chlorostyrene	1.025± .05	do	[35]
Do	.695± .02	p-Bromostyrene	0.99 ± .07	do	[35]
Do	.62 ±.05	p-Iodostyrene	1.25 ± .30	do	[35]
Do	.64 ±.05	m-Chlorostyrene	1.09 ± .23	do	[35]
Do	.55 ±.03	m-Bromostyrene	1.05 ± .21	do	[35]
Do	.28 ±.025	p-Cyanostryrene	1.16 ± .13	do	[35]
Do	.19 ±.02	p-Nitrostyrene	1.15 ± .20	do	[35]
Do	.20	2,5 Dichlorostyrene	0.80	70° C, 0.4 mole % benzoyl peroxide, bulk	[3]
Do	.56 ±.03	o-Chlorostyrene	1.64 ± .07	60° C, 0.5 mole % benzoyl peroxide, bulk	[46]
Methyl methacrylate	.67 ±.10	Methacrylonitrile	0.65 ± .06	60° C, 0.1 mole % benzoyl peroxide, bulk	[43]
Do	1.2 ±.14	Acrylonitrile	0.15 ± .07	60° C, 0.1 mole % benzoyl peroxide, bulk	[15]
Do	2.53 ±.1	Vinylidene chloride	.24 ± .03	do	[15]
Do	20 ±3	Vinyl-acetate	.015± .015	do	[44]
Do	10	Vinyl chloride	.1	68° C, 0.2-0.4 weight % benzoyl peroxide bulk.	[38]
Do	0.395± .025	α-Vinyl pyridine	0.86 ± .06	60° C, 0.5 mole % benzoyl peroxide, bulk	[46]
Do	.25 ±.03	Butadiene	.75 ± .05	60° C, 0.1 mole % benzoyl peroxide, bulk	[43]
Do	.29 ±.03	p-Methoxystyrene	.32 ± .05	do	[35]
Do	.205± .02	p-Dimethylaminostyrene	.11 ± .02	do	[35]
Do	.405± .025	p-Methylstyrene	.44 ± .02	do	[35]
Do	.53 ±.025	m-Methylstyrene	.49 ± .02	do	[35]
Do	.415± .02	p-Chlorostyrene	.89 ± .05	do	[35]
Do	.395± .02	p-Bromostyrene	1.10 ± .25	do	[35]
Do	.36 ±.03	p-Iodostyrene	0.95 ± .20	do	[35]
Do	.47 ±.075	m-Chlorostyrene	.91 ± .11	do	[35]
Do	.48 ±.02	m-Bromostyrene	1.17 ± .25	do	[35]
Do	.22 ±.02	p-Cyanostyrene	1.41 ± .13	do	[35]
Do	.50 ±.03	o-Chlorostyrene	1.37 ± .10	60° C, 0.5 mole % benzoyl peroxide, bulk	[46]
Do	.50 ±.03	α-Methyl styrene	0.14 ± .01	do	[46]
Do	.41	2,5 Dichlorostyrene	2.55	68° C, 0.2-0.4 weight % benzoyl peroxide, bulk.	[38]
Vinyl acetate	0.1 ±.1	Methyl acrylate	9 ±2.5	60° C, 0.1 mole % benzoyl peroxide, bulk	[44]
Do	.7	Allyl chloride	0.67	68° C, 0.2-0.4 weight % benzoyl peroxide, bulk.	[38]
Do	.60 ±.15	Allyl acetate	.45 ± .15	60° C, 0.1 mole % benzoyl peroxide, bulk	[43]
Do	.1	Vinylidene chloride	6	68° C, 0.2-0.4 weight % benzoyl peroxide, bulk.	[38]
Do	.0 ±.03	do	3.6 ± .5	60° C, 0.1 mole % benzoyl peroxide, bulk	[40]
Do	.3	Vinyl chloride	2.1	68° C, 0.2-0.4 weight % benzoyl peroxide, bulk.	[38]
Do	.35	Vinyl bromide	4.5 ±1.2	60° C, 0.1 mole % benzoyl peroxide, bulk	[44]
Do	3.0 ±.1	Vinyl ethyl ether	0	do	[44]
Do	.23 ±.02	Vinyl chloride	1.68 ± .08	60° C, 0.1 mole % benzoyl peroxide, bulk	[44]
Do	0.17 ±.01	Diethyl maleate	.043± .005	60° C, 0.2 mole % benzoyl peroxide, bulk	[41]
Do	.011± .001	Diethyl fumarate	.444± .003	do	[41]
Do	.67	Trichloroethylene	0	68° C, 0.1 weight % benzoyl peroxide, bulk	[39]
Do	.66 ±.04	do	.01 ± .01	60° C, 0.5 mole % benzoyl peroxide, bulk	[44]
Do	5	Tetrachloroethylene	0	68° C, 0.2-0.4 weight % benzoyl peroxide, bulk.	[38]
Do	6.8 ±.5	do	0	60° C, 0.1 mole % benzoyl peroxide, bulk	[40]
Do	0.85	trans-Dichloroethylene	0	68° C, 0.1 weight % benzoyl peroxide, bulk	[39]
Do	2.8	cis-Dichloroethylene	0	do	[39]

TABLE 2. *Reactivity ratios σ and μ for various monomer pairs*—Continued

Monomer A	σ	Monomer B	μ	Conditions	Reference
Vinyl Acetate	0.99±0.02	*trans*-Dichloroethylene	0.086±0.01	60° C, 0.2 mole % benzoyl peroxide, bulk	[41]
Do	6.3 ± .2	*cis*-Dichloroethylene	.018± .003	do	[41]
Acrylonitrile	.61± .04	Methyl vinyl ketone	1.78 ± .22	60° C, 0.1 mole % benzoyl peroxide, bulk	[43]
Do	.91± .1	Vinylidene chloride	0.37 ± .1	do	[15]
Do	4.05± .3	Vinyl acetate	.061± .013	60° C, 0.1 mole % benzoyl peroxide, 45 mole % monomer in acetonitrile.	[44]
Do	3.28± .06	Vinyl chloride	.02 ± .02	60° C, 0.1 mole % benzoyl peroxide, bulk	[43]
Do	0.0 ± .04	Butadiene	.35 ± .08	50° C, 0.1 mole % benzoyl peroxide, bulk	Footnote 3
Do	.03± .03	Isoprene	.45 ± .05	do	Do.
Do	.01± .01	Chloroprene	6.07 ± .53	do	Do.
Do	470	Tetrachloroethylene	0	60° C, 0.1 mole % benzoyl peroxide, bulk	[40]
Vinyl chloride	0.14	Vinylidene chloride	Large	68° C, 0.2-0.4 weight % benzoyl peroxide, bulk.	[38]
Do	.77	Diethyl maleate	.009± .003	60° C, 0.2 mole % benzoyl peroxide, bulk	[41]
Do	.42	Dioctyl maleate	0	68° C, 0.2-0.4 weight % benzoyl peroxide, bulk.	[38]
Do	.12± .01	Diethyl fumarate	.47 ± .05	60° C, 0.2 mole % benzoyl peroxide, bulk	[41]
Do	5.0	Pentene 1	.2	68° C, 0.2-0.4 weight % benzoyl peroxide, bulk.	[38]
Do	2.05± .3	Isobutylene	.08 ± .10	60° C, 0.1 mole % benzoyl peroxide, bulk	[43]
Vinylidene chloride	0.35	Ethyl methacrylate	2.2	68° C, 0.2-0.4 weight % benzoyl peroxide, bulk.	[38]
Do	.35	Butyl methacrylate	2.2	do	[38]
Do	12.2 ±2.0	Diethyl fumarate	0.046± .015	60° C, 0.1 mole % benzoyl peroxide, bulk	[40]
Do	3.8	Allyl chloride	.26	68° C, 0.2-0.4 weight % benzoyl peroxide, bulk.	[38]
Maleic Anhydride	.03± .03	Stilbene	.03 ± .03	60° C, 0.1 mole % benzoyl peroxide, bulk	[41]
Do	.13 up	Allyl acetate	.0075 up	30° and 38.5° C, approximately 0.5 mole %	[7]
β Chloroethyl acrylate	5.5 ±1	do	0	60° C, 0.1 mole % benzoyl peroxide, bulk	[43]
Do	4 ±1	Methallyl acetate	0	do	[43]
Do	0.9 ± .1	Methyl acrylate	.9 ± .1	do	[43]
p-Chlorostyrene	1.15± .05	*p*-Methylstyrene	.61 ± .03	do	[35]
Do	0.86± .08	*p*-Methoxystyrene	.58 ± .03	do	[35]
Do	.70± .08	*p*-Nitrostyrene	.91 ± .37	do	[35]
Chloroprene	3.41± .07	Butadiene	.059± .015	50° C, 0.1 mole % benzoyl peroxide, bulk	Footnote 3
Do	3.65± .11	Isoprene	.133± .025	do	Do.

V. Discussion

1. Remarks on Effect of Substituents in Organic Reactions

Tables 3 and 4 summarize the experimental information in a slightly different way by giving the relative reactivities of a series of different monomers vs a given radical, e. g., styrene. The scale is arbitrarily fixed by setting the reactivity of a monomer toward a radical of its own kind equal to unity. Values above unity then signify a higher activity than that exhibited by the radical in question toward the identical monomer, whereas values below unity signify a lower activity. Some of the values may be affected by large errors, as can be judged by the limits given for the σ and μ values from which they were calculated.

The interpretation of these results in terms of the electronic structure and internal geometry of radical and monomer is no easy task. However, certain qualitative attacks, at least, can be made

TABLE 3. *Relative reactivities of monomers with styrene radical shown in comparison with Hammett's σ-values for the aromatics*

Monomer	Reactivity	Hammett's σ
Vinyl acetate	0.02	
Allyl chloride	.032	
Diethyl maleate	.2	
Diethyl chloromaleate	.4	
Vinylidene chloride	.5	
Isoprene	.73	
p-Methoxystyrene	.86	−0.268
p-Dimethylaminostyrene	.98	−.205
Styrene	1.00	.000
Methyl acrylate	1.33	
p-Chlorostyrene	1.35	+.227
p-Bromostyrene	1.44	.232
m-Chlorostyrene	1.56	.373
p-Iodostyrene	1.61	.276
m-Bromostyrene	1.82	.391
Methyl methacrylate	2.00	
Acrylonitrile	2.50	
p-Cyanostyrene	3.57	1.000
Butadiene	4.45	
Dichlorostyrene	5.02	
p-Nitrostyrene	5.26	1.27
Maleic anhydride	24.0	
Chloroprene	∞	

along the lines established in the study of organic reactions of small molecules. That we are dealing here with large radicals is no objection, since we have established within the limits of the system studied, that the growth rates are independent of molecular size.

TABLE 4. *Relative reactivities of various monomers with various radicals*

Monomer	Radical type						
	Styrene	Methyl methacrylate	Acrylonitrile	Vinylidene chloride	Isoprene	Butadiene	Chloroprene
Styrene	1.0	2.0	25	7	0.5	0.7	0.2
Methyl methacrylate	2.0	1.0	7	4.1	....	1.3	....
Acrylonitrile	2.5	0.8	1.0	2.7	2.2	3.1	.2
Vinylidene chloride	0.5	.4	1.1	1.0	....	....	....
Isoprene	.7	....	33.0	....	1.0	....	.3
Butadiene	4.5	4.0	∞	....	....	1.0	.3
Chloroprene	∞	....	200	....	7.5	17.0	1.0

It is perhaps worthwhile to precede the discussion of the subject proper with a cursory and necessarily simplified summary of certain results and concepts regarding organic reactions. We need to consider the influence certain substituent groups such as CH_3, Cl, NO_2, etc., in vinyl-type monomers exert on the electronic configuration in the adjacent double bond. The presence of such groups in a benzene ring leads to a change, as compared with benzene, in the rates of further substitution and affects also the locus of substitution. These facts have been known for some time in classical organic chemistry.[7] They are caused by the tendency of an electrophilic group to attack the ring at the region of highest (relative) electron density. Furthermore, if the over-all density is reduced compared to that in benzene, the rate of reaction is accordingly reduced.

In considering the mechanisms of such distortions of the charge distribution, we shall somewhat arbitrarily separate two factors, inductive effects in the sense of Ingold[8] and resonance effects. The former lead to an increase or decrease of the over-all availability of electrons in the ring, the substituent acting as an electron source or sink. For instance, a methyl group increases the electronic density in the ring and thus should increase the rate of substitution by an electrophilic agent while a chlorine atom, with its strong electron affinity, has the opposite tendency. Similarly, substituents such as NO_2, CN, or COOR tend to diminish the electron density. Analogous effects by such groups are observed in addition reactions to double bonds in simple olefins. Resonance effects can determine the locus of attack. For instance, groups with an unshared pair of electrons such as Cl, OH, NH_2, C_6H_5, contribute structures to the activated complex of the substitution reaction (see footnote 7) which make the ortho- and para-positions more negative

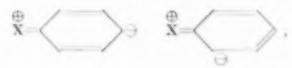

while no structure making the meta-position negative can be written. The resonance effect of NO_2, CN, COOR, and similar groups tends to leave the meta-position relatively more negative. Hence they are meta-directing. These directive effects persist in addition reactions to olefins. In general, ortho-para-directing substituents cause addition to proceed in accordance with Markownikoff's rule, meta-directing ones in opposition to it. These directive effects have also been explained without introducing explicitly the notion of resonance [23].

A quantitative measure of changes in electron density produced by substituents is given by Hammett's σ (see footnote 8), constants. They are defined as the logarithm of the ratio of the ionization constant of the meta or para substituted benzoic acid to that in the unsubstituted acid. A high positive value of Hammett's σ indicates a decrease in electron density. The fundamental correctness of these concepts may be judged from the results of certain calculations regarding the charge distribution in substituted benzenes [37].

2. Induction and Polarization Effects and Relative Reactivities

Reverting now to the problem posed in the beginning, it may be seen that several factors ought to be considered in attempting to account for the relative reactivities obtained and to predict the comparative behavior of monomers toward the same radical. The first ones are the over-all

[7] See for instance, G. E. K. Branch and M. Calvin, The theory of organic chemistry, (Prentice-Hall, Inc., New York, N. Y., 1941).

[8] See, for instance, L. P. Hammett, Physical organic chemistry (McGraw-Hill Publishing Co., Inc., New York, N. Y., 1940).

availability of electrons and, perhaps to a lesser extent, the direction of polarization of the double bond. Let us take first the styrene radical as a basis for comparison. In the stable monomer, the double bond should have a relatively high electron density because of the character of the phenyl group as an electron donor as evidenced by the direction of the dipole moment, which is opposite to that in toluene [45]. It should be remarked, however, that Hammett's σ for the phenyl groups is positive. Thus

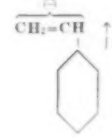

It is reasonable to assume that this over-all negativity carries over to the radical end of a growing vinyl chain [24]:

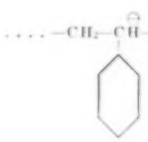

One can then expect that, under otherwise equal conditions (see below) addition to styrene of a monomer in which the inductive effect decreases the over-all availability of electrons in the pertinent double bond is favored in comparison with a monomer in which it is increased. It will be noticed, for instance, in table 3 that out of the three dienes, chloroprene shows the highest activity, isoprene the least and butadiene is intermediate.

Also from tables 3 and 4 it can be seen that acrylonitrile monomer adds preferentially to styrene radical and styrene monomer adds preferentially to acrylonitrile radical because of the opposing effects of the substituent groups. The cyanide group decreases the electronic density.

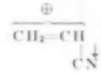

One would similarly expect propylene to show low activity with styrene.

Even allyl chloride has a low reactivity with styrene, as seen in table 3. Contrary to what one might expect by analogous reasoning, methyl methacrylate is slightly more active than methyl acrylate. The difference however, may not be significant.

The data on the substituted styrenes [35] in table 3 provide further support for the viewpoint expressed above. They indicate the existence of a correlation between Hammett's σ values for the respective substituent group and the corresponding relative reactivities of the substituted styrene monomers with styrene radical. A high σ-value, which is characteristic, as said before, for a decreased electron availability on other groups attached to the ring is accompanied by greater reactivity. A similar arrangement can be made in respect to the methyl methacrylate radical. Exceptions are encountered with respect to p-OCH_3, and p-$N(CH_3)_2$-styrene. The reactivities are higher than would correspond to the position of the substituent on the σ-scale. The authors [35] point out that these compounds are particularly effective in forming complexes with conjugated carbonyl systems. Generally such complexes can be formed by electron transfer between constituents of the complex [36]. In this connection the high selectivity (σ and μ very small) of allyl acetate and maleic anhydride is of interest [7]. Here there exists a possibility of resonance structures between radical and monomer which correspond to charge transfer within the activated complex. This possibility appears likely in view of the colors formed by maleic anhydride in mixtures with electron donor-type molecules such as stilbene, indene, and styrene. The difference between maleic anhydride and a quinone-type inhibitor would be a matter of degree and depend on the extent of resonance stabilization of the new radical formed. Inhibition is then effected by the removal of the stable radical through some further side reaction.

The direction and extent of polarization of the double bond can be of importance in favoring

a high reactivity. A monomer such as the one below

should tend to react with a styrene radical by adding head to head, which would bring into play interference by the group X, resulting in decreased activity as compared to the case:

Consideration of the resonance structures in biphenyl (see footnote 8) suggests that the phenyl group should be *o-p*-directing and therefore polarize the double bond in the direction indicated by the first of the above formulas.

The relative stabilities of the radical ends are a second factor governing the propagation rates. The styrene radical is relatively stable because of resonance through the benzene ring. In considering two reactions, the one producing the more stable radical end will be favored. Thus in comparing vinyl acetate with methyl acrylate monomers, the latter will exhibit the greater activity because of conjugation. The inductive effects should be approximately equal in magnitude for these two isomers. Resonance in the styrene radical would be more important than in the acrylate radical. The value for the acrylate monomer is nevertheless slightly larger than unity, probably, because of the direction of the inductive effect away from the double bond. One might expect the formation of acrylonitrile radical to be somewhat favored by the resonance effect. From this point of view all dienes should represent favorable cases.

We have been using for the purpose of illustration almost exclusively the styrene radical because of the wealth of data available. The concepts developed are in fair agreement with experimental results obtained on other radicals. In the case of vinylidene chloride, the radical resonance stabilization can play no significant role. The chloride groups make the monomer positive in the sense previously discussed. Therefore, it shows a high activity, with styrene monomer and a lesser one with methyl methacrylate which would not be extensively polarized because of the opposing effects of the methyl and methyl substituted carboxyl groups. With the more positively polarized acrylonitrile, the activity is still further reduced. For the same reasons, a similar order of activities is obtained, at least in a qualitative way, for acrylonitrile radical and methyl methacrylate radical with the same monomers. The electrostatic effects of groups on diene radicals should be less important than in their monomers, because the effects would be most important on the double bond, and the group is always one or more bond distances away from the activated end in the case of 1,4-addition. The double bond itself should act as an electron source. Actually the few data available could be interpreted by assuming that the diene radicals are somewhat negative regardless of the character of the substituent. However, the values for acrylonitrile relative to the dienes do not appear to fit this picture.

The mass of data given can be summarized in terms of constants that refer to pairs of radicals and monomers (see table 2). It would be desirable indeed to obtain constants characteristic for each monomer as such. This would in principle allow the prediction of reactivity ratios. The complete realization of such a program seems remote in view of the many factors involved and the probable existence of coupling effects.

3. Semiempirical relationships

The preceding discussion makes it evident that the polarity of radical and monomer and the relative stabilities of the radicals are the most important factors to be considered. An attempt to find a set of characteristic numbers in terms of these two effects has been recently made by Alfrey and Price [6]. It is suggested that the various influences are separable and can be represented in the following way:

$$k_{gB}(A) = P_A Q_B exp(-\epsilon_A \epsilon_B),$$

where $k_{gB}(A)$ is the rate of addition of monomer B to radical A. P_A is characteristic for the radical. The ϵ's are a measure of the effective charge on the end of the radical taken to be identical with the charge on the double bond of monomer A and on the double bond of monomer B, respectively. Q_B represents a mean reactivity of monomer B obtained by forming the geometric mean of the reactivities of B with a series of radicals A, B, . . . and then assigning to one monomer a reference value of unity. This equation implies that the free energy of activation for the propagation

step is additive in respect to the above-named effects. In comparing the behavior of monomers A and B toward radical A, P_A cancels out and one obtains for the ratios:

$$\sigma=\frac{k_{gA}(A)}{k_{gB}(A)}=\frac{Q_A}{Q_B}exp[-e_A(e_A-e_B)]$$
$$\mu=\frac{k_{gB}(B)}{k_{gA}(B)}=\frac{Q_B}{Q_A}exp[-e_B(e_B-e_A)] \quad (17)$$

$$\sigma\mu=exp[-(e_A-e_B)^2], \quad (18)$$

By the use of these equations, a set of relative Q- and e-values can be derived from the experimental results. They are presented in table 5 for some typical vinyl monomers. The result for the polarities is in general agreement with the point of view discussed before, styrene being the most negative and acrylonitrile the most positive of the four. The order of the Q's show a parallelism to the stabilities expected on the basis of the possible resonance structures for the radicals previously mentioned. Furthermore, the set of values is self-consistent in as much as they give σ's and μ's that are in agreement with the experimental data on all combinations of these four monomers.

TABLE 5 *Q- and e-values for vinyl compounds*

Monomer	Q	e
Styrene	1.00	−1
Methyl methacrylate	.64	0
Acrylonitrile	.31	+1
Vinylidene chloride	.16	0

Some difficulties arise if one attempts to fit the other olefins studied into the framework represented by table 5. The Q-values are not always consistent with the interpretation given to them and neither are the polarities. No satisfactory results are obtained by applying eq 17 and 18 to the data on dienes obtained by Henery-Logan and Nicholls (see footnote 5). In deriving these results the equality of effective charges for monomer and radical is assumed. As mentioned previously, it seems to us that in the case of dienes a differentiation ought to be made particularly when the inductive effect of a substituent acts to decrease the electron availability [32]. On this basis one can evaluate the pertinent data in conjunction with the values for the vinyl compounds given in table 5. We modify the two eq 17 and 18 by replacing the first factors e_A and e_B by e^*_A and e^*_B and one factor (e_A-e_B) in eq 18 by $(e^*_A-e^*_B)$, respectively. The star refers to the radical. The result of these calculations is summarized in table 6. The differences in sign between the e-values are in the expected direction. All e^*-numbers are negative, the one for chloroprene being the least. The few data available for an independent check are rather well reproduced by using table 6. It can be seen from eq 17 that a large value of the ratio Q_A/Q_B for a set of e's corresponds to large values of σ and small values of μ. Thus monomers with great disparity in the Q's, will copolymerize poorly. Large differences in the e's, of course, lead to good copolymerization.

TABLE 6. *Q, e, and e* for dienes*

Monomer	Q	e	e^*
Chloroprene	2.2	0.9	−0.6
Butadiene	2.5	−1.4	−1.2
Isoprene	3.5	−1.4	−1.3

4. Steric Effects

In considering the copolymerization of compounds such as stilbene, indene, maleic anhydride, the maleates, and the fumarates, another factor becomes important, namely steric hindrance. For example, the symmetrical substitution of another phenyl group in styrene leads to a compound, stilbene, which does not polymerize. Maleic anhydride and other symmetrical disubstituted ethylene derivatives polymerize with difficulty, if at all. However, stilbene and maleic anhydride form copolymers. The hindrance in such a case should still be great but is apparently overcome by the influence of polarity effects since the pertinent double bond can be expected to be positive in maleic anhydride and negative in stilbene.

A striking example of steric hindrance is provided by the comparison of maleic anhydride, diethyl chloromaleate, and diethyl maleate [4, 5]. The reactivities with styrene radical are respectively 24, 0.4, and 0.2. There differences have been ascribed to the opening of the anhydride ring [24]. Diethyl fumarate has a reactivity of 2.5 toward styrene monomer [24]. The increase over that of its cis-isomer can be understood on the

basis of the geometry of the two molecules, if the respective resonance structures of maleates and fumarates are considered.

The preceding discussion dealt entirely with relative rates of propagation in copolymerization, which are the ones determining average composition. Differences between monomers are, of course, to be expected in respect to the other steps of the chain reaction. In considering for instance, the rate of peroxide induced initiation, the polarities of monomer and catalyst radical and the stabilities of the radicals formed are of importance. We would expect the phenyl and the benzoyl radicals to be negative. It is not possible to compare directly the rates of initiation in two binary systems, since the rate of decomposition of the peroxide depends markedly on the medium [22]. This can be minimized by using dilute solutions of the monomers in an identical solvent. It serves no purpose to discuss in any greater detail possible effects of monomer structure on the relative rates of elementary acts other than propagation, until a complete kinetic analysis of the copolymerization of at least some typical pairs has been obtained.

5. Effect of Intramolecular Arrangement on Degradation

The whole discussion has hitherto referred to the building up of copolymer chains. It is of interest to consider also the reverse process. It is not our purpose here to discuss in detail thermal decomposition of polymers. We merely wish to point out briefly the relationship between the structure of the copolymer as considered previously and the results to be expected in its degradation. Studies of the thermal decomposition of various copolymers have shown that in many cases the yield of monomers are much lower than what would be expected from the number of monomer units known to be in the polymer and the behavior of the simple polymer [33]. For example, the yield of styrene from GR-S is much less than the corresponding yield of styrene from polystyrene.

Assuming that the effect of side reactions on the yield of a given monomer remains constant in going from simple polymer to copolymer depolymerizations, the pyrolysis yield of certain types of monomers obtained from a copolymer of given composition may be calculated. Let A represent monomers of the mono or asymmetrical disubstituted ethylene type (CH_2CXY) with head-to-tail arrangement in the simple chain and in the copolymer, and B monomers of the diene of symmetrically disubstituted ethylene types. In comparing the expected yield of A from a copolymer with the corresponding one from a pure polymer A, we proceed in the following manner. Consider a sequence of i A-units, which in the case of the copolymer is bounded by B units. There are $2i$ possibilities of producing a split, $2i-1$ in the interior and $2\times\frac{1}{2}$ at the boundaries, where the factor $\frac{1}{2}$ is included to avoid twofold counting of the bonds joining the sequence to the rest of the chain. $2i-1$ of these splits produce monomer A. If the probability of occurrence of a sequence of length i is denoted by $P_i(A)$ (eq 15), the yield Y_c of A from the copolymer becomes equal to:

$$Y_c = Y_0 \sum_{i=1}^{\infty} \frac{2i-1}{2i} P_i(A), \qquad (19)$$

where Y_0 denotes the expected yield of monomer from the pure polymer A. In deriving eq 19, it has been assumed that splitting occurs at random and independent of the nature of the adjacent units in the chain. Also recombination is excluded. One would expect large positive deviations from the calculated yields to be an indication of head-to-head and tail-to-tail structures in the polymer. For in such a case, the effect of the sequence boundaries considered in eq 19 is absent. In practice, the number of such configurations is usually small and obscured by other factors. Using the expressions (eq 15 and 16), we finally obtain from eq 19:

$$\frac{Y_c}{Y_0} = \frac{A}{A+\mu B}\left[1+\frac{B}{2\sigma A} \ln \frac{B}{\sigma A+B}\right]. \qquad (19a)$$

Since the composition of the copolymer can be determined from eq 4a, the thermal decomposition yield can be plotted against the instantaneous polymer composition as shown in figure 15 for the styrene-butadiene system using the pertinent values of σ and μ. For certain copolymers, such as the polybutenes, where the monomers are isomers or otherwise similar, this may be a useful tool for the development of a pyrolytic analytical technique, particularly since most monomers can be determined spectrometrically, while the copolymers cannot always be analyzed. The full application of this technique

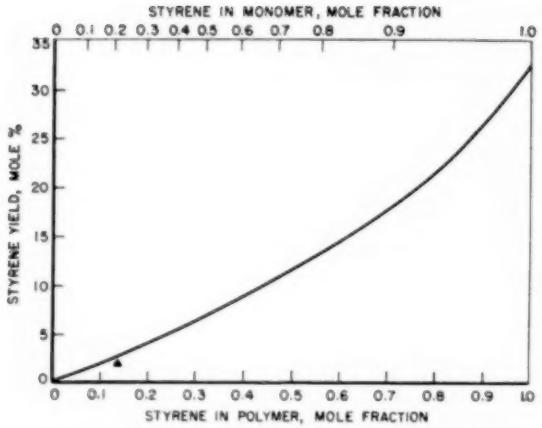
STYRENE IN MONOMER, MOLE FRACTION
0 0.1 0.2 0.3 0.4 0.5 0.6 0.7 0.8 0.9 1.0
STYRENE YIELD, MOLE %
0 5 10 15 20 25 30 35
0 0.1 0.2 0.3 0.4 0.5 0.6 0.7 0.8 0.9 1.0
STYRENE IN POLYMER, MOLE FRACTION

FIGURE 15. *Theoretical yield of styrene from butadiene-styrene copolymer as function of instantaneous polymer composition.*

▲, Experimental for GR-S.

will require precise control of pyrolysis conditions and highly refined analytical methods. At present, the above concepts will account for some of the results found in the depolymerization of copolymers.

6. Conclusion

In conclusion, the obvious main lines for further work may be sketched. Kinetic studies on copolymers are few and will have to be extended to include over-all rates, and at least in some typical cases, determinations of the individual rate constants of the chain reaction. It will be further interesting to see whether the observed reactivity ratios can be related to the structure of the monomer through other constants characteristic of the same. Consideration of dipole moments, polarizabilities, and ionization potentials may offer some clues. Indications as to steric influences in the copolymer chain may be gained by a comparison of the heats of reaction of the pure and mixed species.[9] The preceding discussion dealt primarily with the mechanism of formation and the resulting structure of the copolymer. Apart from the work on GR-S, no systematic studies of the relation between these factors and the thermodynamic [26] and rate properties of copolymer solutions seem to have been undertaken. Some physical properties of certain copolymers besides synthetic rubbers have been systematically investigated.[10]

[9] See in this connection a remark made by M. G. Evans, J. Chem. Soc., **1947**, 264. L. K. J. Tong and W. O. Kenyon, 113th meeting of the American Chemical Society, Chicago, Ill., April 19 to 25, 1948

VI. References

[1] T. Alfrey and G. Goldfinger, J. Chem. Phys. **12,** 20 (1944).

[2] T. Alfrey and G. Goldfinger, J. Chem. Phys. **12,** 32 (1944); **14,** 115 (1946).

[3] T. Alfrey and J. G. Harrison, J. Am. Chem. Soc. **6** 299 (1946).

[4] T. Alfrey and E. Lavin, J. Am. Chem. Soc. **67,** 20 (1945).

[5] T. Alfrey, E. Merz, and H. Mark, J. Polymer Sci. **1** 37 (1946).

[6] T. Alfrey and C. C. Price, J. Polymer Sci. **2,** 10 (1947).

[7] P. D. Bartlett and K. Nozaki, J. Am. Chem. Soc. **6** 1495 (1946).

[8] R. F. Boyer, J. Phys. and Colloid Chem. **51,** 80 (194

[9] R. F. Boyer, R. S. Spencer, and R. M. Wiley, Polymer Sci. **1,** 249 (1946).

[10] H. Branson and R. Simha, J. Chem. Phys. **11,** 2 (1943).

[11] P. J. Flory, J. Am. Chem. Soc. **61,** 3334 (1939).

[12] E. F. G. Herington and A. Robertson, Trans. Farad Soc. **38,** 490 (1942).

[13] E. Jenckel, Zeits. f. physik. Chem. **190A,** 24 (194

[14] F. M. Lewis and F. R. Mayo, Ind. Eng. Chem. Anal. Ed., **17,** 134 (1945).

[15] F. M. Lewis, F. R. Mayo, and W. F. Hulse, J. A Chem. Soc. **67,** 1701 (1945).

[16] I. Madorsky and L. A. Wood, work sponsored by t Office of Rubber Reserve.

[17] C. S. Marvel, G. D. Jones, T. W. Mastin, and G. L Schertz, J. Am. Chem. Soc. **64,** 2356 (1942).

[18] F. R. Mayo and F. M. Lewis, J. Am. Chem. So **66,** 1594 (1944).

[19] E. J. Meehan, J. Polymer Sci. **1,** 175 (1946).

[20] E. Merz, T. Alfrey, and G. Goldfinger, J. Polym Sci. **1,** 75 (1946).

[21] R. G. W. Norrish and E. F. Brookman, Proc. Ro Soc. London [A] **171,** 147 (1939).

[22] K. Nozaki and P. D. Bartlett, J. Am. Chem. Soc. **6** 1686 (1946).

[23] C. C. Price, Chem. Rev. **29,** 37 (1941); Reactions carbon-carbon double bonds (Interscience Pu lishers, Inc., New York, N. Y., 1946).

[24] C. C. Price, J. Polymer Sci. **1,** 83 (1946).

[25] R. Simha, J. Am. Chem. Soc. **63,** 1479 (1941).

[26] R. Simha and H. Branson, J. Chem. Phys. **12,** 2 (1944).

[27] H. Staudinger and J. Schneiders, J. Ann. **541,** 1 (1939).

[28] W. H. Stockmayer, J. Chem. Phys. **13,** 199 (194

[29] T. Wagner-Jauregg, Ber. **63,** 3213 (1930).

[10] See, for instance, W. O. Baker, in Advancing fronts in chemistry, High polymers (Reinhold Publishing Corp., New York, N. Y., 194

[30] F. T. Wall, J. Am. Chem. Soc. **62,** 803 (1940); **63,** 821 (1941).
[31] F. T. Wall, J. Am. Chem. Soc. **66,** 2050 (1944).
[32] L. A. Wall, J. Polymer Sci. **2,** 542 (1947).
[33] L. A. Wall, J. Research NBS **41,** 315 (1948) RP 1928.
[34] C. Walling and E. R. Briggs, J. Am. Chem. Soc. **67,** 1774 (1945).
[35] C. Walling, E. R. Briggs, K. B. Wolfstirn, and F. R. Mayo, J. Am. Chem. Soc. **70,** 1537 (1948).
[36] J. Weiss, J. Chem. Soc. (London), 245 (1942).
[37] T. Ri and H. Eyring, J. Chem. Phys. **8,** 433 (1940).
[38] P. Agron, T. Alfrey, J. Bohner, H. Haas, and H. Wechsler, J. Polymer Sci. **3,** 157 (1948).
[39] T. Alfrey and S. Greenberg, J. Polymer Sci. **3,** 297 (1948).
[40] K. W. Doak, J. Am. Chem. Soc. **70,** 1525 (1948).
[41] F. M. Lewis and F. R. Mayo, J. Am. Chem. Soc. **70,** 1533 (1948).
[42] F. M. Lewis, C. Walling, W. Cummings, E. R. Briggs, and F. R. Mayo, J. Am. Chem. Soc. **70,** 1519 (1948).
[43] F. M. Lewis, C. Walling, W. Cummings, E. R. Briggs, and E. J. Wenisch, J. Am. Chem. Soc. **70,** 1527 (1948).
[44] F. R. Mayo, C. Walling, F. M. Lewis, and W. F. Hulse, J. Am. Chem. Soc. **70,** 1523 (1948).
[45] M. M. Otto and H. H. Wenzke, J. Am. Chem. Soc. **57,** 294 (1935).
[46] C. Walling, E. R. Briggs, K. B. Wolfstirn, J. Am. Chem. Soc. **70,** 1543 (1948).

WASHINGTON, November 25, 1947.

U. S. GOVERNMENT PRINTING OFFICE: 1948